2019-09-12

Characterization of interactions between DmsD, DmsA, and TatB for the docking step for the bacterial twin-arginine translocase

Levchenko, Elina

UNIVERSITY OF CALGARY

Characterization of interactions between DmsD, DmsA, and TatB for the docking step for the bacterial twin-arginine translocase

by

Elina Levchenko

A THESIS

SUBMITTED TO THE FACULTY OF GRADUATE STUDIES

IN PARTIAL FULFILMENT OF THE REQUIREMENTS FOR THE

DEGREE OF MASTER OF SCIENCE

GRADUATE PROGRAM IN BIOLOGICAL SCIENCES

CALGARY, ALBERTA

SEPTEMBER, 2019

Abstract

Tat-pathway is the primary translocation system which deals with fully-folded proteins that all bear a “twin arginine” motif with a consensus sequence S/TRRXFLK. Three major *Escherichia coli* components are TatA, TatB and TatC, where the last two comprise a functional unit responsible for cargo docking. My project utilized a heterotrimer Dimethyl Sulfoxide (DMSO) reductase as a model system with two constituents (DmsA and DmsB) requiring assistance from a DmsD chaperone to reach the translocon. My goal was to study the order of events during the docking of DmsA onto the TatB and potential involvement of DmsD. The work supports that DmsD mediates the PMF-dependent transfer of the substrate to the translocase system. It was also shown *in vitro* (differential scanning fluorimetry; circular dichroism; chromatography) and *in silico* that DmsD has binding sites on its surface for DmsA and TatB, and they are distinct and potentially regulated by Mg^{2+} and GNP.

Preface

Portions of the work described in this thesis (Chapters 3 and 4) were presented as a poster at the 61st CSMB Membrane Proteins in Health and Disease Conference (2018) in Banff, Canada and oral presentation at PUBS (2018) in Calgary, Canada. The thesis is original and independent work by Elina Levchenko.

Acknowledgments

I would first like to thank Dr. Raymond Turner, my supervisor, mentor and personal hero. Dr. Turner has been key to just about everything I have done in the past two years. When I think of his role in my story, I always go back to that scene in "Balto 2" animated film where people choose copper husky puppies from the box and pay little attention to the silver-shaded Aleu, their sibling. I want to thank Dr. Turner for picking me from that box. I would like to say here "Thank you for giving me a chance, for your faith and vision".

I am very grateful for the members of my committee: Dr. Noskov and Dr. Moorhead. They never missed a single seminar or presentation by me. They always had a couple of challenging questions that would inevitably deepen my understanding of the project (and make me sweat uncontrollably in the process). Furthermore, I would like to thank our permanent lab members (Damon Brown, Nadia Monych and Natalie Gugala) as well as visiting scientists (Greta Baggio, Drs. Elena Piacenza and Alessandro Presentato) for keeping me laughing in the moments of ill luck (Plenty of those!!!) and applauding on small successes. I would like to express my deepest appreciation for scientists from other research groups who always had a piece of advice and required instrument available for me: Dr. Hynes, Dr. Ishida, Dr. Arias, Dr. Fraser, Dr. Winstone and Dr. Chaudhuri. Finally, I would like to thank anyone who at least once carried a liquid nitrogen tank with broken wheels across the campus (see chapter 5). I hope in the end you get a well-paying job with the insurance that covers massages and chiropractic services.

Finally, I am indebted to my family, especially my mother. Mindy Kaling wrote "…there is virtually no difference between an acquaintance and a friend. But the gulf between a friend and a best friend is enormous and profound…" I would like to thank her for being my Absolutely Best Friend during all these years, cheering me up and feeding hot chocolate and cookies after stressful Chemistry midterm exams or screaming with joy on victories.

I dedicate this work

to Victor and Tamara,

my maternal grandparents.

You set my standards for Love, Family and Partnership.

Table of Contents

List of Tables

List of Figures and Illustrations

List of Symbols, Abbreviations and Nomenclature

Symbol	Definition
A_{280}	Absorbance at 280 m
Amp	Ampicillin
ATP	Adenosine Triphosphate
BSA	Bovine Serum Albumin
CD	Circular Dichroism
CISM	Complex Iron-Sulfur Molybdoenzyme
D	Dilution
DMSO	DiMethyl SulfOxide
DSF	Differential Scanning Fluorimetry
DTT	Dithiolthreitol
EcDmsD	*Escherichia coli* DmsD
GDP	Guanosine Diphosphate
GMP	Guanosine Monophosphate
GST	Glutathione-S-Transferase
GTP	Guanosine Triphosphate
IPTG	Isopropyl β-D-1-thiogalactopyranoside
K_{ave}	Partition Coefficient
K_d	Dissociation Constant
LB	Luria Bertani
LC MS/MS	Liquid Chromatography Tandem-Mass Spectrometry
MalE	Cytosolic Maltose-Binding Protein
MBP	Maltose-Binding Protein
MobisPGD	Molybdenum-Bis Pyranopterin Guanine Dinucleotide

Native-PAGE	Native Polyacrylamide Gel Electrophoresis
Ni-NTA	Nickel-NitriloTriacetic Acid
OD_{600}	Optical density at 600 nm
PMSF	PhenylMethaneSulfonyl Fluoride
REMP	Redox Enzyme Maturation Protein
RR	Twin-arginine
Sec	Secretory
SEC	Size-Exclusion Chromatography
SDS-PAGE	Sodium Dodecyl Sulfate-Polyacrylamide Gel Electrophoresis
SmTorD	*Shewanella massilia* TorD
SRP	Signal Recognition Particle
SSE	Secondary Structure Estimation
StDmsD	*Salmonella typhimurium* DmsD
Tat	Twin-Arginine Translocase
T_m	Melting Temperature
UV-vis	Ultraviolet–visible
V_e	Elution Volume
V_o	Void Volume
V_t	Total Volume
WT	Wild-Type

Chapter 1. Background

Any living cell requires exchange of nutrients, solutes, and information with the outer environment. While for smaller molecules like ions, gases and water this can be achieved relatively easily (passive and active diffusion), whereas proteins require assistance due to varying size, charge and conformations (Yan and Wu, 2015).

1.1 Sec Pathway

In Gram-positive and Gram-negative bacteria most of the protein transport happens via general secretion system (Sec). While there are slight differences between the two types of bacteria due to their wall structure, major components and steps of the route are highly conserved (Freudl, 2013). Bacterial Sec system encompasses seven proteins of SecA to G and SecY (Yan and Wu, 2015). The integral pore is comprised of SecYEG, with the SecG being responsible for increased efficiency, yet not essential (Hanada et al, 1994). SecDF promote final stages of translocation of the substrate and SecA was shown to be an ATPase which drives the transport (Yan, Wu, 2015). As export can occur in two mechanisms, post-translational or co-translational manner, additional cell machinery may be required (Stephenson, 2005). In the case of the first one, SecB, a chaperone that is believed to recognize mature part of pre-protein, may target the substrate towards the SecA which will insert it into the membrane and employ ATP hydrolysis to move the pre-protein (de Keyzer J et al, 2003; Freudl, 2013). It is worth noting that the mechanism by which SecA transfers the substrate is still debated. At the moment three models exist: “power stroke” (each ATP hydrolysis cycle is believed to result in a “push” from SecA leading to a transport of 20-30 amino acids), “diffusion” (ATP is only utilized by the SecA to prevent backsliding of the sequence) and “SecA dimerization” (one monomer of SecA will be interacting with the pore, while its counterpart will hydrolyze the ATP) (Corey et al, 2016).

Co-translation from the ribosome is another option for delivery of the substrate across the membrane. It will require two more molecules in addition to already existing SEC apparatus: signal recognition particle (SRP), consisting of RNA and Ffh, and targeting FtsY protein (Giner et al, 1992). Combined activity of the two leads to hydrolysis of GTP molecule and transfer of the substrate to the SecYEG (Valent et al, 1998).

Finally, other proteins may become involved in targeting and insertion of the substrates into the membrane. One example would be YidC which is known to act independently as well as in combination with Sec. The following protein is regarded as only specializing on the membrane proteins (not exported substrates) and is believed to recognize hydrophobic patches which it subsequently inserts into the membrane (van den Berg et al, 2004). Following this event YidC recruits Sec apparatus to proceed with the translocation (Shanmugam et al, 2019).

Presence of a signal peptide is typically regarded as the feature of a non-cytoplasmic protein (Park et al, 1988). Proteins to be transported via general secretion pathway typically include an N-terminal signal sequence, which can be divided into three segments: positively-charged N-region, hydrophobic central section and C-terminal that contains a peptidase cleavage site (Kudva et al, 2013). Amino-terminal region with several basic residues was suggested to create a positive charge that allows for phospholipid and Sec proteins binding while hydrophobic segment assists with the successful insertion into the SecYEG pore (Akita et al, 1990).

This system is universal and it is found in all domains of life. However, the eukaryotic Sec is not identical to the bacterial version with an example being GTP and co-translation is used to drive the transport instead of ATP (Yan and Wu, 2015). Overall machinery involved is also more sophisticated with SRP particle consisting of 7s RNA and 6 proteins and a high number of accessory proteins (Lichi et al, 2004).

1.2 Tat pathway

An alternative to Sec is the twin-arginine translocation (Tat) pathway which transports exclusively folded proteins that all bear a distinct sequence with two arginine residues. Notably, only bacterial and the plant cell organelle chloroplasts contain a Tat system. Both Gram-positive and Gram-negative bacteria utilize the following pathway, but the former does not seem to employ any Tat-specific chaperone that assist in targeting. Nevertheless, the standard set of components remains unchanged with only minor fluctuations (number and identity of TatA and TatA-like proteins) (Goosens et al, 2014). While typically being longer and having SRRxFLK motif between the N-terminal and the hydrophobic domain, the signal sequence is very similar to the one in Sec (Keon et al, 1996). As Tat is assumed to be coupled to proton-motive force, it is considered a form of active transport (Berks, 2015), which makes it potentially dependent on changes in local pH (section 1.6.1).

The main components of the system are TatA, TatB and TatC (Figure 1.1); all are coded in the same operon.

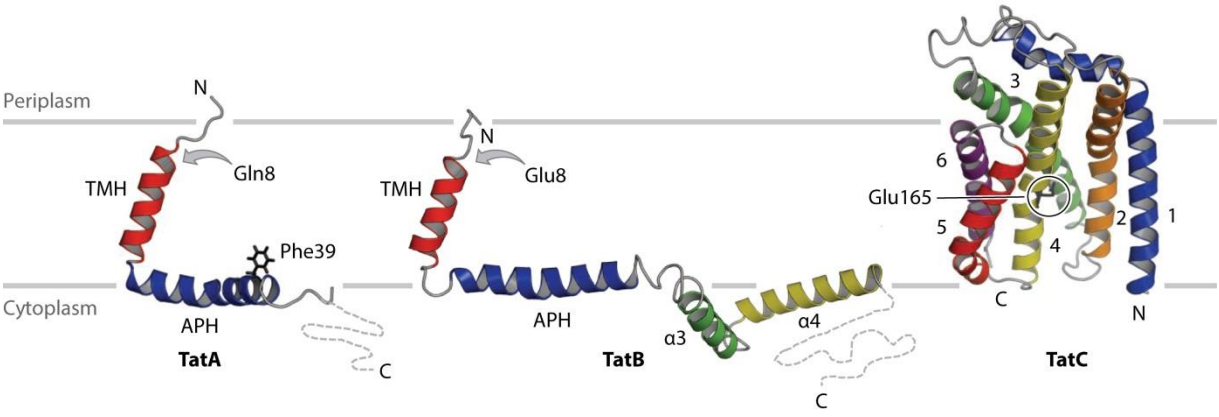

Figure 1.1. Structures of the Twin Arginine translocase (Tat) components. TatA and TatB were products of the NMR technique (both proteins were from *E. coli*), while TatC was solved using high-resolution X-ray structure (Aquifex Aeolicus). Helices were presented with ribbons and any disordered regions- as dashed lines. Functionally conserved residues are highlighted. Used with permission from Berks, 2015 (see Appendix).

TatA and TatB are integral membrane proteins, with the first known to oligomerize and potentially form a channel for substrate translocation (Kostecki et al, 2010). The number of TatA components in the ring varies and might depend on the size and/or diameter of the substrate being transported (Berks, 2015). TatC was shown to include six transmembrane spans and form a complex with TatB which is believed to form a substrate-binding site, which is a crucial interaction prior to actual translocation (Kostecki et al, 2010). Furthermore, TatBC is currently viewed as a functional unit with a 1:1 ratio, with recently identified critical contact sites within the transmembrane helices between the two proteins (Alcock et al, 2016).

It is not known how the pathway discerns between folded and unfolded proteins, but it is clear it transports folded proteins and multi subunits. The sequence of events involved in the translocation is also speculative (Berks, 2015). Nevertheless, it was determined that TatB interacts with a hydrophobic segment of the leader substrate. It was also suggested that this happens after an interaction of the protein with TatC (Alami et al, 2003). The *in vitro* result was later supported by *in vivo* studies: using bimolecular fluorescence complementation researchers were able to show that TatB interacted with the RR-leader of the substrate (Kostecki et al, 2010). One of the recent models suggests that TatB forms a dome-like structure and prevents the substrate to be exposed to the other side of the membrane prematurely (Blümmel et al, 2015). In addition, it might control access of TatA to TatC based on the observation that crosslinking contacts between the two increase in the absence of TatB (Blümmel et al, 2015).

Another proposed model offers little role to TatB and instead claims that TatA and TatB are competing for the polar amino acids cluster on TatC which has two binding sites on the opposite sides of the molecule. During the resting mode TatB contacts two TatC entities, but once the signal peptide binds to one of the TatC, the latter dissociates from the TatB and recruits TatA to

the same binding site which was recently employed by the TatB (Alcock et al, 2016). Finally, there exist more speculative options on how the system functions with models that include the oligomerized TatB assembly with TatC interacts in an octopus-like manner with the substrate (Maurer et al. 2010).

TatB itself is modeled as an L-shaped membrane protein (Fig 1.1) consisting of four helices (transmembrane helix (α1), amphipathic helix (α2), two additional hydrophilic helices (α3 and 4)) and a disordered C-terminal (Zhang et al, 2014). It has been shown that contacts with TatC happen via the TMH with residues Leu9/10, Phe6 and Glu8 (Rollauer et al, 2012; Kneuper et al, 2012; Alcock et al, 2016). Maurer *et al*. discovered that amino acids Gly34, Trp35, Ile36, Leu54, Leu56 and Leu78 may be involved in signal peptide binding (Maurer et al, 2010). However, the cytosolic segment of the molecule had not been studied extensively. Recently, the NMR structure of TatB in DPC micelles in solution was solved and it was found that while packing of TMH and amphipathic helices seemed rigid, α3 and α4 were very flexible in agreement with previous predictions of this region potentially intrinsically disordered. It was also noted that the α3 has a majority of its charged residues conserved, while the α4 did not (Zhang et al, 2014). Using their results and residues identified via cross-linking study (Maurer et al, 2010), Zhang *et al*. proposed that the cytoplasmic helices adjusted to the shape of the substrate and "hugged" it during the docking event (Zhang et al, 2014). That would explain the observation that TatB demonstrated binding towards the substrate throughout its length (Maurer et al, 2010).

1.3 Dimethyl sulfoxide reductase

When oxygen is unavailable or limited, *E. coli* switches to anaerobic respiration during which various compounds such as nitrate, fumarate and dimethyl sulfoxide may be used as terminal electron acceptors (Cole et al, 1985). The reduction in such cases is performed by enzymes that

have specificity towards the mentioned substrates. In case of dimethyl sulfoxide (DMSO), bacteria utilizes DMSO reductase, an enzyme present in a variety of organisms including *E. coli*, *P. vulgaris*, and *R. capsulatus* (Weiner et al, 1988; Styrvold et al, 1984; Satoh and Kurihara, 1987)

The anaerobic respiratory enzyme DMSO reductase belongs to the molybdoenzyme superfamily, a category of enzymes that require a molybdenum atom to be able to catalyze redox reactions. As DMSO reductases also include [4Fe-4S] clusters, they are additionally classified as members of CISM (complex iron-sulfur molybdoenzyme) family (Ray et al, 2003).

The model system our laboratory utilizes is DMSO reductase from *E. coli*, a heterotrimer comprised of units DmsA, B and C (Figure 1.2).

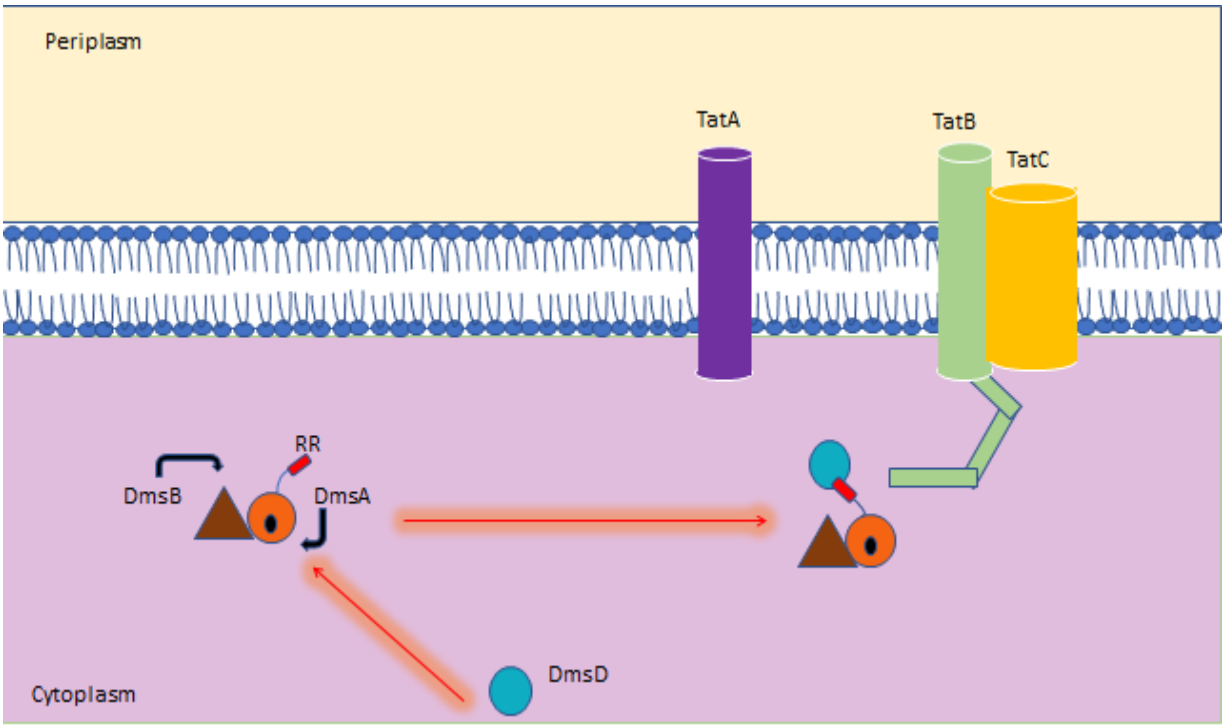

Figure 1.2. Complete Twin Arginine Translocase (Tat) which is involved in targeting of constituents of our model enzyme (DmsAB) to the periplasm. DmsD is the Redox Enzyme Maturation Protein (REMP) which is not part of the final holoenzyme, but targets the RR-bearing substrate to the membrane and potentially assists it in folding.

DmsA is the largest component of the enzyme and the only one that includes a twin-arginine signal sequence (Figure 1.2). DmsB dimerizes with DmsA in the cytoplasm after folding and [Fe-S] cofactor loading, as it cannot pass the membrane on its own. DmsA is also the subunit that has the molybdo- *bis* pterin guanosine dinucleotide (Mo*bis*PGD) co-factor installed in it along with a [2Fe-2S] cluster. DmsB is the electron conduit containing four [4Fe-4S] clusters. Finally, DmsC is a protein with eight transmembrane helices incorporated into the membrane and holding DmsAB attached on the periplasmic side of the membrane (Ray et al, 2003).

It was recently shown via bimolecular fluorescence complementation that the twin-arginine leader sequence of DmsA as well as the full-length protein interacts with both TatB and TatC proteins (Kostecki et al, 2010). Furthermore, the same tool was utilized to test whether mutating key arginines to lysines would affect the interaction. Interestingly, the signal only became stronger. That led to suggestion that this binding is not RR-dependent. Another important observation came from the poles of the cells where TatBC complexes were appeared to be localized; ssDmsA::DmsD complexes were targeted to that region and, thus, prepared for interaction with the TAT translocon (Kostecki et al, 2010).

1.4 Redox enzyme maturation proteins

It has been established that Tat system utilizes general chaperones such as DnaK and GroEL (Graubner et al, 2007). However, the following translocation pathway also employs a specialized group of chaperons named redox enzyme maturation proteins (REMPs). A REMP protein is a molecule that participates in the assembly of a complex redox enzyme, but is not part of the final structure. Turner *et al*. classified these molecules based on the phylogeny using *E. coli* organism as a basis (2004). They identified a group of oxidoreductases that employed chaperones in order to mature and managed to expand the analysis to other species. As a result, they grouped the

related REMP proteins into the following families: DmsD family (includes DmsD, NarJ, TorD and YcdY), NapD family (nitrate reductase-related proteins), FdhE family (formate-dehydrogenase-related proteins) and hydrogenases (HyaE and HybE) (Turner et al, 2004). While all substrates of DmsD family were determined to contain a molybdopterin co-factor, twin-arginine signal sequence and, thus Tat dependence, was not a uniform feature (Turner et al, 2004). Ten years later the DmsD family was later redefined as the NarJ superfamily (Chan et al, 2014).

Several functions had been proposed for the REMPs, but the debate is ongoing mostly due to the facts that A) the behavior of these molecules substantially differs among its representatives and B) different techniques and protein regions were utilized for the studies (Shanmugham et al, 2012).

The first suggested role is mediation of the targeting of the cofactor-containing respiratory enzyme to the Tat pathway with the initial idea that twin-arginine signal sequence was crucial for the interaction (Stevens et al, 2009). While the binding itself was detected, the N-terminal region (containing the SRRxFLK motif) was found to be essential for the binding, but hydrophobic and C-terminal ones (Shanmugham et al, 2012; Winstone et al, 2013). Moreover, one of the studies even casted doubts on DmsD being the targeting factor of DmsA since DmsA-GFP was delivered into the periplasm even in the absence of DmsD. Instead, the authors claimed that the REMP proteins should perform some other function (Ray et al, 2003). Nevertheless, it needs to be noted that the experiments did not test for the presence of other chaperones that could have assisted DmsA.

The second function proposed was to preserve the substrate in a conformation that would allow co-factor insertion. Ilbert *et al*. showed that *E. coli* TorA was activated (from its apo-form) only

in the presence of its chaperone TorD. Moreover, they determined that an additional step existed before insertion of the co-factor into the substrate and, thus, concluded that the REMP "prepared" its substrate for maturation (Ilbert et al, 2003).

Finally, there appears to be the third assigned REMP`s role which is protection of a signal peptide from degradation. This was demonstrated by purification of apoTorA protein in the absence of TorD: the substrate would be lacking the first 35 residues in cells with REMP protein deleted (Genest et al, 2006).

A common sequence of events was proposed to explain the interaction with their substrates (Figure 1.3) (Cherak and Turner, 2017):

1. Subunit of the future holoenzyme is released from the ribosome and is bound by the REMP (step 1 in Figure 1.3);
2. Chaperone assists in folding and (or) shields from incorrect co-factors, metals, and proteases (Berks, 2015) (steps 2-5 in Figure 1.3);
3. When the folding of the primary substrate is complete, a co-transported protein may join the complex (step 7 in Figure 1.3);
4. Docking to the TAT apparatus happens and REMP is released (steps 9-10 in Figure 1.3);
5. Following the translocation, the substrate is commonly attached to the awaiting integral membrane component (step 14-15 in Figure 1.3).

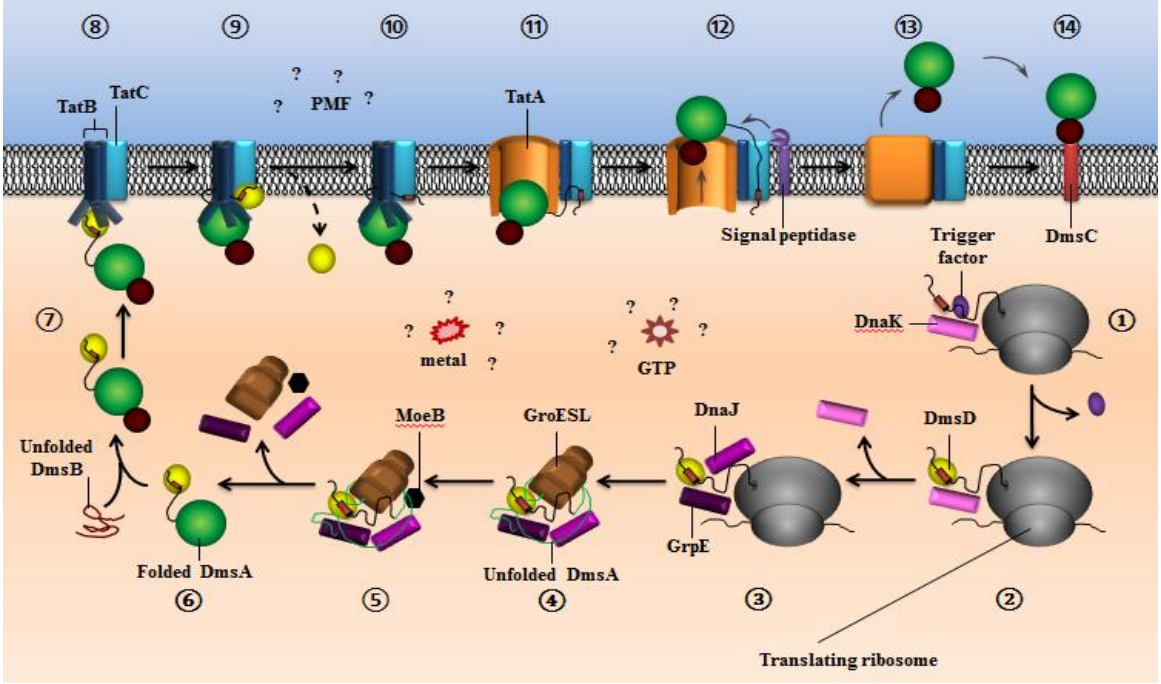

Figure 1.3. Maturation pathway model for DMSO reductase. Initially the substrate bearing a RR-signal sequence (red) (DmsA) is represented as a disordered black string of amino acids. Upon insertion of a co-factor, the depiction is changed to a green sphere (step 6). The number of TatBC units is reduced to one for simplification, while TatA oligomerized pore is shown as a whole structure. Adapted from Cherak and Turner (2017).

1.5 DmsD

1.5.1 Structural information

DmsD is the REMP for DMSO reductase and the model system our laboratory employs to study the Tat pathway. It is a small 23 kDa protein which was initially identified together with DnaK as DmsA-binding proteins (Oresnik et al, 2001). The protein`s structure was solved for *E. coli* and *S. typhimurium*: *Escherichia coli* (PDB: 3EFP, 3CW0, and 3U41) and *Salmonella typhimurium* (PDB: 1S9U) (Stevens et al, 2009; Ramasamy and Clemons, 2009; Qiu et al, 2008; Stevens and Paetzel, 2011). As seen in Figure 1.4 it was found to be mostly α-helical with a hydrophobic pocket that was suggested (through mutagenesis and molecular simulations) as the binding site for DmsA (see Chapter 6; Stevens et al, 2009). Upon inspection it is visible that one

of the fronts has multiple grooves present which may be important for the function (i.e. potential binding sites).

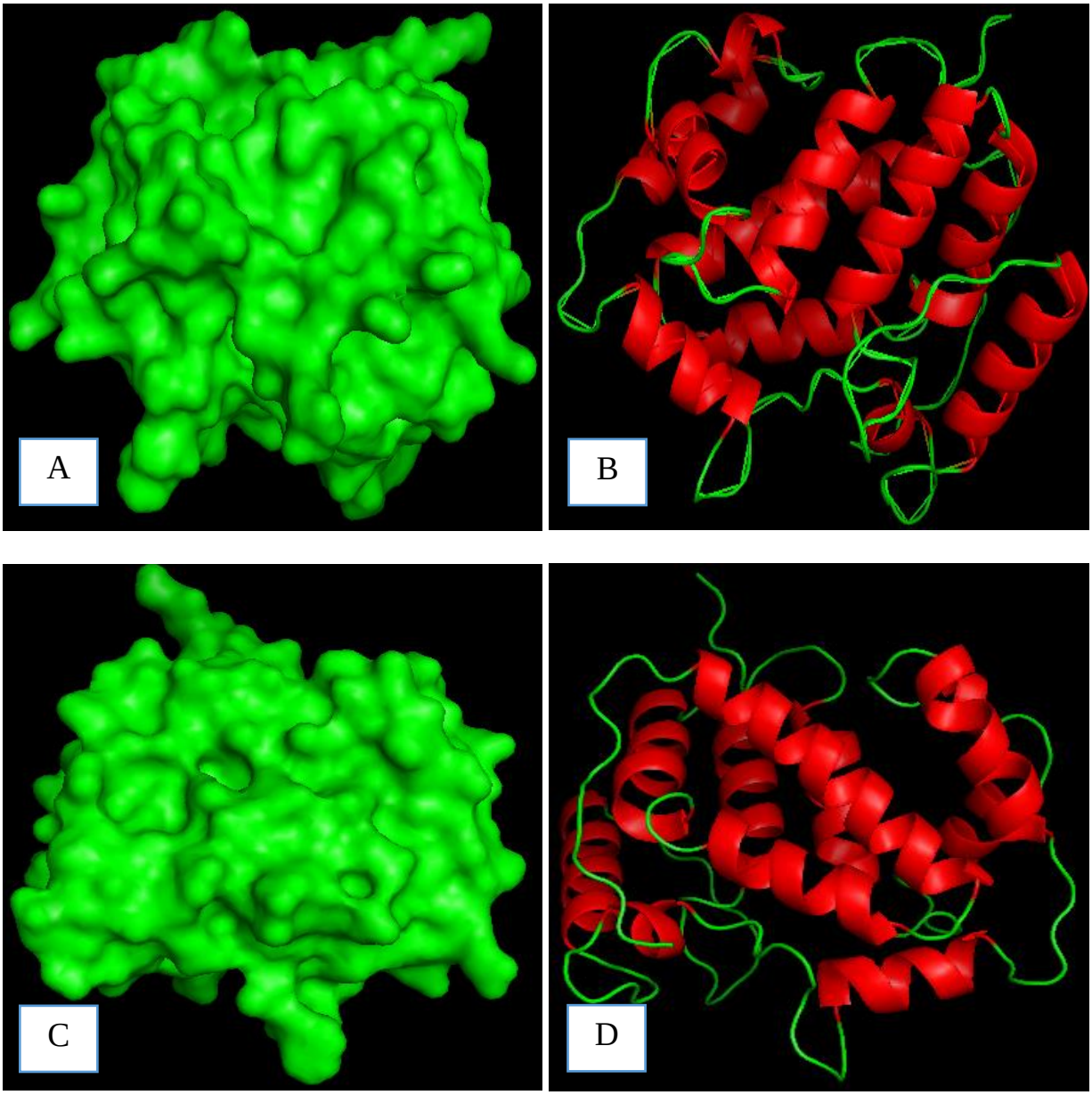

Figure 1.4 Crystal structure of DmsD from *E. coli.* A. Surface representation facing the side bearing the majority of cavities. **B.** Ribbon diagram of **A** with shading based on the secondary structure: helices are highlighted in red and loops-in green. **C**. Surface representation facing the "smooth" side. **D**. Ribbon diagram of **C** with shading based on the secondary structure: helices are highlighted in red and loops-in green. Crystal structure of *E. coli* DmsD (PDB: 3EFP) was used to generate a monomer from the asymmetric unit consisting of a dimer. Image was rendered using PyMOL.

DmsD exists in several folding forms all of which are "active" (demonstrate binding to DmsA RR-leader): monomer, dimer and pH 5-induced form "D" (Sarfo et al, 2004; Winstone et al, 2006).

1.5.2 Interactions with DmsA

While it was shown that chimeric (GFP-fused) DmsA protein can be delivered to the periplasm in a DmsD-deficient strain, it is also true that anaerobic growth using DMSO is impossible. Therefore, this REMP carries out some essential function for its substrate, but not directly related to the twin-arginine signal sequence (Ray et al, 2003). Still, it is now established that DmsD binds to the middle (H-section) part of the RR-leader peptide (Figure 1.2, Winstone et al, 2013; Connelly et al, 2016). Residues identified as a hot pocket on the surface of *E. coli* DmsD are the following: W72, F76, V77, P86, W87, P124, D126, and H127 (Chan et al, 2008). Interestingly, a genetic screen in *S. enterica* found only three residues that influenced the interaction between the chaperone and its cognate reductase substrate: W91Q and G100Q (abrogated selenite reductase activity, but did not influence signal sequence interaction) and V16Q (no signal sequence interaction) (Connelly et al, 2016). As seen from Figure 1.5, *S. enterica* key residues are located on opposite sides of the DmsD molecule, while DmsAl hot pocket on *E. coli* DmsD - between the two.

The binding with DmsAl occurs in a 1:1 ratio even if dimeric DmsD is employed and with a good biological affinity (0.2 μM for DmsAl-GST protein and 1.7 μM DmsAL $_{15\text{-}41}$) (Winstone et al, 2006; Winstone et al, 2013). The following values were consistent with other previously reported REMP-substrate interactions: 1.7 μM signal peptide TorA-TorD and 0.16 μM NarG-NarJ (Hatzixanthis et al, 2005; Chan et al, 2006). It had also been determined though use of differential scanning fluorimetry (DSF) that DmsD demonstrates an increase in melting

temperature with the addition of DmsA. Moreover, narrowing of the curve signaled of an increase in melting cooperativity (Cherak and Turner, 2015).

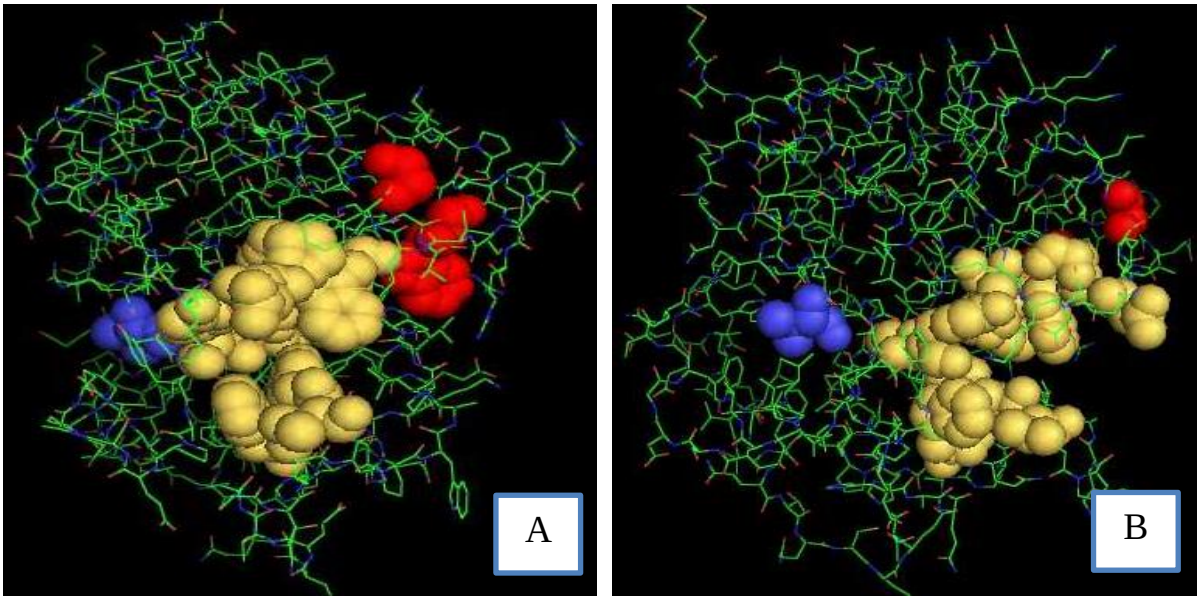

Figure 1.5. Comparison of alternative DmsAl-binding sites` position. A, B "Hot pocket" residues identified experimentally are colored in yellow (Chan et al, 2008), while those determined by Connelly *et al*. are shaded in red (W91Q and G100Q) and blue (V16Q) (2016). Crystal structure of *E.coli* DmsD (PDB: 3EFP) was used to generate a monomer from the asymmetric unit consisting of a dimer. Image was rendered using PyMOL.

1.5.3 Interaction with TatB and TatC

Apart from interacting with its substrate DmsA leader, DmsD was shown to interact with Tat pathway components, TatB and TatC. Using Bacterial two-hybrid system Kuzniatsova et al. determined that residues from the second and third cytoplasmic helices of TatB had a higher affinity towards DmsD compared to the fourth helix and the disordered C-terminal. All cytoplasmic loops of TatC except for the third one also appeared to be interacting with DmsD. Next, they attempted isothermal titration calorimetry (ITC) with peptides mimicking cytoplasmic loops on TatC and only detected heat consumption in the case of TatC4 (aa 233-258) with a K_d of 150 μM. When DmsD was pre-incubated with TatC4 and $DmsAl_{15-41}$ was co-titrated, the

dissociation constant would decrease by a factor of 2 compared to the original DmsD::$DmsAl_{15-41.}$ This implied that TatC increased the tightness of the interaction between the cargo and its REMP. Finally, the same article presented the data from a sandwich ELISA assay where TatB biotin-tagged peptides were tested for their interaction with DmsD. Again, the chaperone preferentially bound to third helix, but not the C-terminal. However, the fourth (hydrophilic helix) also yielded a significant signal while the amphipathic (α2) did not (Kuzniatsova et al, 2016).

1.6 Effector molecules and special conditions

1.6.1 PMF and its importance for the translocation

Proton motif force (PMF) consists of transmembrane potential (*Δψ)* and pH gradient. The effect of increased transport rate under its influence was originally observed in Sec pathway where inverted inner membrane vesicles containing SecA and SecYE were promoted to function and move substrates even in the absence of ATP (Driessen et al, 1991). It is now known that the Tat pathway and its substrates are also influenced by PMF. Firstly, proton electrochemical gradient was shown to be important at least for the first (binding) stage of the translocation when the TatA forms the pore to pass the mature protein out into the periplasm (Mori and Cline, 2002). It was also shown to play a role in the interaction between TatA and twin-arginine signal sequence where a collapse of a transmembrane gradient led to a loss in cross-linking (Alami et al, 2003). Moreover, our laboratory was able to demonstrate that the structure of DmsD is influenced by the pH: varying the pH across 3 units led to an emergence of different active, but structurally-different form (Sarfo et al, 2004; Winstone et al, 2006). Finally, data from Cherak and Turner further convinced us that varied sequence of events using alteration in pH and GTP molecules cause drastically different melting profiles in DmsD (2016). It thus can be hypothesized that

proton electrochemical gradient, particularly minor changes in pH may alter the interaction between DmsD and DmsA.

1.6.2 Purine nucleoside mono/di/triphosphates

When the affinity of TorD towards the TorA twin-arginine signal peptide was determined, it was proposed that the interaction should be regulated by some additional mechanism (Buchanan et al, 2008). Involvement of ATP was a reasonable theory due to its involvement in the Sec translocation (Hunt et al, 2002). However, when Hatzixanthis *et al*. employed fluorimetry to detect whether it would quench the tryptophans, no signal was observed (2005). Meanwhile, GTP, GDP, and GMP all showed binding to TorD (homologue of DmsD) which led the researchers to propose that a guanosine moiety was implicated. As the K_d was calculated to be approximately 370 µM for all three molecules and the concentration of di- and monophosphate is believed to be 10 and 1000 less, the authors deduced that it was only GTP that carries out some role *in vivo*. Notably, the dissociation constant for TorD already in complex with TorA (homologue of DmsA) was much smaller (200 µM) and, thus, implied a certain conformation change triggered by the substrate in its chaperone (Hatzixanthis et al, 2005). Another study concluded that TorD is a GTPase with a slow intrinsic rate which acts as a "switch" during maturation of TorA (Guymer et al, 2010).

In our lab differential scanning calorimetry was utilized to explore relationship of DmsD with GTP/ATP molecules. While no change in transition temperatures were detected, it was noted that addition of GTP resulted in enthalpy decrease for a less stable DmsD calculation. The authors then assessed possible GTPase activity in DmsD by completing a malachite green assay and ^{31}P NMR study. A signal from inorganic phosphate was observed only using the latter technique and in the presence of Mg and signal peptide (Tran, 2011). Finally, Cherak and Turner explored the

influence of GTP on DmsD::DmsAl complex: Not only does GTP lead to a decrease in the stability of DmsD and rise of a mixed DmsD population(s), but triggers dissociation from the DmsAl-GST (2015).

1.6.3 Metals

Mg and Mn are frequently associated with GTP molecules in the cell and it was shown that a domain-swapped TorD dimer has magnesium-dependent GTPase activity (Guymer et al, 2010). Tran even reported that GTP hydrolysis by DmsD was only possible in the presence of Mg (Tran, 2011). Sarfo noticed that multimeric changes took place when Ni or Zn were present in the assay (Sarfo et al, 2004; Rivardo et al, 2014).

Finally, experiments involving metals such as Ni, Zn, Fe, Mg, Mn, Cd and Cu demonstrated some conformational changes in DmsD. More specifically fluorescence intensity and far-UV Circular dichroism signal decreased in the order of $Cu^{2+} > Cd^{2+} > Zn^{2+}$ (Cherak and Turner, 2016). All these observations contribute to an expansion of the physiological conditions that may influence DmsD structure/function.

1.7 Research objectives:

While it has been identified that DmsD, DmsA leader and TatB interact with each other, the sequence of events and the mechanism involved are still unclear (Figure 1.6). In my research, I will focus to increase our understanding of the interactions between these three components (REMP, twin arginine leader peptide of the substrate protein and the TatB component of the Tat translocase) using *in vitro* approaches.

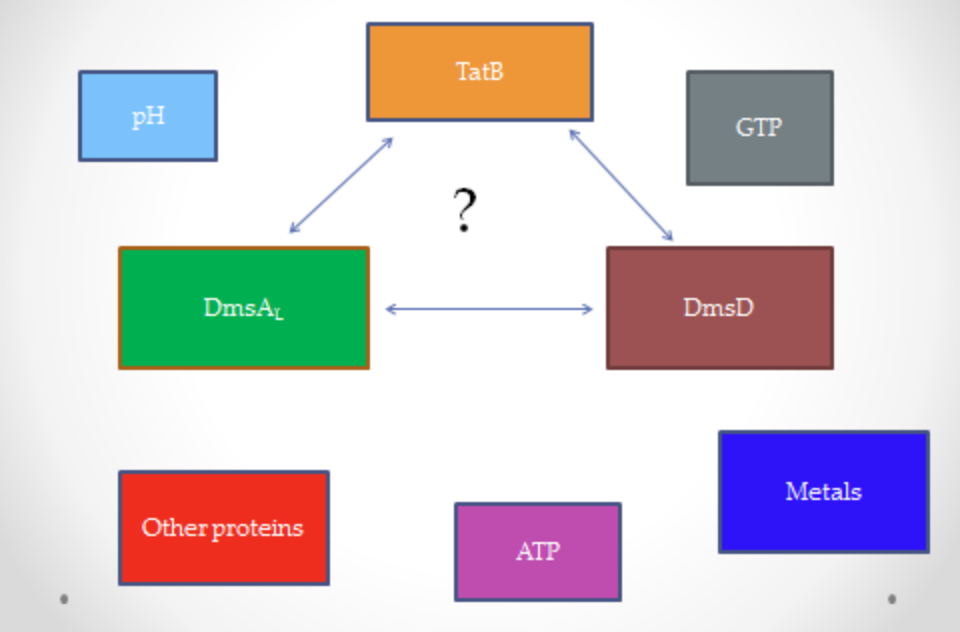

Figure 1.6. Interaction triangle that includes three proteins of interest to study (TatB, DmsD and DmsA), as well as potential effectors (small ligands, other proteins and conditions such as pH).

More specifically, my specific objectives are:

1. To develop and optimize purification method for MBP-TatB$_{fr}$, GST-TatB$_{fr}$ and MalE in order to employ those in *in vitro* approaches (Chapter 3).
2. To study the effect of TatB on DmsD by utilizing recombinant MBP-TatB$_{fr}$ protein as well as synthesized peptides (Chapters 4 and 5).
3. To explore the role of proton motif force by altering pH and observing the effect on TatB-to-DmsD interaction (Chapters 4 and 5).
4. To understand whether TatB needs to displace the leader peptide from the binding site on DmsD surface by performing circular dichroism with WT and mutant DmsD and comparing dissociation constants complemented with modeling of the putative TatB binding site and juxtaposing it to the previously-proposed leader peptide binding site (Chapters 5 and 6).

5. To learn if the transfer of the substrate is likely to happen if DmsD is already in complex with TatB or still bound to DmsA and ready to interact with TAT apparatus for subsequent substrate translocation. For this circular dichroism is employed and the order of peptide addition, pH and DmsD variants (WT versus mutant) (Chapter 5).
6. To determine if MBP-$TatB_{fr}$ is able to form stable complexes with H_6T_7-DmsD or DmsAl-GST by subjecting mixture to analytical size-exclusion chromatography (Chapter 7).
7. To probe DmsD surface for GTP-binding site and determine if it has any shared areas with TatB and/or DmsA leader peptide (Chapter 6).
8. To study the influence of GTP on DmsD when in complex with DmsA leader peptide by utilizing circular dichroism and size-exclusion chromatography (Chapters 5 and 7).
9. To use circular dichroism and analytical size-exclusion chromatography to assist in learning about any effect that the metal (Mg^{2+}, Ni^{2+} and Mn^{2+}) might have on DmsD::DmsAl complex (Chapters 5 and 7).
10. To compare the effects on DmsD::DmsAl complex when a combination of GNP and metal is added versus only metal or GNP in order to understand if any of the components intensify the effects such as dissociation of the substrate. (Chapter 5 and 7).

Chapter 2. Materials and methods

2.1. Protein preparation

2.1.1 H_6T_7-DmsD. WT DmsD was expressed, purified and/or prepared as described previously (Winstone et al, 2006). *E. coli dmsD* gene was cloned into the pRSETA expression vector with a N-terminal His_6 tag and T_7 epitope (Winstone et al, 2006). The plasmid was then transformed into the *E. coli* strain C41 (genotype: F^-ompT $hsdS_B$ ($r_B^-m_B^-$) gal dcm (DE3)). Cultures were grown in Luria Bertani (LB) media (6x1L) with ampicillin (0.1mg/ml final concentration) at 37^oC until OD_{600}=0.5 was reached. Next, induction with 1mM Isopropyl β-D-1-thiogalactopyranoside (IPTG) as final concentration was performed and expression occurred for 3 hours at room temperature ~21°C. The cells were then harvested by centrifugation at 4000rpm, resuspended in lysis buffer (50 mM Tris-HCl, 1M NaCl, 5 mM imidazole, 2mM DTT, pH 8.0) and centrifuged again at 4000 rpm. Phenylmethylsulfonyl fluoride (PMSF) was added at a final concentration of 10 mM just prior to the cell breakage with a French Press. DTT was also added at a final concentration of 10 mM (1 M stock was prepared using 1.54 g of DTT and 10 ml of ddH_2O). Next, a lysis with French Press (11,000 psi) was done and supernatant was obtained upon ultra-centrifugation at 40000 rpm for 90 minutes.

Using an Akta purifier, 2ml of cytosol was passed through the 5 ml HisTrap FF column (GE healthcare) at a flow rate of 3 ml/min. Column was flushed with 5 column volumes (CV) wash buffer (50 mM Tris-HCl, 1M NaCl, 5 mM imidazole, pH 8.0) and the monomer of His_6-T_7-DmsD was eluted using HisElution buffer (50 mM Tris, pH 8.0, 1M NaCl and 250 mM imidazole). The corresponding fractions were then concentrated with Amicon 10 kDa cut-off filters and subjected to a desalting 10 ml HiTrap column (GE Healthcare) to remove any excessive salts and imidazole with Exchange buffer (25 mM Tris, 100 mM NaCl, 1 mM

dithiothreitol (DTT), pH 8.0). The flow rate was 3 ml/min. The purification from 6 L of culture gave a yield of 55-60 mg (~10 mg/L) at ~ 98% purity.

2.1.2 DmsAl-GST

DmsAl-GST was expressed, purified and/or prepared as described previously (Winstone et al, 2006). *E. coli dmsA leader* gene was cloned into the pTDMS24 expression vector with a C-terminal GST tag. The plasmid was then transformed into the *E. coli* strain C41 (DE3). Cultures were grown in LB (6x1L) with ampicillin (0.1mg/ml final concentration) at 37^{o}C until OD_{600}=0.8 was reached.

Next, induction with 1mM IPTG was performed and expression occurred for 3 hours at room temperature ~21°C. The cells were then harvested by centrifugation at 4000rpm, resuspended in Lysis buffer (50 mM Tris-HCl, 200 mM NaCl, 2 mM EDTA, 5 mM DTT, pH 7.5) and centrifuged again at 4000 rpm. Phenylmethylsulfonyl fluoride (PMSF) was added at a final concentration of 10 mM just prior to the cell breakage with a French Press. DTT was also added at a final concentration of 10 mM (1 M stock was prepared using 1.54 g of DTT and 10 ml of ddH_2O). Next, a lysis with French Press (11,000 psi) was done and supernatant was obtained upon ultra-centrifugation at 40000 rpm for 30 minutes.

Using an Akta purifier, 2ml of cytosol was passed through the 5ml GS Trap HP column (GE Healthcare) at a flow rate of 3 ml/min. Column was flushed with 5 CV Wash buffer (50 mM Tris-HCl, 200 mM NaCl, 2 mM DTT, pH 7.5), 2 CV of DnaK buffer (50 mM Tris-HCL, 200 mM NaCl, 10 mM $MgSO_4$, 10mM ATP, pH 7.5) and DmsAl-GST was eluted using 5 CV GST Elution buffer (50mM Tris-HCL, 200mM NaCl, and 10mM reduced glutathione, pH 8.0). The corresponding fractions were then concentrated with Amicon 10 kDa cut-off filters and subjected

to a desalting 10 ml HiTrap column (GE Healthcare) to remove any excessive salts, ATP and reduced glutathione with Exchange buffer (25 mM Tris, 100 mM NaCl, 1 mM DTT, pH 8.0). The flow rate was 3 ml/min. The purification from 6 L of culture gave a yield of 12-18 mg (~2.5 mg/L) at ~ 98% purity.

2.1.3 MBP-TatB$_{fr}$.

Maltose binding protein (MBP) was used as a carrier for the *E. coli* TatB cytosolic fragment starting from amino acid 27 and MBP tag. Primers to amplify the gene fragment for this clone were designed by previous Turner lab member (Erik Tralman-Baker). The PCR product was purified and cloned as a EcoRI–BamHI fragment into EcoRI–BamHI digested pMAL-c2g. The system utilizes tac promoter (P_{tac}). The nucleotide sequence of the clone was validated and this construct was then transformed into *E. coli* strain C43 (DE3).

For expression the culture was grown in LB broth supplemented with ampicillin (0.1 mg/mL final concentration) and glucose (2 g per liter). The cultures were grown at 37^{o}C until OD_{600} was equal to 0.5. Next, IPTG was added at a final concentration of 0.5 mM. The incubation of cultures continued for 2 hours at 37^{o}C and overnight (16 additional hours). The cells were harvested within two 10 minute rounds of centrifugation at 4000 rpm (Sorvall SLC4000 rotor). The pellets were then washed with 80-100 ml of MBP column buffer (20 mM Tris-HCl, 200 mM NaCl, 1 mM EDTA, 1 mM DTT, pH 8.0) and transferred into 250 ml pre-weighted vessels for another 10 min centrifugation at 5000 rpm (Sorvall SLA1500). The supernatant was decanted and the bottles with pellets were reweighted.

Next, the pellet was homogenized and additional 5-10 ml of lysis buffer was added. Phenylmethylsulfonyl fluoride (PMSF) was added at a final concentration of 10 mM just prior to

the cell breakage with a French Press. DTT was also added at a final concentration of 10 mM (1 M stock was prepared using 1.54 g of DTT and 10 ml of ddH_2O). The cell free extract was centrifuged for 30 min at 5000 rpm (Sorvall SS34 rotor). The supernatant was collected and poured into Beckman centrifuge tubes (Beckman 70Ti rotor) and centrifuged for 30min at 40000 rpm. Upon centrifugation the cytosol was collected in a 50 ml Falcon tube. The concentration was determined via a Bradford assay and aliquots of protein were frozen in liquid nitrogen and stored at -80 ^{o}C until the purification step.

Purification was a two-step process on an AKTA Purifier system: passing 2ml portions of cytosol from 6x1 L through the 5ml amylose column followed by size exclusion chromatography with Superose 12 10/300 GL. First, the cytosol was thawed in a water bath inside the cold room, centrifuged for 10 min at 4000 rpm (Sorvall SLC4000 rotor), collected the supernatant, passed through 0.45 µm membrane filters (Sterile Acrodisc ®Syringe Filter with Supor®Membrane) and prepared 2 ml portions for loading onto the amylose column. Next, the column was equilibrated with 1 column volume of MBP column buffer (20 mM Tris-HCl, 200 mM NaCl, 1 mM EDTA, 1 mM DTT, pH 8.0). The sample was loaded on a 2 ml loop. The flow rate was 2 ml/min. After the unbound sample had been washed with 5 CV, elution of the identified contaminating Ef-Tu chaperone (see section 3.4) was removed using 2.5 CV ATP-containing buffer (50 mM Tris-HCL, 200 mM NaCl, 10 mM $MgSO_4$, 10 mM ATP, pH 7.5). Upon completion of segment 1 (2 CV), segment 2 followed where the elution with maltose-containing MBP buffer (20 mM Tris-HCl, 200 mM NaCl, 1 mM EDTA, 1 mM DTT, 10 mM maltose, pH 8.0) was performed over 5 CV. Product of elution step was collected with all the fractions being subject to SDS-PAGE. The fractions were then pooled and concentrated with an Amicon filter (30 kDa cut-off) to produce a volume of 10 ml of less. To achieve this Sorvall SLC4000 was

used for three 10 min runs at 4000 rpm. Next, the protein was filtered using 0.45 μm syringe filter (Sterile Acrodisc ®Syringe Filter with Supor®Membrane) and divided into 0.5 ml portions for the second purification step. Superose 12 10/300 GL column was washed with 42 ml of Hi-Trap (Exchange) buffer (10mM Tris-HCl, 100 mM NaCl, 2 mM DTT pH 8.0) and equilibrated with 0.5 column volumes. The flow rate was 0.7 ml/min. Enriched MBP-TatB samples were loaded in 0.5ml portions and the second eluted peak was collected (first peak was identified as MBP-TatB dimer and a third peak contained remaining Ef-Tu). All fractions were concentrated using a new Amicon filter (30 kDa cut-off). The concentration of protein was measured using the spectrophotometer (Hitachi U2000) with a 10x dilution. Extinction coefficient of 1.293 and molecular weight of 56 kDa were employed to perform the necessary calculations and determine molarity and concentration in mg/ml. The purified product was frozen in 1ml aliquots and kept at -80°C. The purification of the MBP-TatB from 6 L of culture gave a yield of 40-50 mg (~7.5 mg /L) at ~ 90% purity (see Figure 3.7, section 3.3).

2.1.4 MalE (cytosolic maltose-binding protein)

DMSO stocks with *E. coli* strain TL212 that had full-length cytosolic maltose-binding protein were created by a previous member of the Turner lab (Catherine Chan). Purification of native MalE as a control was performed in an equivalent fashion, expressing in the pMAL-c2 vector, but without the need for an ATP containing elution step as no Ef-Tu is co-purified without the TatB peptide (see sections 2.1.3 and 3.4).

2.1.5 GST-$TatB_{fr}$

Glutathione S-transferase (GST) was used as a carrier for the *E. coli* TatB cytosolic fragment starting form amino acid 27. Primers to amplify the gene fragment for this clone were designed

by previous Turner lab member (Erik Tralman-Baker). The PCR product was purified and cloned as a EcoRI–BamHI fragment into EcoRI–BamHI digested pGEX-3X. The system utilizes tac promoter (P_{tac}).The sequence validated construct was then transformed into *E. coli* strain C43 (DE3), which was then grown in LB broth supplemented with ampicillin (0.1 mg/mL final concentration).The cultures were grown at 37^{o}C until OD_{600} was equal to 0.5. Next, IPTG was added at a final concentration of 0.5 mM. The incubation of cultures continued for 3 hours at 37^{o}C. The cells were harvested within two 10 minute rounds of centrifugation at 4000 rpm (Sorvall SLC4000 rotor). The pellets were then washed with 80-100 ml of lysis buffer (20 mM Tris-HCl, 200 mM NaCl, 2 mM EDTA, 5 mM DTT, pH 8.0) and transferred into 250 ml pre-weighted vessels for another 10 min centrifugation at 5000 rpm (Sorvall SLA1500). The supernatant was decanted and the bottles with pellets were reweighted.

Next, the pellet was homogenized and additional 5-10 ml of lysis buffer was added. PMSF was added at a final concentration of 10 mM just prior to the cell breakage with a French Press. DTT was also added at a final concentration of 10 mM. The cell free extract was centrifuged for 30 min at 5000 rpm (Sorvall SS34 rotor). The supernatant was collected and poured into Beckman centrifuge tubes (Beckman 70Ti rotor) and centrifuged for 30min at 40000 rpm. Upon centrifugation the cytosol was collected in a 50 ml Falcon tube. The concentration was determined via a Bradford assay and aliquots of protein were frozen in liquid nitrogen and stored at -80 ^{o}C until the purification step.

Purification was a two-step process on an AKTA Purifier system: passing 2ml portions of cytosol from 6x1 L through the 5ml GS Trap HP column (GE Healthcare) followed by size exclusion chromatography with Superose 12 10/300 GL. First, the cytosol was thawed in a water bath inside the cold room, centrifuged for 10 min at 4000 rpm (Sorvall SLC4000 rotor), collected

the supernatant, passed through 0.45 µm membrane filters (Sterile Acrodisc ®Syringe Filter with Supor®Membrane) and prepared 2 ml portions for loading onto the GS Trap HP column. Next, the column was equilibrated with 1 CV Wash Buffer (50 mM Tris-HCl, 200 mM NaCl, 2 mM DTT, pH 7.5). The sample was loaded on a 2 ml loop. The flow rate was 3 ml/min. After the unbound sample had been washed with 5 CV Wash buffer, elution of the contaminating unknown protein(s) (see section 3.5) was removed using 2 CV of ATP-containing buffer (50 mM Tris-HCl, 200 mM NaCl, 10 mM $MgSO_4$, 10 mM ATP). Upon completion of segment 1 (2 CV), segment 2 followed where the elution with GST Elution buffer (50mM Tris-HCL, 200mM NaCl, and 10mM reduced glutathione, pH 8.0) was performed over 5 CV. Product of elution step was collected with all the fractions being subject to SDS-PAGE. The fractions were then pooled and concentrated with an Amicon filter (30 kDa cut-off) to produce a volume of 10 ml of less. To achieve this Sorvall SLC4000 was used for three 10 min runs at 4000 rpm. Next, the protein was filtered using 0.45 µm syringe filter (Sterile Acrodisc ®Syringe Filter with Supor®Membrane) and divided into 0.5 ml portions for the second purification step. Superose 12 10/300 GL column was washed with 42 ml of Hi-Trap buffer (10mM Tris-HCl, 100 mM NaCl, 2 mM DTT pH 8.0) and equilibrated with 0.5 column volumes. The flow rate was 0.7 ml/min. Purified GST-$TatB_{fr}$ was loaded in 0.5ml portions and the first eluted peak was collected (see section 3.5). All fractions were concentrated using a new Amicon filter (30 kDa cut-off). The concentration of protein was measured using the spectrophotometer (Hitachi U2000) with a 10x dilution. Extinction coefficient of 1.172 and molecular weight of 46 kDa were employed to perform the necessary calculations and determine molarity and concentration in mg/ml. The purified product was frozen in 1ml aliquots and kept at -80°C. The purification of the GST-$TatB_{fr}$ from 6 L of culture gave a yield of 12-15 mg (2-3 mg /L) at ~ 90% purity (see Figure 3.5.1, section 3.5).

2.2 Peptides.

Peptides designed based on the *E. coli* K12 genome sequence of TatB (gene accession **P69425**) and were synthesized by GenScript USA Inc. Three peptides demonstrating three distinct segments of TatB cytoplasmic domain (residues 27-171) were constructed and named TatB1/2/3. The sequences were as follows: RALRSLATTVQ (TatB1), LTNLTPELKA (TatB2) and NPVVKDNEAA (TatB3). These regions were selected based on article by Kuzniatsova *et al*. (2016). More specifically, it was determined that peptides comprising two amphipathic helices were the ones that showed a high signal for binding to DmsD (Kuzniatsova et al, 2016). As a result, TatB1 was chosen because it belonged to the end of the first (hydrophilic) helix, a region that had a peptide which produced a single strong signal. TatB2 was the peptide encompassing segments from two amphipathic helixes, while TatB3 peptide was selected based on the idea that the disordered region might accept a more ordered confirmation during the interaction (despite not being shown to participate in the interaction during ELISA or BiFC assays) (Kuzniatsova et al, 2016). Additionally, a peptide from *E. coli* DmsA, DmsAl, the key segment of the DmsA twin arginine leader identified to interact with DmsD (residues 15-41) was synthesized by GenScript USA Inc. This peptide was previously shown to bind DmsD most tightly (K_d=1.7 µM) (Winstone et al., 2013). The sequence of DmsAl is: SRRGLVKTTAIGGLAMASSALTLPFSR. All peptides were solubilized in deionized water to make 1.5mM stocks that were stored at -20°C until use.

2.3 Protein Characterization methods

2.3.1 Bradford Assay

Concentration of protein from multiple purification steps was evaluated using Bradford assay. A standard curve was created using known concentrations of bovine serum albumin and Bradford

reagent (BioRad). 2.5 ml mixture samples received aliquots of 25 µl or 50 µl of protein. Incubation lasted 10-15 minutes and absorbance was then measured at 595 nm. An average of a duplicate was employed to calculate the concentration using the interpolation of the BSA standard curve.

2.3.2 UV-VIS absorption

Absorbance at 280 nm was employed for determination of pure protein concentrations. First, extinction coefficient (ε) was estimated via the online tool ProtParam (https://web.expasy.org/protparam/). The sequence of the protein, including the affinity tag, was used and the software computed the extinction coefficient which was subsequently used together with the A_{280} to calculate the concentration via Beers Law. The protein sample was prepared using elution buffer. A dilution (D) of D10 or D20 was prepared to a final volume of 1 ml.

2.3.3 Sodium Dodecyl Sulfate-Polyacrylamide Gel Electrophoresis (SDS-PAGE)

Protein samples were prepared in order to have a concentration of 1 µg/µl. However, for purified AKTA fractions or analytical SEC samples (also non-concentrated and samples coming directly from AKTA Purifier elution fractions), a 1:1 protein-to-buffer mixture was prepared. Protein samples were prepared using SDS-PAGE loading buffer (50mM Tris-HCl pH 6.8, 2% w/v SDS, 100 mM DTT, 40% W/V glycerol, 0.2% bromophenol blue) and heated at 95 ^{o}C in a water bath for 10 minutes. Next, a centrifugation (4000 rpm, 3 minutes) was performed to ensure homogeneous mixture. Gels for Bio-Rad Mini Protein II were prepared manually using 12% acrylamide stacking gel and 5% acrylamide separating gel. ThermoFischer unstained molecular weight standard was utilized to determine the approximate molecular weight of resolved protein bands. Gels were run at 130 volts for 15 minutes and 180 volts for 45 minutes. A staining step

(10% $^{v}/_{v}$ acetic acid, 0.25 g Coomassie G250 per liter) lasted 1 hour followed by an overnight destaining step (10% $^{v}/_{v}$ acetic acid). Images were taken on a computer via GelDoc software and stored as TIFF files.

2.3.4 Native-PAGE

MBP-$TatB_{fr}$ monomer and dimer samples were resolved using native PAGE (5% stacking and 12% separating). The procedure was identical to section 2.3.3 except that no DTT and SDS were present in buffers and gels. Samples were mixed in a 2:1 protein-to-native-PAGE loading buffer (62.5 mM Tris-HCl pH 6.8, 50% glycerol, 0.1% bromophenol blue) and incubated for 10 minutes at room temperature prior loading. Gels were run at 100 V for 3 hours. Staining and destaining were identical to the steps in section 2.3.3. Images were taken on a computer via GelDoc software and stored as TIFF files.

2.4 Biophysical methods

2.4.1 Differential scanning fluorimetry

2.4.1.1 Background and theory

Differential scanning fluorimetry is a technique that measures fluorescence signal that arises from a fluorescent dye binding to hydrophobic patches of protein that is being gradually heat denatured (Shi et al, 2013). A point of maximum is equivalent to the temperature at which the protein is completely unfolded. After that, the dye dissociates from the substrate and the signal gradually decreases. The first derivative of the raw data yields a peak which determines the melting temperature (Boivin et al, 2013). This method is now common in protein crystallization

field due to the fact that it may be employed to better understand which particular conditions (salts concentrations, pH, buffers) keep the compound most stable (Luft et al, 2010).

This technique is typically performed on a real-time PCR instrument and is generally praised for using small amounts and rather low concentrations of protein which is not the case for isothermal titration calorimetry, a technique that requires high protein concentrations which may be subject to aggregation. Combined with the fact that DSF allows considering the substrate in solution, rather than immobilized like in case of Surface Plasmon Resonance, DSF is an excellent starting point for projects with multiple conditions (Niesen et al, 2007).

2.4.1.2 DSF Protocol

The experiments were performed using Rotor-Gene Quantitative Real Time – PCR (Q RT-PCR) instrument (QIAGEN). Purified DmsD was thawed, centrifuged (10000 × rpm, 4 °C, 30 min) and molarity determined via A_{280}. The protein was diluted with Hi-Trap Buffer (25 mM Tris, 10 mM NaCl) to a final concentration of 2.5 µM. For each trial three PCR tubes received the same condition for a total number of 36 tubes and 12 conditions. Each experimental mix included 5 µl of H_6-T_7-DmsD (12.5 µM stock, 2.5 µM final concentration), 5 µL of D400 SYPRO Orange (Sigma S5692), 5 µl of MBP-TatB (5 µM stock, 1 µM final concentration) and 10 µL of buffer or 15 µL of buffer (if no MBP-TatB was added). pH was maintained at 7.0, 7.5 or 8.0 using the pH adjusted Hi-Trap Buffer. Tubes with protein(s) and buffer were incubated and the dye was added just prior the run. The following parameters were used for experiment: temperature increase starting from 25 to 90 °C with 0.2 °C increments at 5 s intervals with a Gain of 6; excitation of samples happened at 470 nm and emission was collected at 555 nm. In cases where the peptides were employed, 1.5 mM original stock was used to prepared 125 µM experimental stock which was then diluted to 25 µM final concentration.

Data reported was a mean of nine technical replicates which were produced during three biological independent experiments. Standard error was equal to 0.34 ^{o}C.

2.4.2 Circular Dichroism Spectroscopy

2.4.2.1 Background and theory

Circular dichroism utilizes the principle of asymmetry of the protein molecule. More specifically, it records the difference in absorption of right- and left-hand polarized light by certain features such as aromatic chromophores or prosthetic groups (extrinsic or near-UV) and peptide bonds (intrinsic or far-UV) (Adler et al, 1973; Greenfield, 2004). As the content of secondary structures within each protein is unique, it allows for determination of a "fingerprint" that will be exclusive for a molecule. The secondary structures are deconvoluted by one of several existing computational approaches and typically includes α-helix (two minimas at 208 and 222 nm), β-sheet (single minima at 215 nm) , turns and random coil (single minima around 195 nm) (Wei et al, 2014). Additionally, the following method is useful when studying the interactions between protein and the ligand since alteration in the environment (adjustments in pH, addition of nucleotides, peptides or metals) frequently lead to a change in the secondary structure (Attar and Khavari-Nejad, 2016; van Amerongen et al, 1987).

2.4.2.2 CD Protocol

Circular dichroism spectroscopy (CD) experiments were conducted with a Jasco (J-810) spectrometer in 0.1 cm path length cells. Purified DmsD was thawed, centrifuged (10000 × rpm, 4 °C, 30 min) and molarity determined via A_{280} measurement. The protein was diluted with Hi-trap Buffer (25 mM Tris-HCl, 10 mM NaCl, pH 8.0) to a final volume of 500 µl and a concentration of 3.5 µM. Peptide solutions (DmsAl and TatB) were prepared in water (1.5 mM)

and added to His_6-T_7- DmsD at a final concentration of 35 μM. For each sample, ten scans were collected at a rate of 50 nm/min from 260 to 190 nm with a 0.5 nm bandwidth and averaged. Jasco Spectra Analysis software was employed to normalize the files by subtracting the buffer and converting millidegrees to molar ellipticity.

In cases where influence of peptides was investigated, additional data manipulation was performed. For example, when TatB2 peptide was added to DmsD, the following computation was performed:

DmsD file+TatB2 file - (DmsD::TatB2) file.

The resulting data file represented response in the structure of DmsD towards addition of the peptide. It was then compared to mathematical summation of spectra of DmsD and TatB2 alone files. If mathematical and experimental spectra were different, it was concluded that a structural change was taking place when DmsD bound the peptide. Next, CD Multivariate SSE was employed to determine the structural content of the resulting file (percentage of α-helix, β-sheet, turn and random coil). The total structural change was calculated via summation of all four types of structural components.

2.4.3 Analytical size-exclusion chromatography

2.4.3.1 Background and theory

Existence of binding as well as the influence of effectors on the interactions were probed via size-exclusion chromatography. Analytical size-exclusion is based on classical exclusion principles where molecules are separated according to their size (Ingham et al, 1983). Two proteins or the protein and a smaller ligand are equilibrated in the same buffer, then mixed and applied onto the column. If the two substrates interact, the binding will occur and they will elute

together, earlier than their "separate" versions due to the fact that the complex will have greater molecular mass, shape, and stokes radius. As the concentration of the studied protein will be known, dissociation constant, amount of free unbound protein as well as stoichiometry can be determined (Beeckmans, 1999).

Apparent molecular weight of the protein or protein-ligand complex is determined from a calibration curve which is a result of a set of standards with known molecular weights, established Stokes radii and generally spherical in shape (Nguyen et al, 2009).

2.4.3.2 SEC Protocol

An AKTA Purifier system was used with a Superose 12 column equilibrated with 2 column volumes of Hi-Trap buffer (25 mM Tris-HCl, 10 mM NaCl, pH 8.0) at 0.7 ml/min. 1 ml sample loop was attached and cleaned with the same buffer. The Superose column was calibrated with known molecular weight standards and elution volumes (V_e) and partition coefficients (K_{ave}) were determined. Blue dextran (2000 kDa), 7.57 ml, void volume (V_o); aldolase (158 kDa) 11.05 ml K_{ave}=0.385; conalbumin (75 kDa) 11.81 ml K_{ave}=0.470; ovalbumin (43 kDa) 12.45 ml K_{ave}=0.540; carbonic anhydrase (29 kDa) 13.32 ml K_{ave}=0.637; ribonuclease A (13.7 kDa) 14.74 K_{ave}=0.794; aprotinin (6.5 kDa), 16.6 ml, total volume (V_t). DmsD monomer eluted with 13.13 ml (K_{ave}=0.616 and correlated to 33.9 kDa), DmsAl-GST eluted with 11.7 ml (K_{ave}=0.457 and correlated to 87.4 kDa), MBP-TatB eluted with 10.51 ml (K_{ave}=0.326 and correlated to 191.9 kDa), and GTP-TatB eluted to 7.6 ml ($K_{ave}=V_o$ and correlated to unknown molecular mass due to multimerization/aggregation). The formula weight of DmsD monomer is 27.5 kDa, DmsAl-GTP monomer- 30 kDa, MBP-$TatB_{fr.}$ monomer– 56 kDa, and GTP-$TatB_{fr.}$ monomer- 46 kDa. Purified proteins were diluted with Hi-Trap buffer, mixed in a 1:1 ratio and incubated together and/or with effector for 1 hour at 4 ^{o}C. If the mixture contained two proteins and an effector; for

example: H_6-T_7-DmsD, DmsAl-GST and GTP, two subsequent incubations were performed: incubation of two proteins was followed by an incubation with the effector. Next, the 500 µl sample was injected into the column. Protein-containing peaks were collected and SDS-PAGE was performed.

2.5 Data processing and analysis.

2.5.1 Graph Pad Prism 5

Graph Pad Prism 5 software was employed to analyze the data from DSF and CD experiments. One site specific binding with Hill slope was chosen as the best approach to evaluate the data from the "Nonlinear regression (curve fit)" options list. The parameters were computed using the following equation:

$$Y=B_{max}*X^h/(K_d{}^h + X^h)$$

Where B_{max} is the maximum binding possible for the ligand with units identical to the ordinate and h is the Hill slope. The stoichometry for DmsD::MBP-TatB complex was calculated manually; the concentration of ligand that the Bmax related to was employed to find the ratio between the ligand and DmsD which was at a set concentration.

Example:

At pH 7.0 B_{max} is equal to 7.14. It relates to the MBP-$TatB_{cyto}$ at a concentration of 1.3 µM. As the concentration of His_6-T_7-DmsD was consistently kept at 2.5 µM, a ratio between the two molecules can be calculated as $2.5/1.3=y\approx2$. Therefore, the stoichiometry is equal to 1:2 molecules of MBP-$TatB_{cyto}$ to His6-T7-DmsD.

2.5.2 ImageJ software

ImageJ, a Java-based image processing program was utilized for quantification of the protein via density assessment of the bands as well as percentages of loaded protein present in each lane. First, we would set up a rectangular box around each band of interest. Next, we would generate a lane profile plot for each box and outline the peak which would be a representative of the intensity of our protein band. Finally, we would quantify the intensity. Once all the intensities for a particular protein were collected, we would take the sum of those and perceive as 100%. We would take a ratio of each lane`s intensity over the total intensity for specific protein. We could also potentially convert percentage within the lane and relate it to the amount of protein employed for the experiment. For example, in case of MBP-$TatB_{fr}$ which was incubated with H_6T_7-DmsD we determined that 54 μg of MBP-$TatB_{fr}$ was present in lane 13. The following steps were followed:

1. We determined that 5.2% of total amount of MBP-$TatB_{fr}$ was present in fraction 13.
2. We multiplied the loaded volume (500 μl) by the concentration of MBP-$TatB_{fr}$ (2.08 μg/ μl) and obtained 1040 μg.
3. We multiplied total amount of protein loaded (1040 μg) by 0.052. This yielded a number equal to 54 μg.

2.6 Protein-peptide docking

Modeling of DmsD::TatB2 complex was performed using CABS-dock web server (http://biocomp.chem.uw.edu.pl/CABSdock). The following computational method employs coarse-grained representation of the proteins and peptides with each amino acid represented with up to 4 atoms (Blaszczyk et al, 2018). Energy state of the conformations is assessed via Replica

Exchange protocol and 1000 models are selected from the possible 10000 (Blaszczyk et al, 2016). Additional clustering and scoring leads to generation of 10 interactions with highest probabilities (Blaszczyk et al, 2018). For our analysis we chose model #1 due to the fact that it had the highest rating between the suggested 10 options. Crystal structure of *E. coli* DmsD (PDB: 3efp) and sequence of TatB2 peptide was used for analysis.

Additional figures were generated with PyMOL, a molecular visualization system. Information from previous publications and CABS-dock modeling was collected and the binding site(s) would be highlighted on the surface of *E. coli* DmsD using the existing crystal structure (PDB: 3efp).

Chapter 3: Protein purification and optimization

Overall, five recombinant proteins were purified in the context of this thesis work: H_6T_7-DmsD (27 kDa), DmsAl-GST (30 kDa), MBP-$TatB_{fr}$ (56 kDa), GST-$TatB_{fr}$ (42 kDa) and MalE (maltose-binding protein with leader sequence removed) (40 kDa). Existing protocols were utilized for the first two, but the remaining had to be purified according to newly-created procedures.

For clarity throughout the thesis I will use the term MalE for discussion of the control involving experiments with MBP-tag. Nevertheless, sequences of MBP from TatB and MalE were identical.

3.1 H_6T_7-DmsD Purification

DmsD was expressed as an N-terminal fusion which included a hexa-histidine sequence for affinity interaction with a Ni-bound resin, followed by the peptide sequence of a T7 epitope facilitating antibody related experiments. The purification here was established previously (Winstone et al, 2006). To date these affinity tags have not affected the functional binding activity of this protein (Tran, 2011). H_6T_7-DmsD purifies primarily as a monomer with some dimer (Winstone et al, 2006). The protein migrates on gels on occasion as a doublet accounting for cystine oxidation (Figure 3.1). Additionally, folding forms that migrate at higher molecular may also be seen which are a function of pH (Sarfo et al, 2004).

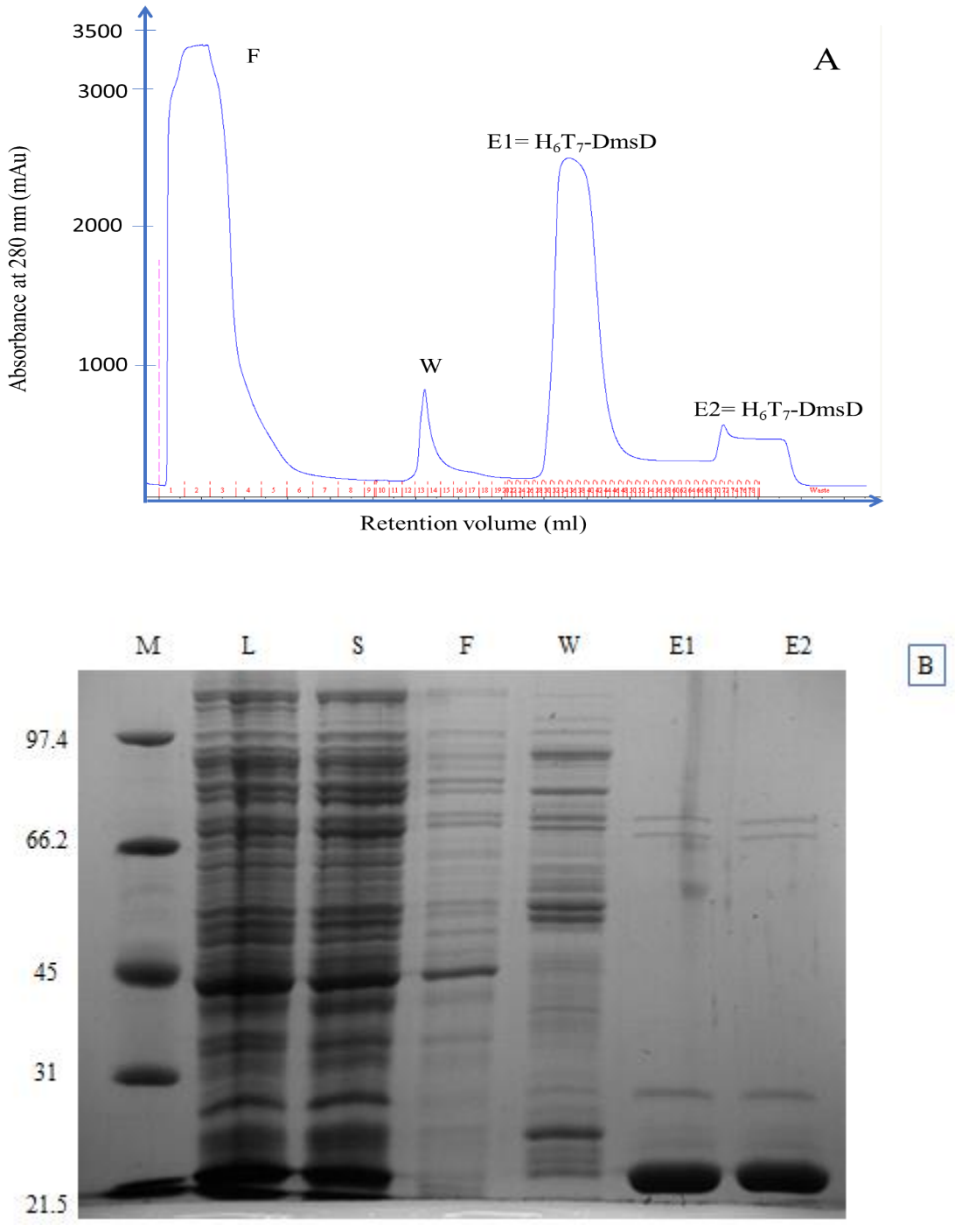

Figure 3.1. Affinity Purification of H_6-T_7-DmsD.
Cytosolic cell free extract sample was applied to a 5 ml nickel affinity column, and elution monitored at 280 nm (mAU). **A**. Elution Profile, Histidine tag binding to column allowing all other proteins to flowthrough (F), 15% (elution) buffer B (at final imidazole concentration of 37.5 mM) applied to elute non-specific interacting proteins (W), 50% (elution) buffer B (at a final concentration of 125 mM) applied to elute DmsD monomer (M) and 100% (elution) buffer B (at a final concentration of 250 mM imidazole) applied to elute any dimer present (D). **B**. Coomassie blue stained 12% SDS-PAGE of eluted fractions including molecular weight markers (M), low-spin pellet (L), cell lysate (S), flowthrough (F), wash (W), DmsD monomer elute (E1) and DmsD dimer elute (E2). All fractions except the molecular weight marker, flowthrough and wash were loaded at 1 mg/ml. The latter were mixed with loading dye in a 1:1 ratio for a final volume of 30 µl.

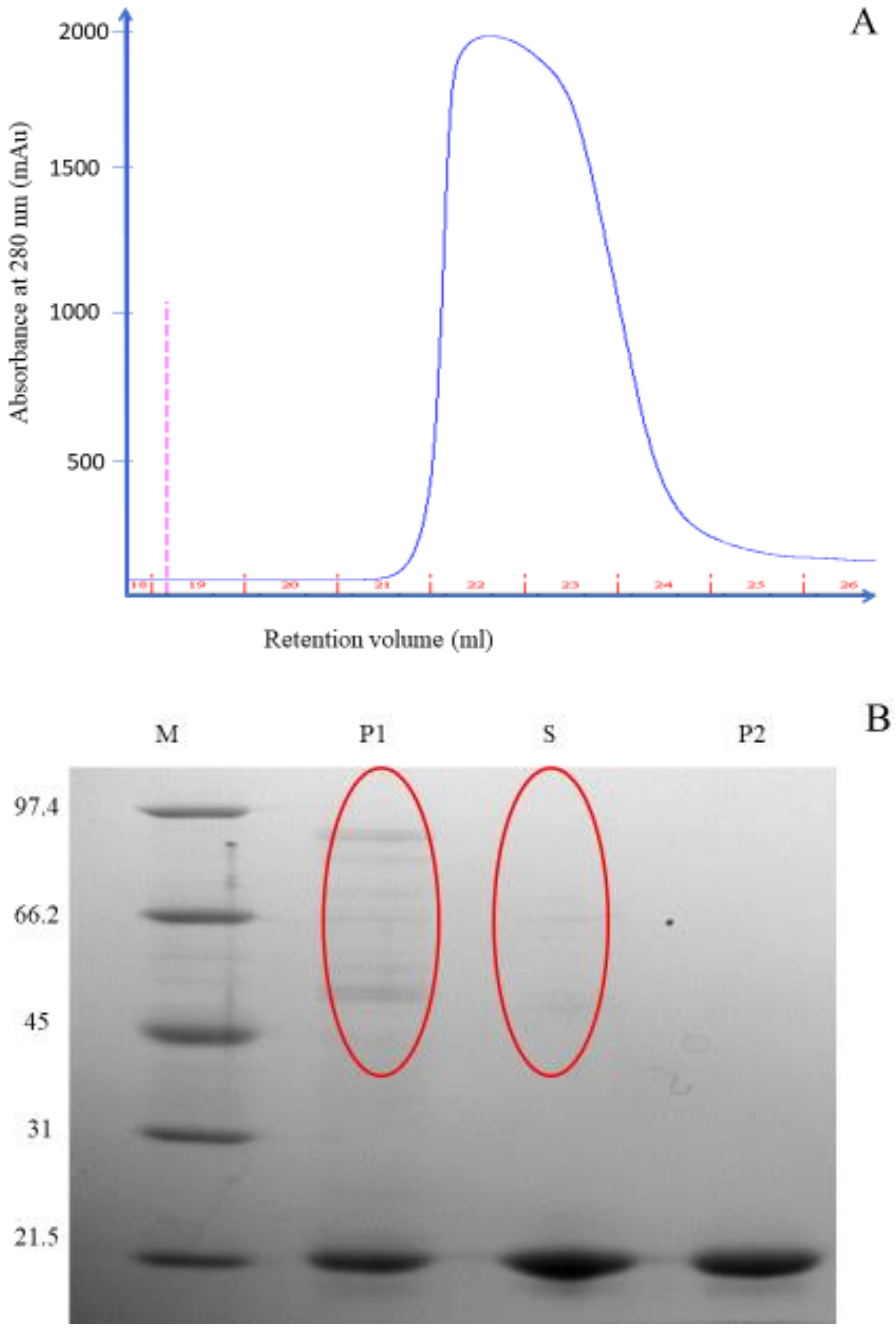

Figure 3.2. Removal of excess salts/imidazole from H_6-T_7-DmsD Protein.
Concentrated DmsD monomer was applied to a desalting 10 ml HiTrap column, and elution monitored at 280 nm (mAU). **A**. Elution Profile, HiTrap desalting buffer applied to elute the DmsD monomer free of excess salts and imidazole. **B**. Coomassie blue stained 12% SDS-PAGE with molecular weight markers (M), purified DmsD at 1 µg/µl (P1(previously frozen and thawed preparation) and P2 (fresh preparation)), and DmsD stocks obtained from a previous member of the laboratory (Stephana Cherak) (S). DmsD folding form "D" is highlighted with red circles. All fractions except the molecular weight marker were mixed with loading dye in a 1:1 ratio for a final volume of 30 µl.

Purified DmsD (lanes with P1 and P2 in Figure 3.2 B) was compared to existing laboratory stocks (lane S in Figure 3.2 B) to ensure quality and reproducibility of experiments. Chromatographic runs and samples not showing good purity were discarded. As seen in lanes P1 and S of Figure 3.2 B, some DmsD purifications had a greater quantity of heterogeneously folded protein (so-called from D). The latter was observed previously along with forms A and B (dimer and monomer of DmsD). However, it was detected primarily at low pH (5.0) (Sarfo et al, 2004). During my project I observed content of these form(s) to increase after prolonged storage at -20 and -80 ^{o}C (see Figure 3.2 with P1 which is frozen and thawed preparation of monomer DmsD). Binding experiments used P2 in Figure 3.2.

3.2 DmsAl-GST Purification

The RR-Leader sequence of DmsA consists of 43 residues and was expressed with a Glutathione S-transferase tag at the C-terminal and purified using initially GSH agarose beads and later GST-affinity column as described previously (Oresnik et al, 2001). The purification had a modification step introduced by Dr. Winstone who noticed that DnaK, a chaperone, was co-purifying with the construct: an ATP-containing buffer was utilized as a wash step between a flow through and the elution with reduced glutathione (Winstone, 2013). An identical construct with a GST-tag at the N-terminal did not demonstrate any binding to the DmsD and, thus, was not used for any experiments (Winstone et al, 2006).

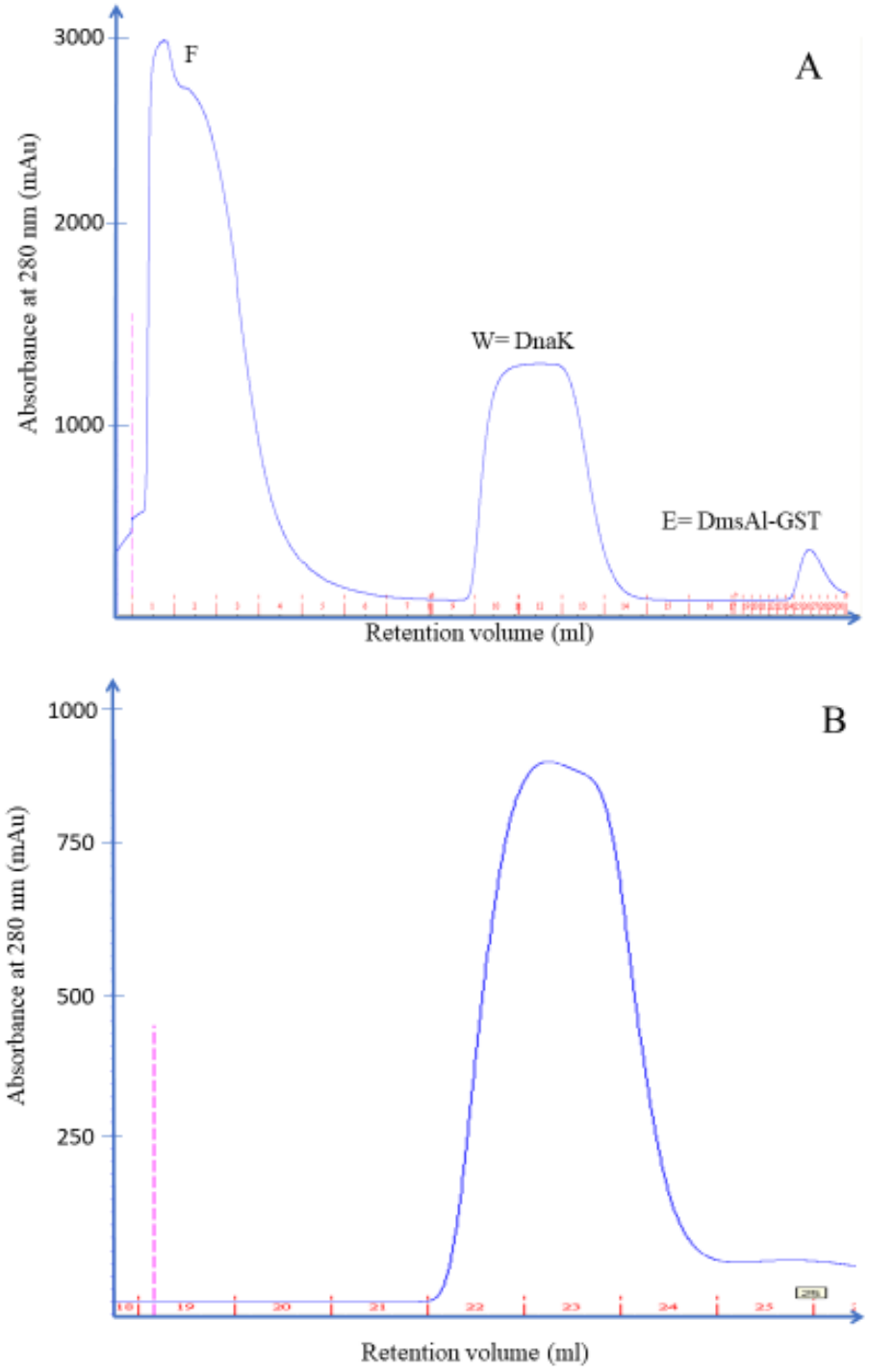
A
3000
2000
1000
Absorbance at 280 nm (mAu)
F
W= DnaK
E= DmsAl-GST
Retention volume (ml)
B
1000
750
500
250
Absorbance at 280 nm (mAu)
Retention volume (ml)

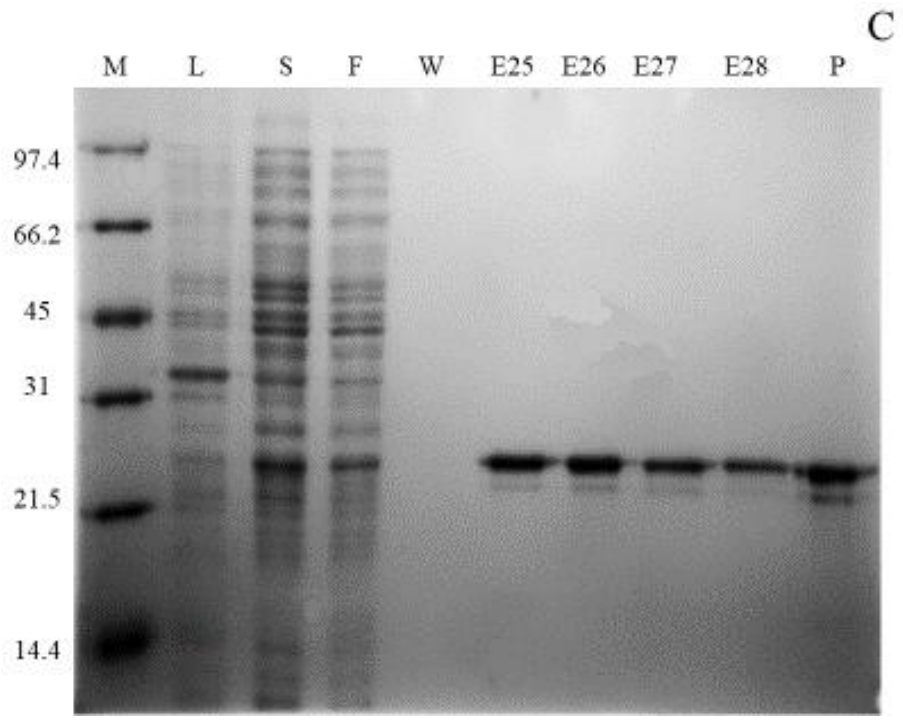

Figure 3.3. Purification of DmsAl-GST.
Cytosolic protein sample was applied to a Glutathione Affinity column, and elution monitored at 280 nm (mAU). **A**. Elution Profile, GST binding to column allowing all other proteins to flowthrough, buffer containing ATP applied to elute DnaK and Glutathione applied to elute GST protein. **B**. Elution Profile, HiTrap desalting buffer applied to elute the DmsAl-GST from HiTrap column free of excess salts and gluthathione. **C.** Coomassie blue stained 12% SDS-PAGE of eluted fractions including molecular weight markers (M), low-spin pellet (L), cell lysate (S); flowthrough (FT); wash (W); fractions 25, 26, 27 and 28 which represent GST elute with highest DmsAl-GST concentration (E) and final concentrated and desalted protein (P). All fractions except the molecular weight marker, wash and immediate elutions were loaded at 1 μg/μl. The latter were mixed with loading dye in a 1:1 ratio for a final volume of 30 μl.

Purified DmsAl-GST was compared to existing laboratory stocks to ensure quality and reproducibility of experiments. Unsuccessful purification samples as well as purifications still containing DnaK contaminations were discarded. The quantity of chaperone DnaK varied highly between preparations and frequently was hardly detected (see Figure 3.3 C). It was noted that the addition of ATP used to elute DnaK produces a fairly large peak, which is a false-positive protein signal on chromatogram as GTP also adsorbs at 280 nm (see Figure 3.3 A). This was

confirmed by SEC experiments where GTP was added and an extra peak was observed, but the SDS-PAGE did not demonstrate any protein present (see section 7.2).

The lower band of the doublet that is observed for the purified DmsAl-GST. It was detected previously by the former members of the laboratory and suggested to be a version of the protein with cleaved signal peptide, i.e. just GST (Winstone, 2013).

3.3 Purification of MBP-TatB$_{fr}$

TatB protein lacking first 26 amino acids comprising a transmembrane helix was expressed with an N-terminal Maltose-Binding protein tag allowing affinity purification with amylose column. As a result, I was dealing with a cytosolic and soluble version of TAT complex component starting from amino acid 27. The protein consisted of three helices and one disordered C-terminal region. The following construct had not been purified before. For information on protein preparation see section 2.1.3.

Initial, attempts to purify MBP-TatB$_{fr}$ used a 3-step process using amylose (maltose polymer associated with agarose), MonoQ (anion exchange column) and HiTrap (buffer exchange) columns (Figure 3.4). I calculated the isoelectric point of MBP-TatB$_{fr}$ using ExPASy Bioinformatics Resource Portal (https://web.expasy.org/compute_pi/) by inputting the sequence of my protein. It was determined to be equal to 5.17. Upon loading the protein sample onto the MonoQ column and increasing buffer concentration via gradient (20 mM Tris-HCl + 1.0 M NaCl, pH 8.0), I would consistently get multiple protein populations. Next, I combined the fractions that I suspected would contain MBP-TatB$_{fr}$ and concentrated them. As the HiTrap did not allow for an adequate separation of a potential dimer/monomer mixture, the initial differential scanning fluorimetry experiments did not yield consistent results.

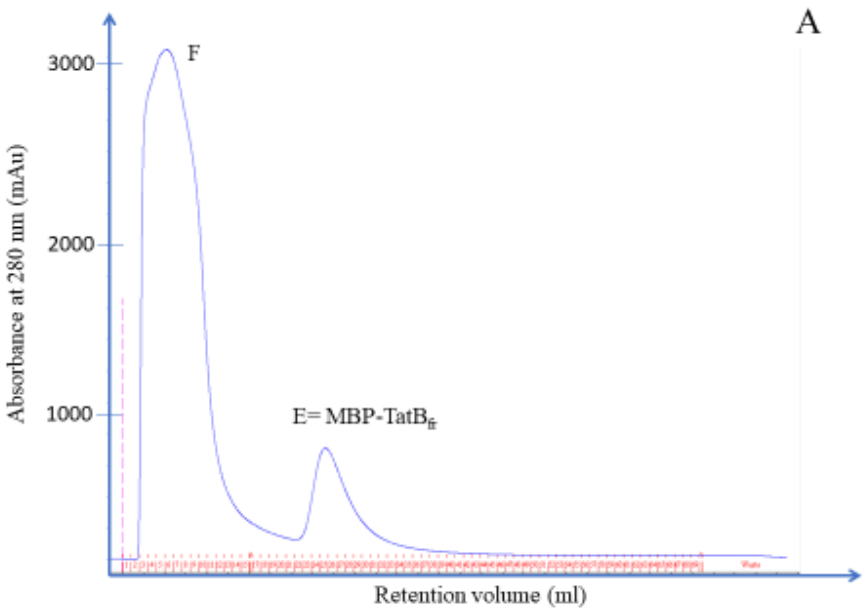
A
3000
2000
1000
F
E= MBP-TatB$_{fr}$
Absorbance at 280 nm (mAu)
Retention volume (ml)

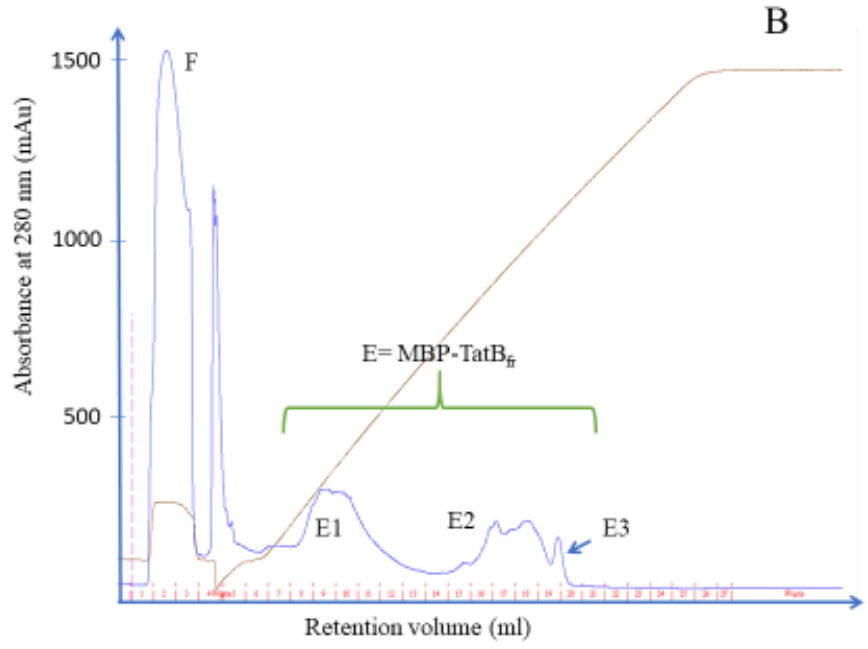
B
1500
1000
500
F
E= MBP-TatB$_{fr}$
E1
E2
E3
Absorbance at 280 nm (mAu)
Retention volume (ml)

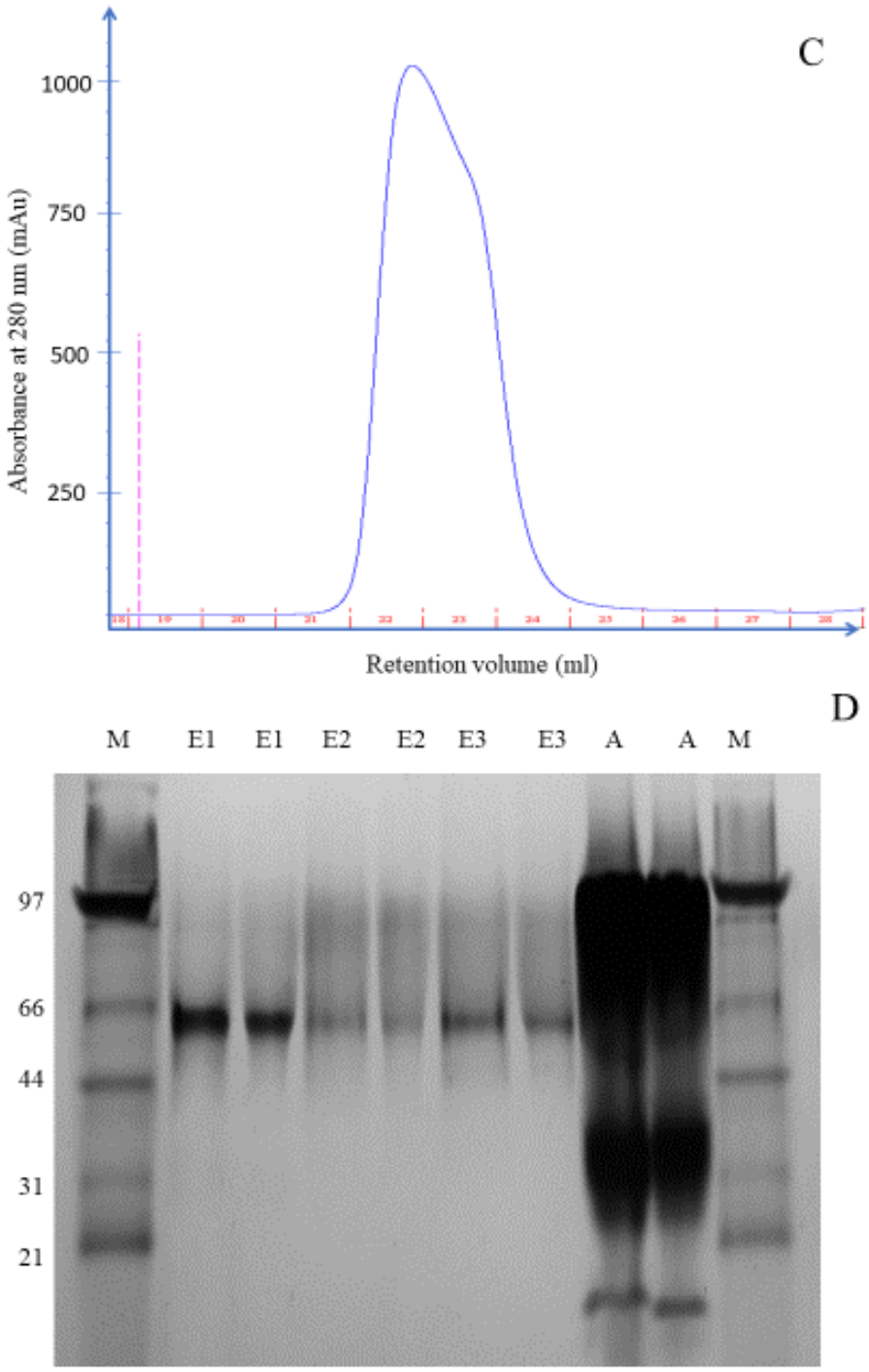

Figure 3.4. Purification elution profiles of MBP-TatB$_{fr}$ using amylose and MonoQ columns. Cytosolic protein sample was applied to a 5ml amylose column, and elution monitored at 280 nm (mAU). **A**. Elution Profile, MBP tag binding to amylose column allowing all other proteins to flow through (F) and elution buffer applied to elute MBP-TatB$_{fr}$ (E). **B.** Elution Profile, binding of negative charges of MBP-TatB$_{fr}$ to MonoQ column allowing all other protein to flow through (F) and elution buffer applied to elute MBP-TatB$_{fr}$ (E). **C.** Elution Profile, HiTrap desalting buffer applied to elute the MBP-TatB$_{fr}$ from Hi-Trap column free of excess

salts and maltose. **D**. Coomassie blue stained 12% SDS-PAGE of eluted fractions including amylose column elution (A); pooled MonoQ eluted fractions (E1, E2 and E3) overloaded in order to see contaminants, molecular weight markers (M) and desalted and purified MBP-$TatB_{fr}$ (P). All fractions except the molecular weight marker were loaded at 1 μg/μl.

As protein of lower molecular weight was still present, two possibilities existed: either another protein was co-purifying with MBP-$TatB_{fr}$ or degradation took place. Therefore, size-exclusion chromatography was explored for further purification.

Performing SEC on a Superpose 12 column allowed for the separation of MBP-$TatB_{fr}$ sample into 3 molecular weight species (Figure 3.5 B). The first two peaks were suggested to correspond to the dimer of MBP-$TatB_{fr}$ (E1) and monomer MBP-$TatB_{fr}$ (E2). The third peak was unknown protein (E3). Importantly, SEC calibration curve equation (see chapters 2 and 7) provided us with a much greater molecular weight than anticipated for a monomer MBP-$TatB_{fr}$: 191.9 kDa versus theoretical 56 kDa. To determine a true state of the "monomer" molecule, we attempted a native-PAGE (Figure 3.6). Interestingly, in the absence of SDS and DTT MBP-$TatB_{fr}$ remained at the position between 66 kDa and 44 kDa. Therefore, we deduced that the second peak was truly a monomer, but probably had rather an elongated shape which resulted in a unique migration pattern.

To determine the identity of unknown protein we sent the sample for proteomics analysis by trypsin treatment LC MS/MS analysis at the SAMS center. The result was returned to us as Ef-Tu, a 43 kDa protein, with function defined as a protein synthesis elongation factor involved in translation, but also believed to have additional functions such as important for cell shape (Fu et al, 2012; Soufo et al, 2010).

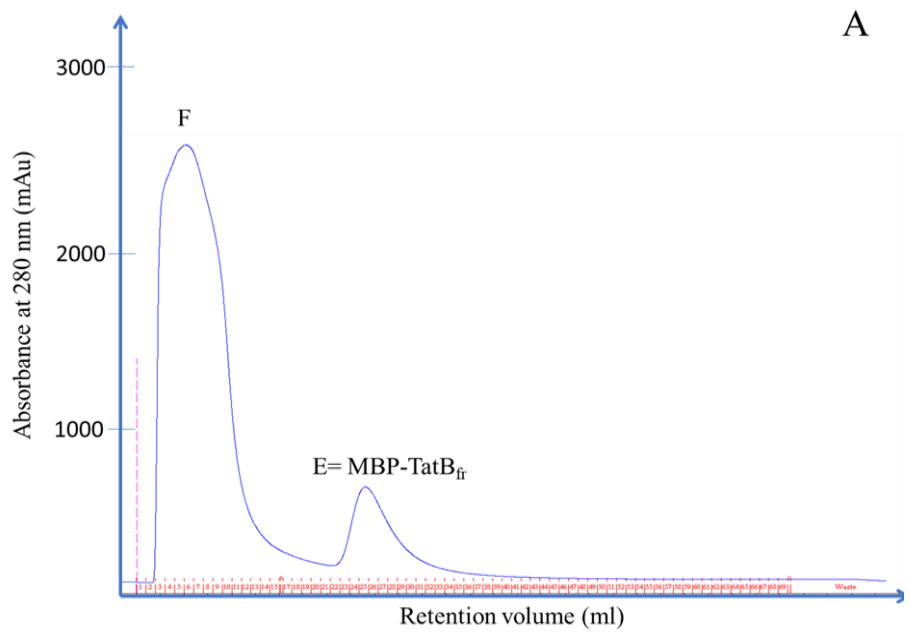
A
3000
2000
1000
Absorbance at 280 nm (mAu)
F
E= MBP-TatB$_{fr}$
Retention volume (ml)

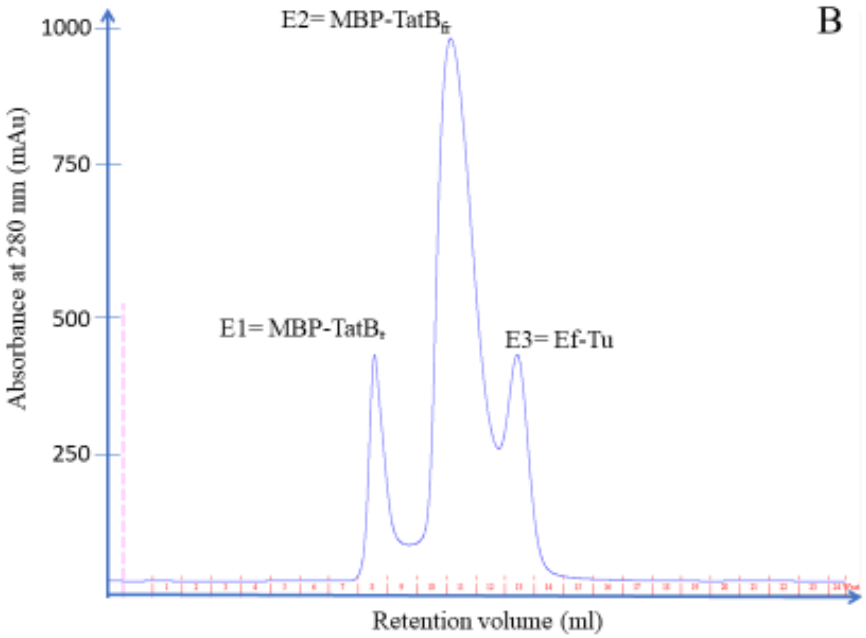
B
1000
750
500
250
Absorbance at 280 nm (mAu)
E2= MBP-TatB$_{fr}$
E1= MBP-TatB$_{r}$
E3= Ef-Tu
Retention volume (ml)

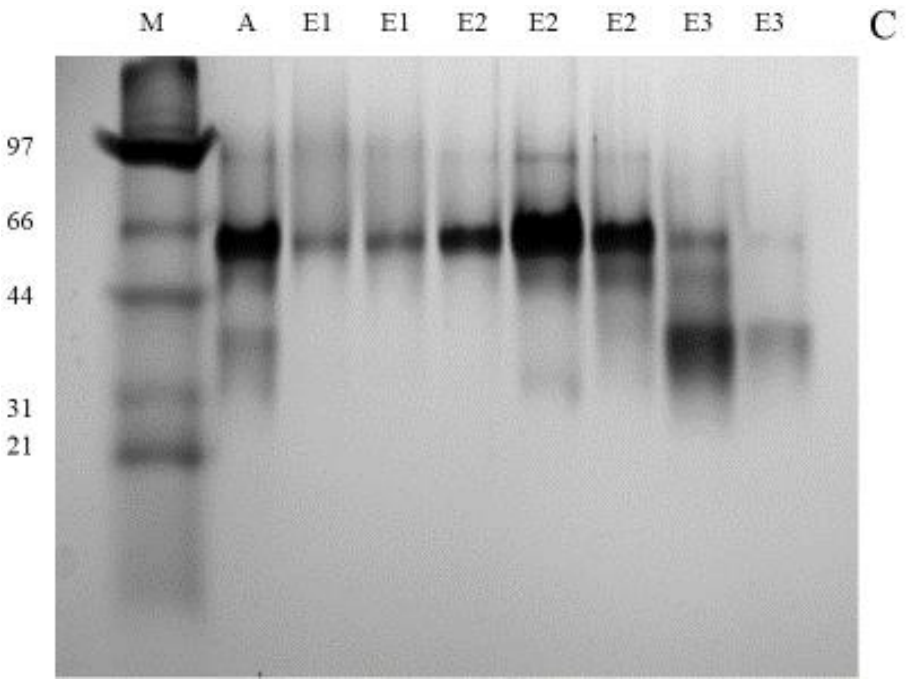

Figure 3.5. Purification of MBP-TatB$_{fr}$ using SEC column.
Cytosolic protein sample was applied to a 5ml amylose column, and elution monitored at 280 nm (mAU). **A**. Elution Profile, MBP tag binding to amylose column allowing all other proteins to flow through (F) and elution buffer applied to elute MBP-TatB$_{fr}$ (E). **B**. Elution Profile, HiTrap desalting buffer applied to elute the dimer MBP-TatB$_{fr}$ (E1), monomer MBP-TatB$_{fr}$ (E2) and unknown protein (E3) from Superose 12 column. All three proteins were now free of excess salts and maltose. **C.** Coomassie blue stained 12% SDS-PAGE of eluted fractions including molecular weight markers (M), amylose column elution (A); three eluted at 5 and 10 μg load (E1, E2 and E3). All fractions except the molecular weight marker were loaded at 1 μg/μl.

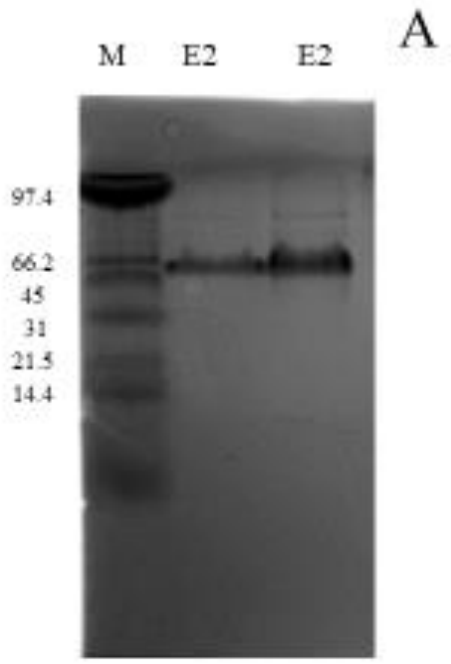

Figure 3.6. Native-PAGE of second peak of MBP-TatB$_{fr}$ demonstrates that it is indeed a monomer. (A) Coomassie blue stained 12% native-PAGE of pooled and concentrated eluted fraction 12/13 (5 µl and 10 µl loaded) and molecular weight markers (M). Sample was mixed with loading dye in a 2:1 ratio for a final volume of 30 µl.

Importantly, this protein had already been recorded as part of DmsD`s interactome. Li and others in the Turner laboratory reported the potential of this protein-protein interaction from *in vitro* (cross-linking and co-precipitation) as well as *in vivo* (BiFC) techniques (Li et al, 2010). It was proposed that the interaction takes place as part of the chaperone cascade during synthesis of DmsA (Li et al, 2010; Cherak and Turner, 2017).

As the three peaks from SEC column were all located in close proximity to each other, I further optimized the purification by introducing an additional step during the amylose column purification: addition of ATP-containing buffer as a wash step between flow through and elution stages led to removal of a significant portion of Ef-Tu (Figure 3.7). The decision regarding the buffer was made based on the notion that Ef-Tu interacts with GTP and ATP molecules (Soufo et al, 2010; Cruz et. al, 2014) and may regulate its protein-protein interactions.

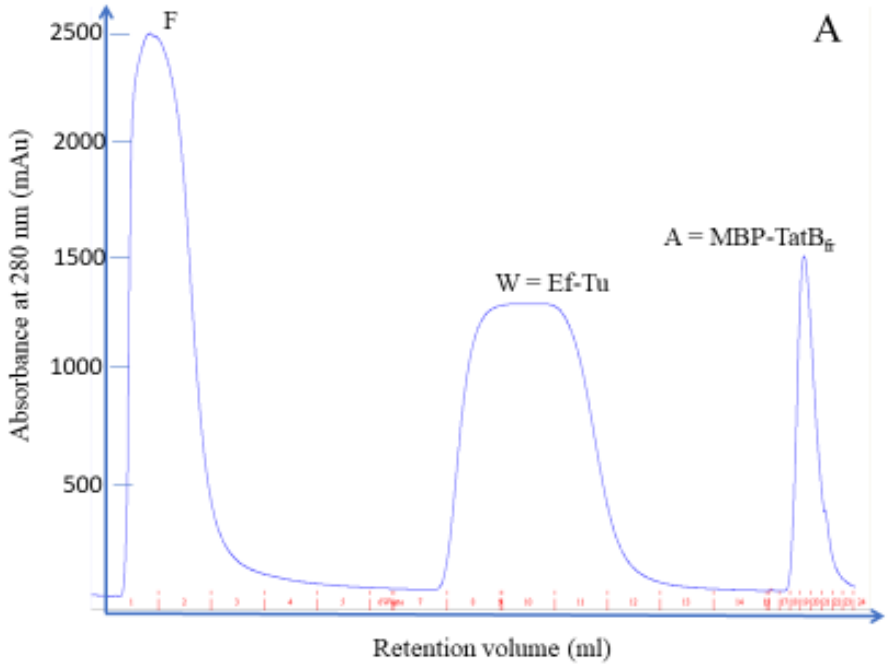
A
F
W = Ef-Tu
A = MBP-TatB$_{fr}$
2500
2000
1500
1000
500
Absorbance at 280 nm (mAu)
Retention volume (ml)

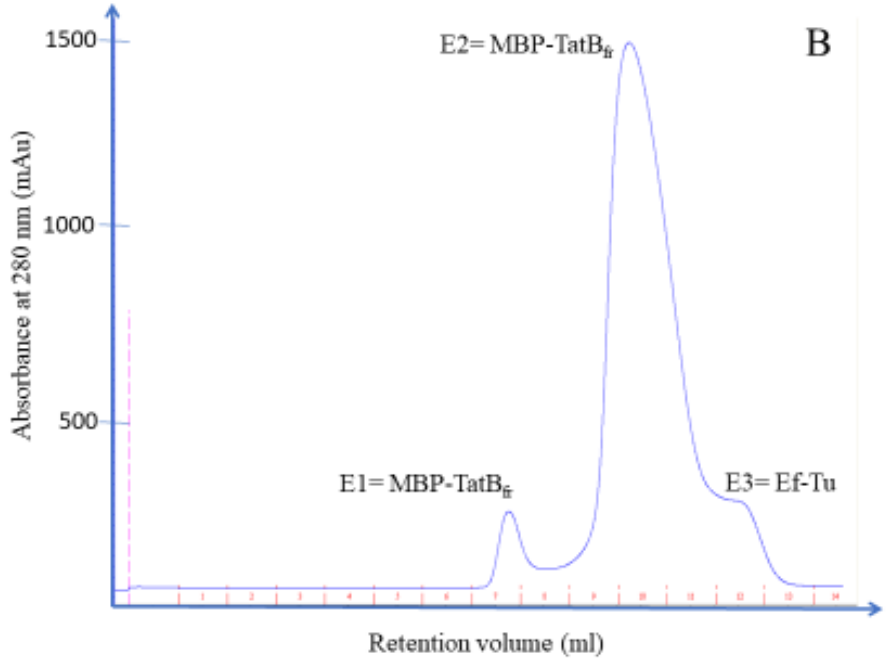
B
E2= MBP-TatB$_{fr}$
E1= MBP-TatB$_{fr}$
E3= Ef-Tu
1500
1000
500
Absorbance at 280 nm (mAu)
Retention volume (ml)

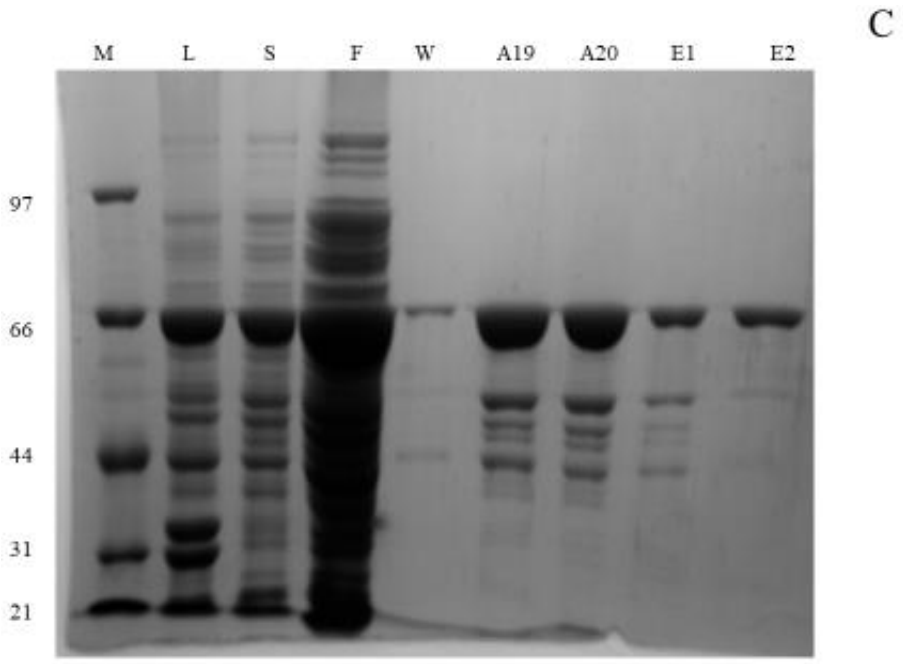

Figure 3.7. Final version of MBP-TatB$_{fr.}$ purification.
Cytosolic protein sample was applied to a 5ml amylose column, and elution monitored at 280 nm (mAU). **A**. Elution Profile, MBP tag binding to amylose column allowing all other proteins to flowthrough (F), buffer containing ATP applied to elute Ef-Tu (W) and elution buffer applied to elute MBP-TatB$_{fr}$ (E). **B.** Elution Profile, HiTrap desalting buffer applied to elute the dimer MBP-TatB$_{fr}$ (E1), monomer MBP-TatB$_{fr}$ (E2) and Ef-Tu (E3) from Superose 12 column. All three proteins were now free of excess salts and maltose. **C.** Coomassie blue stained 12% SDS-PAGE of eluted fractions including molecular weight markers (M), low-spin pellet (L), cell lysate (S), flowthrough (F), wash containing EfTu (W), amylose column elutions 19 and 20 (A19 and A20); MBP-TatB$_{fr}$ dimer (E1)after SEC column and MBP-TatB$_{fr}$ monomer (E2)after SEC column. All fractions except the low-spin pellet (5 µg load), cell lysate (5 µg load) and molecular weight marker were mixed with loading dye in a 1:1 ratio for a final volume of 30 µl.

3.4 Purification of MalE

Obtaining pure MalE was important as it was required as a control for some of the interaction studies. During the purification of this maltose-binding protein version (signal sequence removed so accumulates in cytoplasm), same challenges were faced similar to MBP-TatB$_{fr}$ (see section 3.3). Ion exchange chromatography was tried noting the isoelectric point was determined

to be equal to 5.22. The purification elution profiles and outcome is shown in Figure 3.8 and the SDS-PAGE shows a poorly purified sample (P).

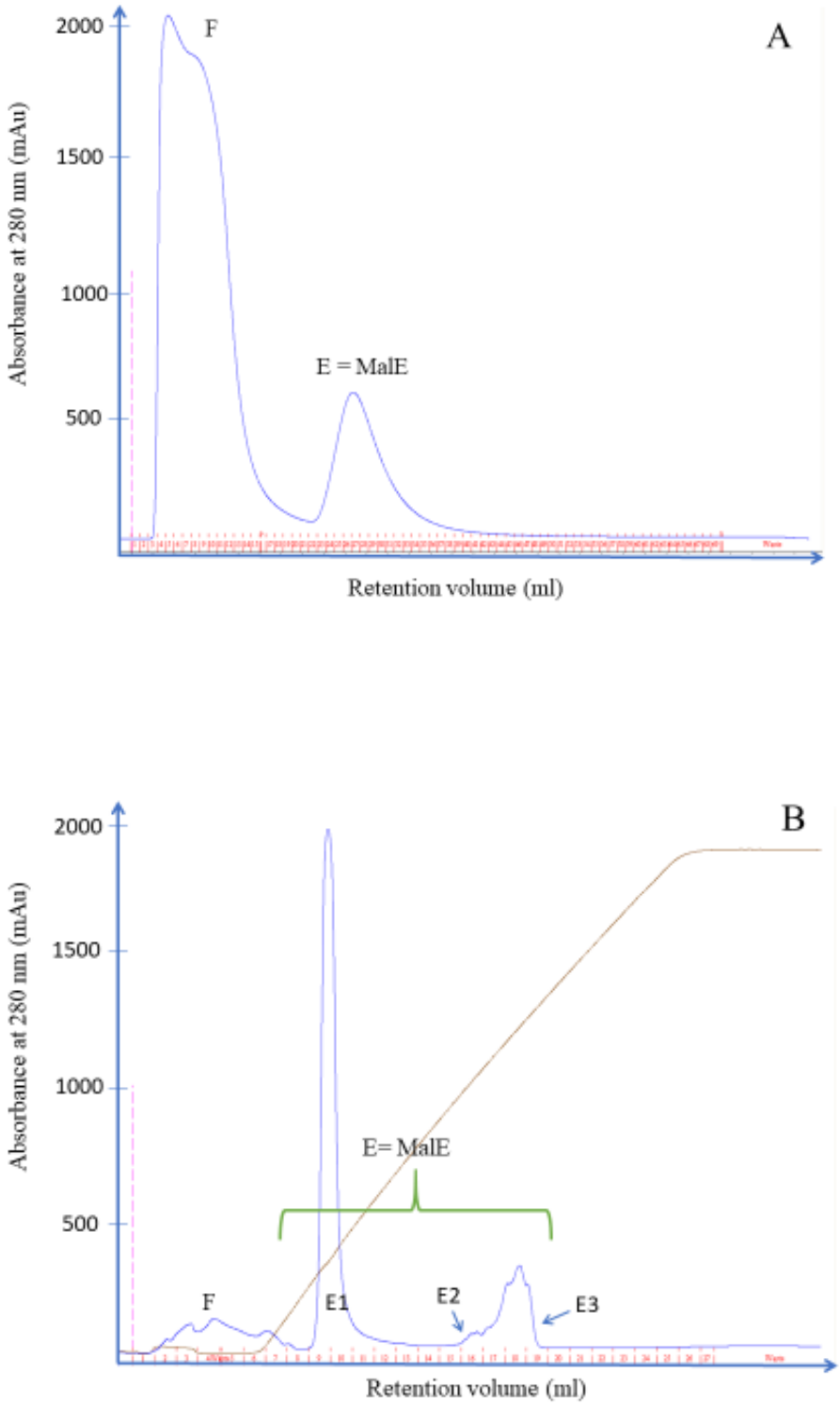

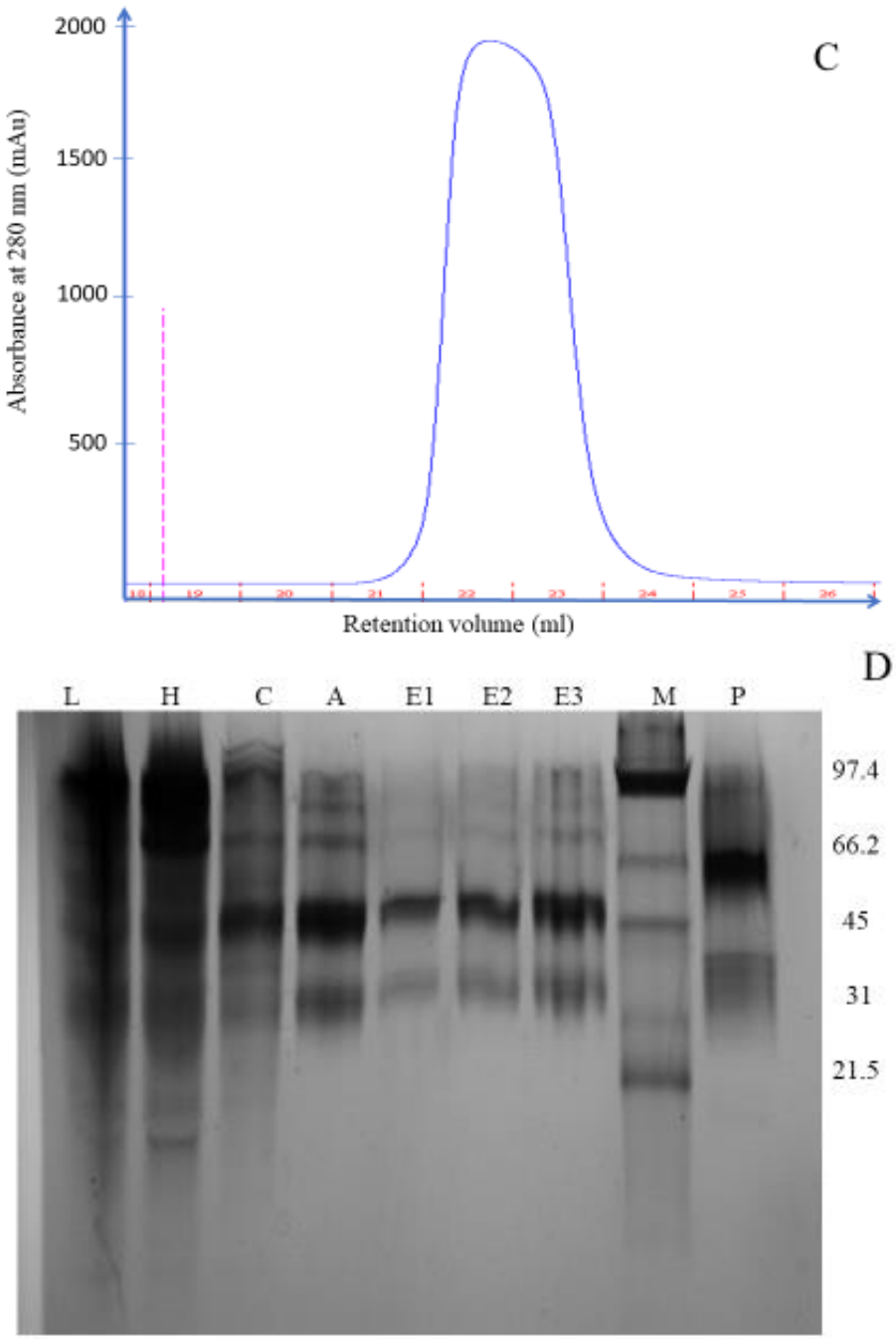

Figure 3.8. Purification of MalE protein.
Cytosolic cell free extract sample was applied to a 5 ml amylose column, and elution monitored at 280 nm (mAU). **A**. Maltose affinity elution profile using amylose column, flow through (F) and elution buffer applied to elute MalE (E). **B.** Anion exchange elution profile using MonoQ column, flow through (F) and elution buffer with gradient applied to elute MalE (E). **C**. HiTrap desalting elution profile to elute MalE free of excess salts using HiTrap desalting column. **D**. Coomassie blue stained 12% SDS-PAGE of eluted fractions including low-spin pellet (L), cell lysate (C); amylose column elution (A); pooled MonoQ eluted fractions (E1, E2

and E3), molecular weight markers (M) and desalted and purified MalE (P). All fractions except the molecular weight marker were loaded at 1 μg/μl.

The optimization of purification of MalE was considered to follow the same approach as MBP-$TatB_{fr}$ (see section 3.3). Therefore, the final purification consisted of two steps of affinity followed by SEC. Chromatography elution profiles are shown in Figure 3.9. Importantly, Ef-Tu did not co-purify with cytosolic MalE and, thus, additional step with ATP-containing buffer was not required. This also provided additional level of confidence that the MBP-$TatB_{fr}$ -Ef-Tu interaction is via the TatB component.

It is important to note that another protein of higher molecular weight that also bound to the amylose affinity column and eluted together with MBP-$TatB_{fr}$ was separated during the second (size-exclusion) step. This protein migrated at approximately 50 kDa and thus could not be Ef-Tu. This unknown molecule was discarded and not employed for the experiments. Second elution from the SEC column was, thus, concentrated and employed for the control experiments.

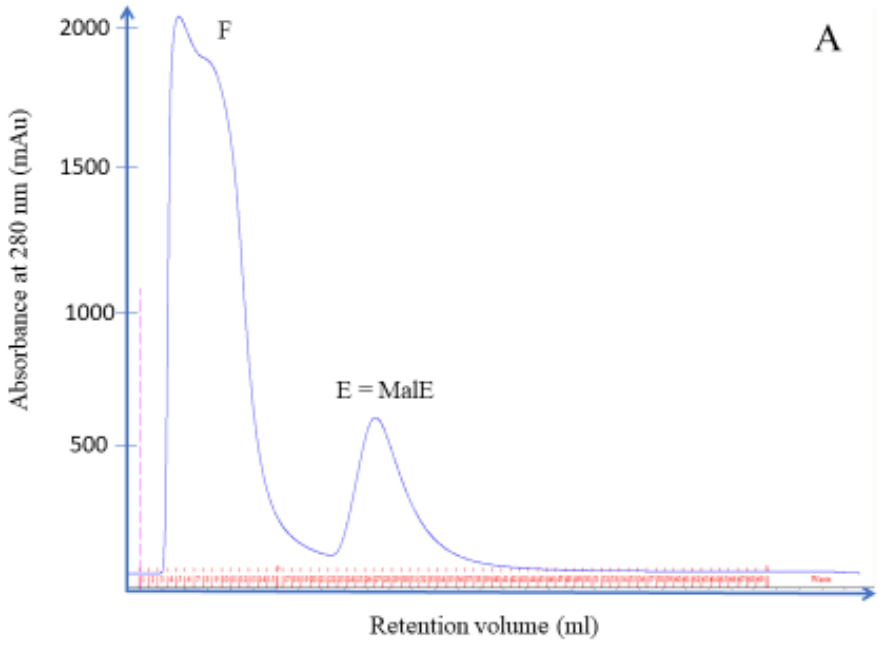
A
2000
1500
1000
500
F
E = MalE
Absorbance at 280 nm (mAu)
Retention volume (ml)

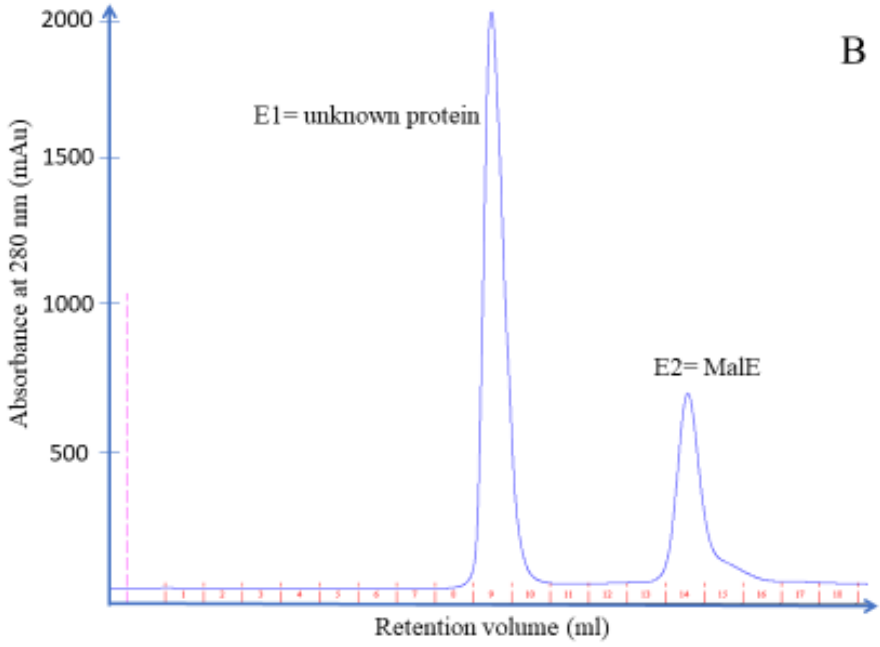
B
2000
1500
1000
500
E1= unknown protein
E2= MalE
Absorbance at 280 nm (mAu)
Retention volume (ml)

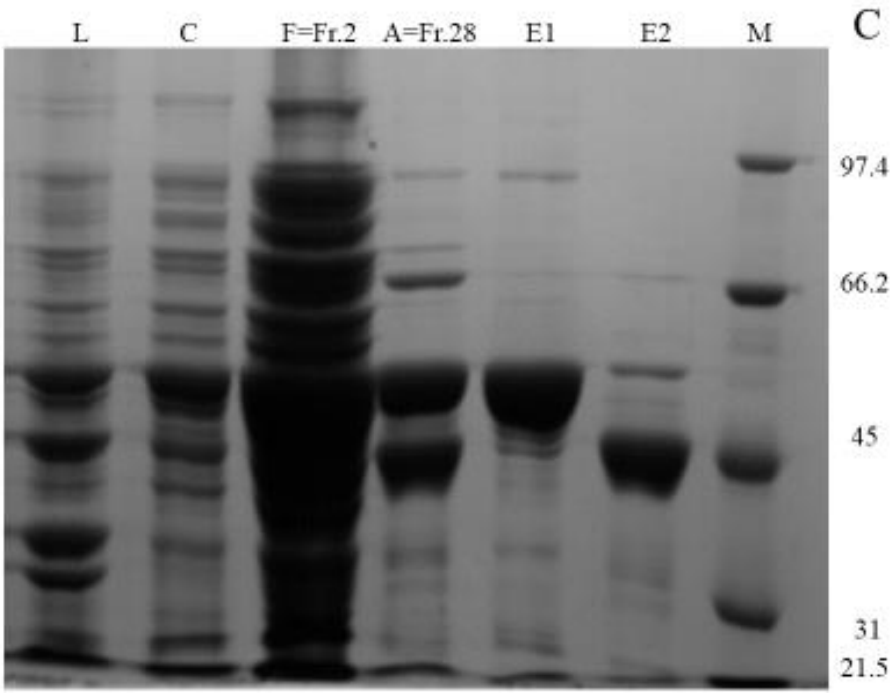

Figure 3.9. Final version of MalE purification.
Cytosolic cell free extract sample was applied to a 5 ml amylose column, and elution monitored at 280 nm (mAU). **A.** Elution Profile of amylose affinity column allowing all other proteins to flow through (F=Fr. 2) and elution buffer applied to elute MalE (A). **B.** Elution Profile, HiTrap desalting buffer applied to elute the dimer MalE (E1) and monomer MalE (E2) from Superose 12 column. Both proteins were now free of excess salts and maltose. **C.** Coomassie blue stained 12% SDS-PAGE of molecular weight markers (M), low-spin pellet (L), cell lysate (S), flowthrough (F=Fr. 2), amylose column elution (A=Fr. 28), unknown protein and MalE (E1 and E2). All fractions except the low-spin pellet (5 µg load), cell lysate (5 µg load) and molecular weight marker were mixed with loading dye in a 1:1 ratio for a final volume of 30 µl.

3.5 GST-TatB$_{fr}$ purification

As an alternative purification host for interaction experiments, we considered GST. After some inconsistent initial trials, I hypothesized that perhaps again another molecule was being co-purifying with my protein of interest and their affinity towards each other was higher than the affinity of GST tag towards the GSTrap column. As two previous purifications involved ATP-dependent molecules (DnaK and Ef-Tu) (see sections 3.2 and 3.3), I included an ATP-containing

buffer as a wash step. This resulted in obtaining a well resolved elution peak containing GST-$TatB_{fr}$ which I concentrated and subjected to size-exclusion chromatography (Figure 3.10). SEC granted me with two well resolved peaks with the first one containing a multimer of GST-$TatB_{fr}$ (elution at 7.5 ml) and the second elution peak contained two unknown proteins of low molecular weight (elution at 12.09 ml). This second peak elution time is quite close to that of Ef-Tu (elution at 12.49 ml). It is possible in this preparation that Ef-Tu was bound to $TatB_{fr}$ as in the MBP fusion construct, but Ef-Tu became hydrolyzed into two fragments which remained interacting until the SDS-PAGE. This is possible as the two bands in fraction E2 of panel D Figure 3.10, ~21 kDa and ~23 kDa roughly add up to the size of Ef-Tu (43k Da). Alternatively, based on the SEC standard calibration curve we could have had three small proteins with a molecular weight of 21-23 kDa each. That would result in the final molecular weight of 67 kDa which was the predicted molecular weight of the complex eluted at 12.09 ml. That option would be consistent with the lane E2 (SDS-PAGE gel in Figure 3.10 C), where the amount of protein in the lower band seems to be twice compared to the amount in the upper band. As time did not allow and was not the focus here these bands were not identified by proteomics methods at the time of this thesis.

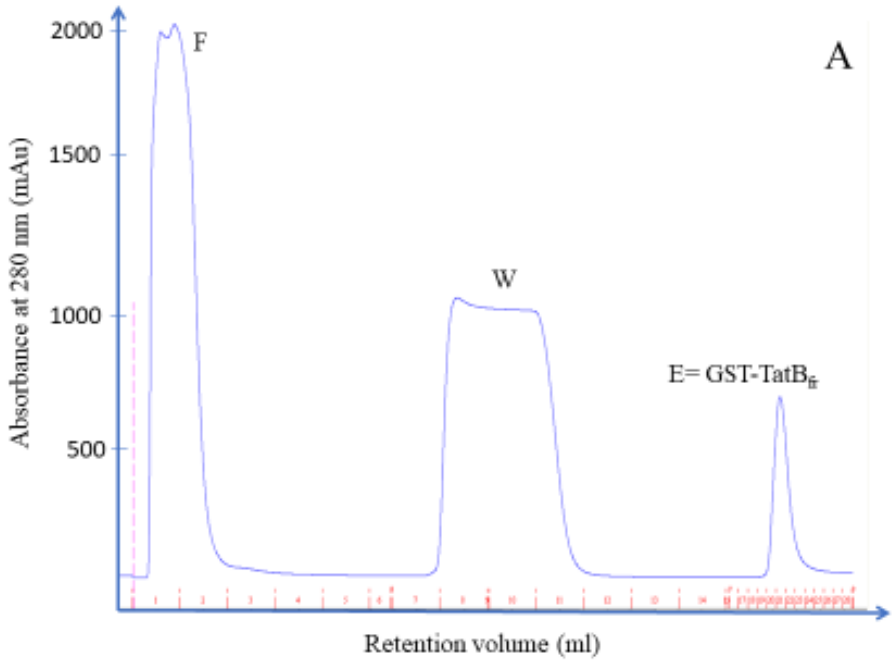
A
2000
1500
1000
500
Absorbance at 280 nm (mAu)
F
W
E= GST-TatB$_{fr}$
Retention volume (ml)

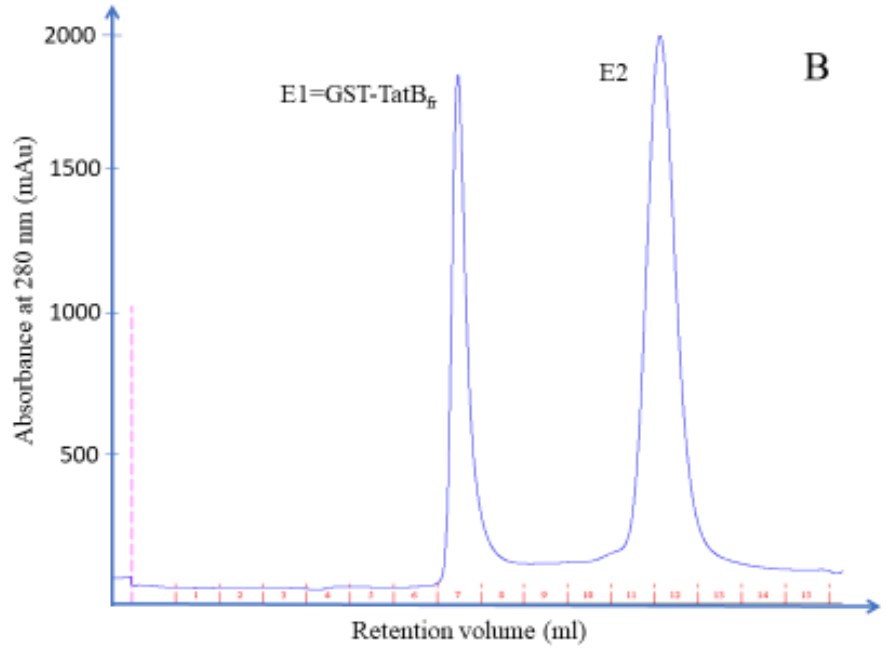
B
2000
1500
1000
500
Absorbance at 280 nm (mAu)
E1=GST-TatB$_{fr}$
E2
Retention volume (ml)

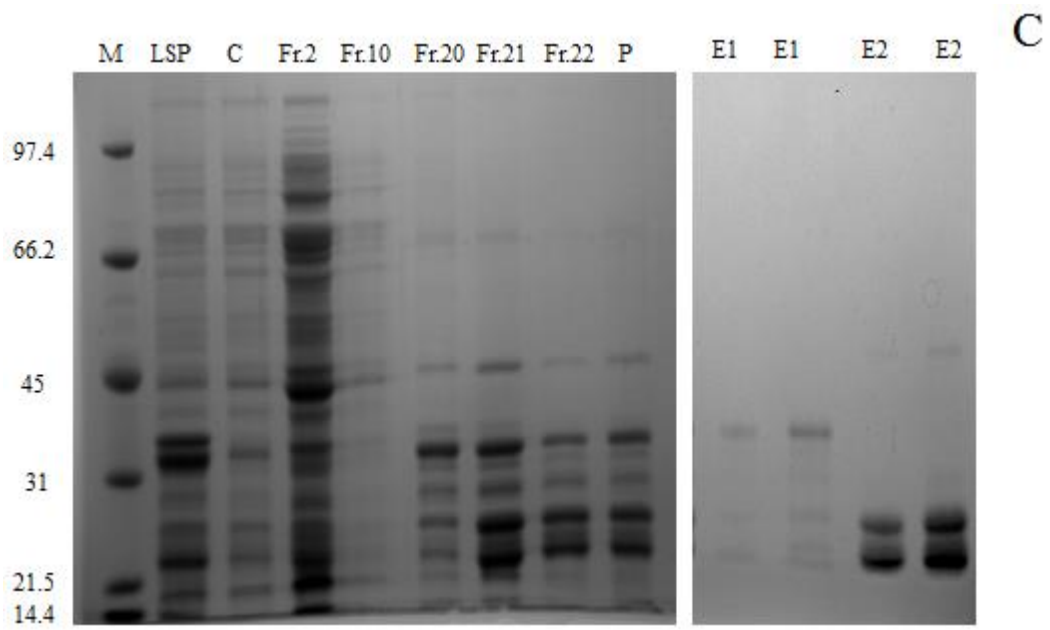

Figure 3.10. Purification of GST-TatB$_{fr}$.
Cytosolic cell free sample was applied to a Glutathione Affinity column, and elution monitored at 280 nm (mAU). **A**. Elution Profile from GST binding to column allowing all other proteins to flow through (F), buffer containing ATP applied to elute unknown protein (fraction W) and glutathione applied to elute GST protein. **B**. Elution Profile from Superose 12 SEC to elute GST-TatB$_{fr}$ (E1) and unknown proteins (E2). All proteins were now free of excess salts and glutathione. **C.** Coomassie blue stained 12% SDS-PAGE of eluted fractions including molecular weight markers (M), cell lysate (C); flowthrough (F); wash (W); GST elute (Frs. 20, 21 and 22), pooled and concentrated elute (prior loading onto the SEC column) (P). **C.** Coomassie blue stained 12% SDS-PAGE of eluted fractions from SEC: GST-TatB$_{fr}$ (E1) and unknown proteins (E2).

Table 3.1. Summary of protein purification.

Protein	**Molecular weight**	**Final yield**	**Purity**	**Comments**
H_6T_7-DmsD	27 kDa	10 mg/L	98%	A single 6 L purification gave enough product to employ for SEC (complete experiment), DSF (complete experiment).CD experiments required more conditions. Therefore, two separate purifications were used for a complete experiment
DmsAl-GST	30 kDa	3 mg/L	95%	Two 6 L purifications were required for a complete SEC experiment.
MBP-$TatB_{fr}$	56 kDa	8 mg/L	90%	A single 6 L purification gave enough product to employ for SEC and DSF (complete experiment).
GST-$TatB_{fr}$	42 kDa	2.5 mg/L	90%	A single 6 L purification gave enough product to employ for SEC due to a low number of trials performed.
MalE	40 kDa	7 mg/L	85%	The protein was only utilized for the DSF experiments due to absence of binding between MBP-$TatB_{fr}$ and H_6T_7-DmsD /DmsAl-GST

Discussion

Here we purified proteins H_6T_7-DmsD and DmsAl-GST using existing protocols and established novel purification protocol for MBP-$TatB_{fr}$, MalE and GST-$TatB_{fr.}$ In addition, we learned that $TatB_{fr}$ tends to co-purify with other proteins. This was true for both affinity tags that we employed. Interestingly, another group that purified full-length GST-TatB from *S. lividans* did not report presence of Ef-Tu or any other proteins that would be bound to TatA or TatB. The buffer they employed was very similar to ours and only differed by 0.5% Triton X-100 and

absence of 1 mM DTT (De Keersmaeker et al, 2005*).* The difference may be explained by expression and purification conditions or the fact that the proteins came from a different bacterial system, or they simply did not notice.

Another important aspect is the multimerization state that the MBP-TatB purifies as. From the SDS-PAGE of MBP-$TatB_{fr}$ purification, we learned that two different types of molecules/ complexes eluted. We initially suggested that we were dealing with a dimer (~112 kDa) and a monomer (~56 kDa). However using the calibration curve equation (Chapter 7), we determined that the apparent molecular weight of our suspected monomer was much higher (191.9 kDa). This would be more consistent with a trimer of MBP-$TatB_{fr}$. De Keersmaeker *et al.* reported that their purified membrane TatAB complexes were generally 200 to 400 kDa in size and thus, different multimer numbers, consistent with our results. Furthermore, their cytosolic version of TatB component also existed in monomer and homo-oligomeric forms (2005). Nevertheless, native-PAGE which we performed on the suspected "monomer" of MBP-$TatB_{fr}$ in the absence of DTT supported our initial idea of a monomer present. As could be seen in Figure 3.6, non-reducing conditions and absence of heating did not alter the migration pattern of the protein collected from the second peak of the Superose 12. Therefore, we propose here that MBP-$TatB_{fr}$ has an elongated shape leading to larger hydrodynamic size, which leads to a much earlier than expected elution.

Finally, it is not surprising that Ef-Tu was identified as part of the system. The list of TAT system associated chaperone molecules is rather long and includes DnaK and trigger factor (TF) which are believed to interact with TAT substrates once they start to appear from the ribosome. DnaJ that was demonstrated to bind DmsD, GroEL which was hypothesized to provide a cavity for further folding of the substrate and enzymes MoeA and MoeB (Chan et al, 2014; Li et al,

2010; Chan et al, 2015; Solomon et al, 1999). Ef-Tu was previously shown to assist in refolding rhodanese with a higher efficiency in the presence of GTP as well as increase the yields of refolded citrate synthase and α-glucosidase (Kudlicki et al, 1997; Caldas et al, 1998). However, interaction of Ef-Tu with TatB was unexpected in the absence of TAT substrate. It may be suggested that Ef-Tu has a bigger role in transport of the folded substrates than anticipated. Alternatively, this chaperone could have co-purified with TatB due to the fact that it was a cytoplasmic segment of a full-sized protein that has a disordered C-terminal and required assistance in folding. Therefore, follow-up experiments could include identification of protein(s) that had co-purified with GST-$TatB_{fr}$ as well as interaction experiments between Ef-Tu and components of TAT system.

Chapter 4: Protein-protein interactions evaluated by differential scanning fluorimetry.

We made a decision to employ differential scanning fluorimetry due to a number of advantages: small amount of protein required, instrument-controlled conditions, and a wide selection of states and/or effectors to be sampled (DeSantis et al, 2012). Additionally, DSF was previously used in our lab to show that the addition of the DmsA leader peptide shifted the melting point of DmsD and increased its stability (Cherak and Turner, 2016). Therefore, an existing protocol was employed and optimized further for a combination of two protein constructs undergoing melting together.

4.1 Cytosolic fragment of TatB protein stabilizes DmsD.

Our goal here was to employ the same technique in order to study the interaction of DmsD with cytosolic soluble domain of TatB which lacks the transmembrane segment. We constructed a $TatB_{fr}$ protein fusion with a maltose binding protein (MBP) which acts as a peptide carrier and purification handle.

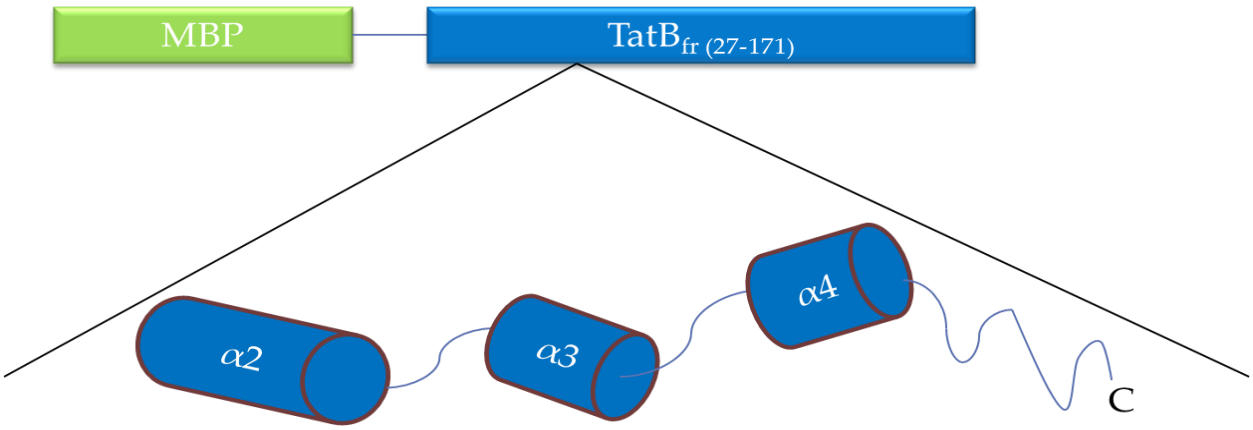

Figure 4.1. Depiction of cytosolic TatB construct with an N-terminal MBP tag utilized for differential scanning fluorimetry. The C-terminal domain after helix 4 is considered intrinsically disordered.

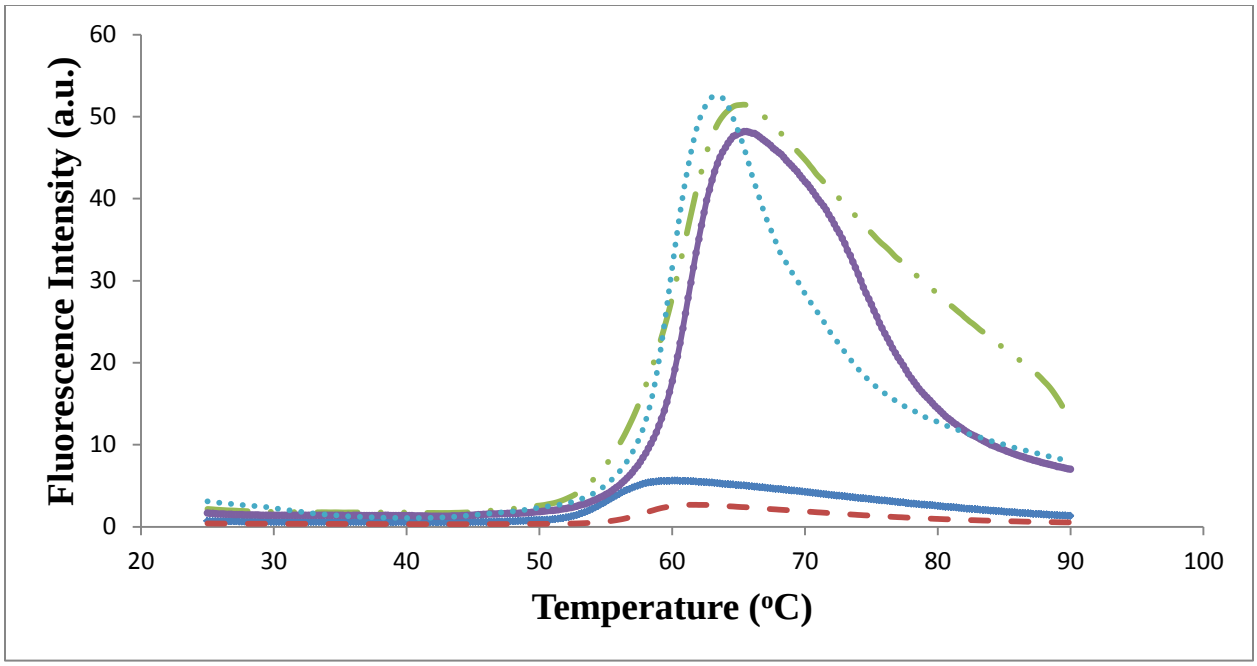

Figure 4.2. Thermal unfolding curves of wild-type H_6T_7-DmsD and MBP-$TatB_{fr}$ alone and in complex with each other. DmsD alone is depicted in dotted light blue, MBP-$TatB_{fr}$ alone - in solid dark-blue, MalE - in dashed red. Combination of DmsD and MBP-$TatB_{fr}$ is shown in dashed-double dot green line; combination of DmsD and MalE – in solid purple line. Final concentration of H_6T_7-DmsD was 2.5 µM and of MalE/MBP-$TatB_{fr}$- 1µM. Differential scanning fluorimetry monitored the change in Sypro orange fluorescence intensity at 555 nm emission (excitation at 470 nm). Experiment was performed at pH 7.0.

As can be seen from Figure 4.2, addition MBP-$TatB_{fr}$ led to a change in melting profile of DmsD. Additionally, the addition of MalE on its own as a control also led to a shift to higher temperatures. More specifically, the shift suggests a move towards a greater level of stability as well a change in cooperativity as seen by the peak broadening. However, the two profiles were not the same and, thus, it was concluded that while the presence of maltose-binding protein appears to interact with or influence DmsD, the $TatB_{fr}$ segment of the recombinant construct contributes additionally to the interaction.

In order to determine what is the effect of the $TatB_{fr}$ fragment to DmsD, experimental curves of combined proteins were normalized by subtracting "DmsD+MalE" data files from

"DmsD+MBP-TatB$_{fr}$" to generate "DmsD+TatB$_{fr}$" curve. The curves at three different pH values are shown in Figure 4.3. While curves at pH 7.0 and 7.5 look quite similar and almost overlap, the curve at pH 8.0 is dramatically different past 70^{o}C. This supports previous findings regarding a different conformational folding of DmsD exists at different pHs observed previously (Sarfo et al, 2004).

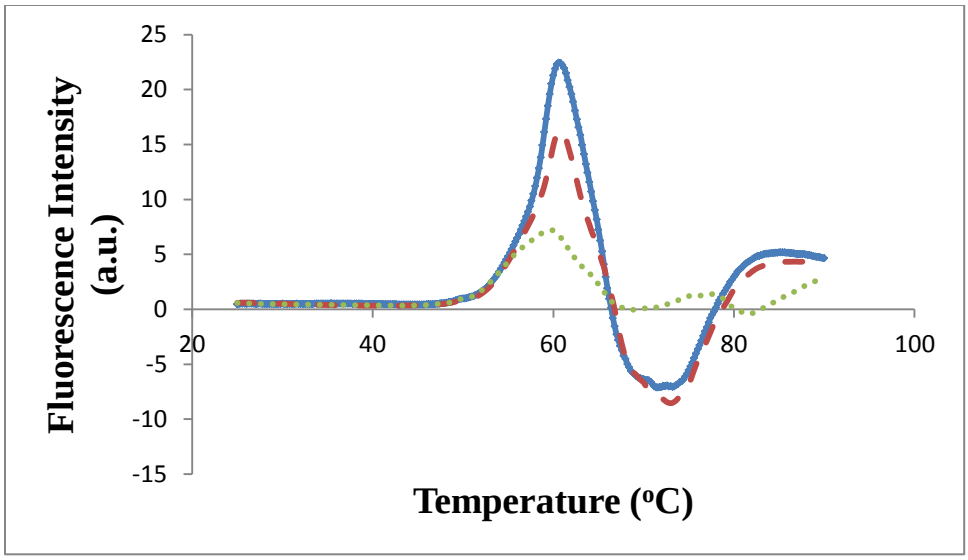

Figure 4.3. Normalized thermal unfolding curves of H_6T_7-DmsD under the influence of TatB$_{fr}$ at pH 7.0, 7.5 and 8.0. Ligand was added at a 1:2.5 molar ratio. Data at pH 7.0 is shown in solid blue, pH 7.5- dashed red and pH 8.0- dotted green.

We utilized this TatB$_{fr}$ fragment influence on the melting curve for the determination of an apparent dissociation constant by titrating MBP-TatB$_{fr}$ into H_6T_7-DmsD at pH 7.0 (Figure 4.4), 7.5 and 8.0 (data not shown). Figure 4.4 demonstrates that increasing concentrations of MBP-TatB$_{fr}$ led to a shift of DmsD curve towards a higher melting temperature and the stabilization was observed at just 0.1µM MBP-TatB$_{fr}$ ligand added. Half-widths of the melting curve were plotted as functions of concentration of the ligand (Figure 4.4 insert) and K_d values were found for pH 7.0, 7.5 and 8.0: 0.08+/-0.027 (µM), 0.11+/-0.037 (µM) and 0.15+/-0.06 (µM), respectively. Stoichiometry was calculated from B_{max} values and equal to 1 molecule of MBP-

$TatB_{fr}$ and 2 molecules of H_6T_7-DmsD for pH 7.0 and 7.5 and 1 molecule of MBP-$TatB_{fr}$ and 3 molecules of H_6T_7-DmsD for pH 8.0 (See Table 4.1).

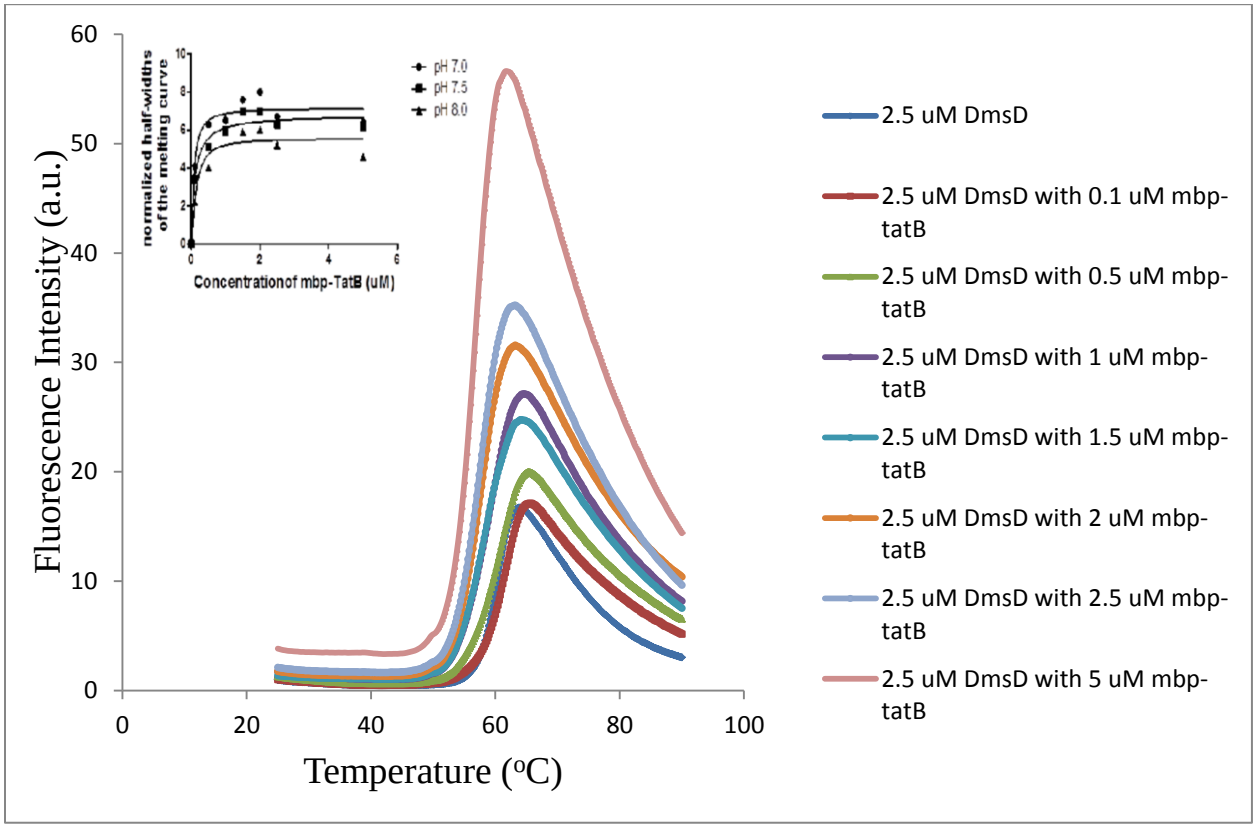

Figure 4.4. Effect of MBP-$TatB_{fr}$ on DmsD. Increasing concentrations of MBP-$TatB_{fr}$ led to a shift of the DmsD curve towards a higher melting temperature. The experiment was performed in triplicated at pH 7.0, 7.5 and 8.0 with addition of 0.1, 0.5, 2 and 5 µM MBP-$TatB_{fr}$. The insert shows normalized half-width of the melting curve as a function of MBP-$TatB_{fr}$ concentration. Differential scanning fluorimetry monitored decrease in Sypro orange fluorescence intensity at 470 nm excitation and 555 nm emission following MBP-$TatB_{fr}$ binding and stabilization. Best-fit values are presented in Table 4.1.

Table 4.1. Best-fit values for the titration of MBP-TatB$_{fr}$ (DSF) or TatB peptide (CD) into H$_6$-T$_7$-DmsD at pH 7.0, 7,5 and 8.0. The dissociation constant was obtained using GraphPad Prism 5 via the one site/specific binding with Hill slope nonlinear fit. Circular dichroism data from chapter 5 was also included here.

pH	DSF (Differential scanning fluorimetry)		CD (circular dichroism) (see chapter 5).	
7.0	B_{max}	7.14+/-0.53	B_{max}	31838+/-634.5
	h	1.27+/-0.93	h	1.20+/-0.09
	K_d	0.08+/-0.027 (µM)	K_d	4.7+/-0.20(µM)
	R^2	0.95	R^2	0.99
7.5	B_{max}	6.8+/-0.65	NA	
	h	0.96+/-0.46		
	K_d	0.11+/-0.037 (µM)		
	R^2	0.97		
8.0	B_{max}	5.6+/-0.55	B_{max}	26246+/-409.6
	h	1.4+/-0.82	h	1.78+/-0.16
	K_d	0.15+/-0.06 (µM)	K_d	5.4+/-0.26 (µM)
	R^2	0.92	R^2	0.99

4.2 Peptides derived from TatB affect melting cooperativity of DmsD

Next, we chose to explore short synthetic peptides that represented potential areas of TatB to bind to the DmsD based on previous experiments (Kuzniatsova et al, 2016). Utilizing these studies from a Sandwich ELISA peptide array assay we chose to work with three peptides that we name TatB1 (residues 37-47), TatB2 (71-80) and TatB3 (113-122).

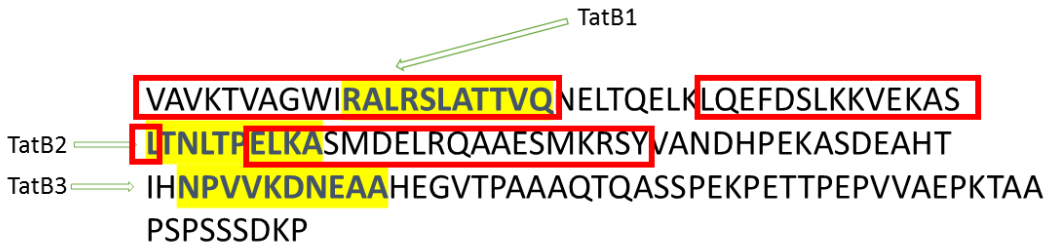

Figure 4.5. Cytoplasmic domain of TatB protein employed for the study (amino acids 27-171). Residues highlighted in yellow represent three synthesized peptides. Residues shown in red boxes indicate predicted helical regions of the protein. Any non-highlighted amino acids belong to disordered regions.

Utilizing these peptides allows analyzing effects without the influence of the MBP carrier. We performed experiments again using differential scanning fluorimetry at three different pH values and three different peptide concentrations (5 µM, 12.5 µM and 25 µM). We found that only at pH 7.0 did all three peptides show a change in melting profile; neither pH 7.5, not pH 8.0 demonstrated any change (Figure 4.6). Only TatB1 at pH 7.5 showed a change in melting profile. Most pronounced was a decrease in melting cooperativity in case of TatB1 at pH 7.0 (Figure 4.7). The following was observed via broadening of the curve with addition of peptide. While this was consistent with the recombinant TatB protein that we employed above, the melting temperature (the mid-point of the curve) changed by 0.8 degrees for a single (TatB1) peptide at pH 7.0 (Figure 4.7).

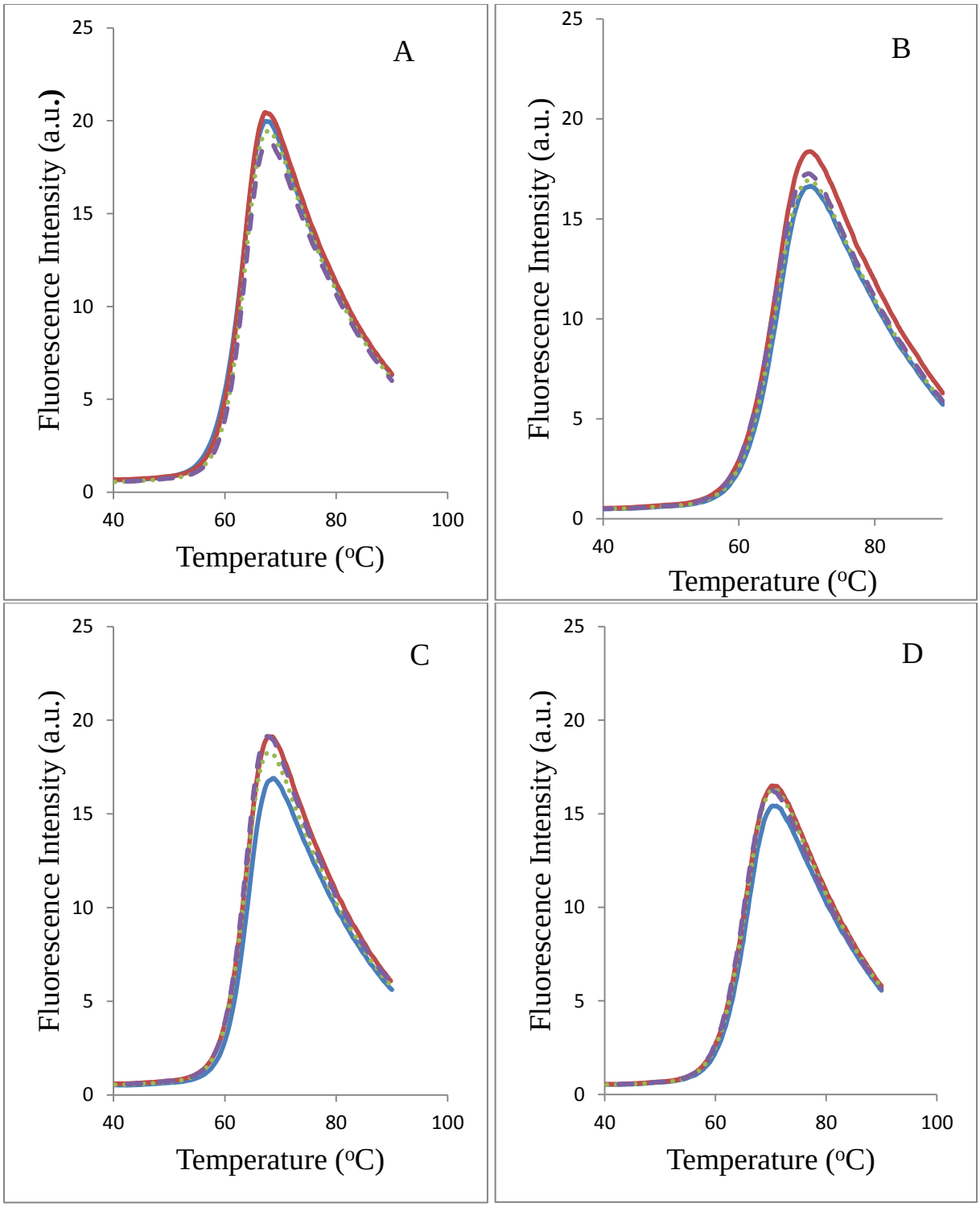

Figure 4.6. TatB2 (A, B) or TatB3 (C, D) peptides, do not affect melting cooperativity of DmsD at pH 7.5 or 8.0. Experiment was monitored with Sypro Orange (SO) at pH 7.5 (A, C) and pH 8.0 (B, D). DmsD alone is depicted in solid blue, 5 μM TatB2/3 added- dashed purple, 12.5 μM TatB2/3 added- dotted green, 25 μM TatB2/3 added- solid red. Final concentration of H_6-T_7-DmsD was 2.5 μM.

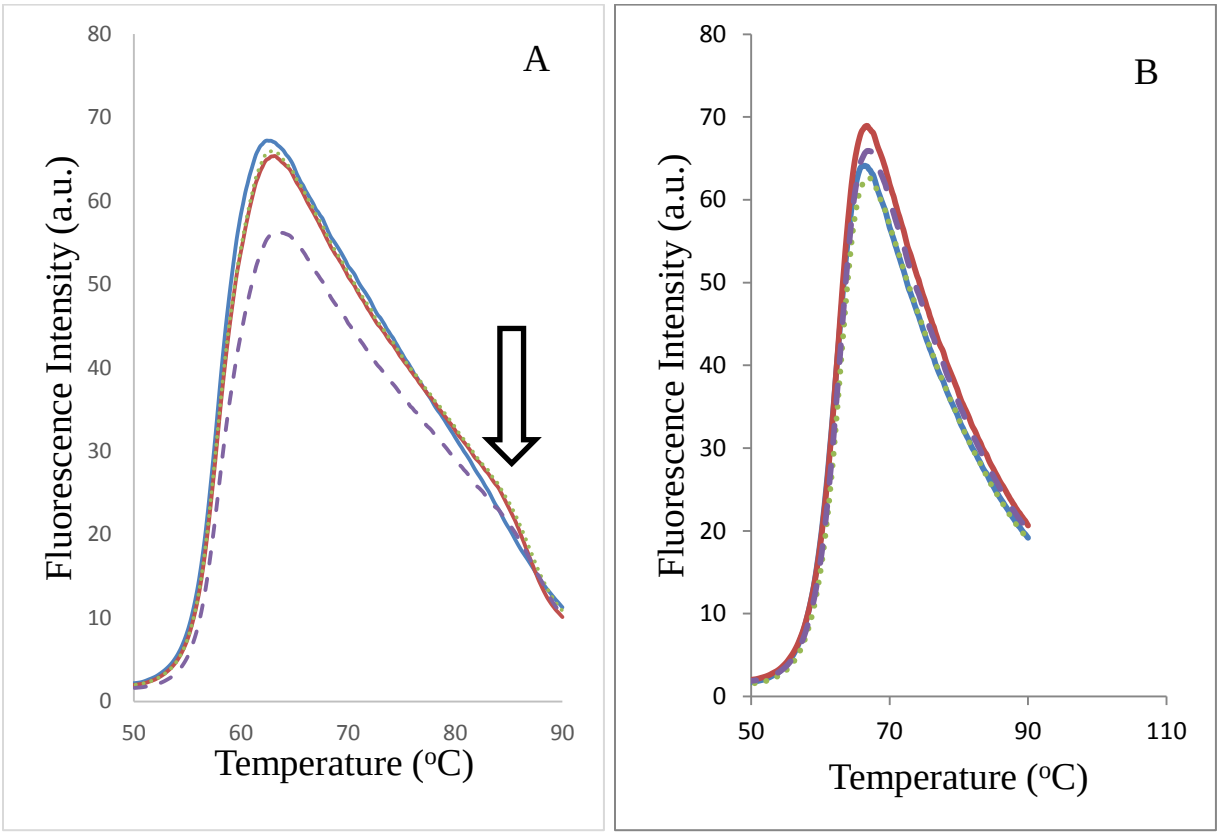

Figure 4.7. TatB1 peptide, residues 37-47, alters melting cooperativity of DmsD at pH 7.0, but not pH 8.0. Experiment was monitored with Sypro Orange (SO) at pH 7.0 (A) and pH 8.0 (B). DmsD alone is depicted in solid blue, 5 μM TatB1 added- dashed purple, 12.5 μM TatB1 added- dotted green, 25 μM TatB1 added- solid red. Final concentration of H_6-T_7-DmsD was 2.5 μM. Arrow in panel A highlights a shoulder feature of the melting profile.

When TatB1 peptide was added at a concentration of 5 μM, which was twice the molar amount of DmsD, no shift in Tm was observed, but the intensity was lost and the shape of the curve was altered suggesting different cooperativity. It was noted that only at a higher concentration of TatB1 (12.5 μM) a shoulder melting transition was observed at higher temperatures suggesting a secondary domain melting differently as well as previously mentioned 0.8 ^{o}C increase. The broadening of the peak was also attributed to a decrease in melting cooperativity. A further increase to 25 μM of TatB1 did not result in additional changes with the shoulder remaining

identical to the one at 12.5 µM. The two other peptides, TatB2 and TatB3, did not reveal a presence of a shoulder.

Discussion

Here we further studied the interaction between DmsD and TatB which was previously shown *in vivo* by a Bacterial two-hybrid assay and an *in vitro* ELISA peptide array (Kuzniatsova et al, 2016). Both of those techniques demonstrated binding, but provided no information on structural changes. Therefore, Differential Scanning Fluorimetry (DSF) was chosen to learn more about potential changes within DmsD for structural thermal stability.

When DmsD and MBP-$TatB_{fr}$ were combined for DSF experiments, the peak of the melting curve shifted towards a higher temperature which suggested a higher level of stabilization. A similar stabilization was detected in an earlier experiment, but with the addition of DmsAl peptide (Cherak and Turner, 2015). Notably, the profile became broader and a shoulder was observed at higher temperatures (Figure 4.2). This was interpreted as a change in the level of cooperativity of DmsD domains upon MBP-$TatB_{fr}$ binding or emergence of new species such as DmsD::MBP-$TatB_{fr}$ complex that unfolds as one (Englander et al, 2016). Addition of DmsAl peptide, on the other hand, was reported to give a more homogeneous population of DmsD due to narrowing of the melting profile peak (Cherak and Turner, 2016). This may imply that conformations of DmsD when bound to TatB and DmsA are quite different.

Stoichiometry calculated for the DmsD::MBP-$TatB_{fr}$ complex demonstrates that REMP protein may dimerize (pH 7.0 and 7.5) or even trimerize (pH 8.0) during the interaction. It is not surprising considering that the following translocation system highly relied on multimerization with one group reporting up to 7 TatBC heterodimers present within an assembly complex (Tarry

et al, 2009). Other researchers claimed that four TatB monomers form an oligomer that makes contact with the substrate (Fröbel et al, 2012). Substrates were also proposed to multimerize; Ma and Cline performed a cross-linking study where they were able to show that up to four leader peptides may be bound to the TAT system at one time. While the authors admitted that disulfide bonds could have enforced the transport, they presented an appealing argument regarding a known *Zymomonas mobilis* oxidoreductase, which has to be transported in a folded form and bears a signal sequence on each of its four monomers (2010). However, while for the TAT translocon components and majority of RR-leader substrates, the function of oligomerization may be explained more or less easily, the purpose oligomerization serves for DmsD, on the other hand, is not so obvious. It could potentially be the need of the cell to keep a centered pool of REMP when no excess substrate is present. The following idea would be consistent with an observation recently reported by Connelly *et al*. who believed that dimerization of DmsD is abrogated during signal peptide binding: once more DmsA would be available, the dimer would dissociate and chaperone the substrate in a 1:1 ratio (Connelly et al, 2016).

Another physicochemical parameter could be the dependence of oligomerization of DmsD on the environment`s pH. Two separately-reported crystal structures of *E. coli* from DmsD were a dimer (pH 6.5) (Stevens et al, 2009) and a tetramer (pH 7.5) (Ramasamy and Clemons, 2009). These structures suggest a tendency towards a higher oligomerization state with increasing pH which is supported in part by our protein-protein interaction experiments in this thesis.

Hill coefficient is a modeling approach that describes cooperative binding and is equal to “n” term. With n values greater than one, a positive cooperativity is assumed and affinity of a binding site is believed to be increased with the binding of a ligand to a different site. Negative cooperativity ($n<1$), on the other hand, suggests that the second binding is highly unlikely due to

the effect from the first molecule-to-ligand binding (Cattoni et al, 2015). Based on our data, Hill coefficient also changes with increasing pH. Initially equal to 1.27 (DSF at pH 7.0) and 1.20 (CD at pH 7.0), it was determined as 1.40 (DSF) and 1.78 (CD) at pH 8.0. This implies that as the local chemical environment is altered, DmsD is prone to offer more than a single binding site for TatB. The following finding would be consistent with the data from Alder and Theg who reported Hill coefficient of 1.80 for the translocon and suggested that either two binding sites with strong affinity or multiple binding sites with weak affinity exist (2003). Another research group reported Hill coefficient equal to 2.09 when GTP was added to DmsD::DmsAl complex and caused dissociation of the substrate from the chaperone (2015). Therefore, it is likely that the following observation has biological relevance and is utilized by DmsD during later stages of translocation.

Affinity of DmsD towards MBP-$TatB_{fr}$ was shown to be 0.15 μM compared to 0.2 μM $DmsAl_{1-43}$-GST at pH 8.0 (Winstone and Turner, 2015). However, the authors pointed out that the interaction is highly dependent on the kind of fusion tag, the position of the tag, and the pH. They compared K_d values with the second measured at pH 7.4 and the construct bearing a Streptavidin-Binding Peptide (SBP) tag. The latter had a dissociation constant equal to 0.06 μM (Winstone and Turner, 2015). It is, therefore, conceivable to suggest that, based on a similar dissociation constants, DmsD has equal chances of interacting with DmsA and TatB, but the first one is more likely to happen when the chaperone is in close proximity to the ribosome translating the mRNA for DmsA since the concentration of the substrate in that region will be locally very high and DmsD was found previously to bind to ribosomal proteins (Li et al, 2010).

Addition of TatB derived peptides did not result in such dramatic changes as in the case of recombinant MBP-$TatB_{fr}$ protein. Nevertheless, we observed a decrease in melting cooperativity

as well as a slight increase in melting temperature for TatB1 added at pH not greater than 7.0. Cherak and Turner reported that adding a GTP and then increasing the pH from 6.0 to 8.5 led to an emergence of a pre-transition peak while the reverse order of addition resulted in an increase of the melting temperature and a uniform DmsD population (2016). Moreover, adding DmsAl peptide at pH 8.0 would also result in an increase in the melting cooperativity (Cherak and Turner, 2016). Comparing their and our results obtained via the same technique (DSF), we conclude here that any affect produced by the TatB-derived peptides could not overcome the "barrier" of the pH (pH 7.5 and 8) which seemed to offer DmsD a degree of stabilization and prevent any further changes.

In conclusion, we were able to demonstrate that TatB in a form of a recombinant protein (MBP-$TatB_{fr}$) as well as three small cytoplasmic segments (TatB1, TatB2 and TatB3) influenced the structure of DmsD leading to a decrease in melting cooperativity and slight increase in melting temperature. This was more prominent at lower pH (7.0) and could be interpreted as a more stable REMP protein with differently-melting domains. Furthermore, the affinity and stoichiometry of DmsD towards MBP-$TatB_{fr}$ decreased at increasing pH.

Chapter 5. Evaluation of secondary structural changes by circular dichroism.

The differential scanning fluorimetry technique provided me with some useful insights into the DmsD to TatB binding at different pH values. While it was elucidated that ligand provided an additional level of stabilization, it was still unclear whether any secondary structure changes were taking place. Therefore, I attempted to evaluate the interaction of the REMP with TatB peptides via circular dichroism (CD). It should be noted that the same set of peptides and the same buffer as in section 4.2 were utilized for all CD experiments.

We initially planned to utilize Isothermal Titration Calorimetry (ITC) which proved to be informative for DmsD-DmsAl interaction (Winstone et al, 2015). However, upon several pilot experiments we determined that the technique was not particularly useful for studying DmsD-TatB interaction (no heat of enthalpy involved). As a result, we chose CD, a method where extensive amounts of information can be obtained for a complex which may not be dissociating and just undergoing shape changes. We also considered relative sensitivity, small amounts of material required, and ability to rescue to the sample for downstream analysis (SDS-PAGE) (Attar and Khavari –Nejad, 2016).

5.1 CD spectra of DmsD and peptides alone

Prior to performing any experiments involving a protein-peptide mixture, I needed to test whether the buffer that I had been using for my DSF experiments was compatible with the CD equipment. It was also important to verify that the CD profile from DmsD alone was comparable with the one previously reported by Winstone *et al*. (2013). Finally, spectra of peptides had to be collected in order to perform normalizations for the combinations of the molecules. Spectra for the individual biomolecules studies are shown in Figure 5.1.

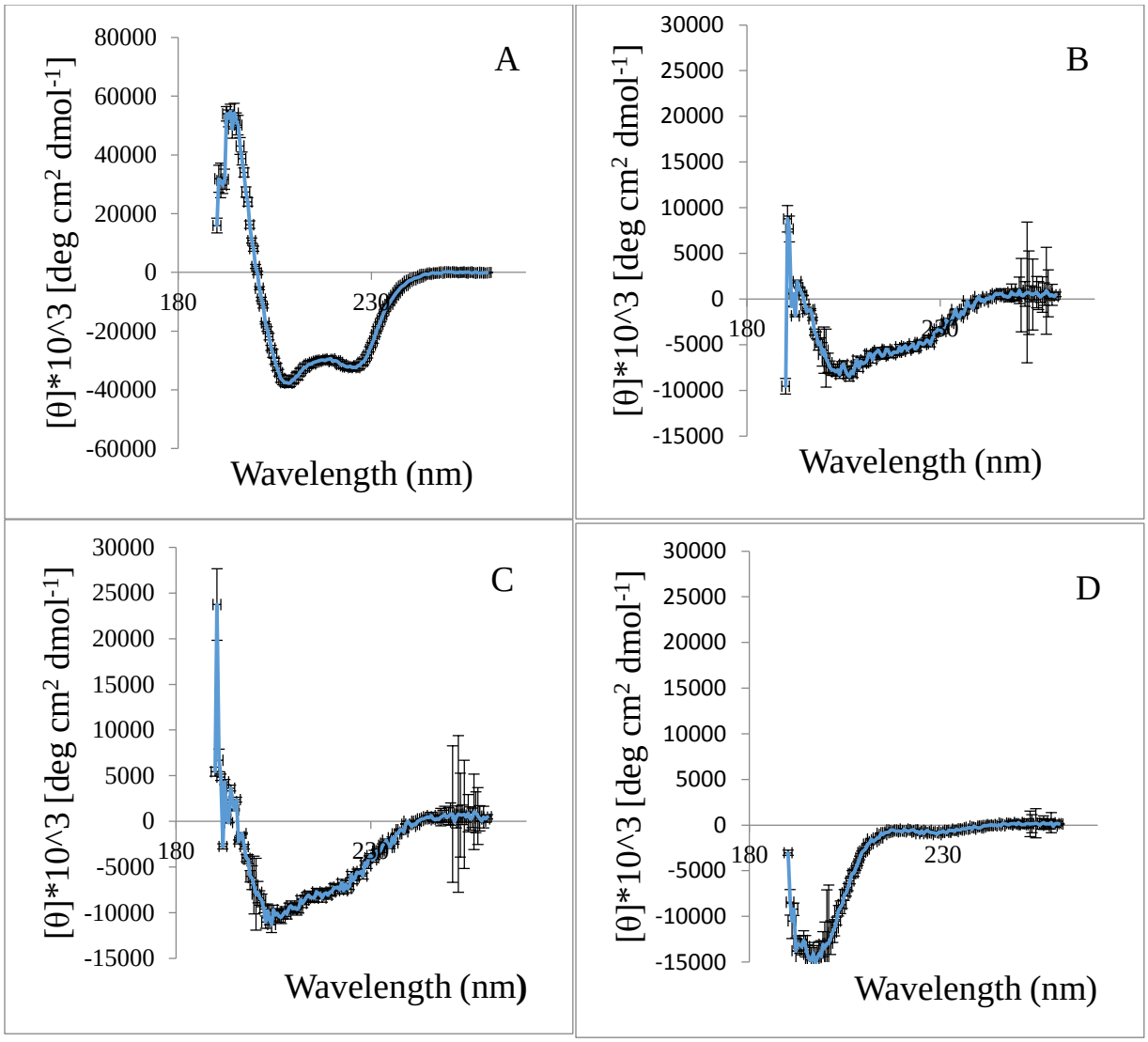

Figure 5.1. Circular dichroism spectra of individual biomolecules. A. DmsD at pH 7.0. **B.** TatB1peptide at pH 7.0. **C.** TatB2 peptide at pH 7.0. **D.** $DmsAl_{15\text{-}41}$ at pH 7.0. Circular dichroism data was collected in the far-UV range (190-260 nm) of samples with 3.5 μM concentration of DmsD and 35 μM any peptide. Shown is an averaged spectrum from 10 scans. Standard error was calculated via standardization method using a replicate of five samples.

All CD spectra were normalized to moles of polypeptide in the cuvette. It is important to note that the scale magnitude between the protein and the peptides is quite different with signal for DmsD being between -60000 and 80000 while only -15000 to 15000 for TatB1, reflecting the minor amount of structure in the peptides. The CD spectra of DmsD and $DmsAl_{15\text{-}41}$ were compared to Winstone *et al*. and it was concluded that secondary structure content was quite similar to the previously reported (2013). At pH 7.0 and pH 8.0 we determined $DmsAl_{15\text{-}41}$ to

have 6.5% and 10.5% helix, respectively, versus 5% reported by Winstone *et al*. (at pH 5). This showed a trend towards increasing helical content at higher pH values (2013).

5.2 TatB2 peptide leads to changes in DmsD secondary structure

It was previously shown that TatB interacts with DmsD (Kuzniatsova et al, 2016). In chapter 4 DSF demonstrated that DmsD melting profile was affected by the complete TatB cytoplasmic domain and peptides from selected regions. Additionally, these experiments demonstrated that these changes were pH dependent. Here, experiments to understand conformational changes were explored, to see if there was any influence of $TatB_{fr}$ interaction with DmsD on secondary structure of DmsD. The three selected peptides were added to DmsD and circular dichroism performed at pH 7.0 and 8.0.

There was no apparent secondary structure change in case of TatB1 (Figure 5.2. A, B) or TatB3 (data not shown). However, secondary structure was altered with the addition of TatB2 (Figure 5.2 C, D). The total structural change upon addition of TatB2 at pH 7.0 was 14%, where 6.4% of helix and 0.6% of turn are gained, while 7% of random coil was lost. With 1 unit increase in pH the total change in secondary structure was equal to 10.6% (gain in 4% helix and 1.3% turn, loss of 5.3% random coil).

Based on these CD results and the DSF results (Chapter 4) we chose to base further investigations of the DmsD to TatB interaction on the peptide TatB2 at pH 8.0. Nevertheless, we performed a titration of peptide into the protein at both pH 8.0 and 7.0 as shown in Figure 5.3. Data could be fit via the one site/specific binding of nonlinear fit with K_d values of 5.40 µM and 4.70 µM were obtained at pH 8.0 and 7.0, respectively.

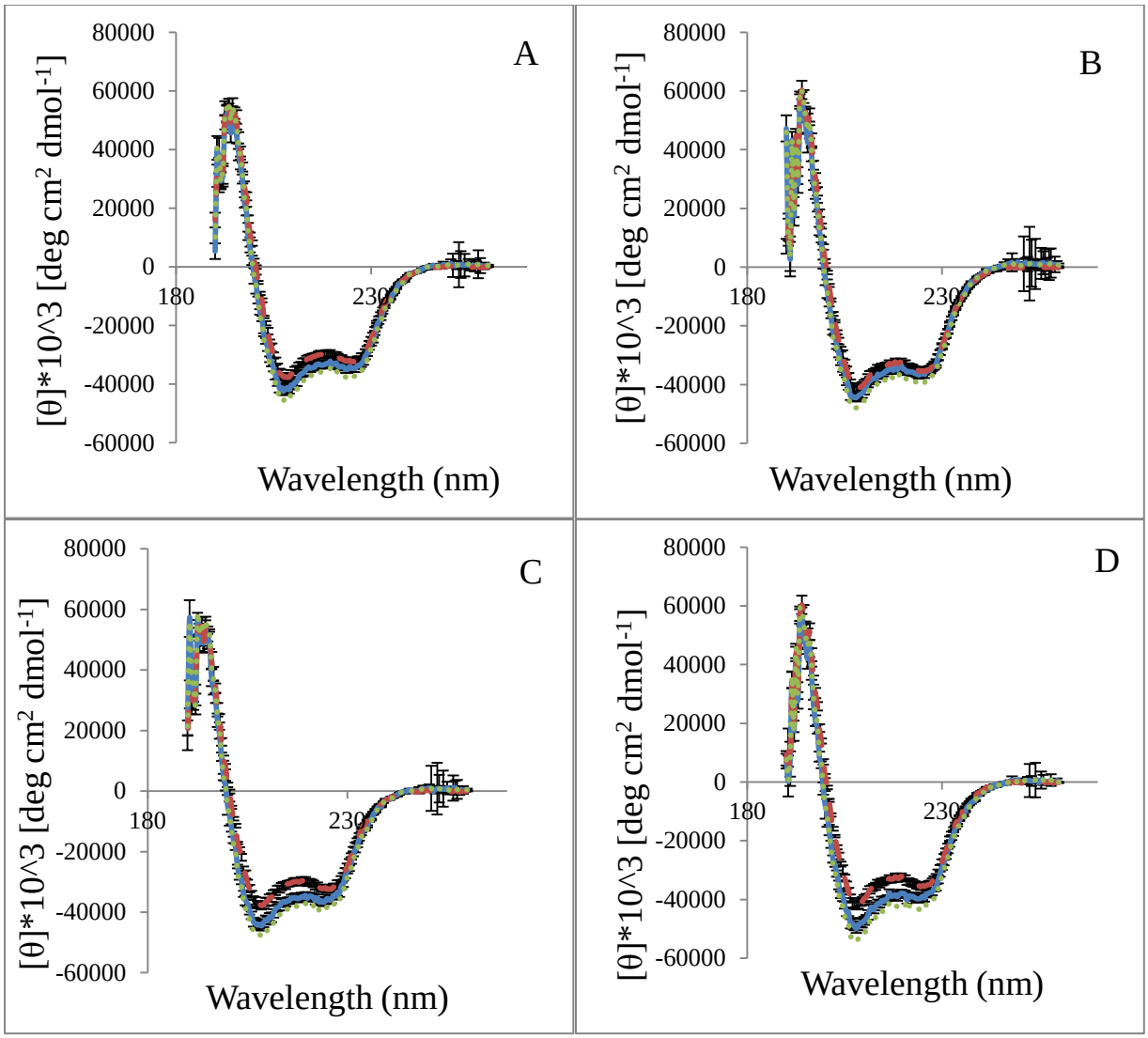

Figure 5.2. Secondary structure of DmsD changes in response to TatB2, but not TatB1 or TatB3 peptides. A. DmsD exposed to TatB1 at pH 7.0. **B.** DmsD exposed to TatB1 at pH 8.0. **C.** DmsD exposed to TatB2 at pH 7.0. **D.** DmsD exposed to TatB2 at pH 8.0. Circular dichroism data was collected at pH 7.0 (A, C) and 8.0 (B, D) and in the far-UV range (190-260 nm) of samples with 3.5 μM concentration of DmsD and 35 μM TatB peptide. Normalized spectrum where spectra of DmsD alone and TatB peptide alone were subtracted from experimental data is shown in solid blue line (DmsD+TatB-(DmsD::TatB)). DmsD protein alone (red dashed line) is provided for comparison. Theoretical combination of DmsD and TatB peptide spectra (see section 5.1) is depicted in dotted green line. Shown is an averaged spectrum from 10 scans. Standard error was calculated via standardization method using a replicate of five samples.

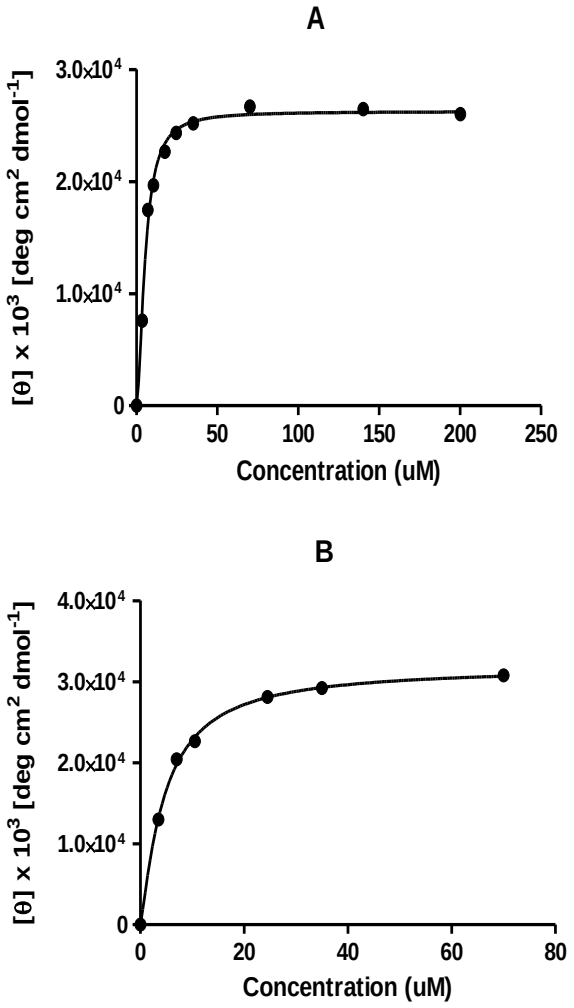

Figure 5.3. DmsD binding curve titrated with TatB2 peptide at pH 8.0 (A) and pH 7.0 (B). The circular dichroism spectrum was collected in the far-UV range (190-260 nm) at different concentrations and normalized. Molar ellipticity at 222 nm was plotted versus the concentration of TatB2. Best-fit values are shown in Table 4.1.

5.3 DmsAl itself does not lead to a dramatic change in DmsD secondary structure

Standard error of the plot between trials was similar to previous spectra and thus were left off in order to see the overlapping spectra more easily. This remained consistent starting from section 5.3 and till the end of the chapter except from Figure 5.6. As in the latter figure the standard error was relatively high in the region of 180-200 nm, we decided to present it with standard error.

It was previously shown via isothermal titration calorimetry and differential scanning fluorimetry that DmsD interacts with the leader sequence on DmsA protein (Winstone et al, 2006; Winstone and Turner, 2015; Cherak and Turner, 2015). Furthermore, our lab successfully demonstrated that DmsAl adapts a helical conformation in the presence of the REMP protein (Winstone et al, 2013). Our goal here was to determine whether addition of DmsAl impacts the secondary structure of DmsD and if it is different at pH 7.0 or pH 8.0.

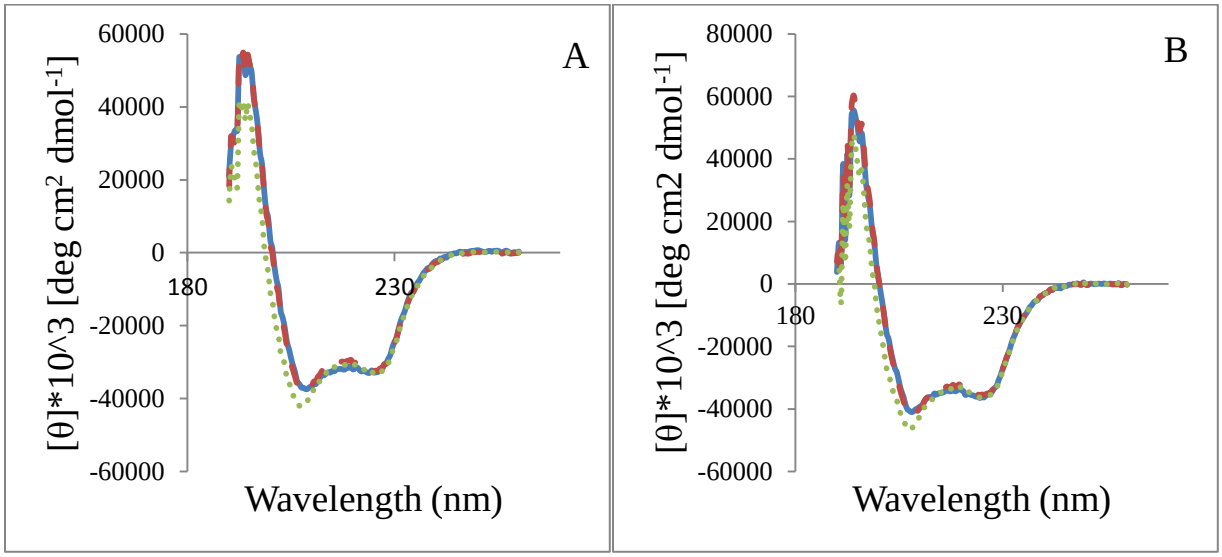

Figure 5.4. DmsAl causes very minor structural changes in DmsD. A. DmsD exposed to DmsAl at pH 7.0. **B.** DmsD exposed to DmsAl at pH 8.0. Circular dichroism data was collected at pH 7.0 (A) and pH 8.0 (B) and in the far-UV range (190-260 nm) of samples with 3.5 µM concentration of DmsD and 35 µM DmsAl peptide. Normalized spectrum where spectra of DmsD alone and DmsAl alone were subtracted from experimental data is shown in solid blue line (DmsD+DmsAl-(DmsD::DmsAl)). DmsD protein alone (red dashed line) is provided for comparison. Theoretical combination of DmsD (see Figure 5.1. A) and DmsAl spectra (see Figure 5.1. D) is depicted in dotted green line.

As seen in Figure 5.4 A and B, very minor conformational changes take place during introduction of DmsAl peptide at pH 7.0 or 8.0. As it has been previously shown that the DmsD binds to DmsA leader sequence, we can deduce that the structure of the chaperone remains unaltered (Oresnik et al, 2001). We proceeded with a titration in order to obtain a dissociation

constant for interaction between DmsD and DmsAl (Figure 5.5). Additionally, we were interested in comparing this new K_d to the one found via ITC experiments.

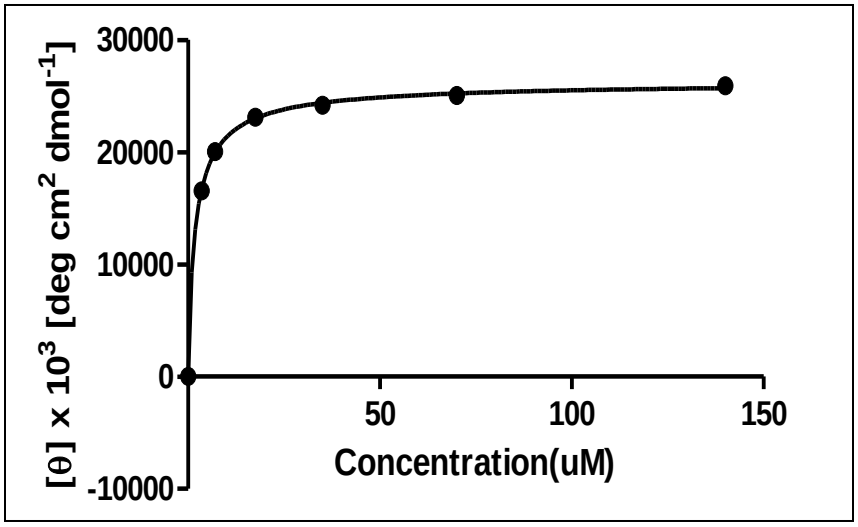

Figure 5.5 DmsD binding curve titrated with DmsAl at pH 8.0. The circular dichroism spectrum was collected in the far-UV range (190-260 nm) at different concentrations and normalized. Molar ellipticity at 222 nm was plotted versus the concentration of DmsAl peptide. The dissociation constant was obtained using GraphPad Prism 5 via the one site/specific binding with Hill slope nonlinear fit. Best-fit value for Hill slope was equal to 0.87.

We found that the K_d that obtained was extremely close to the one calculated from the ITC experiments: 1.89 μM here with circular dichroism versus 1.7 μM via ITC (Winstone et al, 2013). The fact that the two numbers were almost identical implied that this was a reliable dissociation constant for chaperone-leader peptide. It was also the smallest number among all the K_d values that CD titrations yielded. Therefore, it can be speculated that this interaction is most likely the most stable and is key to the translocation event.

5.4 DmsD possesses two distinct sites for interaction with DmsA leader and TatB

From previous studies there is now a good understanding of the interaction between DmsD and the twin-arginine signal sequence of DmsA (DmsAl) (see chapter 1 and section 5.2). Research

from previous studies (Kostecki et al, 2010; Kuzniatsova et al, 2016) and work above in chapters 4 and 5.1 demonstrate that DmsD also interacts with regions in the soluble cytoplasmic domain of TatB. There is also the appreciation that DmsD structure is influenced by pH (Sarfo et al, 2004) and that this pH difference influences DmsD's binding ability. Here we proceeded with exploration of more complex relationship and asked if we could extract structural changes of a trimeric complex of DmsD, DmsAl and TatB. For this the first study was to see if DmsAl influenced the secondary structure of DmsD::TatB (1, 2 or 3) complex?

Addition of DmsAl influenced the secondary structure of DmsD::TatB2 complex at pH 7.0 and pH 8.0 (Figure 5.6 A, B). Conformational change was observed in the case of TatB1 and TatB3, but the theoretical summation of DmsD::TatB3 and DmsAl overlapped the experimental spectra and, thus, it is most likely that we were dealing with the addition of signals from the complex and the ligand rather than the effect of interaction. The total secondary structure change for DmsD::TatB2 complex with DmsAl was 11.2%. At pH 8.0 DmsD::TatB2 demonstrated slightly greater total change in secondary structure and equal to 13.2% (5.5% increase in α-helix, 3.6% loss in β-sheet, 1.1% gain in turn and 3% loss in random coil). Overall, addition of DmsAl to the DmsD::TatB peptide complex leads to replacement of β-sheet structure.

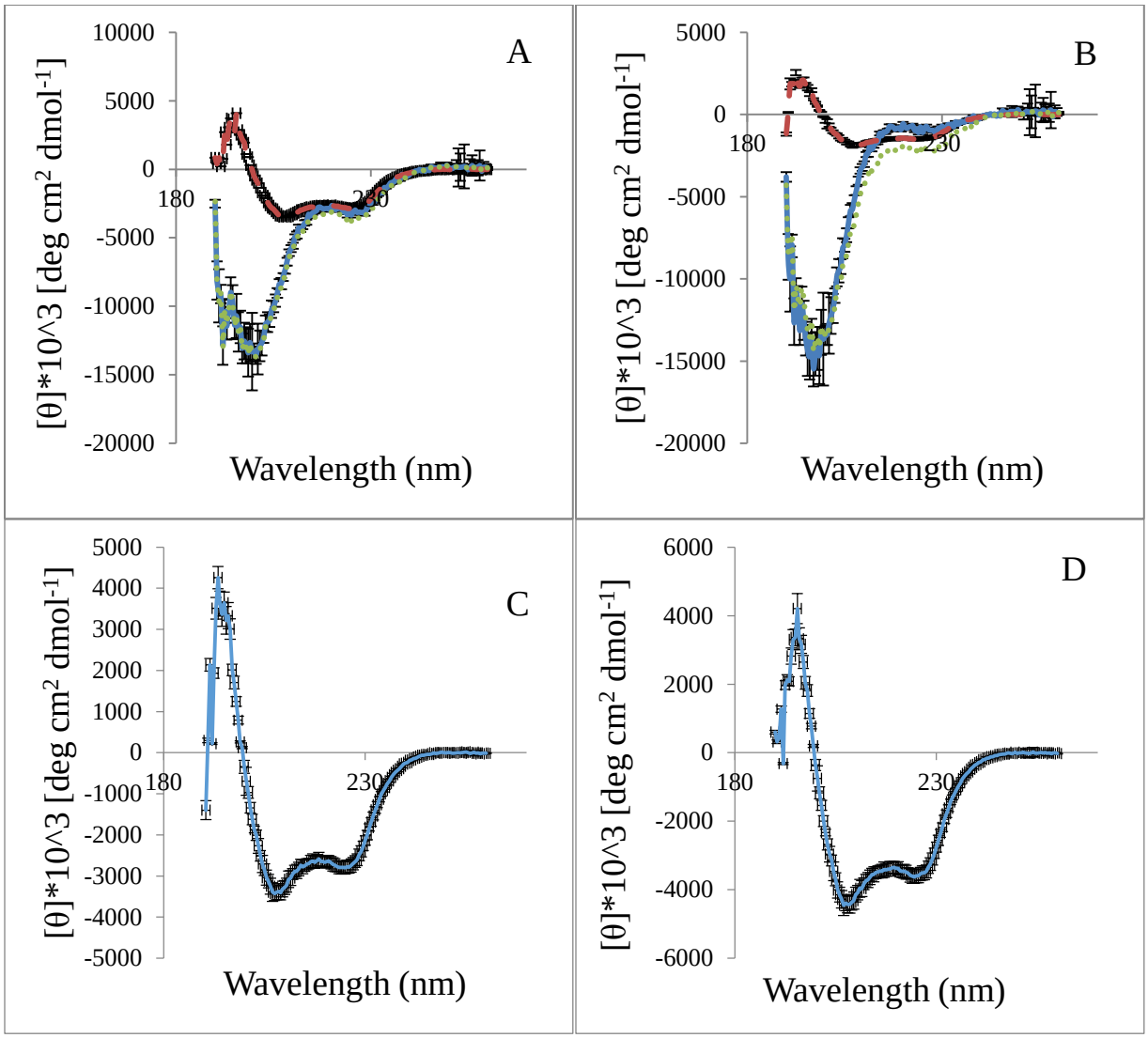

Figure 5.6. Circular dichroism spectra of structural change in DmsD::TatB2 upon addition of DmsAl peptide. The data was collected at pH 7.0 (**A**) and pH 8.0 (**B**) and in the far-UV range (190-260 nm) of samples with 3.5 μM concentration of DmsD and 35 μM concentrations of DmsAl and TatB2. Normalized spectrum where spectra of DmsD::TatB2 and DmsAl were subtracted from experimental data is shown in solid blue line (DmsD::TatB2+DmsAl-(DmsD::TatB2::DmsAl)). DmsD::TatB2 complex (red dashed line) is provided for comparison. Theoretical combination of original DmsD::TatB2 (Figure 5.6 **C** (pH 7.0) and **D** (pH 8.0)) and DmsAl (see Figure 5.1 D) is depicted in dotted green line. Shown is an averaged spectrum from 10 scans. Standard error was calculated via standardization method using a replicate of five samples.

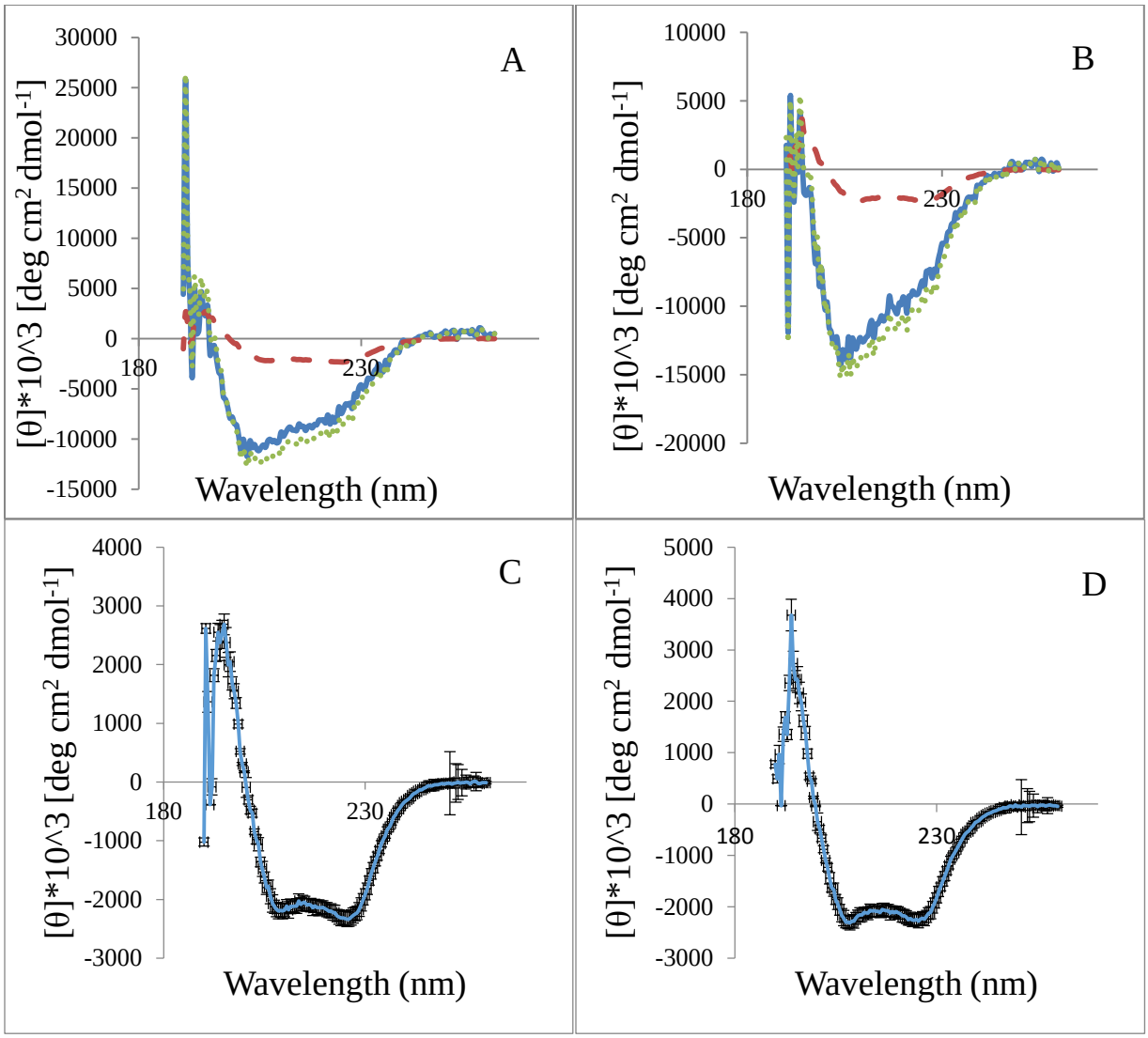

Figure 5.7. **Circular dichroism spectra of structural change in DmsD::DmsAl upon addition of TatB2 peptide at pH 7.0 (A) or 8.0 (B).** The data was collected in the far-UV range (190-260 nm) of samples with 3.5 μM concentration of DmsD and 35 μM concentrations of DmsAl and TatB2. Normalized spectrum where spectra of DmsD::DmsAl and TatB2 were subtracted from experimental data is shown in solid blue line (DmsD::DmsAl+TatB2-(DmsD::DmsAl::TatB2)). DmsD::DmsAl complex (red dashed line) is provided for comparison. Theoretical combination of original DmsD::DmsAl (Figure 5.7 **C** (pH 7.0) and **D** (pH 8.0)) and TatB2 (see section 5.1C) is depicted in dotted green line.

We then reversed the experiment to understand whether the order of addition matters in case of each of the two possible preformed complexes: DmsD::TatB peptide complex vs DmsD::DmsAl complex. The results are presented in Figure 5.7.

We looked at the order of addition of TatB peptide versus DmsAl peptide. It was noted that no conformation change takes place when TatB1 or TatB3 peptides are used. However, a structural change was observed when TatB2 is added to the experimental mixture of DmsD::DmsAl. As seen in Figure 5.7, at pH 7.0 a total conformational change of 51.4% is observed with the major impact coming from a substitution of 20.5% β-sheet with 22.2% α-helix. In case of pH 8.0, the total structural change reached 63.2% with the same trend where 26.6% β-sheet was replaced with 27.7% α-helix (Figure 5.7 B).

This data may provide an insight in the order of steps that takes place during the translocation event. Since we have shown that conformational change of DmsD upon addition of DmsAl was minor in the absence of TatB it may be speculated here that the presence of TatB plays a role in altering the DmsD::DmsAl complex. To explore this relationship further, we attempted two titrations: DmsAl into DmsD::TatB2 complex and TatB2 into DmsD::DmsAl complex (Figure 5.8). This investigated how the dissociation constants compare.

The dissociation constant for TatB2 titration into DmsD::DmsAl was found to be equal to 8.88 μM, while the reverse (DmsAl into DmsD::TatB2) was far weaker at 24.24 μM. The results were placed in Table 5.1.

From a collection of DmsD amino acid variants studied previously (Winstone and Turner, 2015), we picked a single variant of an amino acid in the DmsAl binding pocket for DmsD that presented a 2-fold decrease in binding DmsAl. First, we asked how do dissociation constants of the wild-type and mutant compare when only TatB2 or DmsAl peptides are added to DmsD.

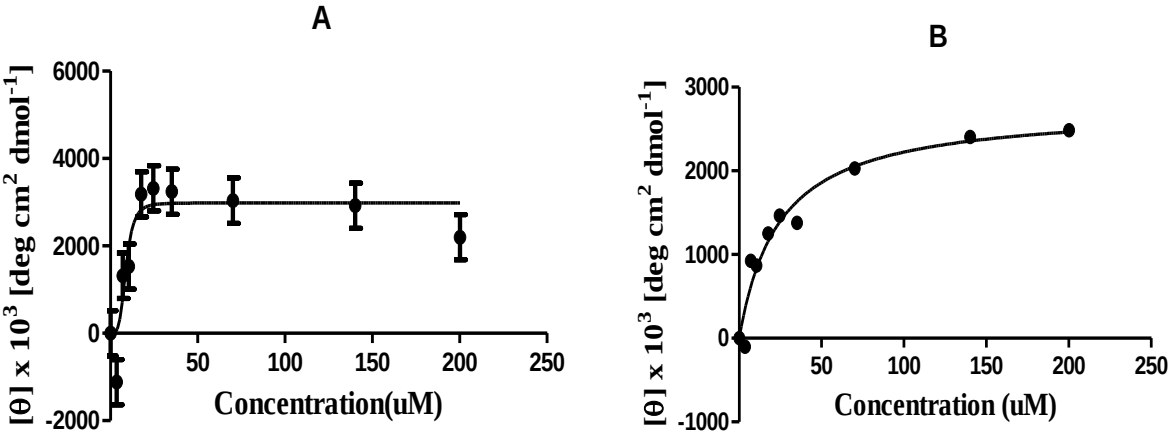

Figure 5.8. DmsD complexed with peptide titrated with competing peptide A. TatB2 as part of the complex; DmsAl as competing peptide. **B.** DmsAl as part of the complex; TatB2 as competing peptide. Experiment performed at pH 8.0. The circular dichroism spectrum was collected in the far-UV range (190-260 nm) at different concentrations and normalized. Molar ellipticity at 222 nm was plotted versus the concentration of a binding partner added to the complex. The dissociation constant was obtained using GraphPad Prism 5 via the one site/specific binding with Hill slope nonlinear fit.

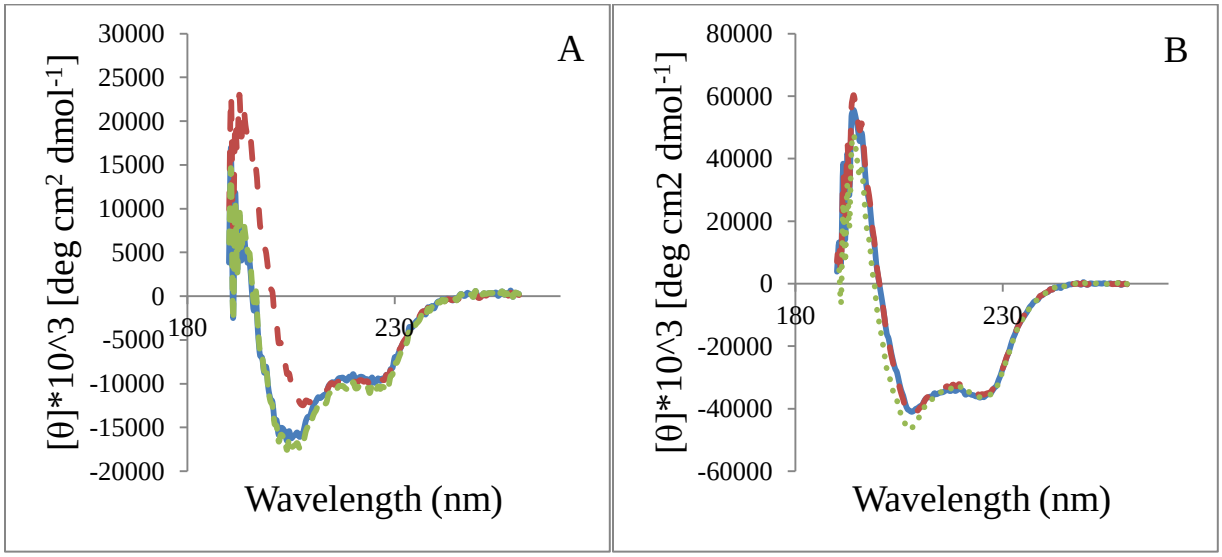

Figure 5.9. DmsD P86Q variant responds to DmsAl differently compared to DmsD wild-type. A.P86Q mutant exposed to DmsAl. **B.** Wild-type exposed to DmsAl. Circular dichroism data was collected at pH 8.0 and in the far-UV range (190-260 nm) of samples with 3.5 μM concentration of DmsD and 35 μM DmsAl peptide. Normalized spectrum where spectra of DmsD alone and DmsAl alone were subtracted from experimental data is shown in solid blue line (DmsD+DmsAl-(DmsD::DmsAl)). DmsD protein alone (red dashed line) is provided for comparison. Theoretical combination of DmsD (see Figure 5.1 A) and DmsAl spectra (see Figure 5.1 D) is depicted in dotted green line.

Figure 5.9 A and B demonstrated that the signals from the wild-type and the mutant are different. Total structural change for DmsD P86Q variant was equal to 26%, while only 4.4% for wild-type DmsD. Notably, the K_d values were extremely close to the previously reported by Winstone and Turner via Isothermal Titration Calorimetry: 1.89 µM (see section 5.3) and 4.27 µM (Figure 5.10) yielded by circular dichroism technique versus 1.7 µM and 3.6 µM obtained through ITC (2015). The authors also reported increased entropic cost in the case of a mutant upon binding to DmsAl. They suggested that substitution of a proline led to a more flexible conformation (Winstone and Turner, 2015). This could explain the 4.8% increase in random coil that we had observed when DmsAl was added to P86Q variant. We then repeated the same procedure for TatB2 peptide.

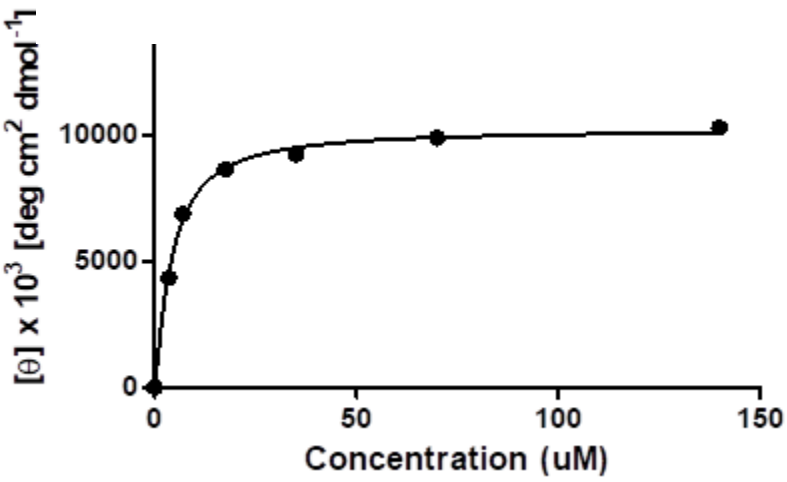

Figure 5.10. P86Q DmsD variant binding curve titrated with DmsAl at pH 8.0. The circular dichroism spectrum was collected in the far-UV range (190-260 nm) at different concentrations and normalized. Molar ellipticity at 222 nm was plotted versus the concentration of DmsAl peptide. The dissociation constant was obtained using GraphPad Prism 5 via the one site/specific binding with Hill slope nonlinear fit. Best-fit value for Hill slope was equal to 1.2.

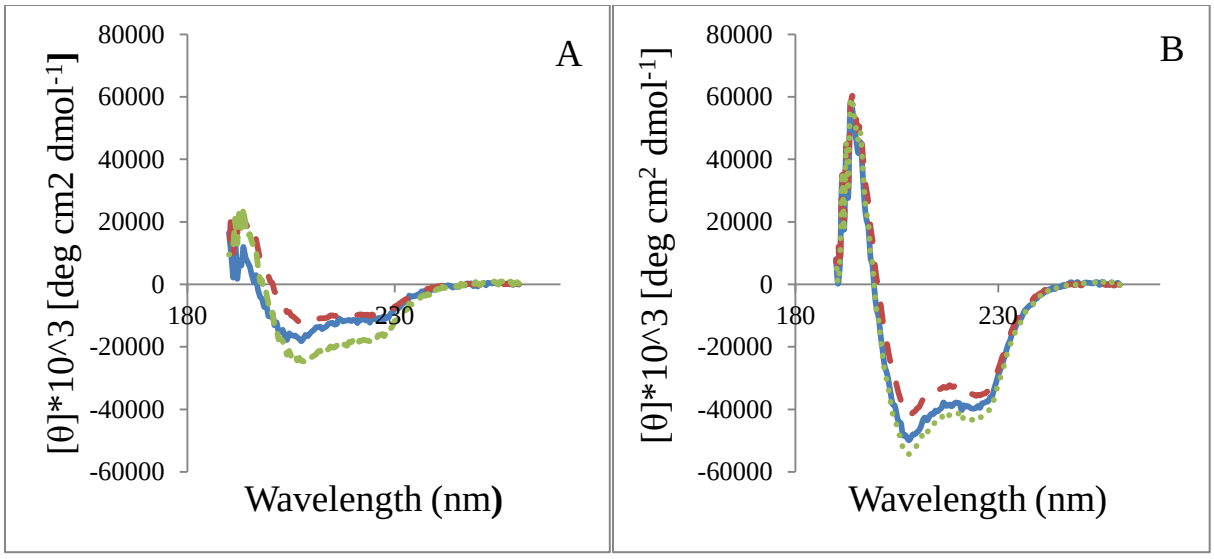

Figure 5.11. DmsD P86Q mutant responds to TatB2 differently compared to DmsD wild-type. A. P86Q mutant exposed to TatB2. **B**. Wild-type exposed to TatB2. The data was collected at pH 8.0 and in the far-UV range (190-260 nm) of samples with 3.5 μM concentration of DmsD and 35 μM TatB2. Normalized spectrum where spectra of DmsD alone and TatB2 alone were subtracted from experimental data is shown in solid blue line (DmsD+TatB2-(DmsD::TatB2)). DmsD protein alone (red dashed line) is provided for comparison. Theoretical combination of DmsD (see Figure 5.1 A) and TatB2 spectra (see Figure 5.1 C) is depicted in dotted green line (A, B).

It was found that there was a greater structural change in the mutant variant: 52.2% versus 10.6% for wild-type with the addition of TatB2 (Figure 5.11). Nevertheless, the perturbations were alike in the type of structural elements. Random coil and β-sheet were replaced with turn and α-helix. The titration curve provided us with a dissociation constant equal to 5.45 μM which was not very different from the wild-type DmsD (5.40 μM) (Figure 5.12). This hinted at two different sites for DmsAl and TatB2 binding. As a result, we sought to investigate if wild-type and P86Q mutant differ in their secondary structure response to addition of TatB2/DmsAl when DmsD already in complex with DmsAl/TatB2.

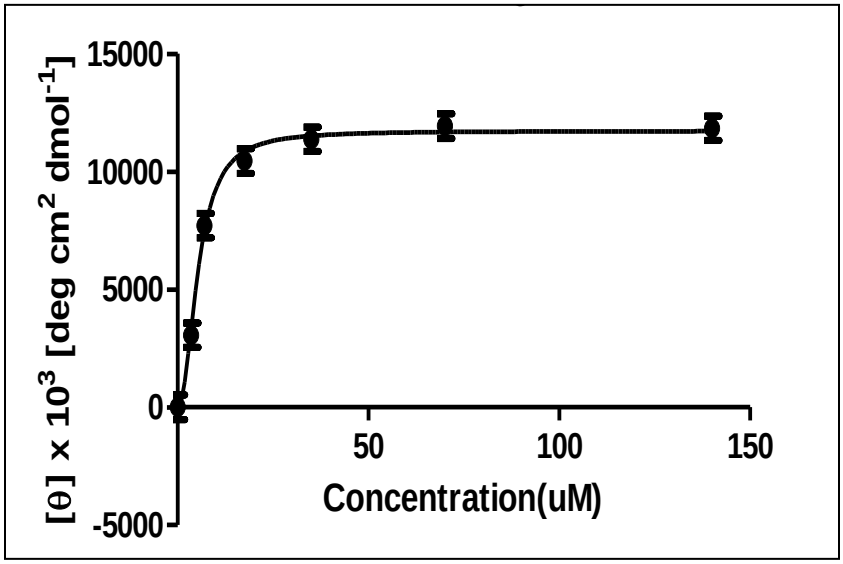

Figure 5.12. P86Q DmsD binding curve titrated with TatB2 at pH 8.0. The circular dichroism (spectrum was collected in the far-UV range (190-260 nm) at different concentrations and normalized. Molar ellipticity at 222 nm was plotted versus the concentration of TatB2 peptide. The dissociation constant was obtained using GraphPad Prism 5 via the one site/specific binding with Hill slope nonlinear fit. Best-fit value for Hill slope was equal to 2.1.

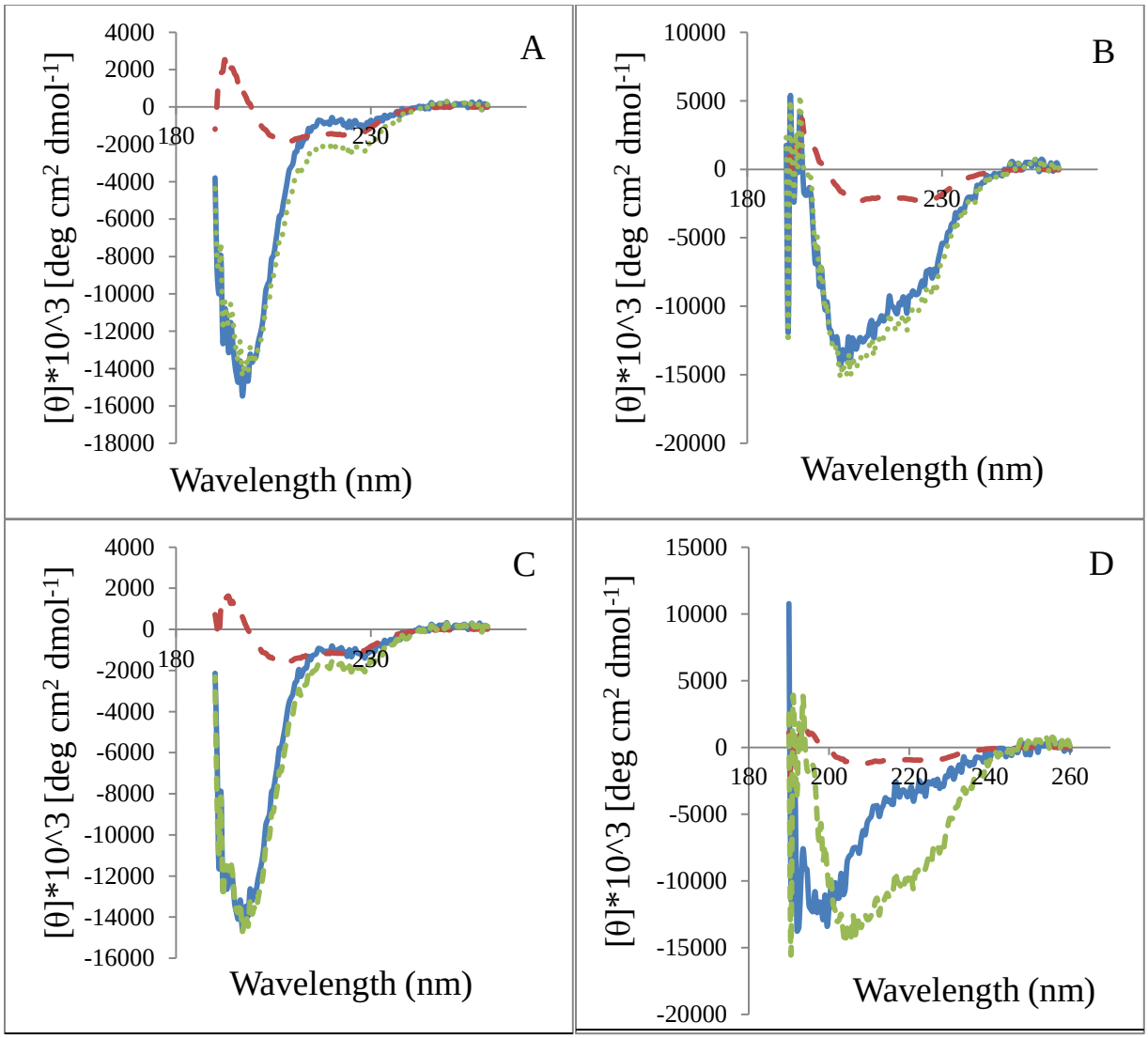

Figure 5.13. Circular dichroism spectra of structural change in DmsD::peptide upon addition of DmsAl (A, C) or TatB2 (B, D) peptide at pH 8.0. A. W-T DmsD::TatB2 exposed to DmsAl. **B.** W-T DmsD::DmsAl exposed to TatB2. **C.** P86Q DmsD::TatB2 exposed to DmsAl. **D.** P86Q DmsD::DmsAl exposed to TatB2.The data was collected in the far-UV range (190-260 nm) of samples with 3.5 μM concentration of DmsD and 35 μM concentrations of DmsAl and TatB2. Normalized spectrum where spectra of wild-type DmsD::peptide1 and peptide2 were subtracted from experimental data is shown in solid blue line (DmsD::peptide1+peptide2-(DmsD:: peptide1::peptide2)). Wild-type DmsD::peptide1 complex (red dashed line) is provided for comparison. Theoretical combination of wild-type DmsD::TatB2 (Figure 5.2) and DmsAl (see Figure 5.1 D) is depicted in dotted green line.

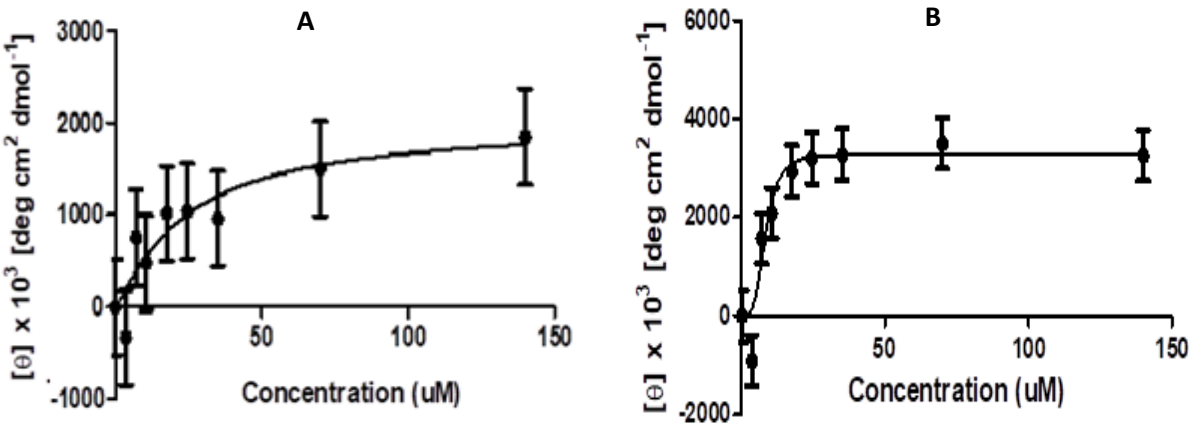

Figure 5.14. P86Q DmsD complexed with peptide titrated with competing peptide. A. TatB2 as part of the complex; DmsAl as competing peptide. **B.** DmsAl as part of the complex; TatB2 as competing peptide. Experiment performed at pH 8.0. The circular dichroism spectrum was collected in the far-UV range (190-260 nm) at different concentrations and normalized. Molar ellipticity at 222 nm was plotted versus the concentration of a binding partner added to the complex. The dissociation constant was obtained using GraphPad Prism 5 via the one site/specific binding with Hill slope nonlinear fit.

As seen in Figure 5.13 B and D, when in complex with DmsAl, wild-type and P86Q mutant differ in their structural change upon addition of TatB2. While there is 63.2% for the wild-type, the total change for the mutant variant was 56.6%. The change in secondary structure was consistent among the different ligand additions in case of P86Q (17.3% and 11% increases in α-helix and turn; 16.7% and 11.6% decreases in β-sheet and random coil), but only demonstrated adjustments in helix and sheet for the wild-type (27.7% gain in α-helix and 26.6% β-sheet). In the case of the reverse experiment (DmsAl titration into DmsD::TatB2 complex) we saw a smaller change: 23.8% total change for wild-type DmsD and 28.8% - for P86Q. Again, there was increase in helical structures as well as the turn and random coil.

Next, we compared the dissociation constants for mutant and wild-type when TatB2 or DmsAl are titrated into DmsD::peptide complex (Figure 5.14). Table 5.1 shows that there is no

difference in the binding of either peptide (DmsAl or TatB2) to wild-type or mutant DmsD when in complex with the other peptide.

Table 5.1. Best-fit values for the titration of DmsAl/TatB2 peptide into DmsD::TatB2/DmsAl at pH 8.0 evaluated by circular dichroism. The dissociation constant was obtained using GraphPad Prism 5 via the one site/specific binding with Hill slope nonlinear fit.

	Titration of DmsAl into DmsD::TatB2		Titration of TatB2 into DmsD::DmsAl	
W-T DmsD	B_{max}	2758 ± 464.4	B_{max}	2983 ± 288.5
	h	1.1 ± 0.32	h	4.18 ± 3.11
	K_d	24.24 ± 1.1 (μM)	K_d	8.88 ± 1.61 (μM)
	R^2	0.95	R^2	0.87
P86Q mutant	B_{max}	2001 ± 693.1	B_{max}	3280 ± 249.2
	h	1.15 ± 0.67	h	3.72 ± 1.95
	K_d	24.43 ± 1.9 (μM)	K_d	8.26 ± 1.14 (μM)
	R^2	0.86	R^2	0.93

5.5 DmsD structure is affected by the addition of GNP, not the guanosine moiety.

It was previously shown using differential scanning fluorimetry (DSF) that GTP with DmsD causes a decrease in the melting temperature (Cherak and Turner, 2015). Our aim was to validate the binding with circular dichroism (CD).

As can be seen in Figure 5.15, GTP alone leads to a change in secondary structure of DmsD. The total structural changes are as follows: 23.8% for pH 7.0 and 19.4% for pH 8.0. In both cases loss of α-helix and increase in random coil are observed. Higher degree of structural disorder supports previously reported 3.8^{o}C shift down from 60.9^{o}C (Cherak and Turner, 2015).

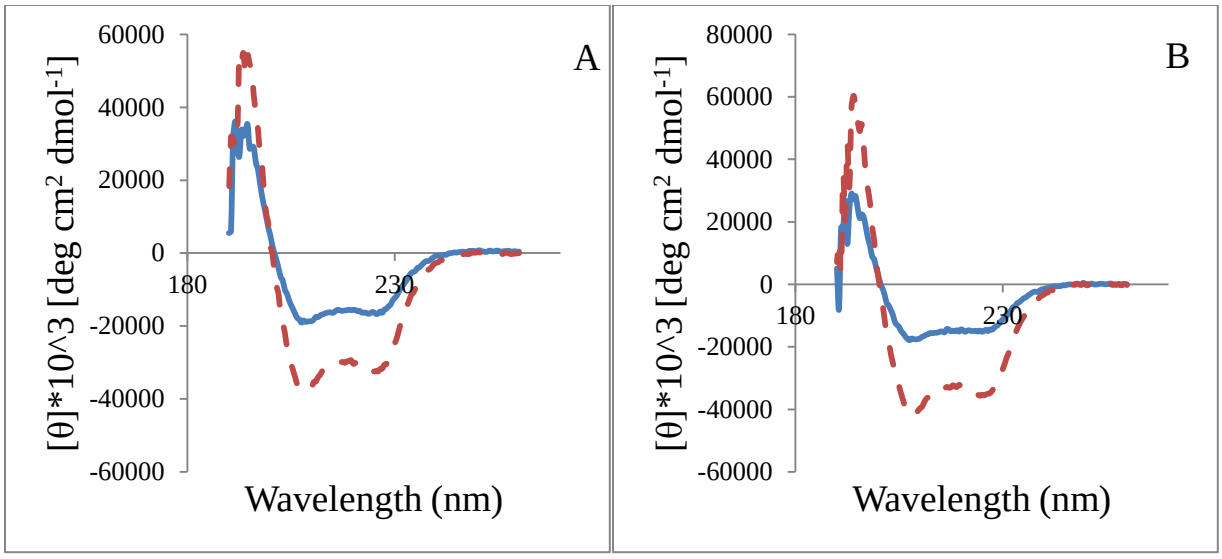

Figure 5.15. GTP binds to DmsD. A. DmsD exposed to GTP at pH 7.0. B. DmsD exposed to GTP at pH 8.0. Circular dichroism data was collected at pH 8.0 and in far UV-range (190-220 nm) of samples with 3.5 μM concentration of DmsD and 35 μM concentrations of GTP. Normalized spectrum with GTP added is shown in solid blue line. DmsD (red dashed line) is provided for comparison.

Once we had demonstrated that circular dichroism technique could be used for DmsD-GTP interactions, we attempted to understand if DmsD::DmsAl complex is influenced by any of the GNP (GTP, GDP or GMP).

As seen in Figure 5.16, all guanosine-containing nucleotides led to a similar change in secondary structure. It was smallest for GDP (8.4% total change) and greatest in case of GTP (15.6% total change). Beta-sheet components and random coil were replaced with alpha-helix and turn. A key observation was that the percentages for α-helix vs β-sheet and random coil vs turn always closely overlapped. For example, in case of GTP added to DmsD::DmsAl 6.5% loss of sheet coincided with 6.1% gain of helical component and 1.3% loss in random coil coincided with 1.7% increase in turn. One possible reason for similar changes in the secondary structure was that the binding site was equally accommodating for GTP, GDP and GMP. A similar trend was detected with hGBP1, a guanylate-binding protein which was discovered to be a GTPase.

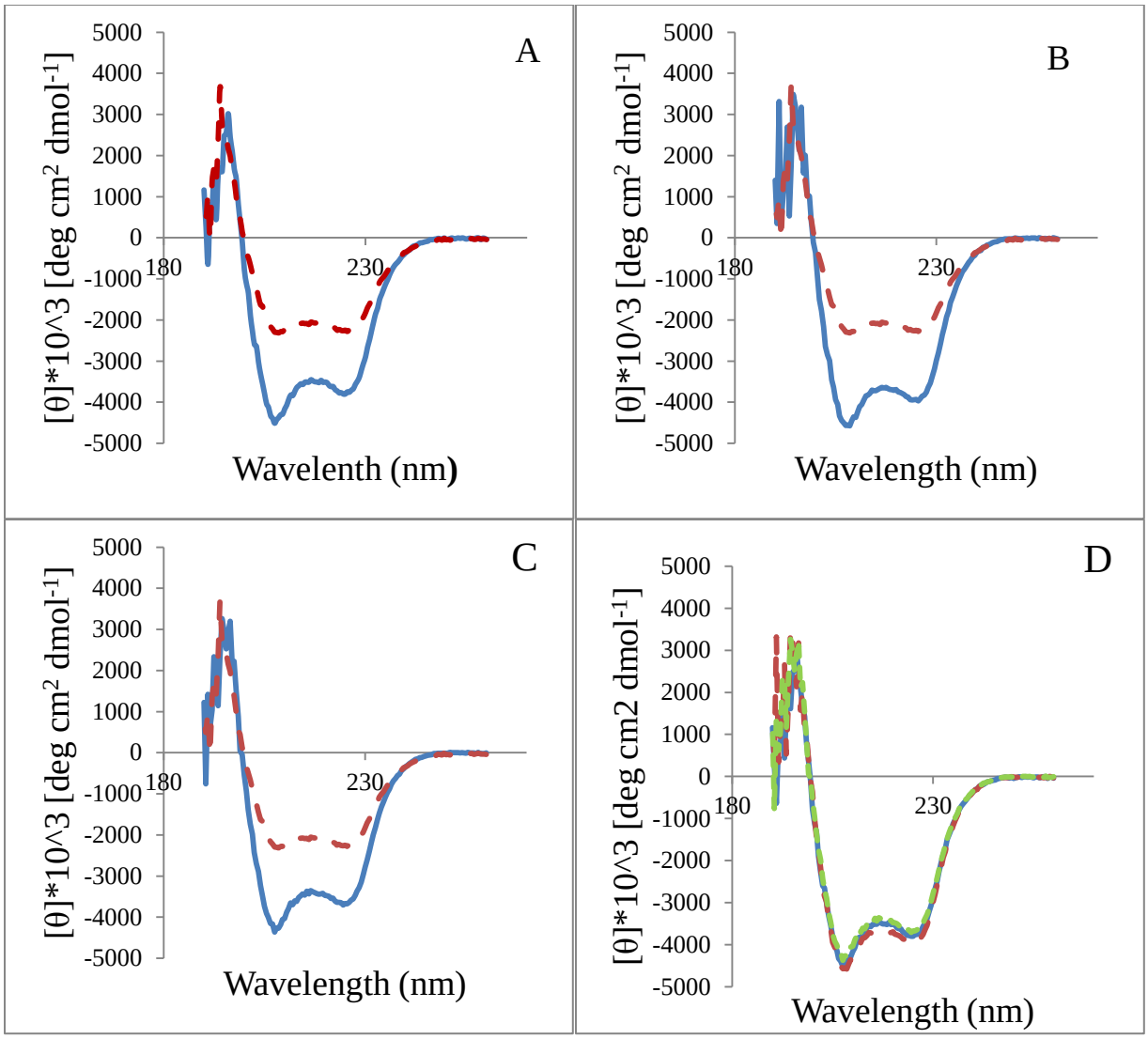

Figure 5.16: Circular dichroism spectra of structural changes in DmsD::DmsAl upon addition of GTP (A), GDP (B) or GMP (C). A. DmsD::DmsAl exposed to GTP. **B.** DmsD::DmsAl exposed to GDP. **C.** DmsD::DmsAl exposed to GMP. **D.** Overlay of the DmsD::DmsAl +GNP spectra. The data was collected at pH 8.0 and in far UV-range (190-220nm) of samples with 3.5 µM concentration of DmsD and 35 µM concentrations of DmsAl and GNP. Normalized spectrum with GNP added (DmsD::DmsAl+GNP) is shown in solid blue line. DmsD::DmsAl complex (red dashed line) is provided for comparison. Complex with GTP is depicted in solid blue, GDP- dashed red and GMP- dotted green line.

Incubated protein would consistently elute together with nucleotide-agarose affinity matrices and demonstrated selective binding to guanine-containing nucleoside phosphates (Schwemmle and Staeheli, 1994).

Our attempt to titrate GTP into DmsD::DmsAl was unsuccessful to generate a binding isotherm. One possible explanation was low affinity of DmsD towards GTP. Guymer et al. reported 340 μM K_D for their TorD, a protein closely related to DmsD (2010) (see section 1.6.2). Another option was that a metal like Mg^{2+} was missing from our experiment. Lastly, there could have been no difference in structural change observed because the protein complex "responds" to the guanosine rather than the phosphate moiety. To test the third hypothesis, we prepared a reaction mixture with sorely a guanosine moiety (no phosphate involved).

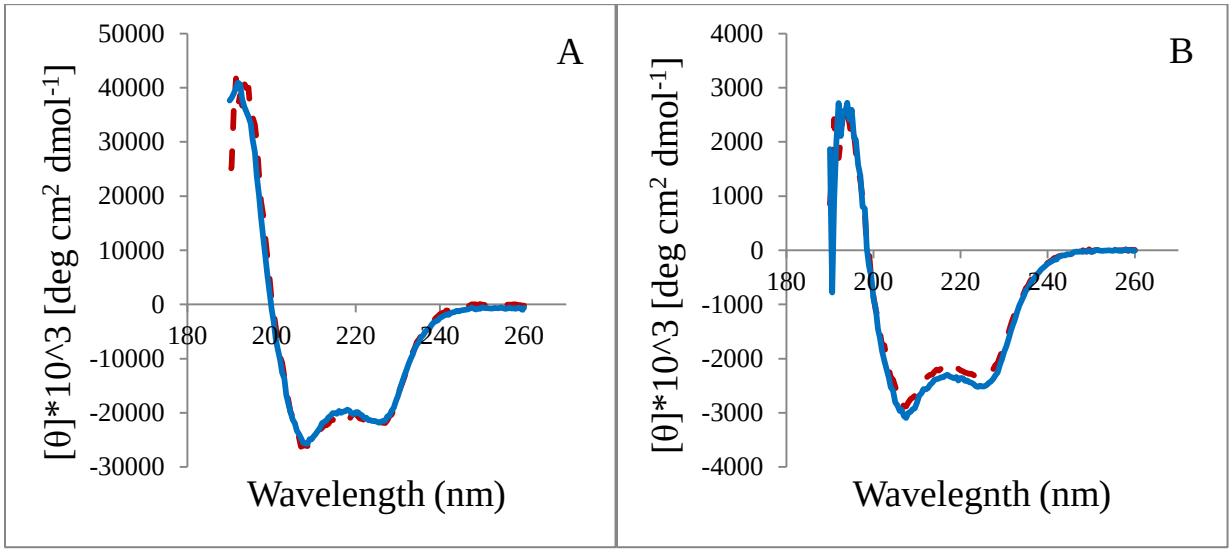

Figure 5.17. Circular dichroism spectra of structural change in DmsD (A) and DmsD::DmsAl (B) upon addition of guanosine. A. DmsD exposed to guanosine. **B.** DmsD::DmsAl complex exposed to guanosine. The data was collected at pH 8.0 and in far UV-range (190-220 nm) of samples with 3.5 μM concentration of DmsD and 35 μM concentrations of DmsAl and guanosine. Normalized spectrum with guanosine added is shown in solid blue line. DmsD (Figure 5.1 A) or DmsD::DmsAl complex (Figure 5.4 B) (red dashed line) is provided for comparison. Shown is an averaged spectrum from 10 scans. Standard error was calculated via standardization method using a replicate of five samples.

In Figure 5.17 we saw no discernible secondary structure conformational change in DmsD or DmsD::DmsAl upon the addition of guanosine base. Based on the absence of change within the secondary structure of DmsD alone and DmsD in complex with DmsAl, the guanosine moiety did not seem to participate in the binding or if it did, there was no secondary structural change.

This data suggested the binding is mediated by the nucleoside and at least one phosphate group as suggested by the earlier GNP experiments.

5.6 Interactions of DmsD and DmsD::DmsAl with metals Mg^{2+}, Mn^{2+} and Ni^{2+}.

5.6.1 Mg^{2+} perturbs secondary structures of DmsD and DmsD::DmsAl, but Mn^{2+} only affects DmsD in complex with the substrate.

It was previously shown that some hydrolysis of GTP happens when $MgCl_2$ is added to the reaction mixture. Before we could check a combination of a GNP and a metal, we had to answer a question if Mg^{2+} alone can affect the secondary structure of DmsD or DmsD::DmsAl. As Mn^{2+} is commonly tested along Mg^{2+} due to its ability to coordinate GTP in a GTPase, we included it in our experiment as well (Rudack et al, 2015).

We found that both metals (Mg^{2+} and Mn^{2+}) led to a change in secondary structure when DmsD associates with DmsAl (Figure 5.18). The total structural changes were comparable to the one caused by the addition of GTP: 12.4 and 16.6%, respectively (see section 5.4). Notably, in the absence of DmsAl, DmsD demonstrated no binding to Mn^{2+}, but had enhanced binding to Mg^{2+}. The total change of the latter was equal to 38.6% and involved 19.3% replacement of helical structure with 10.1% random coil, 6.2% β-sheet and 3% turn.

Metal binding is not unexpected if DmsD is truly a GTPase. As Mondal *et al*. pointed out this metal enhanced the affinity of the protein for the guanine triphosphate and diphosphate (2015). Another possible role of the metal in the following complex is guiding the substrate towards its binding site similar to ARD, a metalloenzyme that binds Ni^{2+} (Pochapsky et al, 2002). This could explain why the structural change was greater in the absence of the leader peptide and differed in the breakdown of components in that the metal "prepares" DmsD for association with the ligand.

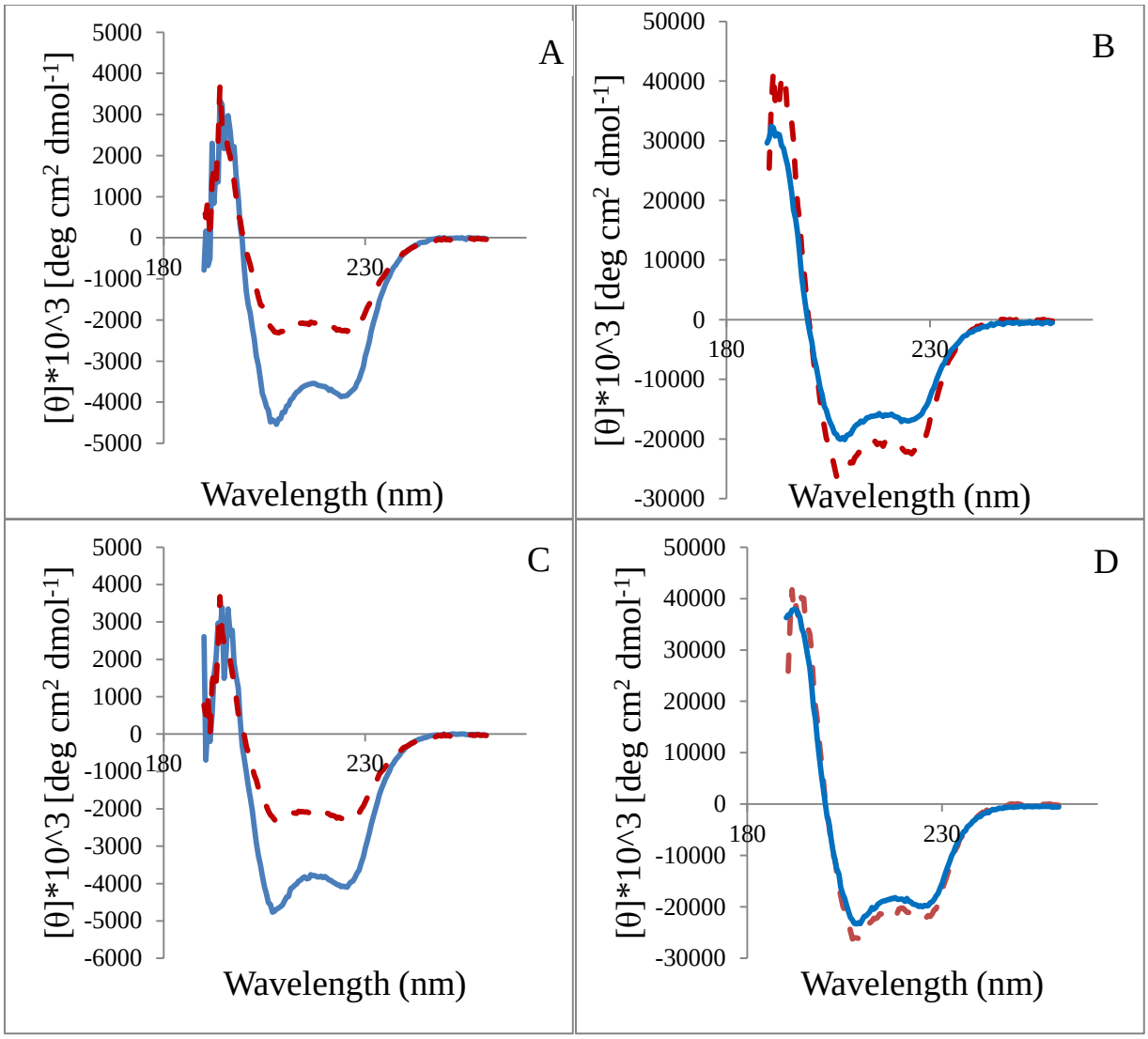

Figure 5.18. Circular dichroism spectra of structural change in DmsD::DmsAl (A, C) and DmsD (B, D) upon addition of Mg^{2+} (A, B) or Mn^{2+} (C, D) metal. A. DmsD::DmsAl exposed to Mg^{2+}. **B.** DmsD::DmsAl complex exposed to Mn^{2+}. **C.** DmsD exposed to Mg^{2+}. **D.** DmsD exposed to Mn^{2+}. The data was collected at pH 8.0 and in far UV-range (190-220 nm) of samples with 3.5 µM concentration of DmsD and 35 µM concentrations of DmsAl and metals. Normalized spectrum with metal added is shown in solid blue line. DmsD or DmsD::DmsAl complex (red dashed line) is provided for comparison. Shown is an averaged spectrum from 10 scans. Standard error was calculated via standardization method using a replicate of five samples.

5.6.2 Ni^{2+} may affect the secondary structure of DmsD::DmsAl complex.

As our DmsD protein was a recombinant product bearing a histidine tag, we needed to test nickel along with other metals. We wanted to determine if Ni^{2+} caused changes in the secondary structure of DmsD or DmsD:DmsAl complex. Ideally, we would see no structural change and this metal would be considered our control.

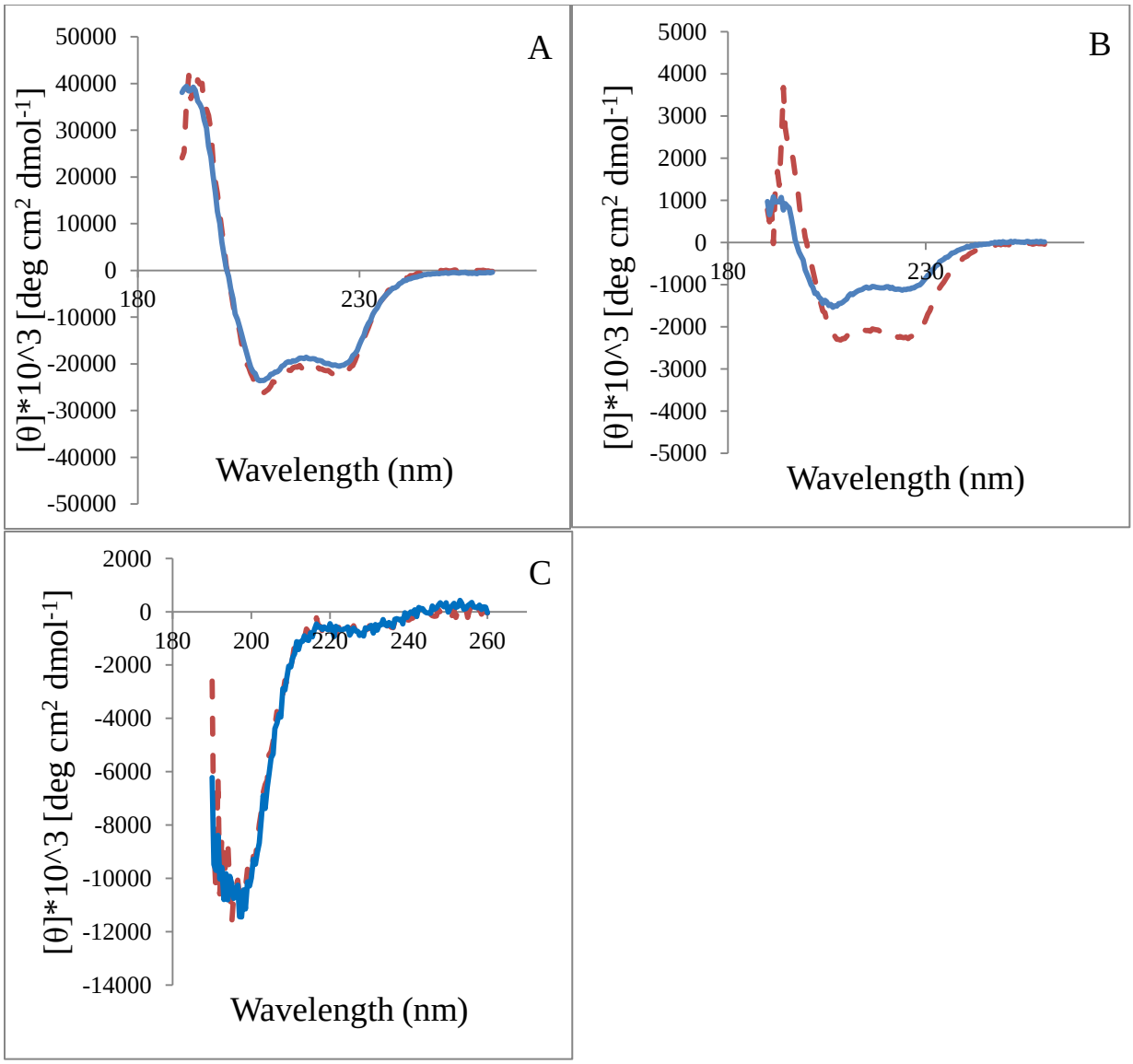

Figure 5.19 DmsD::DmsAl binds Ni^{2+}. A. DmsD exposed to Ni^{2+}. **B**. DmsD::DmsAl exposed to Ni^{2+}. **C.** DmsAl exposed to Ni^{2+}. Circular dichroism data was collected at pH 8.0 and in far UV-range (190-220 nm) of samples with 3.5 µM concentration of DmsD and 35 µM concentrations of DmsAl and metal. Normalized spectrum with Ni^{2+} added is shown in solid blue line. DmsD or DmsD::DmsAl complex (red dashed line) is provided for comparison.

As can be seen from Figure 5.19 A and B, nickel led to structural changes only if DmsAl was present: total change was equal to 8% with a loss of 4% α-helix and gain of 3.7% β-sheet. Therefore, histidine tag either produced a false positive signal for the whole protein::peptide or DmsD::DmsAl complex was truly affected by the addition of Ni^{2+}. If the latter was true, two events were possible: metal led to conformational changes within the complex or it was the leader peptide that interacted with Ni^{2+}. We tested the second case by running a sample in the absence of DmsD. Figure 5.19 C shows that this Ni^{2+} had no influence on DmsAl and, thus, it was either the interaction between the metal and the DmsD::DmsAl or the tag-to-metal binding. At this point we had tested six different permutations with three metals and the effect is summarized in Table 5.2.

Table 5.2. Presence/absence of a secondary structure change within DmsD or DmsD::DmsAl complex upon addition of a metal.

	Mg^{2+}	Mn^{2+}	Ni^{2+}
DmsD	Present	Absent	Absent
DmsD::DmsAl	Present	Present	Present

While addition of Mg^{2+} yielded a signal in both cases (DmsD and DmsD::DmsAl) and Ni^{2+} only caused conformation changes when combined with REMP::substrate, we sought to investigate how the "control" metal (Ni^{2+}) behaved compared to magnesium. Therefore, we compared CD profiles of reaction mixtures with Mg^{2+}/Ni^{2+} and DmsD::DmsAl (Figure 5.20).

A small difference in magnitude was observed: 12.4% (+Mg^{2+}) versus 8% (Ni^{2+}). Moreover, the general trend was opposite for Mg where α-helix replaced β-sheet and turn. It may be speculated that the two metals are both present during the interaction of DmsD with DmsAl, but have different roles. Yang *et al*. reported that addition of Mg^{2+} increased the affinity of UreG, a

GTPase that installs nickel into apo-urease, for the Ni^{2+} 10-fold. Moreover, Mg^{2+} together with GTP were essential for assembly of two hetero-dimers into an active complex (Yang et al, 2015).

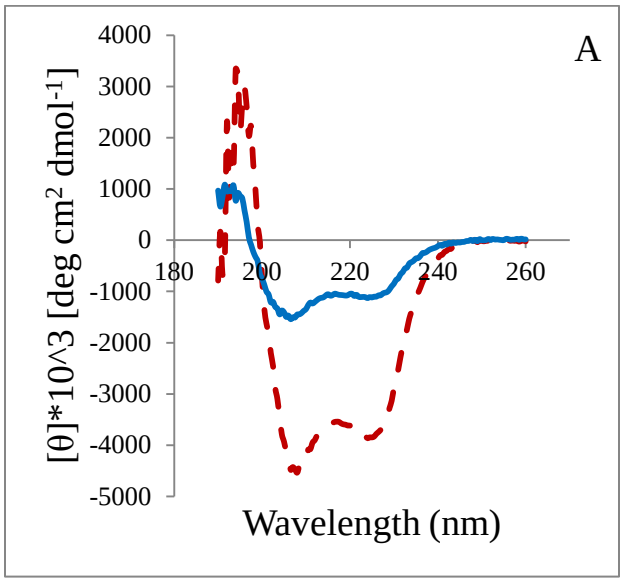

Figure 5.20. DmsD::DmsAl binds to Ni and Mg metals differently. A. Overlay of the DmsD::DmsAl +metal. Complex with Mg^{2+} is depicted in dashed red and Ni^{2+}-solid blue line. Circular dichroism data was collected at pH 8.0 and in far UV-range (190-220 nm) of samples with 3.5 µM concentration of DmsD and 35 µM concentrations of DmsAl and metal. Normalized spectrum with Ni^{2+} added is shown in solid blue line.

5.7 Interactions of DmsD and DmsD::DmsAl with a combination of metal ion and GNP

Here the addition of metals ions of Mg^{2+}, Mn^{2+} and Ni^{2+} along with the nucleotides GTP, GDP and GMP will be discussed.

5.7.1 No difference exists in the observed effect from GNP, Mg^{2+} metal or their combination on DmsD::DmsAl complex

Our next step was to explore the effect of a GNP and an Mg^{2+} metal together. Therefore, we asked the following question- is there any structural change in DmsD::DmsAl complex caused by addition of GTP/GDP/GMP together with Mg^{2+} metal?

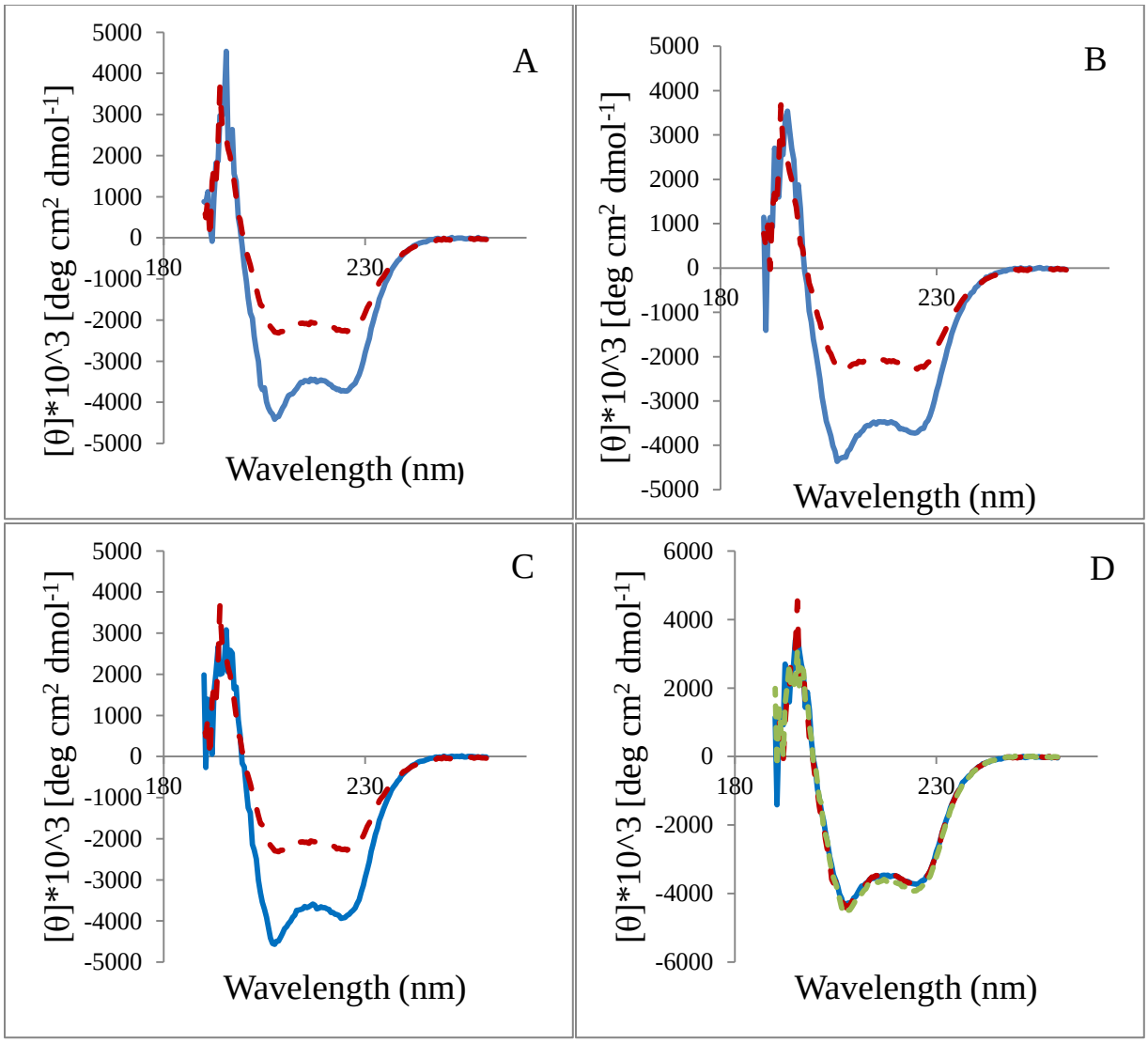

Figure 5.21. Circular dichroism spectra of structural change in DmsD::DmsAl upon addition of GTP (A), GDP (B) or GMP(C) and Mg^{2+} metal. A. DmsD::DmsAl exposed to GTP and Mg^{2+}. **B.** DmsD::DmsAl exposed to GDP and Mg^{2+}. **C.** DmsD::DmsAl exposed to GMP and Mg^{2+}. **D.** Overlay of the DmsD::DmsAl +GNP and Mg^{2+}metal. Complex with is GTP depicted in solid blue line, GDP-dashed red line, GMP-dotted green line. The data was collected at pH 8.0 and in far UV-range (190-220 nm) of samples with 3.5 µM concentration of DmsD and 35 µM concentrations of DmsAl, metal and GNP. Normalized spectrum with GNP and Mg^{2+} is shown in solid blue line. DmsD::DmsAl complex (red dashed line) is provided for comparison.

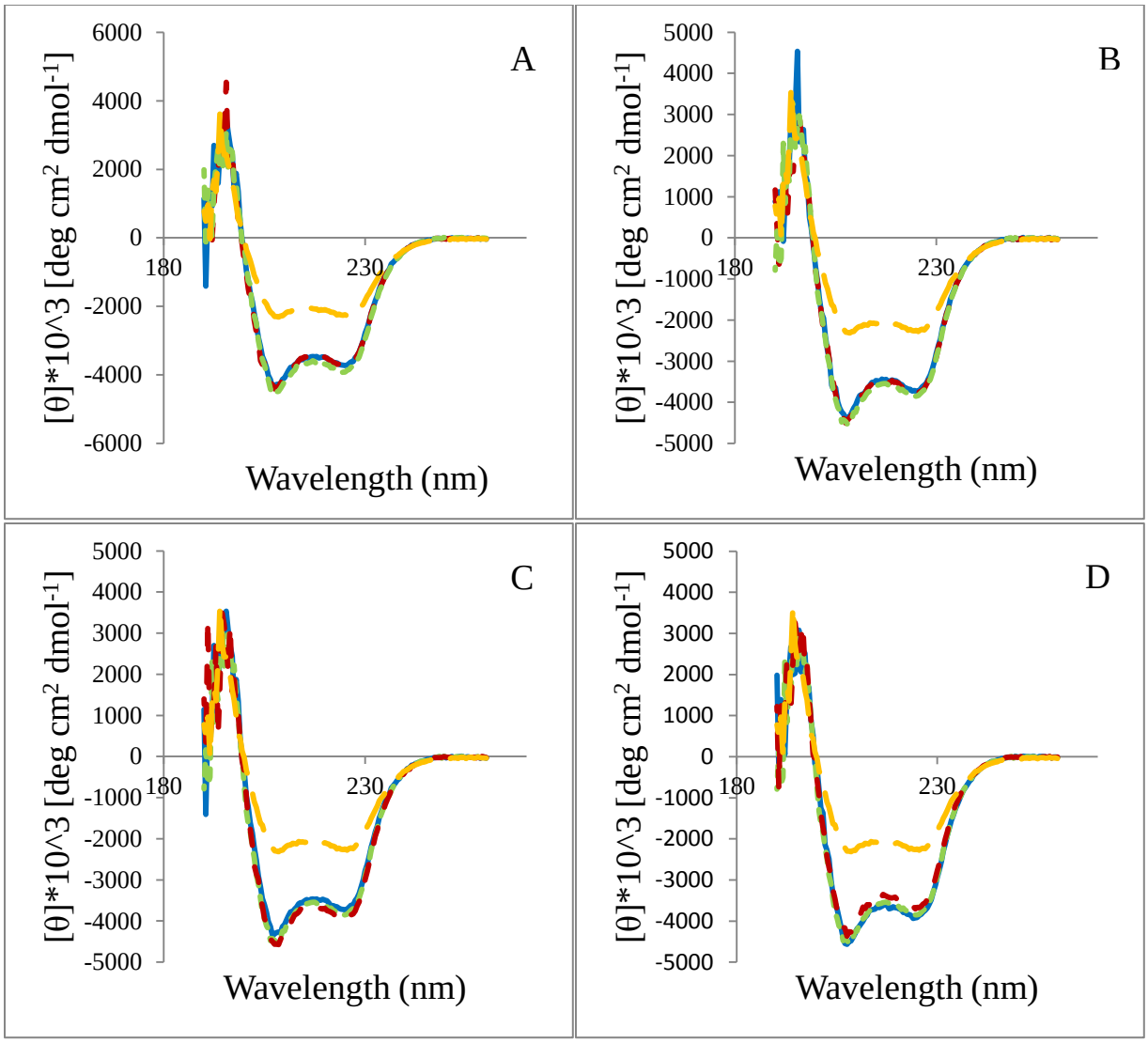

Figure 5.22. Circular dichroism spectra of structural change in DmsD::DmsAl upon addition of GNP, Mg^{2+} or GNP with Mg^{2+} metal. A. Overlay of the DmsD::DmsAl +GNP and Mg^{2+}metal. Complex with is GTP depicted in solid blue line, GDP-dashed red line, GMP-dotted green line. No effector (original DmsD::DmsAl complex) - dashed orange line. **B.** Overlay of the DmsD::DmsAl +GTP and/or Mg^{2+}. Complex with is GTP and Mg^{2+} depicted in solid blue line, GTP only -dashed red line, Mg^{2+} only-dotted green line. No effector (original DmsD::DmsAl complex) - dashed orange line. **C**. Overlay of the DmsD::DmsAl +GDP and/or Mg^{2+}. Complex with is GDP and Mg^{2+} depicted in solid blue line, GDP only-dashed red line, Mg^{2+} only-dotted green line. No effector (original DmsD::DmsAl complex) - dashed orange line. **D.** Overlay of the DmsD::DmsAl +GMP and/or Mg^{2+}. Complex with is GMP and Mg^{2+} depicted in solid blue line, GMP only-dashed red line, Mg^{2+} only-dotted green line. No effector (original DmsD::DmsAl complex) - dashed orange line. The data was collected at pH 8.0 and in far UV-range (190-220 nm) of samples with 3.5 µM concentration of DmsD and 35 µM concentrations of DmsAl, metal and GNP.

As seen in Figure 5.21, all three combinations led to almost identical alteration of DmsD::DmsAl conformational structure. The total structural change determined by the Jasco Software varied between 11.4% and 14.4%. As in the case of GNP alone, percentages for gained helical component (5-5.7%) closely overlapped the decreased β-sheet (5.2-5.9%), while the increases in turn (0.7-1.5%) coincided with loss in random coil (0.5-1.9%). In Figure 5.22, we compared the difference in effects of the metal alone, GNP alone or the metal with GNP on the secondary structure of the DmsD::DmsAl complex. While the structural change took place within DmsD::DmsAl complex, the signals largely overlapped with each other. No difference was observed in the presence of just GTP/GDP/GMP with the metal compared to just GNP or just Mg^{2+}.

5.7.2 Combination of GNP with Mn^{2+} is no different to a change caused by two of those molecules added alone.

Similarly, to Mg^{2} we investigated Mn^{2+} metal. We wanted to know if any structural change in DmsD::DmsAl complex is caused by addition of GTP/GDP/GMP together with Mn^{2+} metal. As seen in Figure 5.23, all three combinations led to an alteration of DmsD::DmsAl conformational structure. The greatest total change was observed in case of GTP where it was equal to 19.4%. Importantly, it was the only one of the three GNPs that led to a loss in random coil.

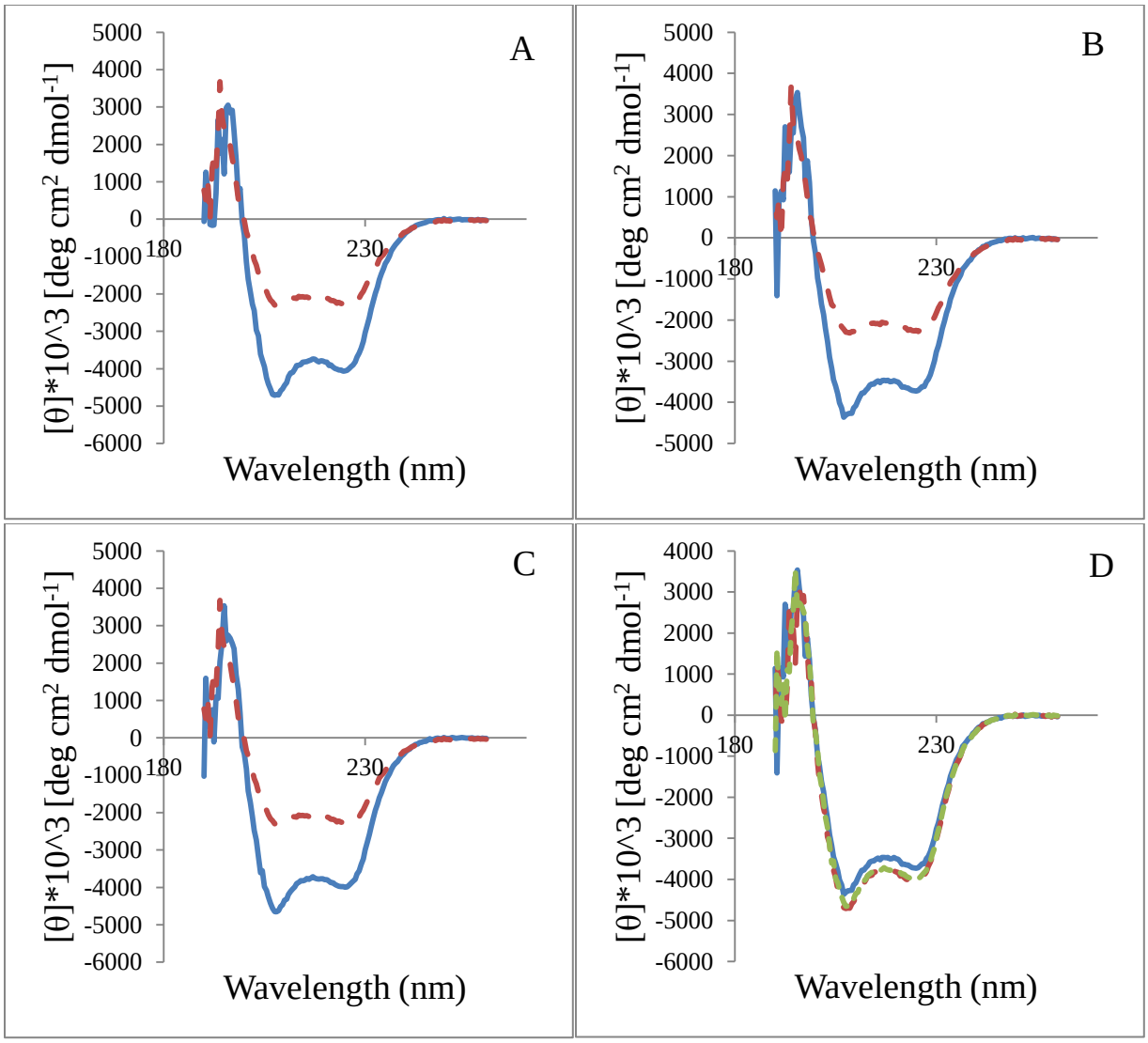

Figure 5.23. Circular dichroism spectra of structural change in DmsD::DmsAl upon addition of GTP(A), GDP (B) or GMP(C) and Mn^{2+} metal. A. DmsD::DmsAl exposed to GTP and Mn^{2+}. **B.** DmsD::DmsAl exposed to GDP and Mn^{2+}. **C.** DmsD::DmsAl exposed to GMP and Mn^{2+}. **D.** Overlay of the DmsD::DmsAl +GNP and Mn^{2+}metal. Complex with is GTP depicted in solid blue line, GDP-dashed red line, GMP-dotted green line. The data was collected at pH 8.0 and in far UV-range (190-220 nm) of samples with 3.5 µM concentration of DmsD and 35 µM concentrations of DmsAl, metal and GNP. Normalized spectrum with GNP and Mn^{2+} is shown in solid blue line. DmsD::DmsAl complex (red dashed line) is provided for comparison.

Next we explored whether there was a difference between adding just the metal or just the guanosine nucleotide (Figure 5.24).

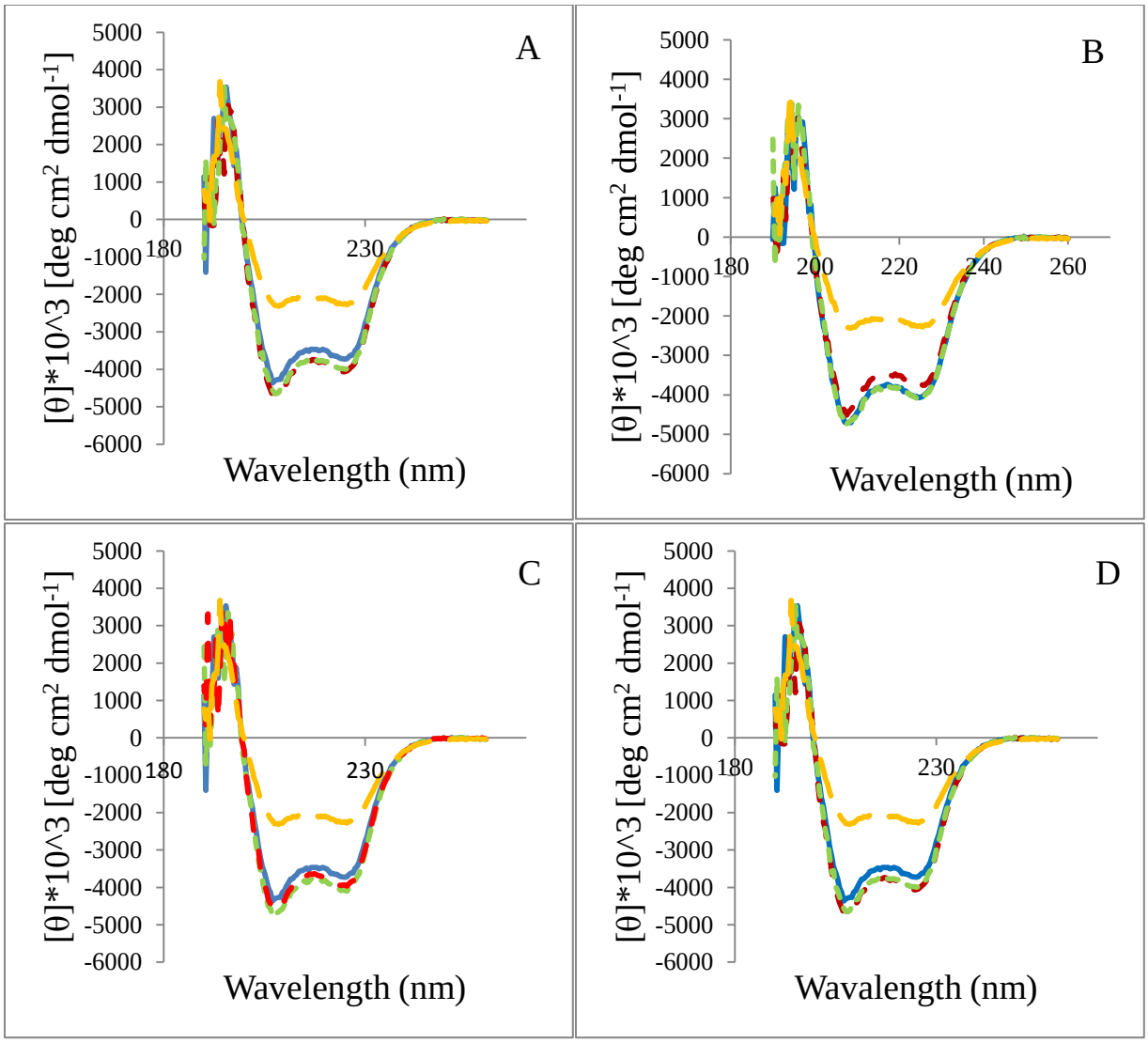

Figure 5.24. Circular dichroism spectra of structural change in DmsD::DmsAl upon addition of GNP, Mn^{2+} or GNP with Mn^{2+} metal. A. Overlay of the DmsD::DmsAl +GNP and Mn^{2+}metal. Complex with is GTP depicted in solid blue line, GDP-dashed red line, GMP-dotted green line. No effector (original DmsD::DmsAl complex) - dashed orange line. **B.** Overlay of the DmsD::DmsAl +GTP and/or Mn^{2+}. Complex with is GTP and Mn^{2+} depicted in solid blue line, GTP only -dashed red line, Mn^{2+} only-dotted green line. No effector (original DmsD::DmsAl complex) - dashed orange line. **C.** Overlay of the DmsD::DmsAl +GDP and/or Mn^{2+}. Complex with is GDP and Mn^{2+} depicted in solid blue line, GDP only-dashed red line, Mn^{2+} only-dotted green line. No effector (original DmsD::DmsAl complex) - dashed orange line. **D.** Overlay of the DmsD::DmsAl +GMP and/or Mn^{2+}. Complex with is GMP and Mn^{2+} depicted in solid blue line, GMP only-dashed red line, Mn^{2+} only-dotted green line. No effector (original DmsD::DmsAl complex) - dashed orange line. The data was collected at pH 8.0 and in far UV-range (190-220 nm) of samples with 3.5 µM concentration of DmsD and 35 µM concentrations of DmsAl, metal and GNP.

The impression from the spectra was that there are only minor differences in signal of GNP+metal versus GNP or Mn^{2+} metal alone only existed. However, standard error calculated using a factor obtained from five replicates of a sample displayed that no significant difference existed between any of the combinations depicted in Figure 5.24.

5.7.3 GTP combined with Ni^{2+} leads to a minor structural change

The last combination to consider was GNP with Ni^{2+}added. While the structural change was taking place in all three cases (Figure 5.25 A, B and C), combination of Ni^{2+} with GMP yielded a signal that was slightly weaker compared to GTP and GDP. Nevertheless, the total changes were almost identical: 17.6% for GTP and GMP and 18% for GDP.

As with Mg^{2+} and Mn^{2+}, we compared the secondary structure difference between just the metal or GTP/GDP/GMP and the combination of the two. The change in secondary structure was different in cases of GTP alone versus metal alone versus GTP combined with Ni^{2+}. However, there was no difference between GDP/GMP and GDP/GMP combined with metal based on the standard error of five replicates (data not shown). The total structural change in the case of just Ni^{2+} was much smaller than when combined with a nucleotide: 8% compared to 17.6% (GTP with the metal) compared to 15.6% (GTP alone). The data suggested that the nucleotide and Ni combined intensified the effect of GTP.

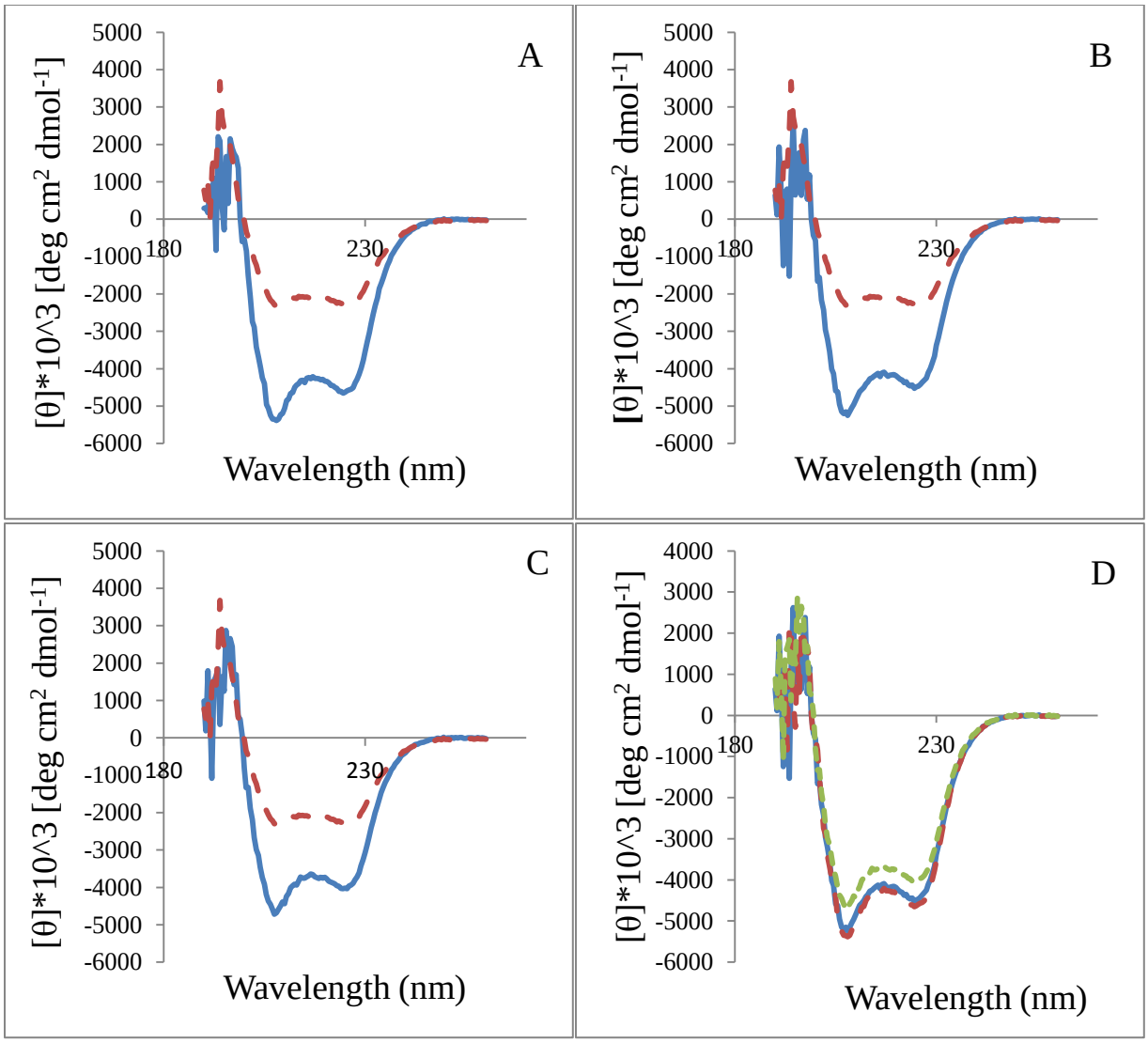

Figure 5.25. Circular dichroism spectra of structural change in DmsD::DmsAl upon addition of GTP(A), GDP (B) or GMP(C) and Ni^{2+}. A. DmsD::DmsAl exposed to GTP and Ni^{2+}. **B.** DmsD::DmsAl exposed to GDP and Ni^{2+}. **C.** DmsD::DmsAl exposed to GMP and Ni^{2+}. **D.** Overlay of the DmsD::DmsAl +GNP and Ni^{2+}metal. Complex with is GTP depicted in solid blue line, GDP-dashed red line, GMP-dotted green line. The data was collected at pH 8.0 and in far UV-range (190-220 nm) of samples with 3.5 μM concentration of DmsD and 35 μM concentrations of DmsAl, metal and GNP. Normalized spectrum with GNP and Ni^{2+} is shown in solid blue line. DmsD::DmsAl complex (red dashed line) is provided for comparison.

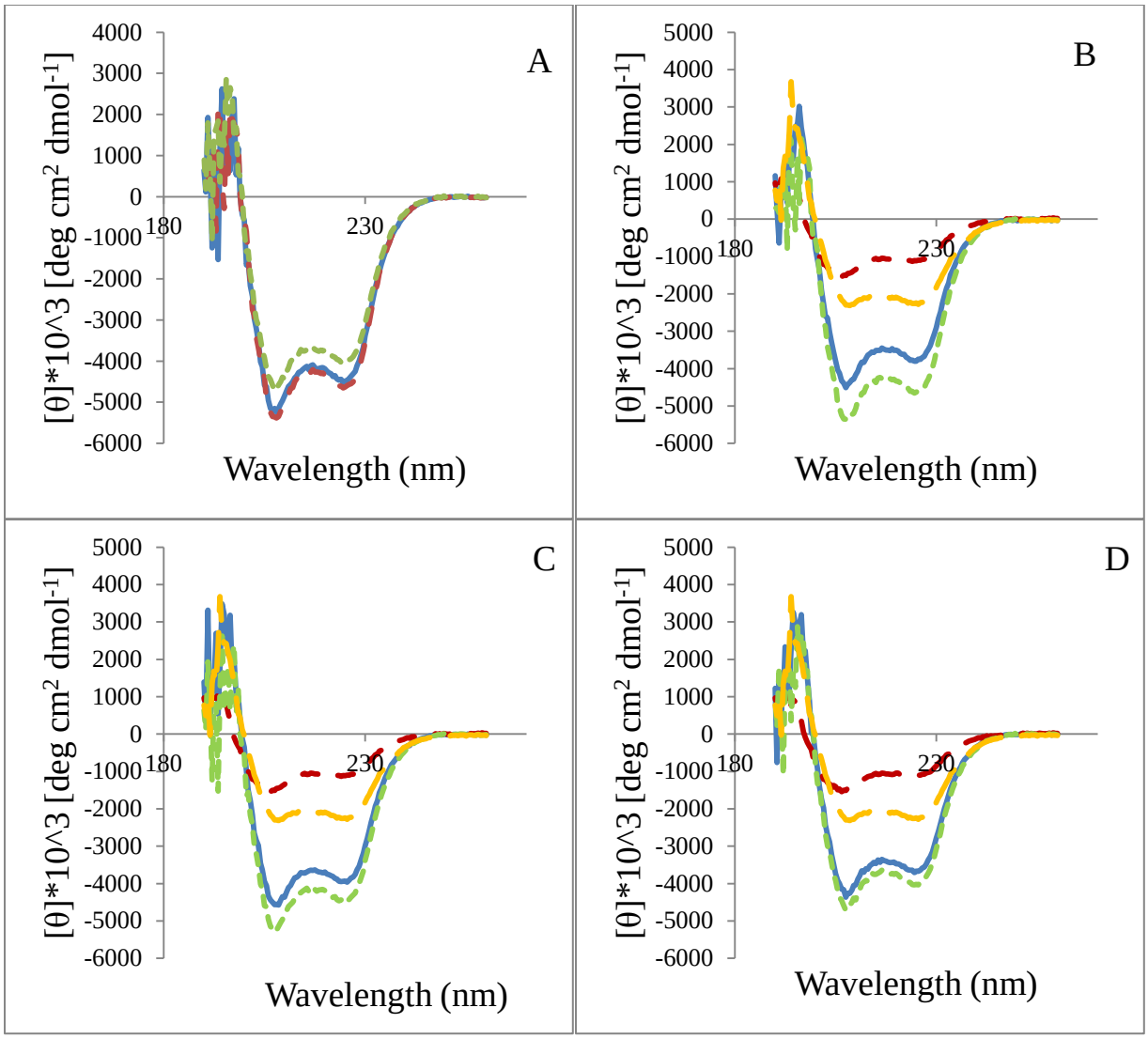

Figure 5.26. Circular dichroism spectra of structural change in DmsD::DmsAl upon addition of GNP, Ni^{2+} or GNP with Ni^{2+} metal. A. Overlay of the DmsD::DmsAl +GNP and NI^{2+}metal. Complex with is GTP depicted in solid blue line, GDP-dashed red line, GMP-dotted green line. **B.** Overlay of the DmsD::DmsAl +GTP and/or Ni^{2+}. Complex with is GTP and Ni^{2+} depicted in solid blue line, GTP only -dashed red line, Ni^{2+} only-dotted green line. No effector (original DmsD::DmsAl complex) - dashed orange line. **C.** Overlay of the DmsD::DmsAl +GDP and/or Ni^{2+}. Complex with is GDP and Ni^{2+} depicted in solid blue line, GDP only-dashed red line, Ni^{2+} only-dotted green line. No effector (original DmsD::DmsAl complex) - dashed orange line. **D.** Overlay of the DmsD::DmsAl +GMP and/or Ni^{2+}. Complex with is GMP and Ni^{2+} depicted in solid blue line, GMP only-dashed red line, Ni^{2+} only-dotted green line. No effector (original DmsD::DmsAl complex) - dashed orange line. The data was collected at pH 8.0 and in far UV-range (190-220 nm) of samples with 3.5 μM concentration of DmsD and 35 μM concentrations of DmsAl, metal and GNP.

5.8 Influence of GTP on DmsD::TatB complex

Similar to an experiment involving DmsAl peptide, we tested GTP influence on the secondary structure of DmsD::TatB (1, 2 or 3) complex.

At pH 7.0 addition of GTP had a significant influence on CD signal of DmsD::TatB which decreased in intensity for all three complexes (data not shown). The total secondary structure change for DmsD::TatB1 was 8% with 3.1% helix and 0.9% random coil being lost to 3.9% sheet and 0.1% turn. The absolute change for DmsD::TatB2 was greater (14.6%) with a slightly different breakdown of secondary structures: loss of 6.2% helix and 1.1% random coil and a gain of 5.9% sheet and 1.4% turn. In case of DmsD::TatB3, the total structural change was slightly decreased compared to DmsD::TatB2 peptide, yet greater then DmsD::TatB1: 12%. Nevertheless, the trend remained with the decrease in helix and an increase in β-sheet with percentages closely overlapping.

At pH 8.0 the magnitude of signal of the DmsD::TatB (1, 2 or 3) complex to GTP was similar to the one at pH 7.0 (Figure 5.27 A, B). The absolute structural change for each of the three peptides was as follows: 10.2%, 23.2% and 7%. Again, a loss in α-helical and a gain in β-sheet structures were observed. Interestingly, the ratio of random coil to turn was almost always 1:1 which implies that one type of secondary structure was replacing another.

We decided to reverse the order of effectors addition and start with GTP instead of the TatB peptide. At this point of the project, TatB2 peptide demonstrated strongest signals. As a result, we decided to test it at pH 8.0. We noted that the order of addition of TatB versus GTP seemed to matter. By comparing the changes in the secondary structure of DmsD::TatB2 and DmsD::GTP, we deduced that order of addition of ligands to DmsD played a significant role.

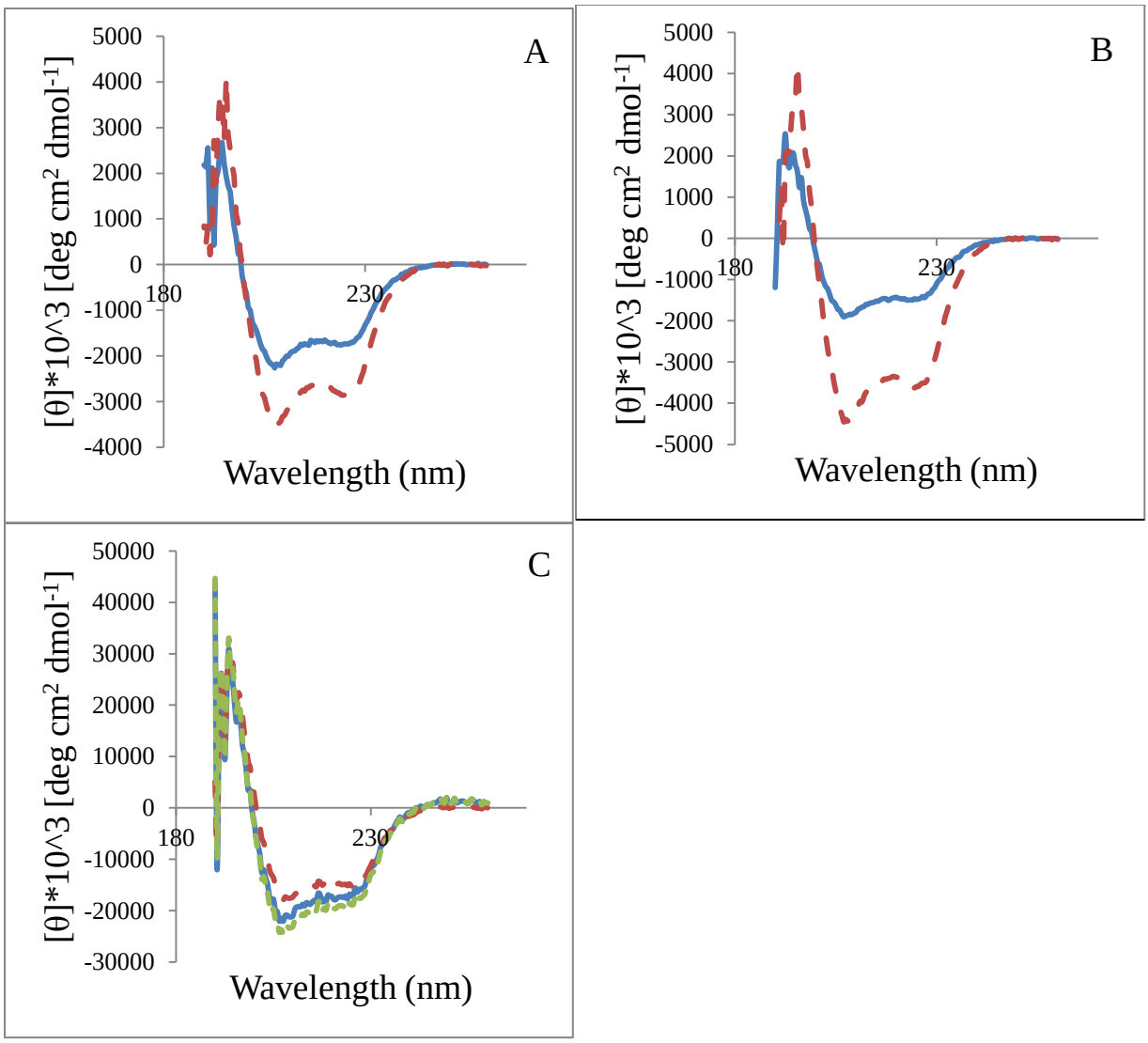

Figure 5.27. Order of addition of GTP to TatB to DmsD matters. A. DmsD::TatB1 exposed to GTP. **B.** DmsD::TatB2 exposed to GTP. **C.** DmsD::GTP exposed to TatB2. Circular dichroism data was collected at pH 8.0 and in the far-UV range (190-260 nm) of samples with 3.5 μM concentration of DmsD and 35 μM TatB peptide, GTP. **For A and B**: normalized spectrum of DmsD::TatB with GTP added is shown in solid blue line. DmsD::TatB complex (red dashed line) is provided for comparison. **For C**: normalized spectrum where spectra of DmsD::GTP and TatB2 peptide alone were subtracted from experimental data is shown in solid blue line (DmsD+TatB2-(DmsD::TatB2)). DmsD protein alone (red dashed line) is provided for comparison. Theoretical combination of DmsD (see Figure 5.1 A) and TatB1 peptide spectra (see Figure 5.1 B) is depicted in dotted green line.

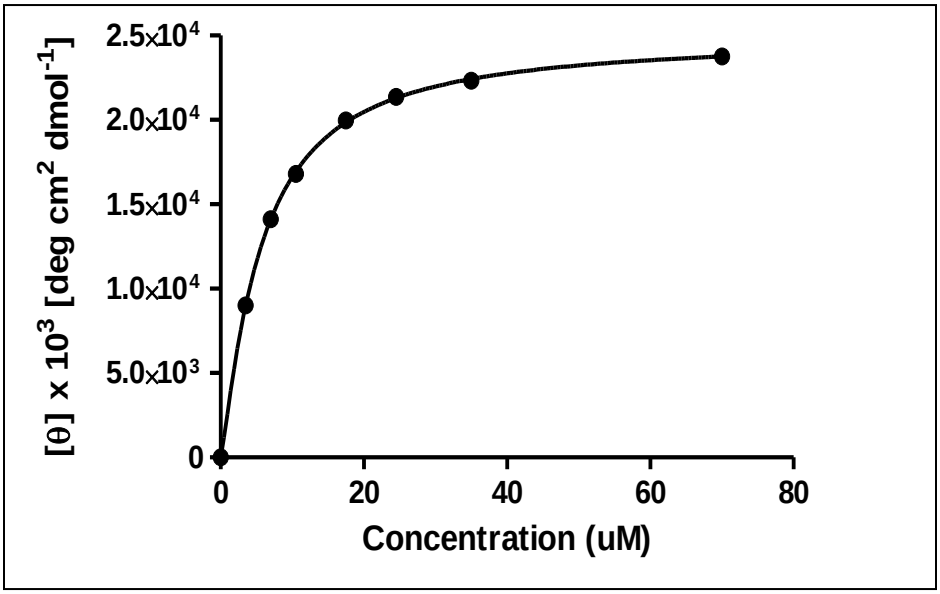

Figure 5.28. DmsD::TatB2 binding curve titrated with GTP at pH 8.0. The circular dichroism spectrum was collected in the far-UV range (190-260 nm) at different concentrations and normalized. Molar ellipticity at 222 nm was plotted versus the concentration of GTP. The dissociation constant was obtained using GraphPad Prism 5 via the one site/specific binding with Hill slope nonlinear fit. Best-fit for Hill slope was equal to 1.2.

Introduction of GTP into DmsD::TatB protein-peptide mix led to considerable conformational change (5.27 A, B), but the reverse step (DmsD::GTP+ TatB2 peptide) did not result in any structural alteration (5.27 C). A very minor difference between normalized (solid blue) and combined (dotted green) data was observed. It may be speculated that GTP "blocks" structural change caused by the addition of TatB. If this is true, two outcomes are possible: either TatB peptide is not able to bind to DmsD::GTP or the binding happens, but with no conformational change. Ray *et al*. recently reported a similar GTP regulation mechanism for a cytokinetic Z-ring formation in bacterial cell division (2013). High GTP concentration prevents binding of MciZ peptide to FtsZ and, thus, allows for successful polymerization and hydrolysis (Ray et al, 2013). Next, we performed a GTP titration to determine what is the K_d for GTP binding to DmsD::TatB2 at pH 8.0 (Figure 5.28). The dissociation constant was found to be equal to 5.60 μM, which was quite similar to 5.40 μM, a K_d obtained from titration of TatB2 into DmsD (section 5.2).

5.9. Adding three different DmsD ligands together helps identify a single potentially-existing complex (DmsD::TatB::GTP) that changes the secondary structure due to DmsAl present.

Having explored the relationship between three molecules at once, we asked if it would be possible to obtain any information from a reaction mixture of four (DmsD, DmsAl, TatB and GTP). As a result, we sought to study how addition of the last one influenced the existing complex. Here we assumed that three previously combined components were interacting when the fourth one was added.

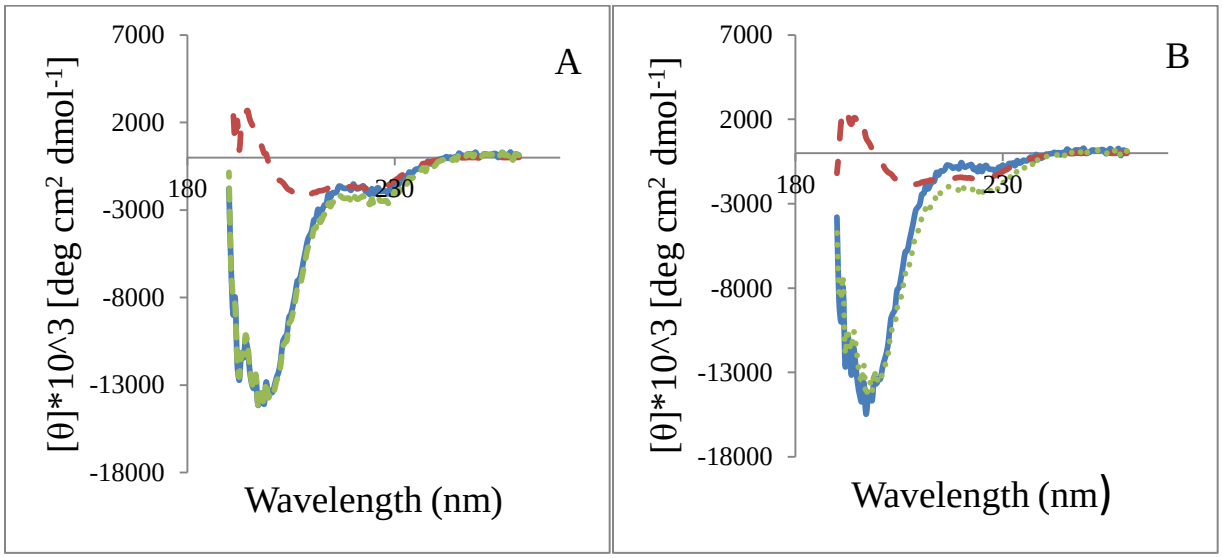

Figure 5.29. Circular dichroism spectra of structural changes in DmsD::TatB(1/2)::GTP upon addition of DmsAl. A. DmsD::TatB1::GTP exposed to DmsAl. **B.** DmsD::TatB2::GTP exposed to DmsAl. The data was collected at pH 8.0 and in far UV-range (190-220 nm) samples with 3.5 μM concentration of DmsD and 35 μM concentrations of TatB, DmsAl and GTP. Normalized spectrum where spectra of DmsD::TatB::GTP was subtracted from experimental data is shown in solid blue line (DmsD::TatB::GTP +DmsAl-(DmsD::TatB::GTP)). DmsD::TatB::GTP complex (red dashed line) is provided for comparison. Theoretical combination of DmsD::TatB::GTP and DmsAl (see Figure 5.1D) is depicted in dotted green line.

We were interested whether the fourth component added altered the structure of the complex.

We started with evaluation of DmsAl peptide influence and obtained a signal only when TatB2 peptide was employed (one of the three components present prior the addition of DmsAl). Both TatB1 and TatB3 (Figure 5.29 A for TatB1) yielded signals which partially overlapped mathematical summation and complex without DmsAl. The total structural change at pH 7.0 was 10.2%, while at pH 8.0- 14.8%. The β-sheet component was the only one that decreased at both pH values.

Neither addition of TatB, nor GTP changed the secondary structure of the DmsD::DmsAl::third component assembly (data not shown). Several explanations are possible. One reason is that no complex of three (DmsD::TatB::DmsAl or DmsD::DmsAl::GTP) existed upon addition of the final effector. As a result, introduction of a TatB peptide or guanosine triphosphate did not lead to any change. The second possible reason – quaternary complex that had formed was no different from its predecessor in terms of secondary structure components. Nevertheless, the following results suggested that we were not dealing with a situation where TatB2 or GTP leads to a dissociation of the complex or any major structural changes that might take place prior the translocation event.

Discussion.

In this chapter we utilized circular dichroism to better understand conformational changes within the structure of DmsD and DmsD::DmsAl complex when effectors such as TatB peptides, GNP and metals were added. The data is summarized in Table 5.3 and visually represented in Figures 5.30 and 5.31. We also considered the existence of other complexes such as DmsD::GTP and DmsD::TatB and attempted to probe changes in conformation of those as well. Finally, we looked into the potential binding site(s) on DmsD surface for DmsAl and TatB peptides by comparing the data from wild-type and a DmsD variant.

In section 5.2 we found out that only TatB2 resulted in secondary structure change with DmsD. This was consistent at pH 7.0 and 8.0. The peptide data from the CD technique did not perfectly overlap with DSF experiments where it was TatB1 that led to greatest change within the melting profile. It may be suggested that both segments of the TatB protein play important, yet slightly different roles. The following logic would be consistent with Kuzniatsova *et al*. who obtained highest binding for second and third helices of TatB via a Bacterial Two-Hybrid assay and for third and fourth helices from ELISA array assay (2016). In our case TatB1 lies within the second helix and TatB2- includes parts of third and fourth.

Table 5.3. Summary table of conformational changes that took place upon addition of an effector to the protein or the protein complex. Deconvolution was performed via Jasco CD Multivariate Secondary Structure Estimation (SSE) program. "Total change" column represents the amendment achieved from the starting complex.

Protein/ Protein complex	Addition	Total structural change	Breakdown of secondary structure content	K_d	Figure Reference
DmsD	TatB1 peptide	-	-	-	5.2 A, B
DmsD	TatB2 peptide	pH 8.0: 10.6% pH 7.0: 14%	pH 8.0: +4% helix +1.3% sheet -5.3% coil pH 7.0: +6.4% helix +0.6% turn -7% coil	5.40 μM (pH 8.0) 4.70 μM (pH 7.0)	5.2 C, D
DmsD	DmsAl	pH 7.0: 3.4% pH 8.0: 4.4%	pH 7.0: +1.7% helix -1.7% random coil pH 8.0: +1.4% helix +0.8% turn -2.2% random coil	1.89 μM (pH 8.0)	5.4 and 5.5
DmsD::TatB2	DmsAl	pH 7.0: 11.2% pH 8.0: 13.2%	pH 7.0 +2.7% helix +2.9% sheet -1.1% turn -4.5% random coil pH 8.0: +5.5% helix -3.6% sheet +1.1% turn -3% random coil	24.24 μM (pH 8.0)	5.6 and 5.8 A
DmsD::DmsAl	TatB2	pH 7.0: 51.4% pH 8.0: 63.2%	pH 7.0 +22.2% helix -20.5% sheet +3.5% turn	8.88 μM (pH 8.0)	5.7 and 5.8 B

			-5.2% random coil pH 8.0: +27.7% helix -26.6% sheet +3.9% turn -5% random coil		
P86Q DmsD	DmsAl	pH 8.0: 26%	pH 8.0: +1.6% helix -13% sheet +6.6% turn +4.8% random coil	4.27 μM (pH 8.0)	5.9 A and 5.10
P86Q DmsD	TatB2	pH 8.0: 52.2%	pH 8.0: +15% helix -14.7% sheet +11.1% turn +11.4% random coil	5.45 μM (pH 8.0)	5.11 A and 5.12
P86Q DmsD::DmsAl	TatB2	pH 8.0: 56.6%	pH 8.0: +17.3% helix -16.7% sheet +11% turn -11.6% random coil	8.26 μM (pH 8.0)	5.13 D and 5.14 B
P86Q DmsD::TatB2	DmsAl	pH 8.0: 28.8%	pH 8.0: +3.5% helix -14.4% sheet +7% turn +3.9% random coil	24.43 μM (pH 8.0)	5.13 C and 5.14 A
DmsD	guanosine	-	-	-	5.17 A
DmsD	GTP	pH 7.0: 23.8% pH 8.0: 19.4%	pH 7.0: -9.9% helix +11.9% turn -3% random coil pH 8.0: -9.7% helix +8% turn -1.7% random coil	-	5.15
DmsD	Mg^{2+}	38.6%	-19.3% α-helix	-	5.18 C

			+6.2% β-sheet +3% turn +10.1% coil		
DmsD	Mn^{2+}	none	-	-	5.18 D
DmsD	Ni^{2+}	none	-	-	5.19 B
DmsD::DmsAl	GTP	15.6%	+6.1% α-helix -6.5% β-sheet +1.7% turn -1.3% coil		5.16 A
DmsD::DmsAl	GDP	8.4%	+3.8% helix -4.2% sheet +0.4% turn	-	5.16 B
DmsD::DmsAl	GMP	10.2%	+4.4% helix -4.9% sheet +0.7% turn -0.2% coil	-	5.16 C
DmsD::DmsAl	guanosine	none	-	-	5.17 B
DmsD::DmsAl	Mg^{2+}	12.4%	+4.2% helix -6.1% sheet -0.1% turn +2% coil	-	5.18 A
DmsD::DmsAl	Mn^{2+}	16.6%	+6.7% helix -6.4% sheet +1.6% turn -1.9% coil	-	5.18 B
DmsD::DmsAl	Ni^{2+}	8%	-4% helix +3.7% sheet +0.2% turn +0.1% coil	-	5.19 A
DmsAl peptide	Ni^{2+}	none	-	-	5.19 C
DmsD::DmsAl	Mg^{2+}+GTP	12.8%	+5.4% helix -5.9% sheet +1% turn -0.5% coil	-	5.21 A
DmsD::DmsAl	Mg^{2+}+GDP	11.4%	+5% helix -5.2% sheet +0.7% turn -0.5% coil	-	5.21 B
DmsD::DmsAl	Mg^{2+}+GMP	14.4%	+5.7% helix -5.3% sheet +1.5% turn -1.9% coil	-	5.21 C
DmsD::DmsAl	Mn^{2+}+GTP	19.4%	+7.6% helix -7.7% sheet +2.1% turn -2% coil	-	5.23 A

DmsD::DmsAl	Mn^{2+}+GDP	15.2%	+6.5% helix -7.5% sheet +1.1% turn -0.1% coil	-	5.23 B
DmsD::DmsAl	Mn^{2+}+GMP	14.4%	+6.3% helix -7.1% sheet +0.9% turn -0.1% coil	-	5.23 C
DmsD::DmsAl	Ni^{2+}+GTP	17.6%	+7% helix -7.7% sheet +1.8% turn -1.1% coil	-	5.25 A
DmsD::DmsAl	Ni^{2+}+GDP	18%	+7.1% helix -7.4% sheet +1.9% turn -0.6% coil	-	5.25 B
DmsD::DmsAl	Ni^{2+}+GMP	17.6%	+6.6% helix -6.5% sheet +2.2% turn +2.3% coil	-	5.25 C
DmsD::TatB1	GTP	pH 7.0: 8% pH 8.0: 10.2%	pH 7.0: -3.1% helix +3.9% sheet +0.1% turn -0.9% coil pH 8.0: -4.1% helix +5.1% sheet -0.2% turn -0.8% coil	-	pH 7.0: Figure not shown pH 8.0: 5.27 A
DmsD::TatB2	GTP	pH 7.0: 14.6% pH 8.0: 23.2%	pH 7.0: -6.2% helix +5.9% sheet -1.1% turn +1.4% coil pH 8.0 -9.5% helix +8.9% sheet -2.1% turn +2.7% coil	5.60 μM (pH 8.00)	5.27 B and 5.28
DmsD::TatB3	GTP	pH 7.0: 12% pH 8.0: 7%	pH 7.0: -5% helix +6% sheet -0.5% turn	-	Figures not shown

			-0.5% coil pH 8.0: -2.9% helix +3.1% sheet +0.4% turn -0.6% coil		
DmsD::GTP	TatB2	pH 8.0: 39.6%	pH 8.0: +16% helix -2.9% sheet +3.8% turn -16.9% coil	-	5.27 C
DmsD::TatB2::GTP	DmsAl	pH 7.0: 10.2% pH 8.0: 14.8%	pH 7.0: +2.6% helix +2.5% sheet -1.4% turn -3.7% random coil pH 8.0: +6% helix -3.9% sheet +1.4% turn -3.5% random coil	-	pH 8.0: 5.29 B

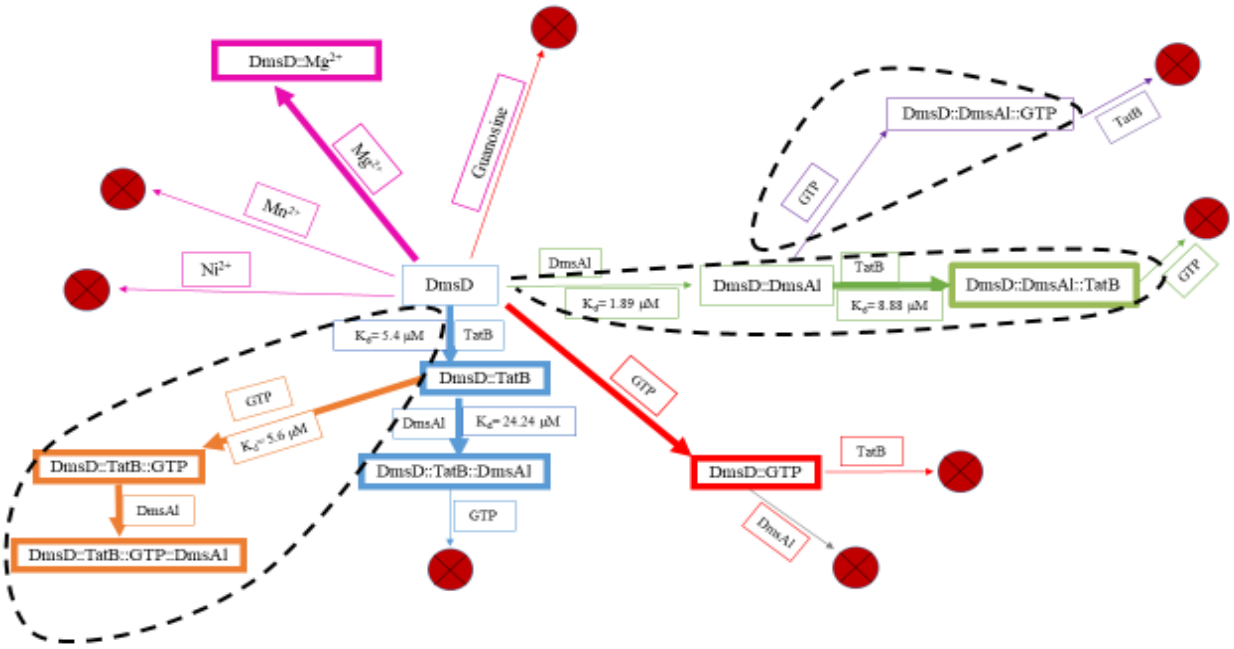

Figure 5.30. Interaction map of DmsD with various ligands. Secondary structure changes greater than 12% are highlighted via thicker arrows. Interactions suspected as biologically-relevant are circled with dashed line and those resulting in no signal change- marked as red X circles.

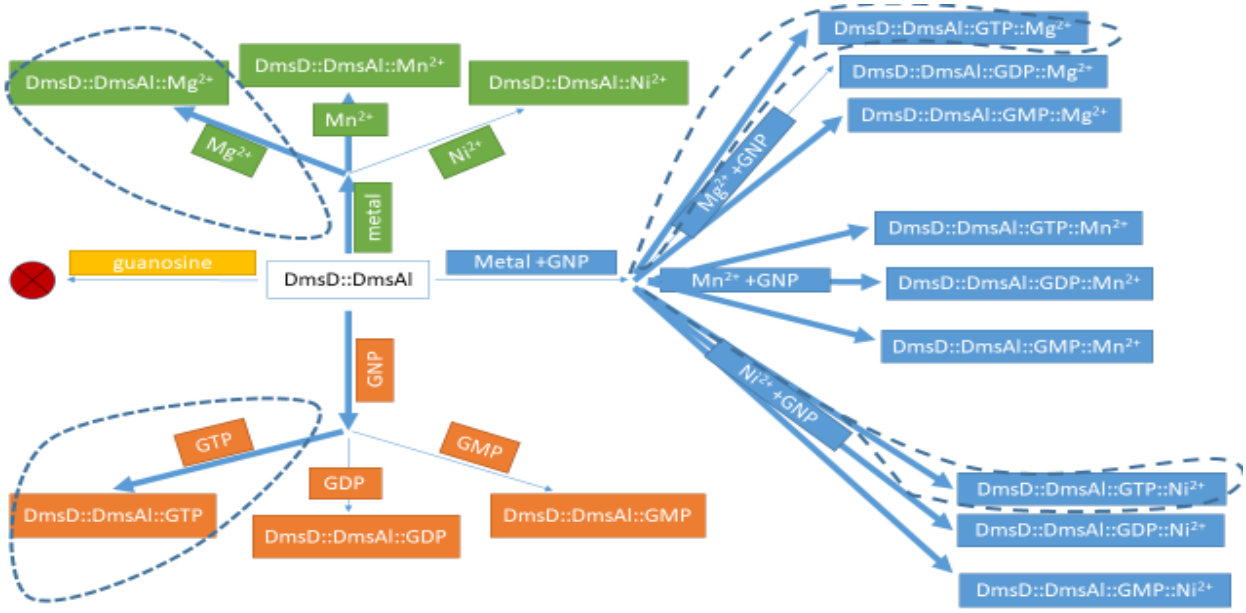

Figure 5.31. Interaction map of DmsD::DmsAl complex with various ligands. Secondary structure changes greater than 12% were highlighted via thicker arrows. Interactions suspected as biologically-relevant are circled with dashed line and those resulting in no signal change- marked as red X circles.

As our obtained K_d for DmsD to DmsAl interaction in section 5.3 was very close to the one previously determined in ITC experiments, this defined that our CD technique and normalization methods yielded reliable results which could be safely utilized for finding other dissociation constants. The difference in K_d for TatB2 with pH relates to a working hypothesis regarding an important role of proton motif force (PMF) for the TAT system (Henry et al, 1997). It is also consistent with the reported strongest binding of DmsAl to DmsD is in the range of pH 5.0 to 6.0 where two *in vitro* protein-protein interaction techniques were utilized (Cherak and Turner, 2017). The interaction between the protein and TatB was also is stronger in the case of lower pH (7.0).

Titrations of TatB2 peptide versus DmsAl peptide into DmsD::DmsAl or DmsD::TatB2 complexes, respectively, demonstrated that dissociation constants are three-fold different with K_d being lower in the case of TatB2 peptide added to the complex. This implies that there is a higher probability of DmsD::DmsAl complex to interact with the TatB. That would be consistent with previously suggested translocation model where the chaperone targets its cargo towards the translocation machinery and transfers DmsAl to TatBC (Cherak and Turner, 2017).

Mutation of proline 86 to glutamine was shown to decrease the affinity of DmsD towards the DmsA leader peptide by two-fold without changing the DmsD monomer percentage or the number of leader peptide binding sites (N=1) (Chan et al, 2008). Our results were also consistent with that previous finding; when the peptide was added to just DmsD, dissociation constant was 2-fold greater in P86Q mutant compared to the W-T (4.27 μM versus 1.89 μM). In section 5.4, we were able to show that the mutant`s ability to bind TatB2 peptide was not perturbed and, thus, the site of interaction between the REMP and one of the TAT system components is likely different from the REMP/cargo complex. We supported the claim by performing experiments

with both peptides added, but added in a different order. Addition of DmsAl or TatB2 to a pre-mix of DmsD with the second peptide would result in almost identical K_d values for the wild-type and the mutant. That implied that DmsD had already obtained the required conformation. Yet, these values were larger than the dissociation constants for TatB2 or DmsAl titration into lone DmsD (see sections 5.2 and 5.3, respectively). Possible reasons for this could be an absence of other crucial components (GTP, metal or another protein) or the state of the environment (pH). Furthermore, a reduced affinity of DmsD towards DmsAl upon pre-incubation with TatB2 (24 μM versus 1.89 μM in the absence of TatB2) might hint at the possibility of an existence of a regulatory mechanism precisely controlling relocation events so that substrate-to-be-transported does not return back to its REMP. Therefore, the pathway where TatB contacts the DmsD::DmsAl assembly for subsequent relocation of cargo is more likely to happen (compared to DmsAl interacting with DmsD::TatB2) based on the obtained K_d values. Finally, as DmsAl would bind to the mutant DmsD::TatB2 complex with the same affinity as to the wild-type, we suggest that TatB2 binding offsets the mutant affect leading to the dissociation constant being similar to the one from the wild-type. Hill coefficients for titration of TatB2 into DmsD::DmsAl complex were equal to 4.18 and 3.72 for wild-type and the mutant. This was similar to the case of TatB2 titration into lone DmsD and pointed at positive cooperativity. However, the following tendency did not exist for the reverse and less likely (based on the K_d values) to happen titration of the substrate into DmsD::TatB2 complex. The following observation provides an additional argument towards biological relevance of increased affinity upon DmsD-to-TatB binding.

We discovered that all three GNP influence the secondary structure of DmsD. However, the effect was more pronounced when the substrate was not present. Cherak and Turner reported a decrease in stability by 3.8 ^{o}C at GTP concentration of 0.1 mM and a rise of a mixed population

of the REMP when no DmsAl peptide was added (2017). This finding would be consistent with a dramatic secondary structure change observed here, that a major α-helix to random coil took place (see Figure 5.16). However, the suggestion of the authors that a guanosine moiety is the key to binding was not supported by our CD work. No conformational change was observed when guanosine was added alone.

Cherak and Turner also determined dissociation constants for DmsD-to-GTP interaction (2.05 mM) and DmsD::DmsAl-to-GTP interaction (0.99 mM) pointing out that addition of GTP led to dissociation of the substrate from DmsD (2017). While we could not obtain K_d values via CD technique due to a high noise from concentrations of GNP higher than 0.1 mM we noted that total secondary structure change for DmsD::DmsAl complex with addition of GTP/GDP/GMP was only ~15% (compared to ~50% for lone DmsD). This may imply that either the concentration of GNP we were working at (35 μM) was too low for the REMP::substrate complex to be affected or that GNP actually leads to the dissociation of DmsAl peptide from DmsD, but the structure of DmsD remains almost intact, unchanged. Moreover, the fact that we were able to obtain a dissociation constant for titration of GTP into DmsD::TatB2 complex and not for DmsD or DmsD::DmsAl complex was quite surprising. If we assume that concentrations in mM range were needed for the latter as suggested by Cherak and Turner, K_d for GTP being added to DmsD::TatB2 was determined as a much smaller number (5.612 μM) (2017). It is, therefore, conceivable that GTP plays some regulatory role, but is not largely implicated in substrate-to-REMP interaction (at least at lower concentrations).

It was rather surprising that Mn^{2+} did not cause any secondary structure change in DmsD alone whereas Mg^{2+} did. The two metals possess similar radii and prefer octahedral coordination (Shannon, 1971). It is, therefore, possible that biological relevance may be implicated:

manganese is generally at lower concentrations inside the cell and demonstrates higher binding affinity towards proteins as per Irving-Williams series (Irving and Williams, 1948). Such selectivity was demonstrated by Lovitt *et al*; addition of Mg^{2+} increased the kinase activity of leucine-rich repeat kinase 2 by only 2-fold, while of Mn^{2+} - 10-fold. Moreover, the authors reported that the 5 mM Mg^{2+} concentration was needed to reach V_{max} versus micromole quantities of Mn^{2+} (2010). It may, thus, be suggested that Mg^{2+} is a true component of TAT system while Mn^{2+} has little to no role.

When exploring the interaction of DmsD and DmsD::DmsAl with metals we noticed that addition of nickel led to structural changes to the REMP::substrate complex. While we did not test if tag-free DmsD::DmsAl complex interacts with nickel, we were able to show that Ni^{2+} has no effect on the structure of DmsD alone, which still has the His6 tag. Furthermore, previous studies had shown that histidine tag does not influence the leader peptide binding (Tran, 2013). Therefore, we believe that both, Mg^{2+} and Ni^{2+} altered the conformation of the DmsD::DmsAl complex. It is feasible that based on their influence of DmsD::DmsAl complex, they have different roles within the translocation pathway based on the opposite effects they have; magnesium results in higher helical content, while nickel increases the percentage of β-sheet within the structure. Yang *et al*. described a process of urease maturation where the nickel metal had to be coordinated by a complex consisting of UreE and apo-UreG dimers that underwent binding to GTP and Mg^{2+} in order to be able to fully transfer Ni^{2+} to apo-UreG which subsequently targeted and installed the metal into the apo-urease. Furthermore, in the absence of Mg^{2+} the affinity of UreG towards Ni^{2+} was 10-times lower and, thus, it was suggested that a structural change at the GTP/Mg^{2+} binding site would trigger the tighter binding (smaller K_d) (2015). Based on the structural changes that resulted from the effectors discussed so far

(peptides and GNP), Mg^{2+} metal was targeting DmsD towards a similar conformation (higher helical content), while Ni^{2+} was reversing the effect. This observation may imply that TAT system may rely on metals as a mode of control and more than one species may be implicated. Lacasse *et al*. reported a HypB to HypA Ni(II) transfer model where another metal (Zn^{2+}) prevented any GTP hydrolysis and dimerization. This helped avoid insertion of an incorrect metal into the binding site of an enzyme (2016). Importantly, this enzyme also utilizes the TAT pathway for the translocation (Sargent, 2016). Perhaps, our system is similar and Ni^{2+} fulfills a different role in the absence/ low concentration of GTP. On the other hand, it is important to remember that intracellular concentration of nickel is extremely low (sub-µM range) and almost all of it will be in a bound form (Ma et al, 2002; Chivers and Sauer, 2002). Therefore, biological relevance of this metal for our model system needs to be verified. One future approach would be to perform titrations of metal with GTP into the complex in order to determine the K_d, which may be subsequently compared to the suggested intracellular nickel within *E. coli*.

Once we had tested metals and GNP alone, we investigated their combined effect. We started with Mg^{2+} metal and utilized all three GNP available (GTP, GDP and GMP). As the structure was ordered to the same level in all the considered cases, it can be speculated that the maximum "natural" change for the complex was achieved. It is conceivable that the binding site for Mg^{2+} metal is the same as for GTP due to the latter help in coordination of the metal. If this is correct, addition of GTP or Mg^{2+} alone may lead to identical structural changes, but biological functionality will be only achieved if both are present. Furthermore, it still remains unclear whether GTP or GDP was hydrolyzed or the role of the molecule is purely regulatory. Another concern that may be raised upon comparing spectra from GNP and GNP+Mg^{2+} cases is the purity of GTP/GDP/GMP that we were using. As the metal could have been present in the

reaction mixture without being accounted for, it might be important to perform a series of future experiments with different concentrations of metal in GNP+Mg^{2+}. If the signals are identical, we will be able to confirm that no difference exists in the structural change in DmsD::DmsAl complex upon addition of GNP with and without the metal.

During our GMP+Ni^{2+} experiment, we observed a small influence on the DmsD::DmsAl complex. However, when standard error was applied to the data, we concluded that the difference was not significant. It should be pointed out that the amount of GMP inside *E. coli* fluctuates between 3.6 and 4.3% depending on the growth phase the bacteria is in. Therefore, it is highly unlikely that DmsD::DmsAl complex is regulated by this particular nucleotide inside the cell. Another important point to consider is that it is not the guanosine moiety alone that binds the complex (as discussed in section 5.5) requiring both the ribose and at least one phosphate. To conclude, we were probably dealing with recognition of GNP molecule by the DmsD::DmsAl complex. Taken together, the fact that structural change observed upon addition of GMP was not significant and the low concentration of this molecule in a live cell, we may suggest that GMP has no regulatory role for the DmsD::DmsAl complex and would only exist if GTP was hydrolyzed to GMP + pyrophosphate rather than GDP + phosphate.

Our final section was dedicated to testing all four molecules (DmsD, GTP, TatB and DmsAl peptides) in a mixture in order to understand better the mechanism of the transfer events that potentially take place prior translocation. The only change in signal (compared to the summed separate files which we considered our control) was when DmsAl peptide was added to the DmsD::TatB2::GTP mixture. We found this finding quite important since adding GTP to DmsD::TatB2 was the only dissociation constant we were able to obtain for GTP earlier (see section 5.8). Therefore, DmsD::TatB2::GTP complex may bear some biological relevance and

exist in the cell. Perhaps, DmsD interacting with DmsAl binds to TatB while the substrate contacts TatC. Next, GTP would serve as a "switch" and control the transfer of substrate to TatB. To conclude, circular dichroism allowed us to gain some insight into the influence of various molecules on the REMP protein alone or in complex with another potential component of the TAT system. We were able to show that GNP as well as TatB2 peptide alter the structure of DmsD and DmsD::DmsAl. Additionally, we showed that metals are important for the system, particularly Mg^{2+}. The involvement of Ni^{2+} which demonstrated somewhat opposite effect compared to Mg^{2+} requires additional verification. Finally, we observed a differential effect of DmsAl on the wild-type versus the P86Q variant of DmsD, while no effect from TatB2. This led us to suggest that the two proteins have distinct binding sites on DmsD's surface.

Chapter 6: Structural analysis and modeling of DmsD target protein interactions.

Currently, crystal structures of DmsD from two organisms are available on Protein Data Bank website; one belonging to *Escherichia coli* (PDB: 3EFP, 3CW0, and 3U41) and referred to here as EcDmsD and the other- *Salmonella typhimurium* (PDB: 1S9U) and referred to as StDmsD. The first structure of EcDmsD (PDB: 3EFP) was solved by our laboratory members and represented a dimer with a resolution of 2.0 Å. It was compared to the existing StDmsD (1S9U) and shown to contain a highly conserved groove that was earlier suggested as a putative leader peptide binding site (Stevens et al, 2009; Qiu et al, 2008). The second structure was published by Ramasamy and Clemons and offered a lower resolution of 2.4 Å (2009). This EcDmsD structure was crystalized as a tetramer and when co-crystallized with leader peptide demonstrated higher quality along with some density that was perceived as the binding site. However, since the peptide was not identified, they were not able to conclusively state specifically where the binding site was located (Ramasamy and Clemons, 2009). Finally, an octamer was published in 2011 with a resolution of 2.5 Å (Stevens and Paetzel, 2011). While no true monomer of EcDmsD had been published, all three publications emphasized that the protein would elute from size-exclusion column as a monomer (Stevens et al, 2009; Ramasamy and Clemons, 2009). Crystal structure of StDmsD was of highest resolution (1.38 Å), monomeric and due to being the first solved DmsD structure was compared to SmTorD (*Shewanella massilia* TorD) (Qiu et al, 2008) solved as a domain swapped dimer.

To date these four structures have been employed for amino acid choice for mutagenesis as well as some small molecule docking studies. More specifically, Qiu *et al*, attempted to computationally determine GTP-binding sites on StDmsD and its close homolog SmTorD (2008). They identified the site using pattern recognition of a known GTP binding site on human

guanylyl cyclase. Figure 6.1 B demonstrates that GTP molecule is positioned close to terminal helices which the authors suggested may provide a supportive role during TatBC interaction (Qiu et al, 2008).

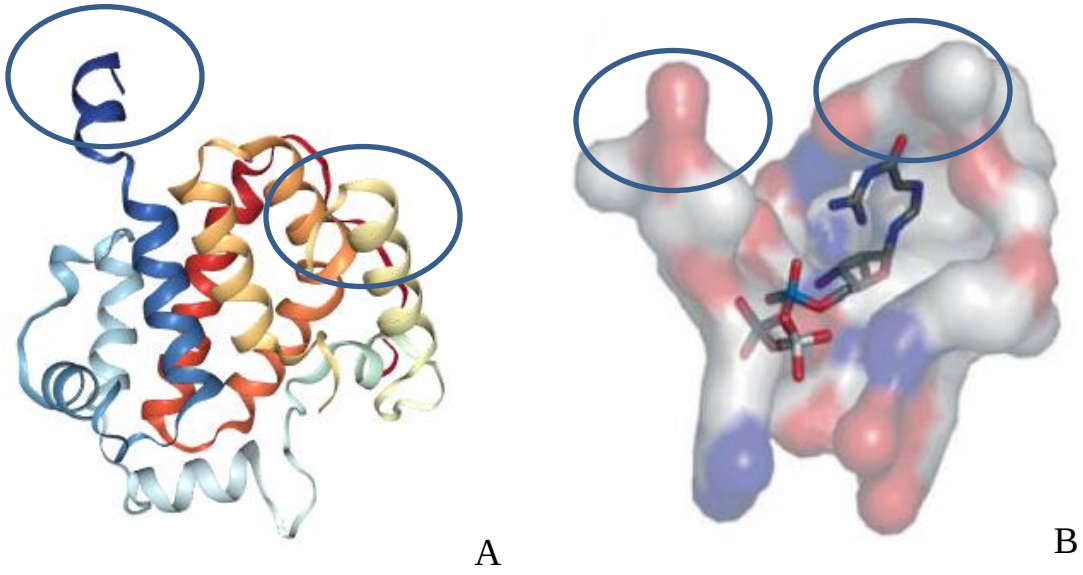

Figure 6.1 Crystal structure of DmsD from *S. typhimurium* L12. A. Ribbon diagram of DmsD with each of the helix strands colored differently. The image was prepared with NGL, a 3D-based viewer (https://www.rcsb.org/3d-view/1S9U/1). **B.** Putative GTP binding site in StDmsD modelled with Global Protein Surface Survey. GTP molecule is depicted in sticks. DmsD is shown using the surface model with charged conserved residues highlighted in red and blue. Blue circles point at N- and C-terminals of StDmsD which the authors believed to be involved in a supportive role for attaching/detaching from the Tat complex. Used with permission from Qiu et al, 2008 (see Appendix).

Stevens et al. utilized molecular modelling to dock the leader sequence on the surface of their DmsD crystal structure (3EFP) (Figure 6.2 A). Importantly, their list of amino acids from the REMP protein was similar to experimentally-identified one by Chan *et al*. (Figure 6.2 B) and included Trp72, Phe76, His127 as well as amino acids between 121 to 126 (Stevens et al, 2009; Chan et al, 2008).

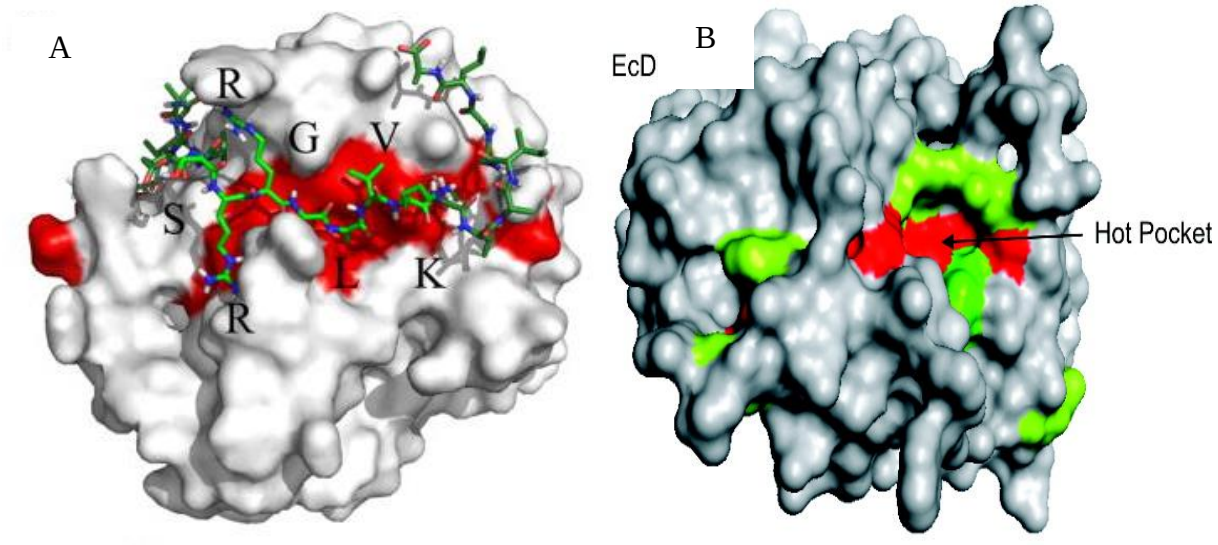

Figure 6.2 Comparison of modelled and experimentally-determined binding site for DmsA leader peptide. A. Molecular dynamics simulation of EcDmsD with the region of EcDmsA leader peptide that harbors the twin-arginine motif. Residues that are part of the twin-arginine consensus motif are labeled. Used with permission from Stevens *et al*, 2009 (see Appendix). **B.** EcDmsD model of the DmsA leader binding site from *in vitro* RR-leader peptide binding assay of site-directed and randomly generated mutants. Surface model of DmsD variants showing less than 0.5-fold relative binding, colored red. Protein variants showing binding above 1.25-fold relative to the WT were colored green. Used with permission from Chan *et al*, 2008 (see Appendix).

CABS-dock software was utilized based on the questions we wanted to address such as what was the putative site for TatB on the surface of DmsD and whether the sites for substrate and TatB are different. The major benefit of CABS-dock compared to other web-servers was the ability to model a flexible peptide on the surface of DmsD compared to what other software could offer (using facets or rigid structures for residue contact evaluation) (Blaszczyk et al, 2018; Lesk and Sternberg, 2008; Pierce et al, 2011). Among other advantages were presence of solvent rather than docking in vacuum and Ligand-RSMD clustering that allowed to remove poses that were too similar to each other (Blaszczyk et al, 2016).

6.1 Modelling the DmsA leader onto DmsD

The protocol for the CABS-dock software is based on a coarse-grained model with up to four centers for each amino acid which allows for longer simulation time. Additionally, it utilizes Replica Exchange Monte Carlo dynamics which allows to sample high and low temperatures on the chosen by the software trajectories. Each of the 10 generated trajectories receives 1000 snapshots of simulation which totals 10000 snapshots. Next, the software excludes all the unbound states and selects only lowest energy-binding models which are in turn clustered 100 times to generate 10 rated alternatives with model 1 bearing the highest probability of being true (Kurcinski et al, 2015).

Prior to exploring the putative binding site for TatB2 peptide via CABS-dock software, an attempt was made to visualize the docking site for the RR-leader peptide with this program. This was done in order to compare the results produced from 3D-Garden, the server employed by Stevens et al., as well as to the amino acids identified via Chan`s mutagenesis study (Stevens et al, 2009; Chan et al, 2008). The model I produced using CABS-dock strongly supported previously identified REMP-peptide residue contacts. The choice of CABS-dock web server for binding site search is based on the fact that it allows for flexible docking and does not require any prior knowledge on the binding site (Kurcinski et al, 2015). 3D-Garden, on the other hand, utilizes the data provided by the user (proposed contacting patches on the surface), creates a small set of guaranteed models using re-weighted Lennard–Jones potential and dedicates the majority of the run time to processing those (Lesk and Sternberg, 2008).

While working with CABS-dock software I generated a PDB file of EcDmsD monomer from PDB 3EFP by highlighting a single chain only. The following decision was based on the earlier mentioned assumption that DmsD likely functions as a monomer (Stevens et al, 2009;

Ramasamy and Clemons, 2009). However, despite multiple attempts docking with DmsA leader peptide would not be accomplished on the surface of a monomer. Therefore, a dimer was utilized for this work. All other modelling experiments (with TatB2 peptide) were completed using the selected monomer with no error message from the CABS-dock software.

Figure 6.3 (A and B) shows the results of the positioning of the RR-leader sequence which is binding in an extended confirmation. Importantly, the peptide still had contacts with only one of the monomers. Table 6.1 lists predicted residue contacts from optimized CABS-dock model 1 which was ranked by the software as most promising.

In order to compare our results to the previously published, we transferred the data to PyMOL (Figure 6.4 A, B) and were able to show that amino acids Phe 76, Trp 87 and His 127 are shared between the sites identified with CABS-dock (grey) and the experimental study by Chan *et al*. (magenta); they can be viewed as spheres highlighted in blue in Figure 6.4 C and D. Another important observation was the region of the signal peptide that made contacts with the mentioned above amino acids: the contacts with Phe 76, Trp 87 and His 127 were created by the C-terminal of the DmsA signal sequence (see Table 6.1).

In order to define a region of RR-leader binding that agrees with all we visualized all three binding sites together. Figure 6.5 demonstrates that there are some shared residues between the two modelling software packages (Trp 80, Gln 121, Glu 123 and Tyr 22, highlighted in blue), experimental and CABS-dock software (Pro 86, Trp 87 and Pro 124, highlighted in green), experimental and 3D-Garden software (Trp 72, highlighted in red), and all the models (Phe 76 and His 127, highlighted in cyan). Nevertheless, the leader binding site from Stevens (2009) seems to be quite differently located from the one generated by CABS-dock: they occupy two

opposite sides of the DmsD molecule/ We also created a comparison table with residues on the surface of DmsD that were suggested to participate in the leader binding (see Table 6.2).

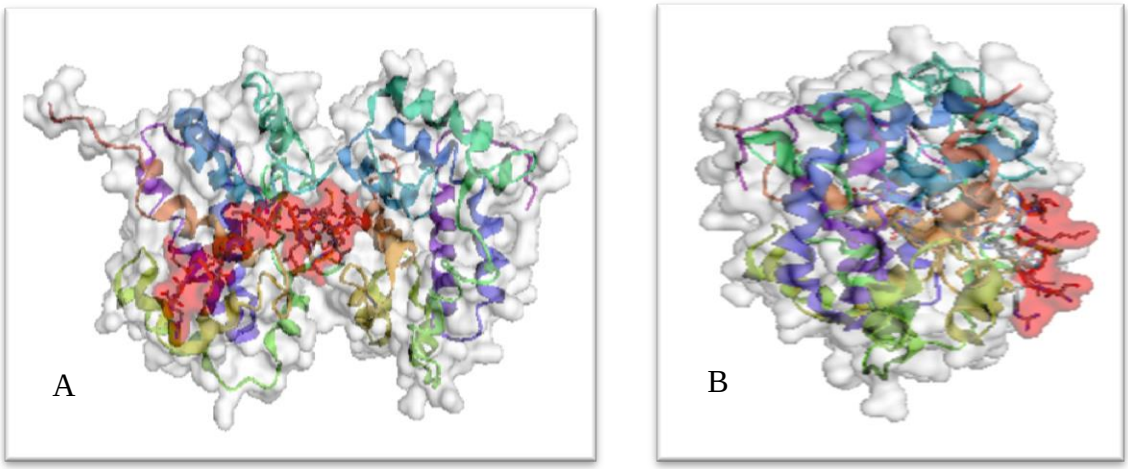

Figure 6.3. Modeling of WT DmsD protein with $DmsAl_{15-41}$ peptide using the CABS-dock. (A, B) Two views rotated by 90° through the y-axis. Structure of *E. coli* DmsD (PDB: 3EFP) was used for analysis. $DmsAl_{15-41}$ peptide is shown in red sticks. Protein is depicted in ribbons and transparent space fill in the dimer version of the protein.

It was noted that Leu 75 and Asp 126 mentioned by Chan et al. as part of the hot pocket (colored in magenta) were not visible on the surface model and are buried within DmsD structure. Also amino acids Phe 76 and His 127 seemed to be key for the interaction and shared among all three models. By comparing the residues and their number to the experimental mutagenesis carried out by Chan *et al*. we found that our model produced more similarities to the DmsAl binding site compared to 3D-Garden: 5 common residues versus only 3 (2008).

Table 6.1. List of DmsD to $DmsAl_{15-41}$ contacting residues generated via CABS-dock docking server. Model 1 was chosen due to its ranking by the software. Colored in orange are rows that contain "hits", residues overlapping with the amino acids identified by Chan et al. as part of the DmsAl-binding "hot pocket" (2008).

$DmsAl_{15-41}$	DmsD
Arg 16	Ser 39, Asp 40, Trp 42, Gln 45, Gly 41, Val 36
Arg 17	Trp 42, Trp 46, Gln 45, Pro 47
Leu 19	Pro 32, Val 36
Val 20	Pro 32, Leu 33
Thr 22	Glu 29
Ala 24	Glu 29
Ile 25	Leu 133, Met 119, Phe 117, Glu 29, Tyr 22
Gly 26	Met 119
Gly 27	Glu 29
Leu 28	Ser 27, Ala 28, Glu 29, Ala 30, Tyr 23
Ala 29	Met 119, Tyr 22, Tyr 23
Met 30	Lys 120, Gln 121, Met 119, Tyr 23
Ser 32	Gln 121
Ser 33	Asn 122, Gln 121, Glu 123
Ala 34	Glu 123
Leu 35	Glu 123, Tyr 22
Thr 36	Val 77
Leu 37	Val 77, Phe 76, Ala 24, Tyr 23
Pro 38	Phe 76, Tyr 22
Phe 39	Trp 80, Pro 79, Val 77, Gly 78, Phe 76
Ser 40	Leu 98, Pro 85, Pro 86, Trp 87, Leu 82, His 127

Arg 41	Leu 98, Lys 120, His 127, Ser 130, Pro 124, Glu 123, Tyr 22

[1] Structure of *E. coli* DmsD (PDB: 3EFP) was used for analysis.

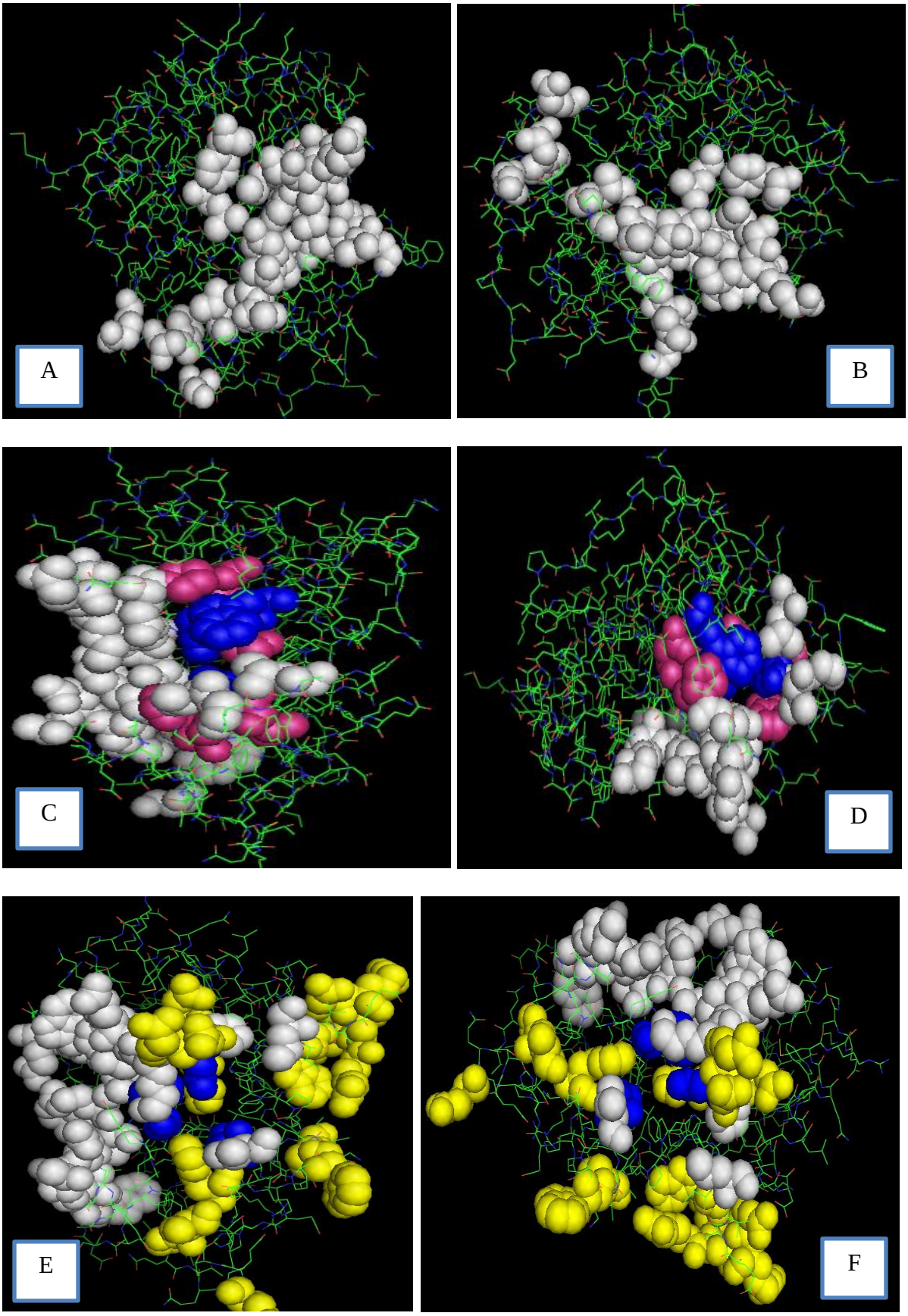
A
B
C
D
E
F

Figure 6.4. Comparison of alternative DmsAl-binding site positions. A, B. Residues of WT DmsD participating in RR-leader peptide binding (two views rotated by 90° through the y-axis) predicted by CABS-dock server. **C, D.** "Hot pocket" residues identified experimentally by (Chan *et al*., 2008) are shown in magenta while those identified via CABS-dock are colored in grey (two views rotated by 90° through the y-axis). **E, F.** Residues of DmsD highlighted by 3D-Garden software as "involved in RR-leader binding" (Stevens *et al*., 2009) are shown in yellow while those identified via CABS-dock are colored in grey (two views rotated by 90° through the y-axis). Crystal Structure of *E. coli* DmsD (PDB: 3EFP) was used for analysis. Residues shared between the two alternative binding models (B-F) are depicted in blue. Image was rendered using PyMOL and only the monomer is shown.

Table 6.2 Comparison of our proposed interactions between EcDmsD and the leader peptide of EcDmsA to the suggested by Stevens et al. (2009) (molecular dynamics study) and Chan et al. (2008) (mutagenesis).

3-D Garden web server (from Stevens et al., 2009)	CABS-dock web server (present study)	Experimental mutagenesis (Chan et al., 2008)
Tyr 22, Glu 65, His 68, Ala 69, **Trp 72, Phe 76, Trp 80**, Pro 83, Trp 91, Asp 93, Arg 94, **Gln 121**, **Asn 122**, **Glu 123**, Glu 125, **His127**, Pro 201, Leu 202, Phe 203, Arg 204,	**Tyr 22**, Tyr 23, Ala 24, Ser 27, Ala 28, Glu 29, Ala 30, Pro 32, Leu 33, Val 36, Ser 39, Asp 40, Gly 41, Trp 42, Gln 45, Trp 46, Pro 47, **Phe 76**, Val 77, Gly 78, Pro 79, **Trp 80**, Leu 82, Pro 85, **Pro 86**, **Trp 87**, Leu 98, Phe 117, Met 119, Lys 120, **Gln 121**, **Asn 122**, **Glu 123**, **Pro 124**, **His 127**, Ser 130, Leu 133,	**Trp 72**, Leu 75, **Phe 76**, **Pro 86**, **Trp 87**, **Pro 124**, Asp 126, and **His 127**.

[1]Residues overlapping among the groups are in bold and underlined.

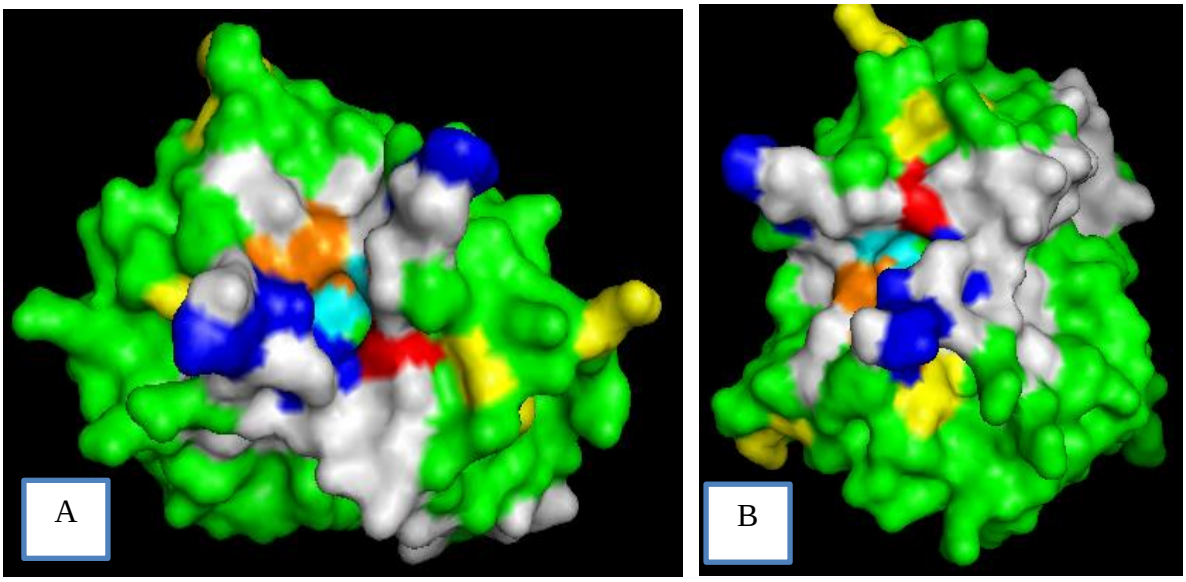

Figure 6.5. Comparison of alternative DmsAl-binding site positions. A, B. "Hot pocket" residues predicted by (Chan *et al*, 2008) are shown in magenta while those identified via CABS-dock are colored in grey (two views rotated by 90° through the y-axis). Residues of DmsD highlighted by 3D-Garden software as "involved in RR-leader binding" (Stevens *et al*, 2009) are shown in yellow. Residues shared between 3-D Garden (Stevens *et al*, 2009) and CABS-dock are shaded in blue; between Chan *et al* (2008) and CABS-dock- in orange; between Stevens *et al*. (2009) and Chan et al. (2008) – in red. Phe 76 and His 127 which are shared between all three models highlighted in cyan. Crystal Structure of *E. coli* DmsD (PDB: 3EFP) was used for analysis. Image was rendered using PyMOL.

6.2 Modeling the TatB peptide site in DmsD

To get an idea if the TatB and RR-leader sequence occupy two different binding sites on DmsD, we attempted a docking experiment of TatB2 peptide onto wild-type DmsD. Using crystal structure of DmsD (3EFP), CABS-dock web server was able to predict a potential binding site of TatB2 peptide.

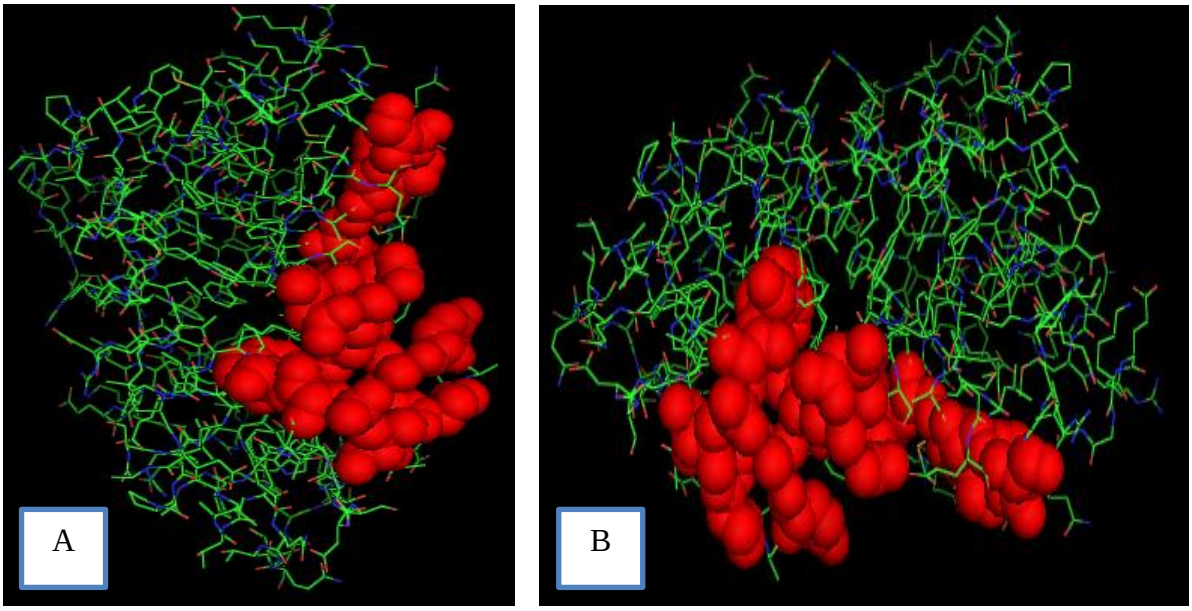

Figure 6.6. Modeling of WT DmsD protein-TatB2 peptide interactions using CABS-dock. A, B. Residues of WT DmsD participating in peptide binding (two views rotated by 90° through the Z-axis) are highlighted in red. (Crystal Structure of *E. coli* DmsD (PDB: 3EFP) was used for analysis. Image was rendered using PyMOL.

Table 6.3 lists DmsD to TatB2 peptide contacts computed by the CABS-dock web server. As can be seen from the list of DmsD residues, the binding site is comprised primarily of nonpolar aliphatic (Val 12, Val 16, Ala 19, Val 36, Leu 33, Leu 133), polar uncharged (Asn 9, Gln 45, Asn 141, Pro 32), and nonpolar aromatic amino acids (Tyr 22, Trp 46, Phe 117, Trp 137). Only two charged residues are present: Arg 15 and Glu 29. Comparing the following result to DmsAl binding site, we noted that the same three groups comprised the majority of the residues making contacts with the leader peptide. However, no aliphatic amino acid was determined to be key for the DmsAl binding. Therefore, if a mutagenesis study is carried out to determine the interaction site for TatB on DmsD surface, it is likely that we would concentrate on polar uncharged, aromatic and charged amino acids.

Table 6.3. List of DmsD-to-TatB2 contacting residues generated via CABS-dock

TatB2	DmsD
Leu 1	Val 16, Gln 45, Trp 46
Thr 2	Asn 9, Val 12, Gln 45
Leu 4	Pro 32, Val 36
Thr 5	Val 12, Arg 15, Val 16
Pro 6	Arg 15, Ala 19, Glu 29, Leu 33
Glu 7	Arg 15
Leu 8	Tyr 22, Glu 29, Phe 117, Leu 133,
Lys 9	Trp 137, Asn 141

Structure of *E. coli* DmsD (PDB: 3EFP) was used for analysis.

6.3 Comparison of the protein-peptide interfaces

Having collected information for both putative binding sites for the RR-leader and TatB2, we compared the CABS-DOC sites to each other using PyMOL. It became evident that while the two sites lie quite close to each other, they do not occupy the same position on DmsD. Nevertheless, some amino acids were shared: Glu 29, Leu 33, Gln 45, Val 36, Pro 32, Phe 117, Leu 133, and Trp 46.

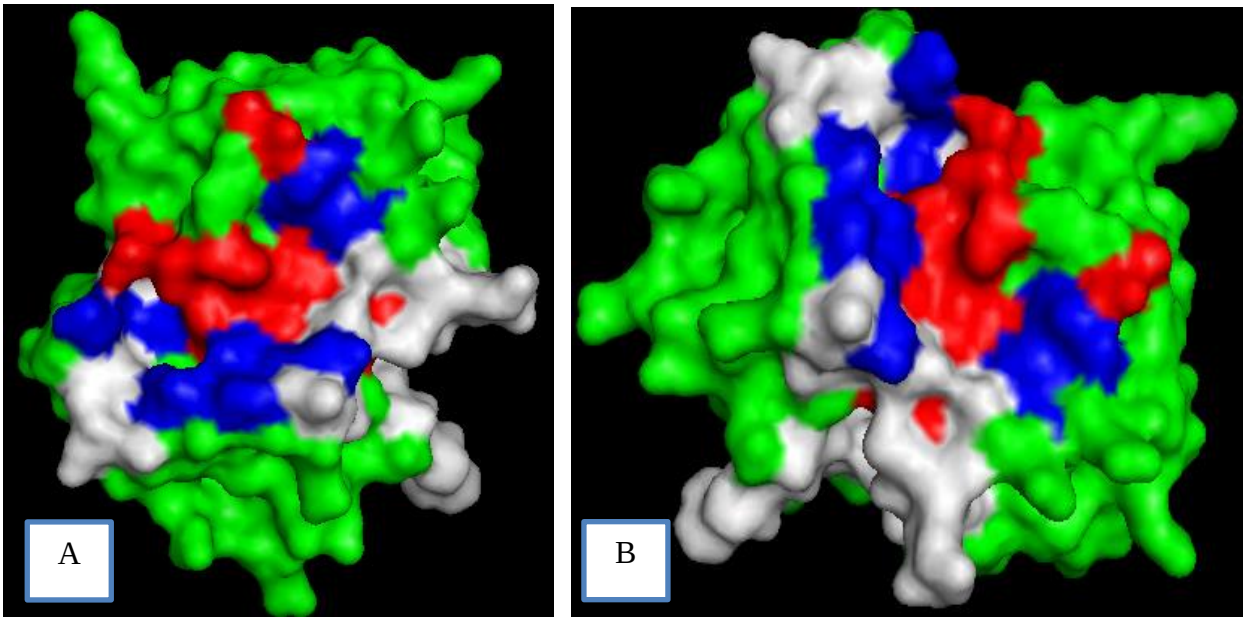

Figure 6.7. Comparison of binding sites of TatB2 and DmsAl peptides on the surface of WT DmsD protein using CABS-dock. Structure of *E. coli* DmsD (PDB: 3EFP) was used for analysis. **A, B.** PyMOL-generated structure of DmsD with predicted binding sites for TatB2 peptide (red) and leader peptide (grey) (two views rotated by 90° through the z-axis). Shared residues are depicted in blue. Figure was rendered using PyMOL.

Focusing on the CABS-doc prediction of TatB and the experimentally defined RR-leader binding site from Chan et al (2008), there is no overlap at all. As seen in Figure 6.8, CABS-dock predicted TatB2 binding site is different from the one suggested for the leader sequence by Chan *et al.* (2008).

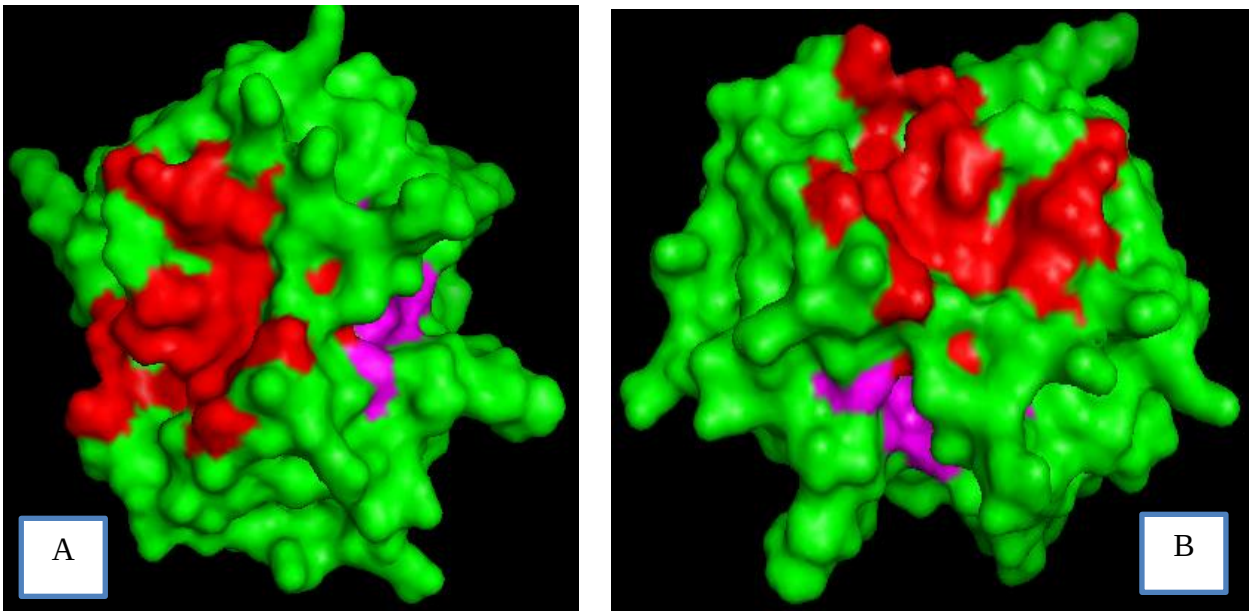

Figure 6.8. Comparison of binding sites of TatB2 and DmsAl peptides on the surface of w-t DmsD protein using the CABS-dock web server (for residues involved in TatB2 binding) and experimentally residues proposed by Chan *et al.* (2008) (for residues involved in DmsAl binding). Structure of *E. coli* DmsD (PDB: 3EFP) was used for analysis. **A, B**. PyMOL-generated structure of DmsD with predicted binding sites for TatB2 peptide (red) and leader peptide (magenta) (two views rotated by 90° through the z-axis). Protein is depicted in sticks. Figure was rendered using PyMOL.

6.4 Modelling GTP binding onto DmsD structure

In an attempt to locate the putative GTP-binding site, Qiu *et al*. employed Global Protein Surface Survey server which compared StDmsD and SmTorD surfaces to 209 known GTP binding sites and yielded a high similarity to guanylyl cyclase from *H. sapiens* (2008). Overall, 11 residues were highlighted as "involved in the interaction with GTP" (see Table 6.4).

Table 6.4. Comparison of proposed interactions between StDmsD and GTP (taken from Qiu et al, 2008) to the manually-identified (current study).

StDmsD and GTP (taken from Qiu et al, 2008)	EcDmsD and GTP (current study)
Arg 7, Asp 8, Phe 10, Thr 13, Glu 140, Asp 142, Cys 147, Glu 148, Leu 151, Leu 193, Ile 194	Ser 27, Ala 28, Glu 29, Asp 126, His 127, Phe 128, Gly 129

[1]StDmsD denotes *Salmonella typhimurium* and EcDmsD- *Escherichia coli*.

According to ExPASy protein sequence comparison tool, there is a 77% sequence identity between EcDmsD and StDmsD. Among all the residues from right column of Table 6.4 (current study) only amino acid 28 is different (His instead of Ala for StDmsD). Whereas in the left column residues 7 (Arg/Gln), 13 (Thr/Ala), 142 (Asp/Gly), and 194 (Ile/Leu) were variable among the two sequences.

Submitting the crystal structure of DmsD into several web-based servers (CRDD, Nucleos, P2RP) did not yield any hints towards a specific nucleotide-binding site. Nevertheless, a putative GTP-binding motif was found during a manual inspection of the sequence: DHFG (residues 126-129). DxxG is known as effector loop in many known GTPases. The Asp in the structure usually participates in metal binding. Additionally, the loop appears to be involved in structure change from GTP to GDP (Kjeldgaard et al, 1996). Indeed, within the crystal structure of DmsD, DxxG is located on the surface and in close proximity to another possible GTP-binding motif which is (C/S)A[x]x (Kjeldgaard et al, 1996). In case of DmsD, it is SAE (residues 27-29). The sequence of StDmsD had DHFG fully-conserved and SAE partially-conserved as SHE. Interestingly, DxxG site is very close to the "hot pocket" of the DmsAl binding site identified by Chan *et al*. and two residues are even shared between the two (D126 and H127) (2008). At the same time, it is rather different from the GTP binding location suggested by Qiu and colleagues (PDB code: 1S9U) (Qiu et al, 2008).

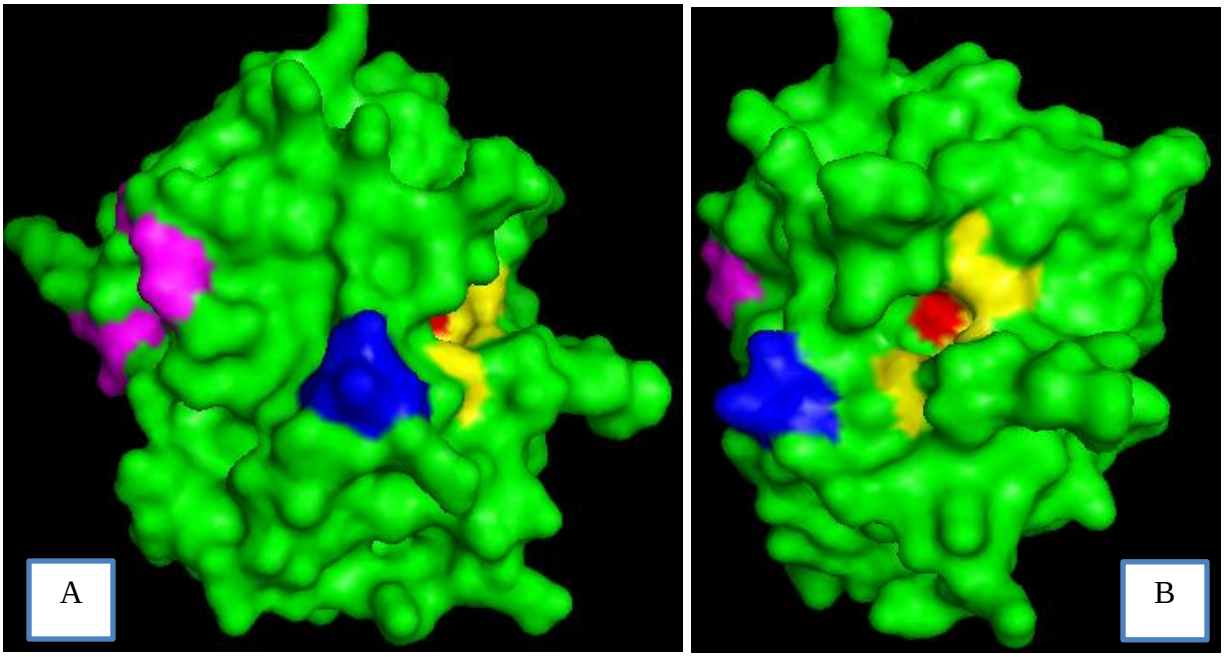

Figure 6.9. Comparison of two alternative GTP-binding site positions in relation to the leader binding peptide in DmsD. Structure of *E. coli* DmsD (PDB: 3EFP) was used for analysis. **A, B.** Residues predicted by Qiu *et al* (2008) are shown in magenta while those identified here (DHFG and SAE) are colored in blue. "Hot pocket" proposed by Chan *et al* are depicted in yellow (2008). Residues shared between the "hot pocket" and manually predicted putative GTP-binding site are shown in red. Image was rendered using PyMOL. Figure rotated through y-axis.

Discussion

In this chapter we attempted to model the interactions that were key for the questions asked in this thesis. More specifically, we were interested in TatB and GTP binding sites. However, as the new docking server was employed, we needed to assess how well the results from the simulations agreed with previously reported by Stevens *et al*. and Chan *et al*. (2009, 2008). While comparing the binding sites for DmsA leader peptide on the surface of DmsD, we were able to identify two key residues that were shared among all three approaches (CABS-dock software, 3D-Garden software, and experimental mutagenesis): His 127 and Phe 76. The first amino acid was found important in DmsD homologue TorD. Hatzixanthis *et al*. reported that the affinity towards TorA signal peptide was reduced two-fold compared to the wild-type (2005).

Moreover, both of the residues were previously identified as parts of two conserved motifs within DmsD sequence: WxxLF (residues 72 to 76) and E(P/x)(x/P)DH (residues 123 to 127) (Turner et al, 2004). Notably, three out of four amino acids shared between 3D-Garden and CABS-dock also belong or are in close proximity to those sections on the surface of DmsD: Trp 80, Gln 121and Glu 123. While they did not demonstrate any significant decrease in affinity towards DmsA leader peptide during the experimental mutagenesis, they could still be part of the binding site. Very similar claim can be made regarding residues Pro 86, Trp 87 and Pro 124 which were shared between the CABS-dock modelling and experimental mutagenesis. They are again either very close to the consensus motif (Pro 86 and Trp 87) or part of it (Pro 124) (Chan et al, 2008). Finally, while it is challenging to state confidently which of the three inspected putative binding sites is most precise, it may be noted that only three amino acids were shared between 3D-Garden and experimental mutagenesis (versus 5 between CABS-dock and Chan *et al*. work). We suggest here that CABS-dock web server offers a benefit of greater flexibility compared to 3D-Garden which highly depends on the stringent conditions that the user applies when selecting a patch for binding on the surface of a protein. Nevertheless, until the two (DmsD and DmsA leader peptide) are co-crystallized, it will be hard to deduce which set of residues is the most correct one.

We also inspected DmsA amino acids which were predicted to participate in the binding. By highlighting the boxes with "hot pocket" residues suggested by Chan *et al*, we noticed that only C-terminal of the leader peptide is expected to interact with the amino acids from the "hot pocket" (see Table 6.1) (2008). The following data is consistent with surface plasmon resonance (SPR) experiments by Shanmugham *et al*. where substitution of C-terminal region of DmsA leader peptide led to the loss of REMP-to-substrate binding (2012). It would also support the

finding by Winstone *et al*. where peptides devoid of residues 34 to 45 demonstrated no binding towards DmsD (2013). Perhaps, the loss of contacts between residues 37 to 41 from the leader peptide abrogates the contacts with Phe 76 and His 127.

Putative binding site for TatB was identified by modelling TatB2 peptide on the surface of DmsD. While the three groups of residues involved (aliphatic, aromatic and polar uncharged) were similar to the leader binding, the two sites did not overlap based on the experimentally-determined "hot pocket" for leader peptide (Chan et al, 2008). Moreover, the amino acids identified did not span 72-76 or 123-127 segments of DmsD`s two consensus motifs. Therefore, WxxLF and E(P/x)(x/P)DH are not likely to be involved in TatB binding.

It is important to note that unlike experimentally-determined set of residues, DmsAl peptide binding site identified via CABS-dock partially overlapped the TatB2 peptide binding site. It is tempting to suggest that the presence of shared amino acids is the result of the web server`s attempt to achieve lowest energy conformation. Blaszczyk *et al*. reported that the quality of the prediction may be increased considerably if restraints on the distances between protein and peptide residues are introduced (2018). Therefore, the next step would be to perform multiple runs on already known model, but with alterations in the distances, in order to determine the cut-offs which will yield optimal results.

In section 6.4 we showed that two conserved GTP-sequence motifs (DxxG and (C/S)A[x]x) are present within DmsD secondary structure. Notably, putative DHFG interaction site lies deep in one of the cavities of the REMP protein and partially overlaps with the leader sequence binding site. Qiu *et al*. believed that the location of a GTP-binding site is important for switching the conformations of DmsD between TatBC-bound and free (2008). However, they also admitted that TorD putative binding site by suggested by Hatzixanthis *et al.* shares very little resemblance

to theirs (2005). Based on the data obtained in chapters 5 and 7 along with the experimental evidence from Cherak and Turner, it is tempting to suggest that GTP and DmsA partially share the same binding site with GTP regulating the interaction between the leader peptide and DmsD (2015). That would explain dissociation that Cherak and Turner observed at high concentration of GTP as well as the change in secondary structure which we noted while performing circular dichroism experiments with DmsD::DmsAl complex and GTP (2015).

Finally, it was mentioned before that Hatzixanthis *et al.* identified a putative GTP-binding site on the TorD surface (2005). The authors performed an *in vivo* screen for hydrolysis activity using TorD variants with mutations of the predicted interaction site. While they could not comment on GTP binding itself, they noted decreased activity in some of the mutants which led them to suggest that certain knock-outs were unable to carry TorA towards the TAT apparatus (Hatzixanthis et al, 2005). This again supports the possibility of existence of one, perhaps, partially-shared binding site for the leader peptide and GTP.

In conclusion, here we showed that His 127 and Phe 76 overlap in all three models (CABS-dock software, 3D-Garden software and experimental mutagenesis) and are likely key for the leader peptide binding. We also demonstrated that it is the C-terminal region of the leader peptide that makes contacts with the “hot pocket” residues (Chan et al, 2008). Furthermore, potential TatB binding knock-outs (for experimental mutagenesis) were identified via CABS-dock and shown to lie in a different region on the surface of DmsD. Finally, we discovered GTP-binding site that is shared with the “hot pocket” of leader sequence which probably is the key to regulation between substrate-bound and unbound forms of DmsD.

Chapter 7. Using analytical size-exclusion chromatography to evaluate protein interaction complexes.

Having observed a number of interactions between the proteins and peptides studied to date, we attempted to evaluate them via size-exclusion chromatography (SEC). Our rationale for choosing this particular technique was an opportunity to identify a particular combination of DmsD and ligands that led to either a stabilization or dissociation of a complex. We were planning to isolate the condition and potentially study it with differential light scattering and/or crystallization. The complete summary list of all experiments as well as the percentage of the ratio of area under the peak/total area is presented in Tables 7.1 and 7.2. In all SEC experiments the chromatographic running conditions were 0.7 ml/min in a Hi-Trap buffer (25 mM Tris-HCl, 10 mM NaCl, pH 8.0).

7.1 Complex with H_6T_7-DmsD and DmsAl-GST migrates as a dimer of each of the two proteins.

Prior to exploring the influence of any effectors on DmsD::DmsAl complex, we obtained chromatograms of H_6T_7-DmsD and DmsAl-GST alone as well as H_6T_7-DmsD::DmsAl-GST complex. As seen in Figure 7.1, the H_6T_7-DmsD elutes at 13.13 ml, DmsAl-GST – at 11.7 ml and complex of the two- at 10.9 ml. Using molecular weight calibration plot we were able to determine the apparent molecular weight of the proteins alone and their complex together. The results for H_6T_7-DmsD were consistent with previously reported values with the elution molecular weight as 33.9 kDa compared to the calculation of 27 kDa based on the sequence. This suggests the protein is an extended shape leading to a larger hydrodynamic radius than a sphere. On the other hand, the apparent weight for DmsAl-GST based on elution volume was approximately 87 kDa which was 27 kDa higher than expected. Winstone *et al.* reported that

DmsAl-GST elutes as a dimer and, thus, the molecular weight was predicted to be equal to 60 kDa (2006). Under the conditions here, the mode of dimerization of the protein led to it migrate faster (elute at an earlier volume) than a standard spherical protein.

It is worth noting that using ITC and analytical SEC, a previous member of our laboratory deduced that monomer H_6T_7-DmsD interacts with a dimer of DmsAl-GST. Therefore, we made sure that the mixing of H_6T_7-DmsD with DmsAl-GST was performed in a 1 to 2 molar ratio. Upon inspecting the elution profile of a latter combination, we detected a single high-intensity peak that represented the predicted monomer-to-dimer complex. We concluded that we successfully reproduced the results published by Winstone *et al*. (2006). Interestingly, neither density assessment by ImageJ, nor apparent weight of the complex supported the following ratio (see Table 7.2). Rather, from the SEC standard curve equation it looked as if we were dealing with a 2:2 ratio of H_6T_7-DmsD to DmsAl-GST: instead of expected 120.9 kDa complex we obtained 148 kDa complex (additional 28 kDa could be a second monomer of H_6T_7-DmsD).

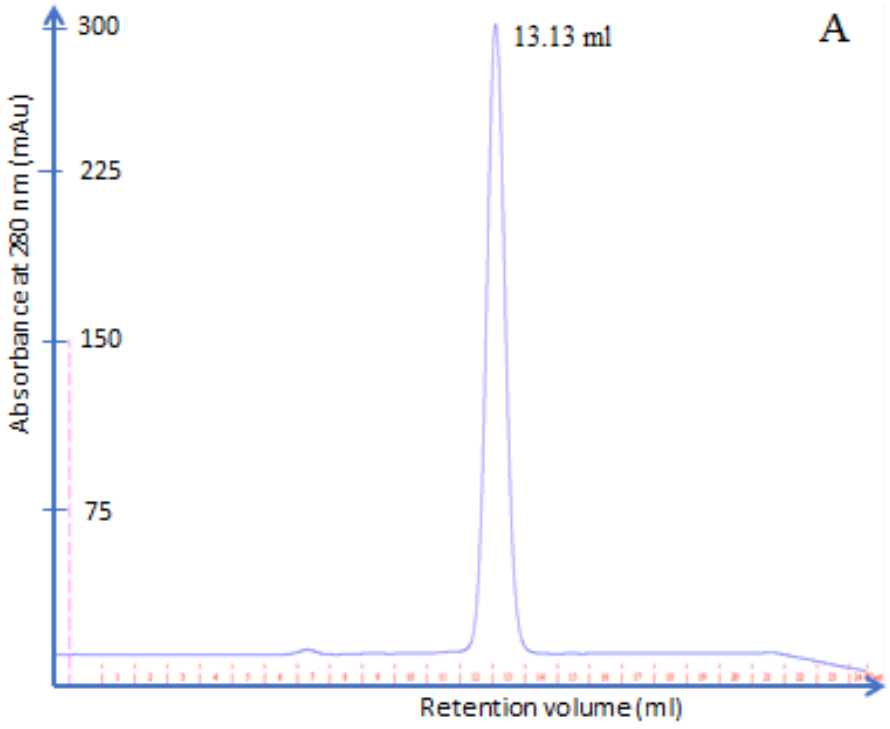
A
13.13 ml
300
225
150
75
Absorbance at 280 nm (mAu)
Retention volume (ml)

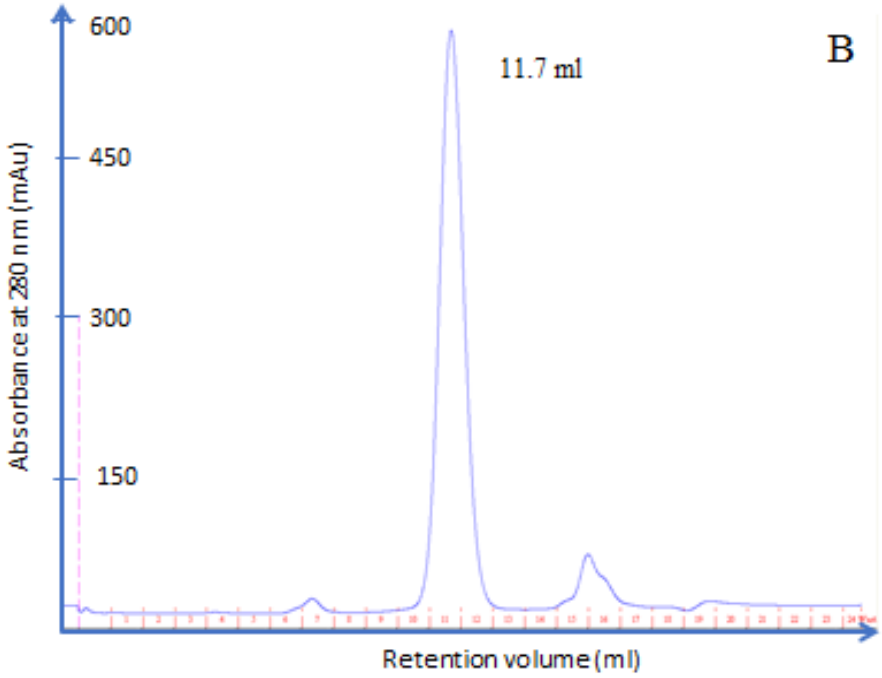
B
11.7 ml
600
450
300
150
Absorbance at 280 nm (mAu)
Retention volume (ml)

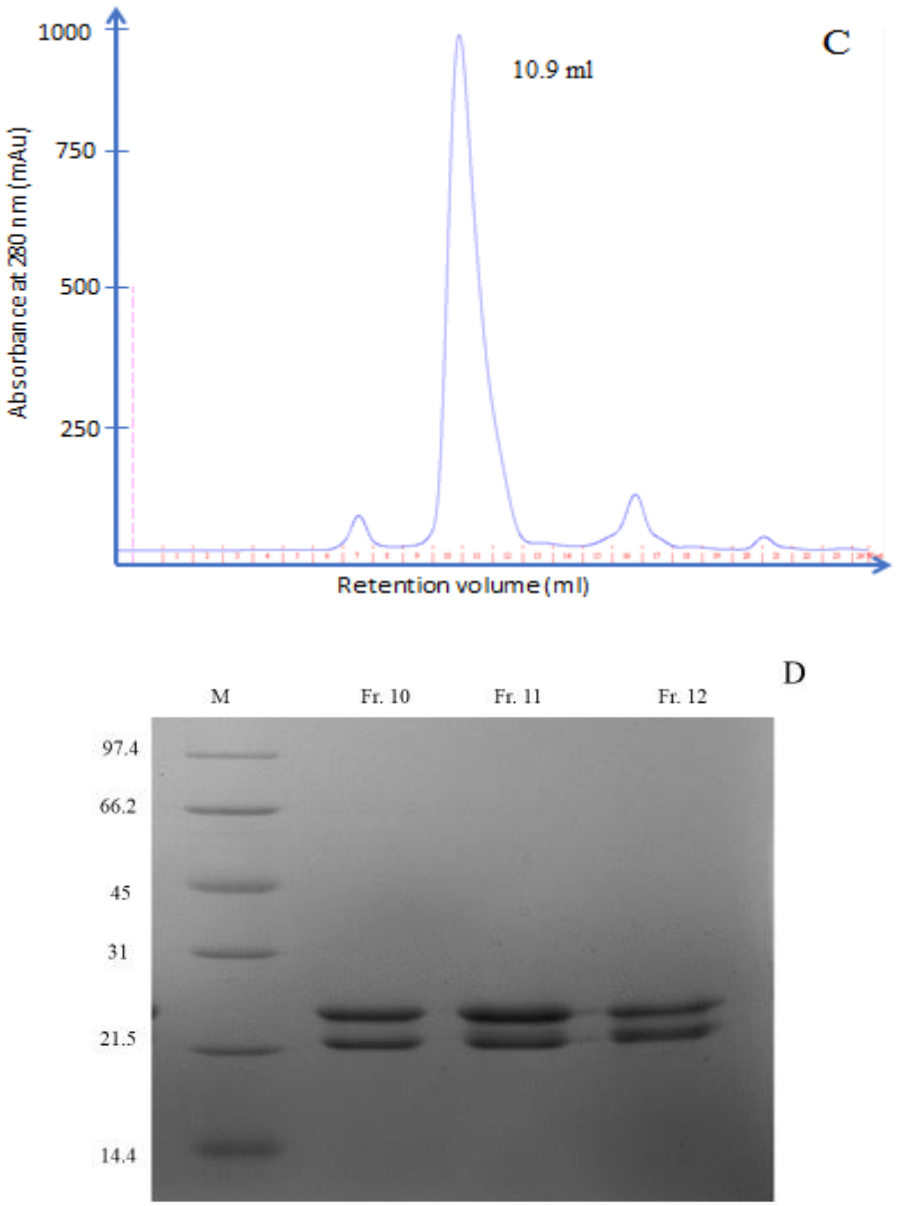

Figure 7.1. Size exclusion chromatography of recombinant proteins. A. Sample chromatogram for H_6T_7-DmsD. **B.** Sample chromatogram for DmsAl-GST. C. Sample chromatogram for H_6T_7-DmsD:: DmsAl-GST. The total area under eluted peaks was determined and main peak area (%) was analyzed for each protein and tabulated. 500µl samples were injected at a 1:1 molar ratio. **D.** Coomassie blue stained 12% SDS-PAGE of SEC eluted fractions including molecular weight markers (M), fractions 10, 11, and 12.

7.2 GTP does not lead to dissociation of DmsAl-GST from H_6T_7-DmsD

To explore the influence of GTP on H_6T_7-DmsD::DmsAl-GST complex, we incubated two proteins together for 1 hour, added 350 μM GTP and incubated for another hour. Next, we loaded the mixture onto the Superose 12 column and compared for the protein-protein reaction mixture alone. As seen in Figure 7.2, H_6T_7-DmsD::DmsAl-GST complex still eluted at 10.89 ml, but another peak (16.4 ml) was observed. As based on the molecular weight this could have only been a structurally-different (moving slower) monomer of either H_6T_7-DmsD or dissociated DmsAl-GST, we collected the peak elution fractions for SDS-PAGE analysis, but we observed no protein in lane 16 (Figure 7.2 B). This observation was similar to a high signal from an ATP-containing buffer during DmsAl-GST purification where very little or no protein was obtained, but absorbance at 280 nm was detected (see section 3.2).

As with the control, we calculated apparent molecular weight of the complex and found it to be almost identical to the uninfluenced complex (149 kDa for complex with GTP added versus 148 kDa for control). It was again consistent with a dimer::dimer complex rather than monomer of H_6T_7-DmsD interacting with two DmsAl-GST molecules. Upon calculating the density of bands from SDS-PAGE we obtained a 1 to 1.5 ratio of DmsD to DmsAl-GST.

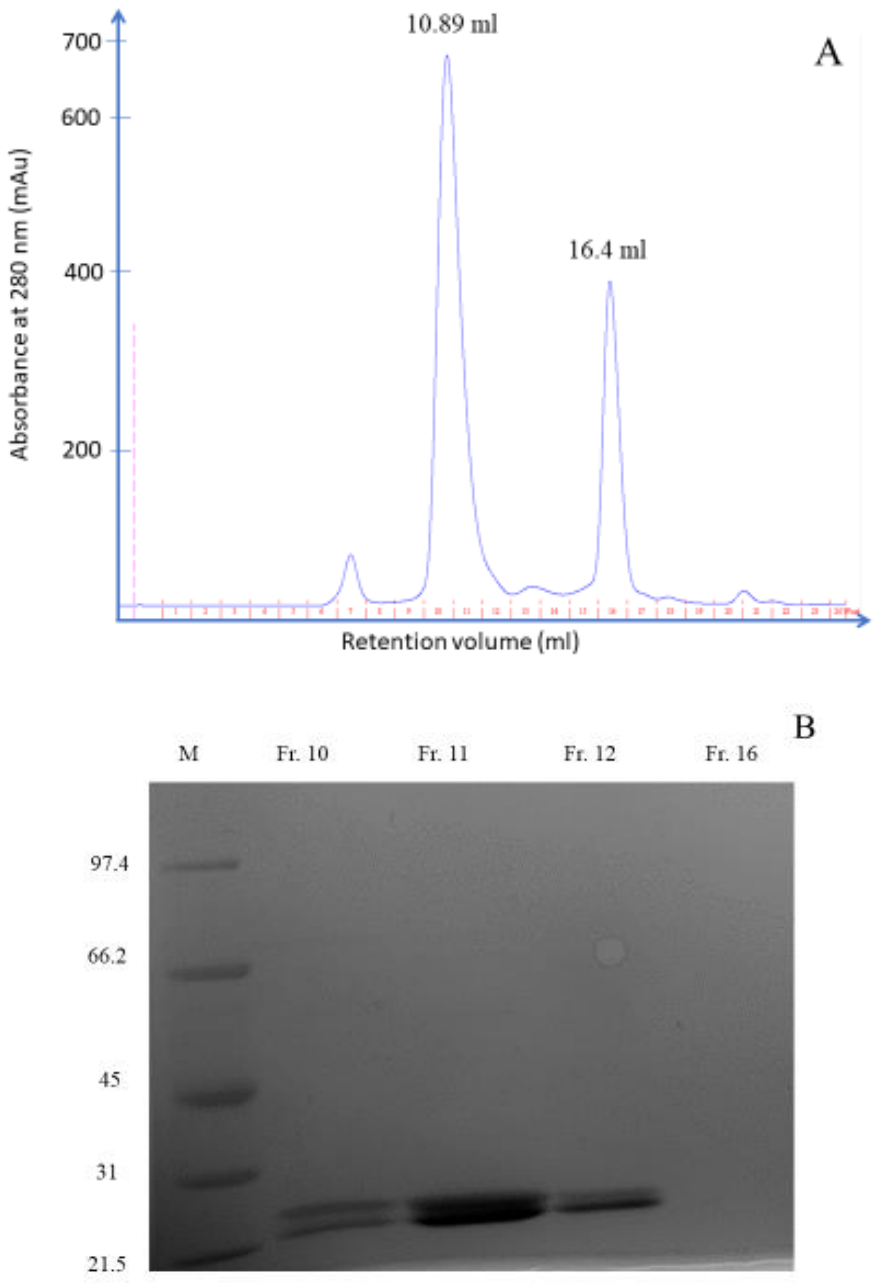

Figure 7.2. Size Exclusion Chromatography of GTP influence on H_6T_7-DmsD::DmsAl-GST complex. A. Sample chromatogram for H_6T_7-DmsD:: DmsAl-GST with GTP added. The total area under eluted peaks was determined and main peak area (%) was analyzed for each protein and tabulated. 500 µl samples were injected at a 1:1 molar ratio. **B.** Coomassie blue stained 12% SDS-PAGE of SEC eluted fractions including molecular weight markers (M), fractions 10, 11, 12, and 16.

7.3 Mg^{2+} does not lead to dissociation of DmsAl-GST from H_6T_7DmsD

Upon performing CD experiments we concluded that Mg^{2+} metal led to a 12.4% total structural change within DmsD::$DmsAl_{15-41}$ complex by increasing α-helix and decreasing β-sheet content (see section 5.6.1), we attempted to explore if recombinant DmsAl (bearing a C-terminal GST tag), would dissociate from its chaperone. The same procedure as in sections 7.1 and 7.2 was performed in order to explore the influence of Mg^{2+} metal. Figure 7.3 demonstrates that no change to the complex was observed and DmsAl-GST remained bound to DmsD. This could be interpreted in two different ways: either the metal did not affect the complex at all due to a variety of reasons (presence of a large GST tag shielded the binding site for the metal or another molecule such as GTP should have been present) or the secondary structure change observed by CD within the complex was not efficient to perturbed the DmsD::DmsAl complex`s structure.

A minor peak around fraction 16 (elution volume 16.44 ml) was similar to the one observed when lone DmsAl-GST was loaded on the column. We attempted to visualize it using SDS-PAGE, but due to a small concentration that was not possible. We hypothesized that it was the cleaved DmsA leader tag since the molecular size at 16.44 ml would be approximately 4.2 kDa, the size that roughly matched the first 41 residues of DmsA.

While no disassembly took place, it was noted that the apparent molecular weight of the complex increased by 5 kDa. That could potentially support the change in secondary structure that led to the H_6T_7-DmsD::DmsAl-GST complex moving faster through the column.

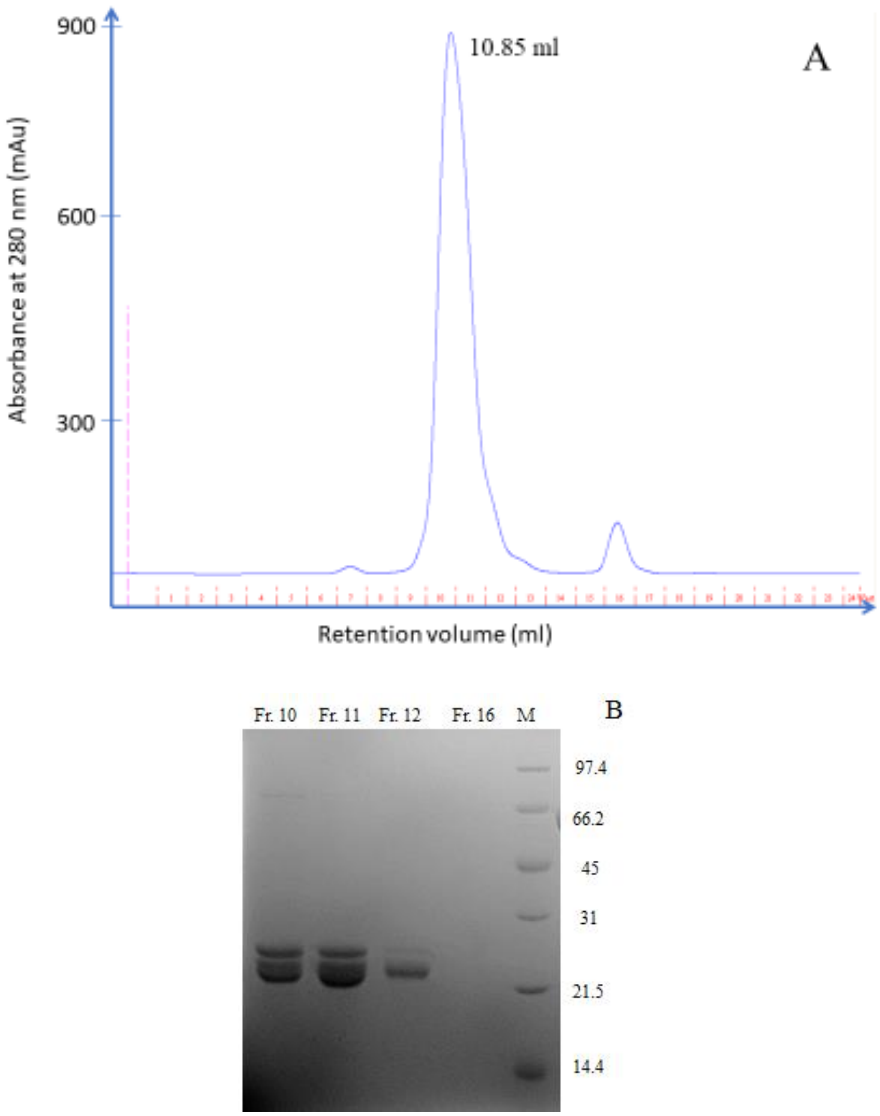

Figure 7.3. Size Exclusion Chromatography of Mg^{2+} influence on H_6T_7-DmsD::DmsAl-GST complex. The total area under eluted peaks was determined and main peak area (%) was analyzed for each protein and tabulated. 500µl samples were injected at a 1:1 molar ratio. **B.** Coomassie blue stained 12% SDS-PAGE of SEC eluted fractions including molecular weight markers (M), fractions 10, 11, 12, and 16.

7.4 Addition of Mg^{2+} with GTP does not lead to dissociation of DmsAl-GST from H_6T_7DmsD

As no dissociation with Mg^{2+} or GTP was detected alone, we attempted to mix the two molecules and add them to the existing DmsD::DmsAl-GST complex. However, the major elution peak (10.8 ml) presented in Figure 7.4 did not change compared to Figure 7.2 and the chromatogram looked very similar to the case where GTP was added alone (see section 7.2). The emerging minor shoulder was observed in cases of GTP and Mg^{2+} alone in several cases and was proposed to be present due to a slightly higher concentration of DmsAl-GST during the mixing. However, upon inspecting the resulting SDS-PAGE we noticed that fraction 12 did not contain a doublet representing DmsD::DmsAl complex anymore. Therefore, some conformational change could have taken place and an additional specie was now present (partial dissociation of one of the proteins). While the Unicorn software did not recognize the shoulder as an independent peak and, thus, did not provide us with an elution volume, an approximation would have granted approximately 11.5 ml which coincides with the elution volume of lone DmsAl-GST (11.7 ml). As with all the previous cases, the two proteins were mixed together in a 1 to 2 ratio since we again expected that a dimer of DmsAl-GST was binding H_6T_7-DmsD monomer. The density of bands was assessed via ImageJ and a ratio of 2:1 was determined for DmsAl-GST to H_6T_7-DmsD (see Table 7.2) with percentages evenly distributed among lanes 10, 11 and 12. The software did not detect any band density in fraction 16 (elution volume 16.45 ml).

Finally, we attempted to determine the molecular weight of the complex using the equation obtained from the molecular weight calibration plot. The calculation yielded a possible dimer::dimer interaction just as in case of H_6T_7-DmsD::DmsAl-GST complex with no effectors present. As seen in Table 7.1, the complex seemed slightly larger with an increase in 6 kDa.

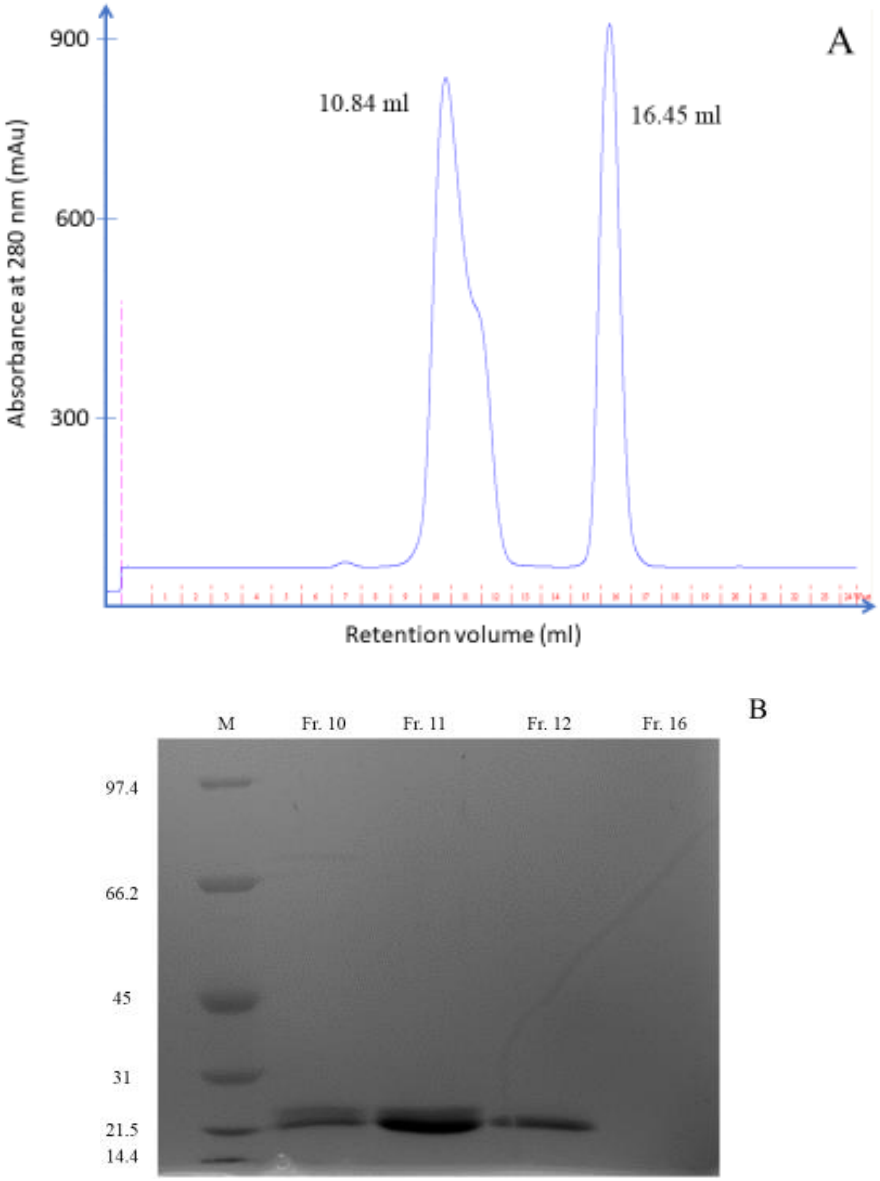

Figure 7.4. Addition of GTP and Mg^{2+} metal does not cause changes in H_6T_7-DmsD::DmsAl-GST complex. A. Elution profile of a combination of GTP and Mg^{2+} influence on. The total area under eluted peaks was determined and main peak area (%) was analyzed for each protein and tabulated. 500µl sample was injected with proteins being at 1:1 molar ratio. **B.** Coomassie blue stained 12% SDS-PAGE of eluted fractions including molecular weight markers (M), fractions 10, 11, 12 and 16.

7.5 MBP-TatB$_{fr}$ does not interact with H_6T_7-DmsD

MBP-TatB$_{fr}$ was mixed with H_6T_7-DmsD for 1 hour or overnight. We expected to detect the presence of any interaction via an elution of a complex of higher molecular weight (at least 56 kDa+ 27 kDa = 83 kDa for H_6T_7-DmsD with MBP-TatB$_{fr}$). Nevertheless, two mixed proteins eluted separately (the results are presented in Figure 7.5).

When inspecting SDS-PAGE, we observed a presence of MBP-TatB$_{fr}$ in fraction 12 in cases of both 1 hour and overnight incubation as well as presence of shoulder on the chromatogram for the overnight incubation which the Unicorn software did not identify as a separate peak. It would be highly unlikely for such a small amount of complex to form during a 16-hour period of time, provided there was some biological relevance to the interaction. Nevertheless, it would be important to mention that normally monomer MBP-TatB$_{fr}$ elutes at 10.5 ml which equals to 191.9 kDa (see chapter 3.3). We interpreted it as a consequence of a non-spherical, probably rod-shape, of the molecule. In both cases of incubation with H_6T_7-DmsD, MBP-TatB$_{fr}$ would not elute until 10.73-10.75 ml (0.2 ml later). That would imply that the molecular weight of the first substrate collected would be 163-165 kDa which was approximately 30 kDa less than MBP-TatB$_{fr}$ observed alone (191.9).

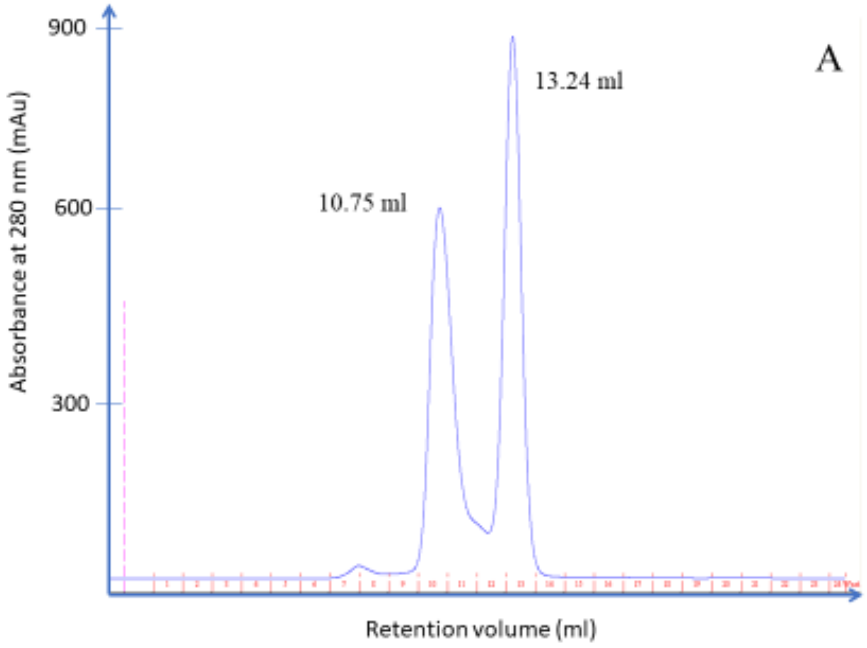
A
900
600
300
Absorbance at 280 nm (mAu)
13.24 ml
10.75 ml
Retention volume (ml)

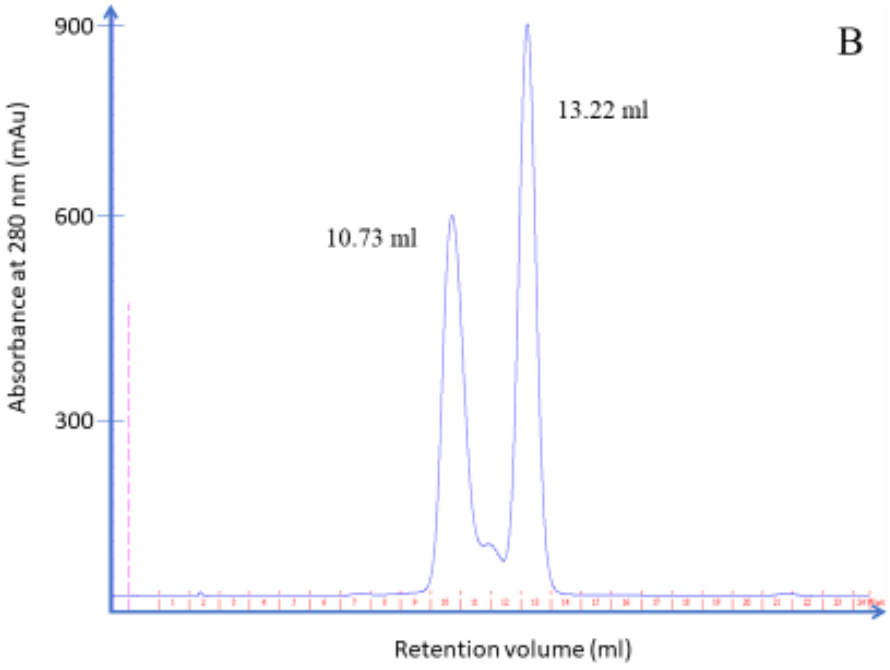
B
900
600
300
Absorbance at 280 nm (mAu)
13.22 ml
10.73 ml
Retention volume (ml)

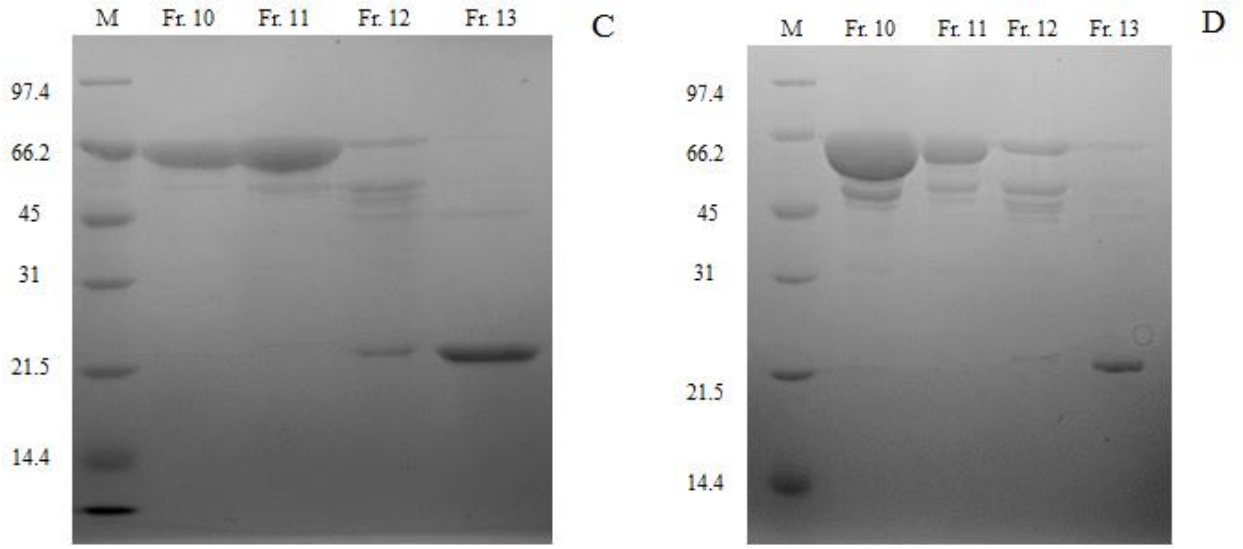

Figure 7.5. Size Exclusion Chromatography of a combination of MBP-TatB and H_6T_7-DmsD. A. 1-hour incubation of the two proteins. **B.** overnight incubation of the two proteins. The total area under eluted peaks was determined and main peaks area (%) was analyzed for each protein and tabulated. 500µl samples were injected at a 1:1 molar ratio. **C.** Coomassie blue stained 12% SDS-PAGE of eluted fractions from 1-hour incubation of MBP-$TatB_{fr}$ and H_6T_7-DmsD including molecular weight markers (M), fractions 10, 11, 12 and 13. **D.** Coomassie blue stained 12% SDS-PAGE of eluted fractions from overnight incubation of MBP-$TatB_{fr}$ and H_6T_7-DmsD including molecular weight markers (M), fractions 10, 11, 12 and 13.

Furthermore, we assessed the density of bands in various lanes for the 1-hour incubation of the proteins (overnight samples were concentrated and, thus, any assessment would not be meaningful). Based on the percentages determined via ImageJ, we calculated that approximately 54 µg of MBP-$TatB_{fr}$ and 79 µg of H_6T_7-DmsD were present in lane 12. Therefore, there was a potential 1:1.5 ratio binding which could probably be rounded to 1:1 based on the fact that free H_6T_7-DmsD is normally present in fraction 12. However, we tend to believe that there was a higher probability of the shoulder being a different species of MBP-$TatB_{fr}$.

7.6 MBP-TatB$_{fr}$ construct is interacting with DmsAl-GST

As cross-linking experiments have previously shown that TatB interacts with the entire signal sequence of the substrate, we attempted to explore the possible binding between DmsAl-GST and MBP-TatB$_{fr}$ (Alami et al, 2003). Similar to incubating DmsD with TatB proteins, we incubated the latter for 1 hour and injected onto the column.

Two peaks were observed across fractions 10, 11 and 12. We collected those for SDS-PAGE and calculated apparent molecular weights. As seen in Table 7.1 the first peak represents a complex consisting of 153 kDa eluting at 10.85 ml, while the second- 68 kDa eluting at 12.07 ml. Neither of those matched the apparent molecular weight of only MBP-TatB$_{fr}$ which eluted at 10.51 ml (earlier) and was considered monomeric (see section 3.3). Based on the calibration curve equation the molecular weight of monomeric MBP-TatB$_{fr}$ from SEC purification (see section 3.3) would be 191.9 kDa which would imply that we were dealing with a trimer (if the shape of the molecule is drastically different from the sphere and it is moving differently than predicted 56 kDa*3=168 kDa). If we were to assume here that the following was true, a decrease in the molecular weight would translate into quite an extreme change in secondary structure. That could have been a result of an interaction with DmsAl-GST. Alternatively, there could have been a transient binding to DmsAl-GST which led to a loss of a monomer. Figure 7.6 B strongly supports the latter interpretation since we observed that each of the lanes contained some of TatB and DmsAl constructs. The last point to consider here is the data from the native PAGE which demonstrated that MBP-TatB$_{fr}$ which we considered a monomer (see chapter 3.3) migrates as a true monomer.

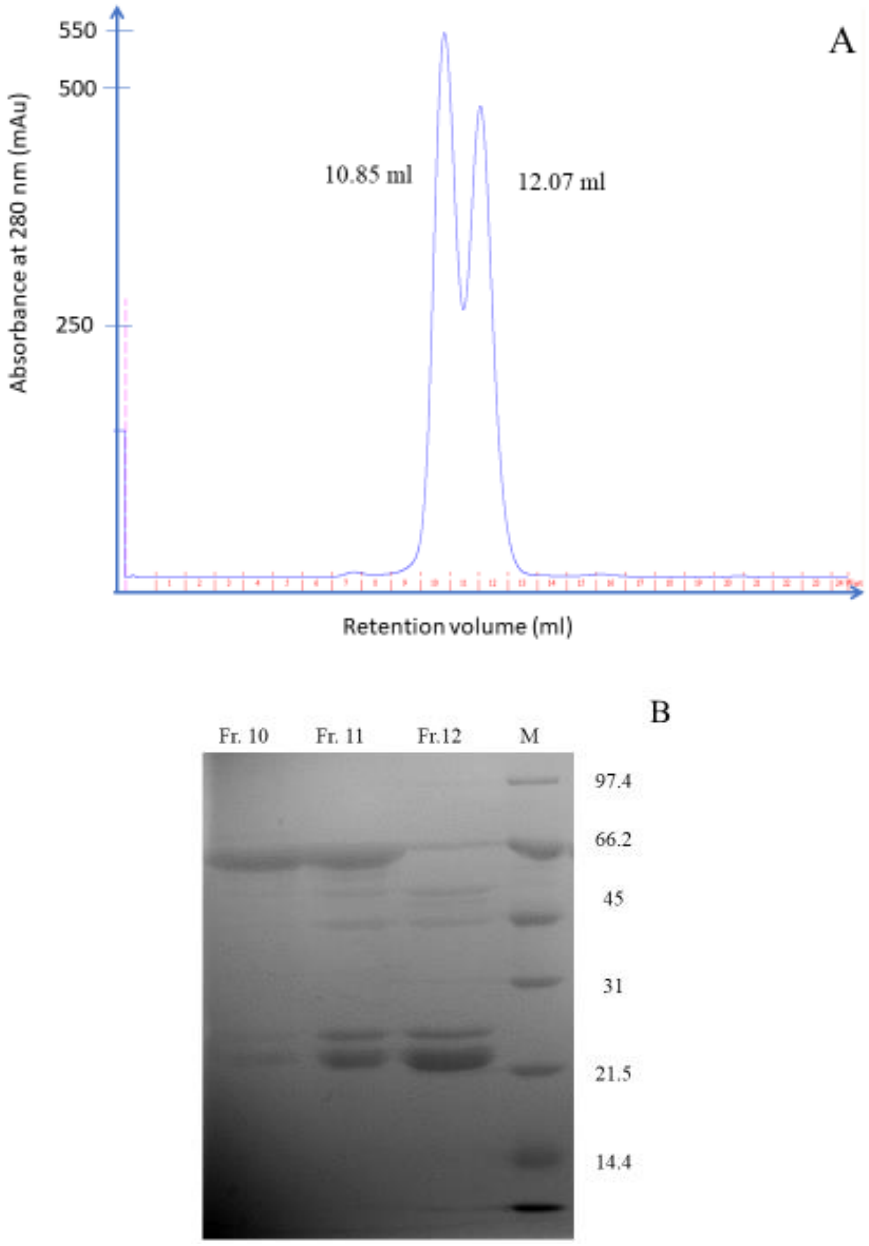

Figure 7.6. MBP-TatB$_{fr}$ and DmsAl-GST constructs interact. A. Elution profile of MBP-TatB$_{fr}$ and DmsAl-GST after 1-hour incubation. The total area under eluted peaks was determined and main peaks area (%) was analyzed for each protein and tabulated. 500µl samples were injected at a 1:1 molar ratio. **B.** Coomassie blue stained 12% SDS-PAGE of eluted fractions from 1-hour incubation of MBP-TatB$_{fr}$ and DmsAl-GST including molecular weight markers (M), fractions 10, 11, and 12.

This led us to modify our initial interpretation and conclude that an interaction between TatB and

DmsAl takes place and results in either an assembly of a complex (which we might not see due

to an overlap of two peaks) or change in secondary structures of both proteins. Based on the binding modes reported by other research groups (weak and strong binding regimes between TatBC and the substrate), both options are possible. Transient interaction, in our case, could have resulted from the absence of TatA and/or TatC which both are needed to be present for strong binding (Whitaker et al, 2012).

Density analysis using ImageJ demonstrated that 14% of all MBP-$TatB_{fr}$ population was present in lane 12 with 59% DmsAl-GST protein

7.7 TatB2 peptide does not cause dissociation of the H_6T_7-DmsD::DmsAl-GST complex, but likely changes its conformation.

As CD studies demonstrated that TatB2 peptide could influence H_6T_7-DmsD::$DmsAl_{15-41}$ peptide complex (see section 5.4), we decided to investigate whether the same peptide could influence the binding between proteins using SEC technique. Upon 1 hour incubation of DmsD with DmsAl-GST, we added TatB2 peptide, incubated for another hour and observed the effect.

As seen in Figure 7.7 no dissociation took place between H_6T_7-DmsD and DmsAl-GST. Density percentages in lanes 10 and 11 between the two proteins were also very similar (see Table 7.2). However, it was noted that the complex eluted at an earlier time point and, thus, the calculated weight increased from 148.3 kDa to 162.7 kDa.

We then reversed the experiment to see whether TatB2 peptide adding before DmsAl-GST would lead to some sort of s structural change and prevent the two recombinant proteins from binding to each other. As seen in Figure 7.8, the complex was still able to be formed.

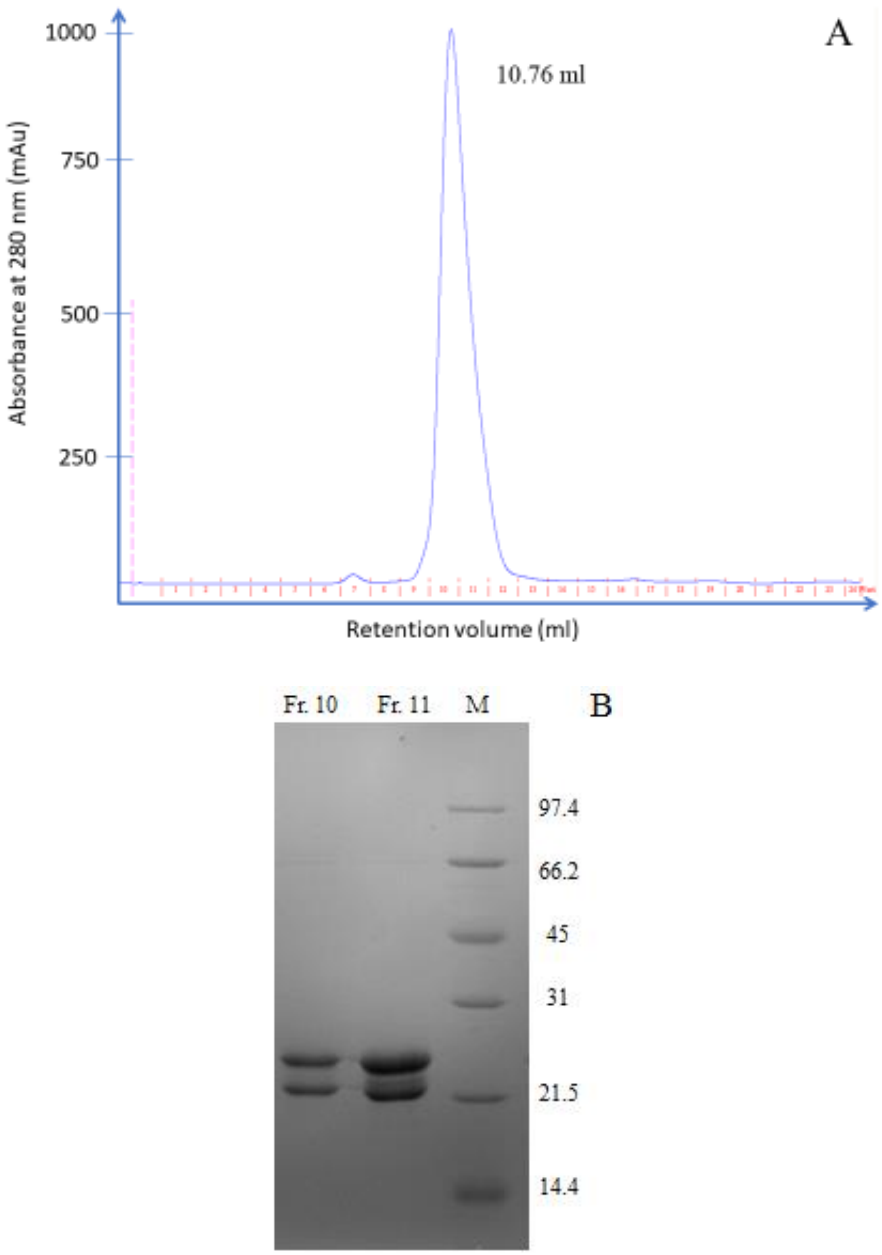

Figure 7.7. TatB2 added after DmsAl-GST does not cause dissociation of the REMP::substrate complex. A. Elution profile of H_6T_7-DmsD::DmsAl-GST complex after 1-hour incubation with TatB2 which was added after DmsAl-GST. The total area under eluted peaks was determined and main peaks area (%) was analyzed for each protein and tabulated. 500 µl samples were injected at a 1:1 molar ratio. **B.** Coomassie blue stained 12% SDS-PAGE of eluted fractions from H_6T_7-DmsD::DmsAl-GST complex after 1-hour incubation with TatB2 which was added after DmsAl-GST including molecular weight markers (M), fractions 10, and 11.

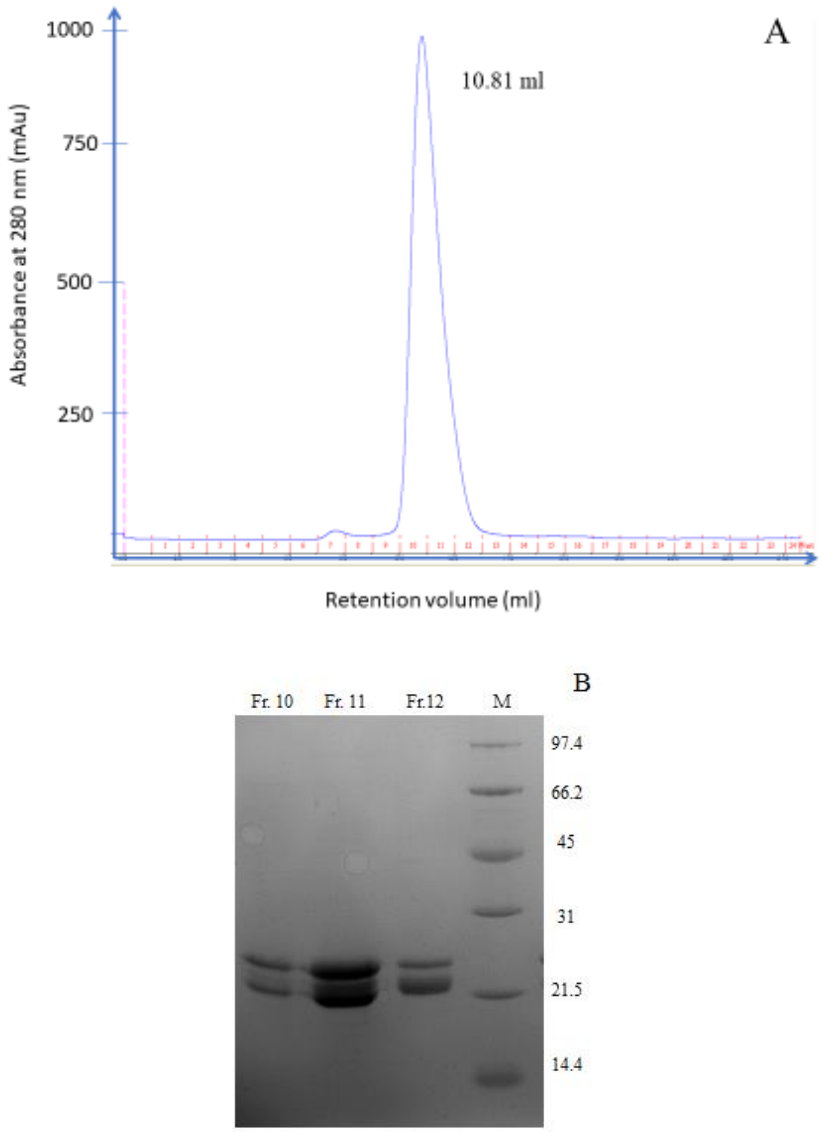

Figure 7.8. TatB2 added prior DmsAl-GST does not cause dissociation of the REMP::substrate complex. A. Elution profile of H_6T_7-DmsD::DmsAl-GST complex after 1-hour incubation with TatB2 which was added prior DmsAl-GST. The total area under eluted peaks was determined and main peaks area (%) was analyzed for each protein and tabulated. 500µl samples were injected at a 1:1 molar ratio. **B.** Coomassie blue stained 12% SDS-PAGE of eluted fractions from H_6T_7-DmsD::DmsAl-GST complex after 1-hour incubation with TatB2 which was added prior DmsAl-GST including molecular weight markers (M), fractions 10, 11, and 12.

Elution time was similar to the peptide added last, but still earlier than the complex alone (10.9 ml). Again, an increase in the apparent molecular weight was observed. This time, however, it

was smaller, by 9 kDa compared to 14.4 kDa for TatB2 added after the incubation of the two recombinant proteins suggesting shape changes.

7.8 GST-$TatB_{fr}$ shows no binding to H_6T_7-DmsD.

As we were not able to show that MBP-$TatB_{fr}$ interacts with H_6T_7-DmsD and other techniques strongly supported that, we attempted to utilize an alternative to MBP tag. Therefore, we employed an N-terminal GST tag with the same fragment of TatB. As in the previous cases, we mixed two proteins in a one-to-one molar ratio. Figure 7.9 A demonstrates that two peaks eluted at 7.6 ml and 13.02 ml. We also inspected the SDS-PAGE gel to determine where each protein was located. As the volume of the assay was slightly smaller than our regular one (300 μl) and fractions 12 and 13 were pooled, we concentrated both fractions and, thus, the density of the bands was not assessed this time.

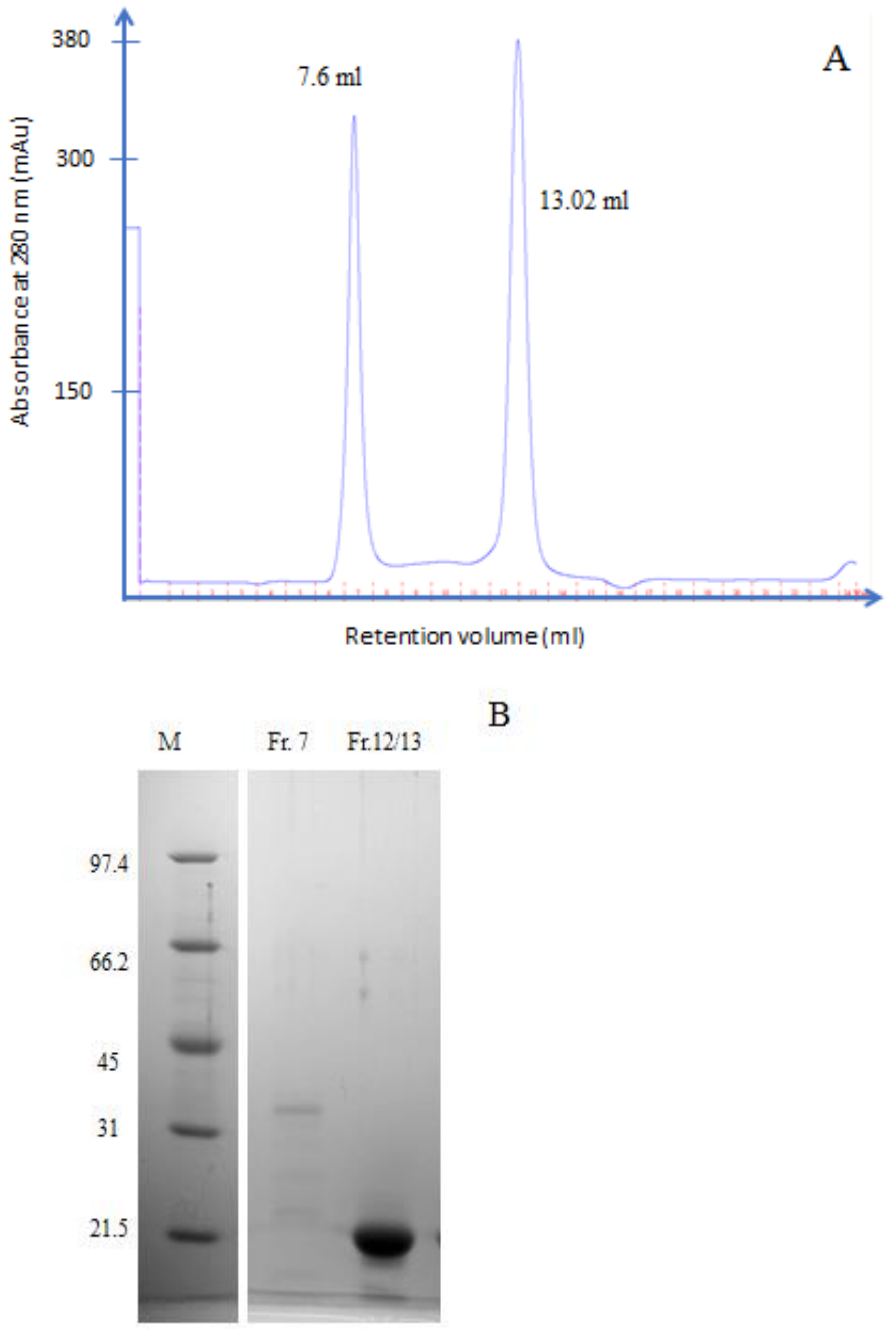

Figure 7.9. No binding is observed between GST-TatB$_{fr}$ and H$_6$T$_7$-DmsD. A. Size Exclusion Chromatography of a combination of GST-TatB and H$_6$T$_7$-DmsD. The total area under eluted peaks was determined and main peaks area (%) was analyzed for each protein and tabulated. 500µl sample was injected at 1:1 molar ratio. **B.** Coomassie blue stained 12% SDS-PAGE of eluted fractions from 1-hour incubation of GST-TatB$_{fr}$ and H$_6$T$_7$-DmsD including molecular weight markers (M), fractions 7 and 12/13.

Each of the proteins was present in a separate lane: fraction 7 contained GST-$TatB_{fr}$, while fractions 12/13- H_6T_7-DmsD. As the elution volume of the first one was very close to the V_o of the Superose 12 column, it was not possible to determine the molecular weight from the calibration curve equation. Nevertheless, the apparent molecular weight of H_6T_7-DmsD migration was calculated as 36.5 kDa.

Discussion

Analytical Size Exclusion Chromatography (SEC) is a powerful method to see changes in multimeric states, and subtle differences in quaternary structure that is illustrated by changes in the Stokes hydrodynamic volume /radius of the protein particle (Cantor and Schimmel, 1980). Such experiments are expected to determine subtle shape changes leading to hydrodynamic volume change as a result of ligand binding. A standard curve using proteins of spherical structure of known molecular weights. This allowed for calculation of the apparent molecular weight. All experiments here were run at pH 8.0 in the same elution conditions (0.7 ml/min) and Hi-Trap buffer (25 mM Tris-HCl, 10 mM NaCl). The variance in elution volumes between runs was on the order of less than 0.8%. Even differences in equilibrium can be sensed by collecting fractions and evaluating by SDS-PAGE the protein content. Here we interpreted the protein levels using Image J intensities obtained from SDS-PAGE gels of samples from peak fractions. Here SEC was employed to explore the behavior of H_6T_7-DmsD when other effectors are added. We decided to explore primarily the influence of other biomolecules on the REMP::substrate complex, but attempted several experiments with sole H_6T_7-DmsD as well. We also addressed the possible binding between DmsAl and TatB which was previously shown by the members of our laboratory (Kostecki et al, 2010). The data is summarized in Tables 7.1 and 7.2.

Table 7.1 Size Exclusion Chromatography analysis of interaction between molecules. Molecular weights were determined using calibration curve equation Log MW=6.1276-2.5933*K_{av} (partition coefficient = $(V_e - V_o)/(V_t - V_o)$). Predicted molecular weights (MW) were calculated based on previously published data (Winstone et al, 2006) or an assumption of a monomer::monomer interaction.

Protein(s) and any effectors added	**Predicted molecular weight (kDa)**	**Peak #1 (elution volume) (ml)**	**Peak #2 (elution volume) (ml)**	**MW of Peak#1 (kDa)**	**MW of Peak#2 (kDa)**	**Interpretation of molecular weight**
H_6T_7-DmsD	27 kDa	13.13	-	33.9	-	monomer
DmsAl-GST	60 kDa (DmsAl-GST was reported to elute as a dimer)	11.7	-	87.4	-	dimer
MBP-$TatB_{fr}$	56 kDa	10.51	-	191.9	-	Trimer
GST-$TatB_{fr}$	42 kDa	7.60	-	NA	-	NA
H_6T_7-DmsD + DmsAl-GST	87 kDa (DmsAl-GST was reported to elute as a dimer)	10.9	-	148.33	-	dimer:dimer
H_6T_7-DmsD + DmsAl-GST + Mg^{2+}	87 kDa (DmsAl-GST was reported to elute as a dimer)	10.85	-	153.3		dimer:dimer with an altered secondary structure
H_6T_7-DmsD + DmsAl-GST + GTP	87 kDa (DmsAl-GST was reported to elute as a dimer)	10.89	14.4	149.3	False positive signal	dimer:dimer
H_6T_7-DmsD + DmsAl-GST + GTP/Mg^{2+}	87 kDa (DmsAl-GST was reported to elute as a dimer)	10.84	-	154.3	-	dimer:dimer with an altered secondary structure
H_6T_7-DmsD + DmsAl-GST + TatB2 (added after dimer:dimer formation).	~88-90 kDa (with attachment of TatB2 peptide(s)) or 30 kDa (monomer of H_6T_7-DmsD) 60 kDa (dimer of DmsAl-GST)	10.76	-	162.7	-	dimer:dimer:peptide complex or dimer:dimer with an altered secondary structure
H_6T_7-DmsD +	~88-90 kDa (with	10.81	-	157.4	-	dimer:dimer:peptide complex or

DmsAl-GST + TatB2 (added prior dimer:dimer formation).	attachment of TatB2 peptide(s)) or 30 kDa (monomer of H_6T_7-DmsD) 60 kDa (dimer of DmsAl-GST)					dimer:dimer with an altered secondary structure
H_6T_7-DmsD + MBP-$TatB_{fr}$	83 kDa	10.75	13.24	163.8	31.5	Change in MBP-$TatB_{fr}$ secondary structure; no interaction between two recombinant proteins
H_6T_7-DmsD + MBP-$TatB_{fr}$ (overnight incubation)	83 kDa	10.73	13.22	165.9	31.9	Change in MBP-$TatB_{fr}$ secondary structure; no interaction between two recombinant proteins
DmsAl-GST + MBP-$TatB_{fr}$	116 kDa (if monomer MBP-$TatB_{fr}$ binds DmsAl-GST dimer) or 86 kDa (MBP-$TatB_{fr:}$::DmsAl-GST complex) and 30 kDa (monomer of DmsAl-GST)	10.85	12.07	153.3	68.4	DmsAl-GST dimer disassembly; MBP-$TatB_{fr}$ Trimer disassembly
H_6T_7-DmsD + GST-$TatB_{fr}$	69 kDa	7.6	13.02	NA (too close to v_o)	36.5	Possible aggregation of GST-$TatB_{fr.;}$ No binding observed. Possible transient interaction leads to change in secondary structure of H_6T_7-DmsD

[1] NA is defined as “not determined”.

Table 7.2. SDS-PAGE analysis of protein-containing fractions collected during SEC experiments.

Protein(s) and any effectors added	**Lane content percentages obtained via ImageJ software and concentration ratios for protein combinations**	**True (loaded) amounts of protein**
H_6T_7-DmsD	NA	500 µg
DmsAl-GST	NA	1150 µg
MBP-$TatB_{fr}$	NA	-
GST-$TatB_{fr}$	NA	-
H_6T_7-DmsD + DmsAl-GST	**H_6T_7-DmsD:** Lane 10: 36.8% Lane 11: 43.7% Lane 12: 19.4% **DmsAl-GST:** Lane 10: 32% Lane 11: 31.7% Lane 12: 36.2% 1:1.2 concentration ratio	H_6T_7-DmsD: 500 µg DmsAl-GST: 1150 µg Expected molar ratio:1:1 Expected concentration ratio: 1:2.3
H_6T_7-DmsD + DmsAl-GST + Mg^{2+}	**H_6T_7-DmsD:** Lane 10: 35.3% Lane 11: 28.1% Lane 12: 36.6% **DmsAl-GST:** Lane 10: 40.6% Lane 11: 40.7% Lane 12: 11.7% 1:1.4 concentration ratio	H_6T_7-DmsD: 500 µg DmsAl-GST: 1150 µg Expected molar ratio:1:1 Expected concentration ratio: 1:2.3
H_6T_7-DmsD + DmsAl-GST + GTP	**H_6T_7-DmsD:** Lane 10: 35.1% Lane 11: 37.7% Lane 12: 27.2% **DmsAl-GST:** Lane 10: 33% Lane 11: 34.9% Lane 12: 32.1% 1:1.5 concentration ratio	H_6T_7-DmsD: 500 µg DmsAl-GST: 1150 µg Expected molar ratio:1:1 Expected concentration ratio: 1:2.3
H_6T_7-DmsD + DmsAl-GST + GTP/Mg^{2+}	**H_6T_7-DmsD:** Lane 10: 35.7% Lane 11: 40.2% Lane 12: 24% **DmsAl-GST:** Lane 10: 29.3%	H_6T_7-DmsD: 500 µg DmsAl-GST: 1150 µg Expected molar ratio:1:1

	Lane 11: 37.9% Lane 12: 32.8% 1:2.2 concentration ratio	 Expected concentration ratio: 1:2.3
H_6T_7-DmsD + DmsAl-GST + TatB2 (added after dimer:dimer formation).	**H_6T_7-DmsD:** Lane 10: 29.5% Lane 11: 70.5% **DmsAl-GST:** Lane 10: 27.9% Lane 11: 72.1% 1:1.04 concentration ratio	H_6T_7-DmsD: 500 µg DmsAl-GST: 1150 µg TatB2: 203.5 µg Expected molar ratio:1:1:10 Expected concentration ratio: 1:2.3:5.7
H_6T_7-DmsD + DmsAl-GST + TatB2 (added prior dimer:dimer formation).	**H_6T_7-DmsD:** Lane 10: 16.5% Lane 11: 66.5% Lane 12: 17% **DmsAl-GST:** Lane 10: 18.4% Lane 11: 63.5% Lane 12: 18.2% 1:0.94 concentration ratio	H_6T_7-DmsD: 500 µg DmsAl-GST: 1150 µg TatB2: 203.5 µg Expected molar ratio:1:1:10 Expected concentration ratio: 1:2.3:5.7
H_6T_7-DmsD + MBP-$TatB_{fr}$	**H_6T_7-DmsD:** Lane 12: 15.8% Lane 13: 84.2% **MBP-$TatB_{fr}$:** Lane 10: 41.1% Lane 11: 53.1% Lane 12: 5.2% Lane 13: 0.5% 1:2.2 concentration ratio	H_6T_7-DmsD: 500 µg MBP-$TatB_{fr:}$ 1040 µg Expected molar ratio:1:1 Expected concentration ratio: 1:2.08
DmsAl-GST + MBP-$TatB_{fr}$	**DmsAl-GST:** Lane 10: 8% Lane 11: 32.8% Lane 12: 59.2% **MBP-$TatB_{fr}$:** Lane 10: 31.8% Lane 11: 54%	DmsAl-GST: 1150 µg MBP-$TatB_{fr}$: 1040 µg Expected molar ratio:1:1 Expected concentration ratio:

	Lane 12: 14% 1:0.95 concentration ratio	1:1.1

[1] NA is defined as "not applicable". [2] Expected concentration ratio was based on the amounts of protein loaded on the column (DmsD was consistently at 1 µg/µl, while concentrations of other effectors were adjusted in order to match molarity). [3] Expected molar ratio was kept at 1:1 and calculated from the concentration of DmsD which was at 1 µg/µl (500 µg of 27 kDa DmsD was equal to 37.04 µM)

It is most likely that the complex of H_6T_7-DmsD and DmsAl-GST consists of a monomer of REMP and a dimer of a substrate. While the ImageJ calculation yielded a 1:1 ratio of proteins present on the SDS-PAGE it is important to remember that for equal molarities of two interacting proteins double the concentration of DmsAl-GST was loaded (based on the molecular weight calculation) onto the column with H_6T_7-DmsD. We were somewhat suspicious of the ImageJ due to the reliance of the software on the loading of the gel, homogeneity of staining, run consistency, and the subjectivity of the run set up of the density determination area around the inspected band. Nevertheless, we continued comparing our results as any error or variability would be consistent throughout the experiments.

As our column was calibrated with molecular weight standards we interpreted the results also based on apparent MW. Thus if the complex consists of a monomer and a dimer, their migration is considerably faster than anticipated (elution volume is smaller due to the complex exiting the column earlier): 148 kDa instead of expected 120.9 kDa, which would have resulted from combining the apparent molecular weight of DmsAl-GST (87 kDa) and H_6T_7-DmsD (33.9 kDa). This difference allows us to imply changes in the complex shape deviations from spherical and subtle shape changes originating from secondary or tertiary structure changes in one or both molecules has taken place.

Addition of GTP alone did not lead to dissociation of one or both molecules of DmsAl-GST from H_6T_7-DmsD. Therefore, we could not support the previous finding by Cherak and Turner where they utilized a dissociation assay on an affinity column to show that GTP abrogated binding between DmsD and DmsAl (2015). Nevertheless, it should be pointed that the authors employed a buffer with 5 mM DTT and of high ionic strength (50 mM Tris–HCl, 200 mM NaCl), while we continued utilizing the same low-salt buffer for all the techniques throughout the thesis (Cherak and Turner, 2015). The following difference could have led to more non-specific (ionic) interactions in our experiments or weaker binding for their experiments. We also had lower GTP concentrations (350 µM or 0.35 mM) compared to Cherak and Turner who used up to 10 mM GTP for their titrations (2015). Moreover, we observed that the complex remained at almost the same apparent molecular weight (149 kDa versus GTP-free experiment 148 kDa). ImageJ yielded a 1:1.5 ratio of the molecules as well as close percentages of proteins present in lanes: 33-35% of DmsAl-GST from each of the lane binding to 27-35% of H_6T_7-DmsD. This made us conclude that under the following conditions GTP has no influence on the interactions of the two proteins under the conditions here.

The H_6T_7-DmsD::DmsAl-GST complex did not undergo disassembly upon addition of Mg^{2+} metal. Still, we observed a change in elution time and consequently an increase in apparent molecular weight. The added molecular weight could not be a protein (5 kDa), but was probably a result of a structural change that took place upon incubation of the formed complex with the metal. A similar change was observed in the case of apo and bound forms of ZneB, a component of a heavy-metal efflux system, which normally has an elongated shape and, thus, elutes earlier (61 kDa). When Zn metal is added, the structural change takes place and the protein::metal complex is collected in later fractions (44 kDa) and matches its real molecular weight (39 kDa)

(Angelis et al, 2010). Density analysis via ImageJ demonstrated a 1 to 1.4 ratio of H_6T_7-DmsD to DmsAl-GST which did not overlap with the concentration applied to the column (1:2.3). Addition of Mg metal and GTP combination also did not result in dissociation of the complex. Nevertheless, this time we were able to obtain a 2:1 density ratio from ImageJ software and confirmed that monomers of DmsD were binding to dimers of DmsAl. Furthermore, we observed a small shift in the elution volume of the complex (0.06 ml from 10.90 ml to 10.84 ml) to the left which translated into extra 6 kDa of weight based on the calibration curve equation. This was almost identical to the addition of Mg^{2+} alone where a complex eluted at 10.85 ml. This results implies that the structural change is mediated primarily by Mg^{2+}. Nevertheless, it is important to remember that magnesium ions bound to proteins are usually coordinated by guanine nucleotides allowing the system to complete hydrolysis and signal transduction (Rudack et al, 2012). Although earlier experiments still suggest GTP is also involved as NMR experiments where GTP hydrolysis by DmsD would only happen in the presence of leader peptide and Mg^{2+} metal (Vy Tran thesis, 2011).

From the SEC data it is highly likely that constructs of MBP-$TatB_{fr}$ and DmsAl-GST interacted with each other. This was supported by a difference in elution times compared to two proteins alone. DmsAl-GST normally elutes at 11.7 ml while here it was collected earlier with it distributed over several fractions (10.85 ml to 12.07 ml): 8% of it even present in fraction 10 (elution volume 10.85 ml), 32.8%- in fraction 11 and 59.2%- in fraction 12 (elution volume 12.07). The opposite was found for MBP-$TatB_{fr}$ which “lost” some of its hydrodynamic volume and initially eluted at 10.85 ml instead of the expected 10.51 ml. While it is hard to state confidently what complexes and in what ratios were assembled, these experiments suggest and support previous findings there is a TatB::DmsAl interaction.

While no binding was detected between GST-$TatB_{fr}$ and H_6T_7-DmsD, an observation regarding a small increase in molecular weight was made. More specifically, the apparent molecular weight of DmsD increased from 33.9 kDa to 36.5 kDa which translated into 2.6 kDa difference. It is tempting to speculate that while no complex was observed, some transient interaction took place leading to a minor secondary structure change. Alternative the interaction on/off kinetics was fast on the timescale of the SEC. A similar claim may be made in relation to another TatB construct. However, we tend to believe that a special orientation is required. Recently another group employed cytoplasmic TatA and TatB proteins from *S. lividans* to explore potential binding with an RR-signal sequence peptide. Both Tat components recognized the substrate via the presence of the twin-arginine signal peptide. Importantly, they utilized TatA and TatB with GST tags, but immobilized on the beads while the substrate was continuously flowing (De Keersmaeker et al, 2007). A similar observation was made during preliminary experiments (unpublished) in our laboratory with gravity-flow amylose column where the binding between MBP-$TatB_{fr}$ and H_6T_7-DmsD was demonstrated. Therefore, we suggest here that the conformation or dynamics of the MBP tag shields the binding site on TatB and makes it inaccessible for DmsD.

Finally, the addition of a peptide did not lead to the dissociation of the complex H_6T_7-DmsD::DmsAl-GST complex when added before or after DmsAl-GST. Nevertheless, an increase in the apparent weight (increase in hydrodynamic volume) of the complex was observed. It was greater in a case where TatB2 was added after incubation of H_6T_7-DmsD with DmsAl-GST (9 kDa) compared to pre-incubation of TatB2 with H_6T_7-DmsD (14.4 kDa). This may be interpreted in two different ways: peptides may be binding to the complex and, thus, making the complex heavier physically or TatB2 may be causing a structure change within the complex leading to a

larger volume/radius. The slight difference in sequence addition of the peptide versus DmsAl-GST is consistent with CD experiments (see section 5.4), where the greater structural change was observed for experimental mix of TatB2 and DmsD::$DmsAl_{15-41}$ compared to DmsD::TatB2 and $DmsAl_{15-41}$.

To conclude, we detected that Mg^{2+} metal on its own, as well as various forms of TatB (two constructs and a peptide) affect the hydrodynamic volume/radius of the complex by potentially making it more elongated. Addition of GTP was the only effector studied that did not lead to any perturbations. Future work could employ dynamic light scattering methods or SEC- Multi-Angle light scattering (SEC-MALS), or small angle x-ray scattering (SAXS) to explore the radius and volume shape of the formed H_6T_7-DmsD::DmsAl-GST upon addition of Mg^{2+} and TatB2.

Chapter 8. Conclusions and future work.

8.1. Summary of thesis results

The following thesis aimed to answer a number of questions regarding the nature of the interaction relationships between DmsD, TatB and DmsA leader peptide.

8.1.1. Targeting of DmsD-to-TatB interaction (Objectives #2 and #6)

By utilizing DSF technique (Chapter 4), we learned that the addition of MBP-$TatB_{fr}$ protein results in stabilization of DmsD through the higher melting temperature as well as a decrease in melting cooperativity. With the same approach we were able to identify a peptide (TatB1) which resulted in a similar effect. In Chapter 5 we followed up on our observations from Chapter 4 and tested how TatB1/2/3 peptides altered the structure of DmsD. While TatB1 was not observed to result in any conformational change of the REMP protein, addition of TatB2 led to a higher helical content within the final structure. We determined the dissociation constants for TatB2 peptide titration into DmsD at pH 7.0 ad 8.0 as 4.70 μM and 5.40 μM, respectively. Therefore, we supported the hypothesis that DmsD interacts with TatB as well as established that the interaction leads to a different structural change in DmsD compared to addition of the substrate DmsA leader. In Chapter 7 we attempted to demonstrate a formation of the complex between recombinant DmsD and TatB proteins using size-exclusion chromatography, but were not successful: only perturbations to the elution volume of the proteins were observed. This led us to suggest that the interaction is transient and we are not able to detect the formation of the complex on the timescale of the employed technique.

8.1.2. Effect of small pH changes (Objective #3).

Another goal of this work was to understand the impact of the pH component of the proton motif force on DmsD-to-TatB relationship. To do this, we varied pH in DSF and CD experiments. It

was found that the melting profile of DmsD with MBP-$TatB_{fr}$ added at pH 8.0 is quite different from pH 7.0 or 7.5. Furthermore, dissociation constants for both techniques increased with increasing pH which implies that the affinity between TatB and DmsD decreased. We interpreted it as a potential step that might take place once the substrate has been transferred to the translocation apparatus and DmsD requires a mechanism that will allow it to return to the free pool of chaperone.

8.1.3. Studying the sequence of substrate transfer and binding site(s) (Objectives #4 and #5)

Our next aim was to investigate if the binding sites for the DmsA leader peptide and TatB were the same. We employed P86Q DmsD variant that was previously shown to have two-fold decreased affinity towards the DmsAl. We hypothesized that if TatB and leader peptide were to share the binding site, the affinity for TatB would be reduced as well. Notably, K_d values for the wild-type and DmsD variant were almost identical (5.40 μM and 5.45 μM). This prompted us to perform experiments with addition of DmsAl/TatB2 into DmsD::TatB2/DmsAl complexes and attempt subsequent titrations. While the dissociation constants were quite similar between W-T DmsD and P86Q variant, the order of addition (TatB2 versus DmsAl) played a significant role with K_d for titration of DmsAl into DmsD::TatB2 complex being 3-fold greater compared to the reverse experiment (24.24 and 24.43 μM versus 8.88 and 8.26 μM for W-T and P86Q, respectively). We, thus, deduced that TatB is more likely to interact with the REMP::RR-leader substrate complex compared to the REMP being already bound to TatB and then interacting with the RR-leader substrate. We also concluded that the binding sites on the surface of DmsD for DmsA leader peptide and TatB are different. Modeling of the putative TatB binding site using CABS-dock web server in and comparison of the residues to the previously-identified by Chan *et*

al. supported our hypothesis that the binding sites for the two proteins on DmsD are distinct (Chapter 6) (2008).

8.1.4. Improving our understanding of role for GTP in DmsD and DmsD::DmsAl complex (Objectives #7 and #8)

Our next goal was to study the effect of GNP with a greater focus on GTP due to its higher concentration within the cell. In Chapter 5 we showed that GTP leads to changes within the secondary structure of DmsD and DmsD::DmsAl complex. However, the K_d could not be established by CD for titrations into these complexes and thus no comparison could be made to the previously determined values via dissociation assay (Cherak and Turner, 2015). As a result, we investigated the influence of GTP on the DmsD::DmsAl complex via size-exclusion chromatography. The complex eluted as in the case of the control which was interpreted as absence of GTP influence under the current experimental conditions. Nevertheless, modeling in Chapter 6 we were able to identify two GTP-binding motifs with one of them sharing some of the residues with experimentally-identified leader binding site (Chan et al, 2008). Moreover, we successfully titrated GTP into DmsD::TatB2 complex during the CD and found the dissociation constant to be equal to 5.60 μM (Chapter 5). Combined together this data implies that GTP has some impact of the conformation of DmsD. However, we cannot confidently state if it plays any role in the REMP-to-substrate interaction. It is likely that the concentration of GTP that we employed was not high enough to influence DmsD-to-DmsAl interaction which resulted in the absence of the effect in the SEC experiments. Still, the concentration was sufficient for the CD experiment involving TatB2 which may point to a regulatory role of GTP within the translocation pathway.

8.1.5. Learning about the effect of metal alone and combined with GNP on DmsD and DmsD::DmsAl structure (Objectives #9 and #10)

By employing CD technique we supported previously reported hypothesis regarding the importance of Mg^{2+} for the system (Tran, 2013). Addition of this metal led to conformational changes in DmsD alone and in complex with the substrate. Combination of the metal with GNP resulted in a similar signal for DmsD::DmsAl (Chapter 5). We further supported this with SEC technique when an increase in apparent molecular weight was detected with addition of Mg^{2+} and GTP/Mg^{2+} (Chapter 7). We, therefore, suggest here that Mg^{2+} is likely coordinated by GTP when bound to DmsD and part of the regulatory mechanism. The other two metals tested (Mn^{2+} and Ni^{2+}) did not perturb DmsD structure when the protein was alone, yet influenced DmsD::DmsAl complex. As their concentration in the cell is much lower compared to Mg^{2+}, we propose here that they do not carry any biological relevance.

8.2. Proposed model

Going back to Figure 1.3 presented in the Introduction, I would like to suggest a more detailed and experimentally-supported sequence of events taking place during steps 8 to 11 in the model from Cherak and Turner (2017). It is important to note that all the steps include TatC protein which was not part of my experiments. However, as I am building on the existing model, it would be incorrect to exclude this component. Moreover, even the research groups that do not completely share out view on the sequence of events, accept that involvement of TatC is crucial for the pathway (Blümmel et al, 2017; Rollauer et al, 2012). My data provides evidence on the transfer of the substrate to the TatBC receptor complex, showing the steps when TatB, DmsD and DmsA follow:

1. DmsD targets DmsA towards the TatBC complex (Step 1).
2. Docking of the substrate on TatC takes place, while DmsD interacts with TatB (Step 2).
3. Leader peptide recognition by the complex triggers the harnessing of the PMF which promotes the flow of protons across the membrane and lowers the local pH (Step 2).
4. DmsA is transferred to TatB which results in formation of DmsD::DmsA::TatB intermediate (Step 3).
5. The interactions between the REMP and its RR-leader substrate are broken as a result of restoration (increase) of the local pH or from an interaction with GTP/Mg^{2+} (Step 4).
6. DmsD dissociates from TatB under the influence of GTP, higher (compared to Step 3) pH or their combination (Step 5).

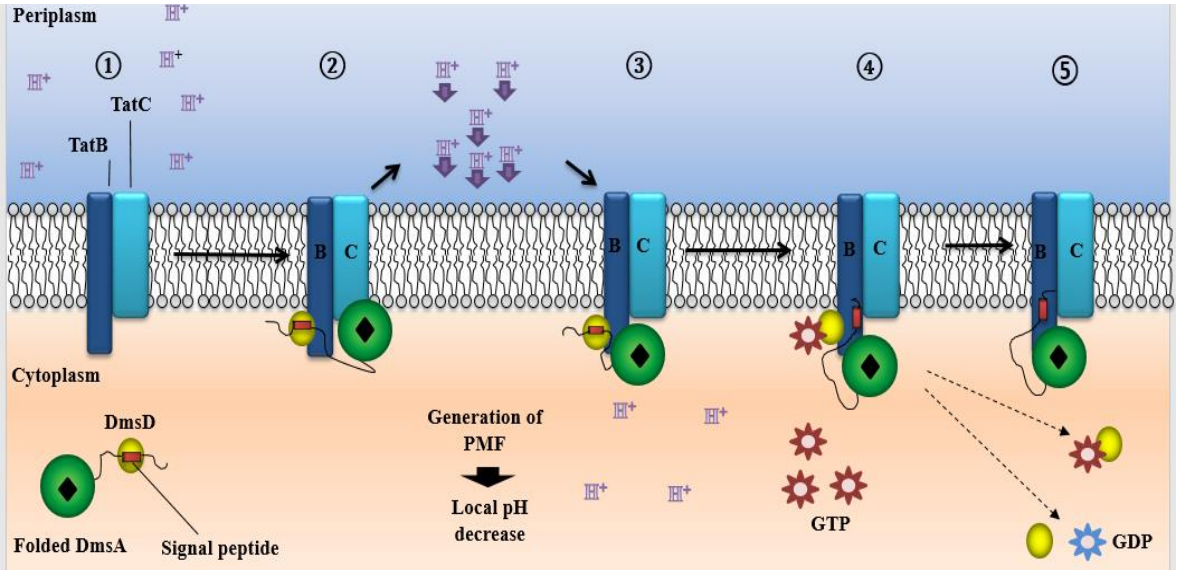

Figure 8.1. Transfer pathway model for DMSO reductase. After DmsA is fully-folded, DmsD targets it towards the membrane where TatBC complex is located (1). Interaction between the substrate and TatC triggers PMF (2). DmsA is transferred from TatC to TatB (3). Binding between the REMP and substrate is abrogated with DmsD and DmsA still bound to TatB (4). Interaction between DmsD and TatB weakens as a result of GTP presence (4). DmsD dissociates from the TAT machinery and returns to the free chaperone pool. Only a monomer of TatBC is shown for simplicity. DmsB was omitted from the cartoon.

In Step 2 we suggest that the interaction between the substrate and TatC takes place prior the contact with TatB. Alami *et al*. reported that in strains lacking TatC the contact between the substrate and TatB was abolished, but the reverse (TatB-deficient strains) was not the case and the substrate would still be detected in contact with TatC (2003). Another research group proposed that TatC makes initial contact with the folded substrate protein and later assists in the insertion of it into the membrane, while TatB may reorient the substrate and safeguard it from the processing of the RR-leader from signal peptidase until it is the time to cleave the signal sequence (Fröbel et al, 2012). This initial binding to TatC, which may be even maintained throughout the translocation according to Fröbel *et al.*, could have been the reason for the absence of a stable complex between TatB and DmsA that we were looking for in our SEC experiments (see Chapter 7) (2012). Perhaps the presence of TatC and/or the chaperone was required for a more long-lived complex to form. As a result, we only observed alterations in elution times of the recombinant proteins which we interpreted as changes in hydrodynamic volumes and, thus, shape changes.

Another important interaction taking place in Step 2 is the binding between DmsD and TatB. This is consistent with our data regarding conformational changes taking place as well as relatively small dissociation constants (0.08, 0.11 to 0.15 µM for MBP-$TatB_{fr}$ at pH 7.0, 7,5 and 8,0, respectively, and 4.70 to 5.40 µM for TatB2). These values are quite similar to what DmsD was found to demonstrate upon binding to DmsAl, but with a greater structural change as supported by the DSF, CD and SEC experiments (see chapters 4, 5 and 7) (Winstone et al, 2013; Winstone and Turner, 2015). Moreover, the following values are also close to 6 µM, the value that Wojnowska *et al.* reported for K_d between a detergent solubilized TatBC complex and a folded substrate (2018).

We positioned the influence of the PMF event between steps 2 and 3 due to the cross-linking data published by Mori and Cline where thylakoid orthologues of Tat A, B and C were employed together with several substrates and a generated pH gradient (2002). The authors showed that the gradient did not affect TatBC interaction with the signal peptide, but prevented Tha4 (thylakoid TatA) from joining the complex. Moreover, they were also able to demonstrate that recognition of the TAT signal peptide binding was crucial for the recruitment of Tha4 (Mori and Cline, 2002). Furthermore, placing PMF event between steps 2 and 3 is also based on our data that association between DmsD and TatB is stronger at lower pH (7.0) and weaker at higher pH 8.0. This is consistent with a sequence where the transfer of the substrate takes place at lower pH and as the system re-equilibrates the affinity between REMP and TatB weakens to eventually achieve separation of DmsD.

It should be noted that in Step 3, we utilized our knowledge on dissociation constants between DmsD::TatB versus DmsD::DmsAl complexes. As 24.24 μM for titration of DmsAl into DmsD::TatB complex is a much greater K_d compared to the 8.88 μM (dissociation constant obtained in a reverse experiment), it is justifiable to propose that the interaction between DmsD::TatB and DmsA is weaker and more likely to be disturbed by increasing pH or an introduction of GTP/Mg^{2+} into the system which as we had showed triggered structural change in the DmsD::DmsA complex.

Two potential mechanisms that lead to dissociation of the REMP from its substrate are presented in Figure 8.2. As can be seen in option 2, we are not excluding a possibility of GTP being hydrolyzed by DmsD as Tran previously suggested in her NMR experiments (Tran, 2013). Therefore, dashed arrow demonstrates an alternative outcome where GDP and Mg^{2+} metal dissociate from the complex once they have fulfilled their role.

In Step 4 we proposed a similar event to Step 3 option #2 mechanism for dissociation of DmsD from TatB. Based on the CD data, we believe that lower concentrations of GTP (compared to Step 3) will be needed to introduce a conformation change in DmsD::TatB since the K_d that was obtained from a titration was equal to 5.60 µM, a value considerably smaller than what Cherak and Turner reported for DmsD alone or DmsD::DmsAl complex (2.05 mM and 0.99 mM) (2015).

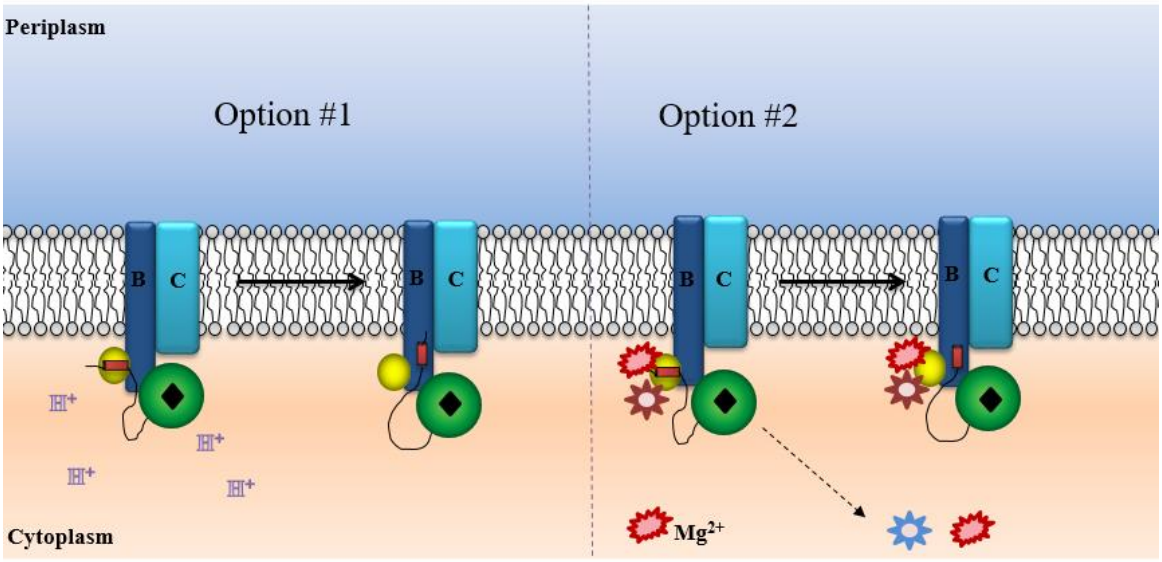

Figure 8.2. Mechanisms triggering dissociation of DmsD from DmsA leader peptide. A. The local pH is being restored by the cell and affinity of DmsD towards the substrate decreases. **B.** Binding of GTP and the metal (Mg^{2+}) results in a structural change with affinity towards the substrate decreasing. Only a monomer of TatBC is shown for simplicity. DmsB was omitted from the cartoon.

There are two key contributions to the field from this thesis:

1. DmsD may have two distinct binding sites for DmsA (the substrate) and TatB (component of the translocon);
2. Ef-Tu is associated with TatB, while previously it was only known as part of the DmsD interactome (Li et al, 2010).

8.3. Future work

As the main focus of this thesis was on DmsD-to-TatB interaction, it would be logical to attempt a mutagenesis study where we could support our findings regarding the distinct binding site for TatB on DmsD surface. We would create specific ligand site variants of DmsD and sample the binding of TatB2 peptide in order to identify variants with decreased affinity. This may be performed using CD technique. Alternatively, we may attempt a cross-linking study where DmsD variants and TatB will be mixed, allow to associate and crosslink, then subject to trypsin and LC-MS/MS in order to determine where exactly the binding is happening. This approach should not only point at the location of the "hot spots" for DmsD-TatB interaction, but resolve the issue of weak or transient binding (Chan et al, 2015). Collecting the data from the amylose-resin dissociation assay where MBP-$TatB_{fr}$ will be tested with DmsD variants will provide an additional layer of confidence for the *in vitro* methods.

Recently, a new purification method of TatBC was suggested where a semisynthetic detergent was utilized and allowed the authors to explore the kinetics with which TatBC binds the substrate. However, the reaction was determined to be quite slow which made the authors suggest that they were missing some components of the system such as phospholipids, yet they were also ignoring the role of a REMP (Wojnowska et al, 2018).. Moreover, ITC data yielded a very weak signal. This was not the case with my own ITC trials (data not shown) where TatB peptides or MBP-$TatB_{fr}$ was titrated into DmsD and no heat of enthalpy was detected. Therefore, working with full-sized native TatB and TatC in membrane vesicles would be more challenging, but would provide more information on that subject. If a similar goal was currently set up in our project, I would attempt utilizing TatBC complex, but isolated with the use of styrene maleic acid lipid particles (SMALPs). I was introduced to the approach during CSMB 2018 Membrane

Proteins in Health and Disease Conference and believe it could resolve many challenges such as non-native lipid population around the proteins as well as complete absence of detergents during the purification (Hardy et al, 2016; Overduin and Esmaili, 2019).

As experiments involving GTP were performed at concentrations which were lower than what the previous laboratory members employed, it would be reasonable to follow up and attempt performing SEC with the ligand being in mM range. Additionally, ITC may be utilized since it was proven to yield results for DmsD::DmsAl complex in the past.

Another important experiment to perform would be a CD titration of DmsA leader peptide into DmsD::TatB2::GTP complex since the following interaction does not fit well with the model proposed in this thesis. Moreover, it would be valuable to include a condition with Mg^{2+} metal added as we saw that it leads to significant structural changes in DmsD alone and in complex with the leader peptide. We could then compare the resulting dissociation constant to titration of DmsAl into DmsD::TatB complex as well as the rest of the K_d values identified. The latter step will assist in determining the biological significance of the step.

Of course, high resolution structures of various complexes using X-ray crystallography or cryo electron microscopy would yield considerable insights into the mechanism. However, these approaches rely on homogenous stable complexes, where our data implies this will be difficult to obtain but worth constant attempts as technologies develop.

Reference:

1. Adler AJ, Greenfield NJ, Fasman GD. Circular dichroism and optical rotatory dispersion of proteins and polypeptides. *Methods in enzymology*. 1973; 27:675.

2. Alder NN, Theg SM. Protein transport via the cpTat pathway displays cooperativity and is stimulated by transport-incompetent substrate. *FEBS Letters*. 2003; 540:96-100.

3. Akita M, Sasaki S, Matsuyama S, Mizushima S. SecA interacts with secretory proteins by recognizing the positive charge at the amino terminus of the signal peptide in *Escherichia coli*. *Journal of Biological Chemistry*. 1990; 265:8164-8169.

4. Alami M, Luke I, Deitermann S, Eisner G, Koch H, Brunner J, Mu M. Differential Interactions between a Twin-Arginine Signal Peptide and Its Translocase in *Escherichia coli*. *Molecular Cell*. 2003; 12:937-946.

5. Alcock F, Stansfeld PJ, Basit H, Habersetzer J, Baker MA, Palmer T, Wallace MI, and Ben C. Berk BCs. Assembling the Tat protein translocase. *eLife*. 2016; 5.

6. Angelis FD, Lee JK, O'Connell JD, et al. Metal-induced conformational changes in ZneB suggest an active role of membrane fusion proteins in efflux resistance systems. *Proceedings of the National Academy of Sciences of the United States of America*. 2010; 107:11038-11043.

7. Attar F, Khavari-Nejad S. In vitro study of drug-protein interaction using electronic absorption, fluorescence, and circular dichroism spectroscopy. *Archives of Razi Institute*. 2016; 71:183-194.

8. Beeckmans S. Chromatographic Methods to Study Protein–Protein Interactions. *Methods*. 1999; 19:278-305.

9. Berks BC. The Twin-Arginine Protein Translocation Pathway. *Annual Review of Biochemistry*. 2015; 84:843-864.

10. Blaszczyk M, Kurcinski M, Kouza M, Wieteska L, Debinski A, Kolinski A, Kmiecik S. Modeling of protein–peptide interactions using the CABS-dock web server for binding site search and flexible docking. *Methods*. 2016; 2015; 93:72-83.

11. Blaszczyk M, Ciemny MP, Kolinski A, Kurcinski M, Kmiecik S. Protein-peptide docking using CABS-dock and contact information. *Briefings in bioinformatics*. 2018.

12. Blümmel A, Haag LA, Eimer E, Müller M, Fröbel J. Initial assembly steps of a translocase for folded proteins. *Nature communications*. 2015; 6:7234-7234.

13. Blümmel AS, Drepper F, Knapp B, Eimer E., Warscheid B, Müller M, Fröbel J. Structural features of the TatC membrane protein that determine docking and insertion of a twin-arginine signal peptide. *The Journal of biological chemistry*. 2017; 292:21320-21329.

14. Boivin S, Kozak S, Meijers R. Optimization of protein purification and characterization using Thermofluor screens. *Protein Expression and Purification*. 2013; 91:192-206.

15. Buchanan G, Maillard J, Nabuurs SB, Richardson DJ, Palmer T, Sargent F. Features of a twin-arginine signal peptide required for recognition by a Tat proofreading chaperone. *FEBS Letters*. 2008; 582:3979-3984.

16. Caldas TD, Yaagoubi AE, Richarme G. Chaperone Properties of Bacterial Elongation Factor EF-Tu. *Journal of Biological Chemistry*. 1998; 273:11478-11482.

17. Cantor CR, Schimmel PR. *Techniques for the Study of Biological Structure and Function*. Vol pt. 2. San Francisco: W. H. Freeman; 1980.

18. Cattoni DI, Chara O, Kaufman SB, González Flecha FL. Cooperativity in Binding Processes: New Insights from Phenomenological Modeling. *PloS one*. 2015; 10:e0146043-e0146043.

19. Chan CS, Howell JM, Workentine ML, Turner RJ. Twin-arginine translocase may have a role in the chaperone function of NarJ from *Escherichia coli*. *Biochemical and Biophysical Research Communications*. 2006; 343:244-251.

20. Chan CS, Winstone TML, Chang L, Stevens CM, Workentine ML, Li H, Wei Y, Ondrechen MJ, Paetzel M, Turner RJ. Identification of residues in DmsD for twin-arginine leader peptide binding, defined through random and bioinformatics-directed mutagenesis. *Biochemistry*. 2008; 47:2749-2759.

21. Chan CS, Bay DC, Leach TGH, Winstone TML, Kuzniatsova L, Tran VA, and Turner RJ. 'Come into the fold': A comparative analysis of bacterial redox enzyme maturation protein members of the NarJ subfamily. *BBA - Biomembranes*. 2014; 1838:2971-2984.

22. Chan CS, Song X, Qazi SJS, Setiaputra D, Yip CK, Chao TC, Turner RJ. Unusual pairing between assistants: Interaction of the twin-arginine system-specific chaperone DmsD with the chaperonin GroEL. *Biochemical and Biophysical Research Communications*. 2015; 456:841-846.

23. Cherak SJ, Turner RJ. Influence of GTP on system specific chaperone – Twin arginine signal peptide interaction. *Biochemical and Biophysical Research Communications*. 2015; 465:753-757.

24. Cherak SJ, Turner RJ. Exploring GTP Control of Bacterial Respiratory System Specific Chaperone Interaction with its Substrate Protein's Twin-Arginine Signal Peptide. *FASEB*. 2016; 30: 810.1.

25. Cherak SJ, Turner RJ. Assembly pathway of a bacterial complex iron sulfur molybdoenzyme. *Biomolecular concepts*. 2017; 8:155.

26. Chivers PT, Sauer RT. NikR Repressor: High-Affinity Nickel Binding to the C-Terminal Domain Regulates Binding to Operator DNA. *Chemistry & Biology*. 2002; 9:1141-1148.

27. Cole ST, Condon C, Lemire BD, Weiner JH. Molecular biology, biochemistry and bionergetics of fumarate reductase, a complex membrane-bound iron-sulfur flavoenzyme of *Escherichia coli*. *BBA Reviews on Bioenergetics*. 1985; 811:381-403.

28. Connelly KRS, Stevenson C, Kneuper H, Sargent F. Biosynthesis of selenate reductase in *Salmonella enterica*: critical roles for the signal peptide and DmsD. *Microbiology (Reading, England)*. 2016; 162:2136-2146.

29. Corey RA, Allen WJ, Collinson I. Protein translocation: what's the problem? *Biochemical Society transactions*. 2016; 44:753-759.

30. Cruz JW, Rothenbacher FP, Maehigashi T, Lane WS, Dunham CM, Woychik NA. Doc toxin is a kinase that inactivates elongation factor Tu. *The Journal of biological chemistry*. 2014; 289:7788-7798.

31. de Keersmaeker D, Mellaert LV, Schaerlaekens K, Dessel WV, Vrancken K, Lammertyn E, Anné J, Geukens N. Structural organization of the twin-arginine translocation system in *Streptomyces lividans*. *FEBS Letters*. 2005; 579:797-802.

32. de Keersmaeker S, Vrancken K, Van Mellaert L, Anne J, Geukens N. The Tat pathway in *Streptomyces lividans*: interaction of Tat subunits and their role in translocation. *Microbiology*. 2007; 153:1087-1094.

33. de Keyzer J, van der Does C, Essen AJM. The bacterial translocase: a dynamic protein channel complex. *Cellular and Molecular Life Sciences*. 2003; 60:2034-2052.

34. DeSantis K, Reed A, Rahhal R, Reinking J. Use of differential scanning fluorimetry as a high-throughput assay to identify nuclear receptor ligands. *Nuclear receptor signaling*. 2012; 10:e002-e002.

35. Driessen AJM. Precursor protein translocation by the *Escherichia coli* translocase is directed by the protonmotive force. *EMBO Journal*. 1992; 11:847-853.

36. Englander SW, Mayne L, Kan Z, Hu W. Protein Folding-How and Why: By Hydrogen Exchange, Fragment Separation, and Mass Spectrometry. *Annual Review of Biophysics*. 2016; 45:135-152.

37. Freudl, R. Leaving home ain't easy: Protein export systems in gram-positive bacteria. *Research in Microbiology*. 2013; 164: 664-674.

38. Fröbel J, Rose P, Lausberg F, Blümmel A, Freudl R, Müller M. Transmembrane insertion of twin-arginine signal peptides is driven by TatC and regulated by TatB. *Nature communications*. 2012; 3:1311-1311.

39. Fu J, Momčilović I, Prasad PVV. Roles of Protein Synthesis Elongation Factor EF-Tu in Heat Tolerance in Plants. *Journal of Botany*. 2012; 2012:1-8.

40. Genest O, Seduk F, Théraulaz L, Méjean V, Iobbi-Nivol C. Chaperone protection of immature molybdoenzyme during molybdenum cofactor limitation: Chaperone protection of immature molybdoenzyme. *FEMS Microbiology Letters*. 2006; 265:51-55.

41. Giner A, Luirink J, High S, Dobberstein B, Wood H, Tollervey D. Signal-sequence recognition by an *Escherichia coli* ribonucleoprotein complex. *Nature*. 1992; 359:741-743.

42. Goosens VJ, Monteferrante CG, van Dijl JM. The Tat system of Gram-positive bacteria. *BBA - Molecular Cell Research*. 2014; 1843:1698-1706.

43. Graubner W, Schierhorn A, Braser T. DnaK Plays a Pivotal Role in Tat Targeting of CueO and Functions beside SlyD as a General Tat Signal Binding Chaperone. *Journal of Biological Chemistry*. 2007; 282:7116-7124.

44. Greenfield N.J. (2004) Circular Dichroism (CD) analysis for protein-protein interactions. *Methods in Molecular Biology, (Clifton, N.J.)*. 2015; 1278:239-265.

45. Guymer D, Maillard J, Agacan MF, Brearley CA, Sargent F. Intrinsic GTPase activity of a bacterial twin-arginine translocation proofreading chaperone induced by domain swapping: The *E. coli* TorD homodimer has GTPase activity. *FEBS Journal*. 2010; 277:511-525.

46. Hanada, M., Nishiyama, K. I., Mizushima, S., & Tokuda, H. Reconstitution of an efficient protein translocation machinery comprising SecA and the three membrane proteins, SecY, SecE, and SecG (p12). *Journal of Biological Chemistry*. 1994; 269:23625-23631.

47. Hardy D, Bill RM, Jawhari A, Rothnie AJ. Overcoming bottlenecks in the membrane protein structural biology pipeline. *Biochemical Society transactions*. 2016; 44:838-844.

48. Hatzixanthis K, Clarke TA, Oubrie A, Richardson DJ, Turner RJ, Sargent F, Randall LL. Signal Peptide-Chaperone Interactions on the Twin-Arginine Protein Transport Pathway.

Proceedings of the National Academy of Sciences of the United States of America. 2005; 102:8460-8465.

49. Henry R, Carrigan M, McCaffery M, Ma X, Cline K. Targeting Determinants and Proposed Evolutionary Basis for the Sec and the Delta pH Protein Transport Systems in Chloroplast Thylakoid Membranes. *The Journal of Cell Biology*. 1997; 136:823-832.

50. Hunt JF, Weinkauf S, Henry L, Fak JJ, McNicholas P, Oliver DB, Deisenhofer J. Nucleotide Control of Interdomain Interactions in the Conformational Reaction Cycle of SecA. *Science*. 2002; 297:2018-2026.

51. Ilbert M, Méjean V, Giudici-Orticoni M, Samama J, Iobbi-Nivol C. Involvement of a Mate Chaperone (TorD) in the Maturation Pathway of Molybdoenzyme TorA. *Journal of Biological Chemistry*. 2003; 278:28787-28792.

52. Ingham K., Busby T, Atha D, Forastieri H. Characterization of Protein-Protein and Protein-Ligand Interactions by High Performance Size Exclusion Chromatography. *Journal of Liquid Chromatography*. 1987; 6:229-248.

53. Kaling M. *Is Everyone Hanging Out Without Me?* New York, NY: Crown Publishing Group; 2011.

54. Keon RG, Voordouw G. Identification of the HmcF and Topology of the HmcB Subunit of the Hmc Complex of *Desulfovibrio vulgaris*: MOLECULAR BIOLOGY/GENETICS. *Anaerobe*. 1996; 2:231-238.

55. Kjeldgaard M, Nyborg J, Clark BF. The GTP binding motif: variations on a theme. *FASEB journal: official publication of the Federation of American Societies for Experimental Biology*. 1996; 10:1347-1368.

56. Kneuper H, Maldonado B, Jäger F, Krehenbrink M, Buchanan G, Keller R, Müller M, Berks BC, and Palmer T. Molecular dissection of TatC defines critical regions essential for protein transport and a TatB–TatC contact site. *Molecular Microbiology*. 2012; 85:945-961.

57. Kostecki JS, Li H, Turner RJ, DeLisa MP. Visualizing interactions along the *Escherichia coli* twin-arginine translocation pathway using protein fragment complementation. *PloS one*. 2010; 5:e9225.

58. Kudlicki W, Coffman A, Kramer G, Hardesty B. Renaturation of rhodanese by translational elongation factor (EF) Tu. Protein refolding by EF-Tu flexing. *The Journal of biological chemistry*. 1997; 272:32206-32210.

59. Kudva R, Denks K, Kuhn P, Vogt A, Müller M, Koch H. Protein translocation across the inner membrane of Gram-negative bacteria: the Sec and Tat dependent protein transport pathways. *Research in Microbiology*. 2013; 164:505-534.

60. Kurcinski M, Jamroz M, Blaszczyk M, Kolinski A, Kmiecik S. CABS-dock web server for the flexible docking of peptides to proteins without prior knowledge of the binding site. *Nucleic acids research*. 2015; 43:W419-W424.

61. Kuzniatsova L, Winstone TML, Turner RJ. Identification of protein–protein interactions between the TatB and TatC subunits of the twin-arginine translocase system and respiratory enzyme specific chaperones. *BBA - Biomembranes*. 2016; 1858:767-775.

62. Lacasse MJ, Douglas CD, Zamble DB. Mechanism of Selective Nickel Transfer from HypB to HypA, *Escherichia coli* [NiFe]-Hydrogenase Accessory Proteins. Biochemistry. 2016; 55:6821-6831.

63. Lesk VI, Sternberg MJE. 3D-Garden: a system for modelling protein-protein complexes based on conformational refinement of ensembles generated with the marching cubes algorithm. *Bioinformatics*. 2008; 24:1137-1144.

64. Li H, Chang L, Howell JM, Turner RJ. DmsD, a Tat system specific chaperone, interacts with other general chaperones and proteins involved in the molybdenum cofactor biosynthesis. *BBA - Proteins and Proteomics*. 2010; 1804:1301-1309.

65. Lichi T, Ring G, Eichler J. Membrane binding of SRP pathway components in the halophilic archaea *Haloferax volcanii*: *H. volcanii* FtsY and SRP54 membrane binding. *European Journal of Biochemistry*. 2004; 271:1382-1390.

66. Lovitt B, Vanderporten EC, Sheng Z, Zhu H, Drummond J, Liu Y. Differential effects of divalent manganese and magnesium on the kinase activity of leucine-rich repeat kinase 2 (LRRK2). *Biochemistry*. 2010; 49:3092-3100.

67. Luft JR, Furlani NM, Nemoyer RE, Penna EJ, Wolfley JR, Snell E, Potter SA, Snell EH. Crystal cookery - using high-throughput technologies and the grocery store as a teaching tool. *Journal of applied crystallography*. 2010; 43:1189-1207.

68. Ma X, Cline K. Multiple precursor proteins bind individual Tat receptor complexes and are collectively transported. *The EMBO Journal*. 2010; 29:1477-1488.

69. Ma Z, Jacobsen FE, Giedroc DP. Coordination chemistry of bacterial metal transport and sensing. *Chemical reviews*. 2009; 109:4644-4681.

70. Maurer C, Panahandeh S, Jungkamp A, Moser M, Müller M. TatB functions as an oligomeric binding site for folded Tat precursor proteins. *Molecular biology of the cell*. 2010; 21:4151-4161.

71. Mondal S, Hsiao K, Goueli SA. A Homogenous Bioluminescent System for Measuring GTPase, GTPase Activating Protein, and Guanine Nucleotide Exchange Factor Activities. *Assay and drug development technologies*. 2015; 13:444.

72. Mori H, Cline K. A Twin Arginine Signal Peptide and the pH Gradient Trigger Reversible Assembly of the Thylakoid ΔpH/Tat Translocase. *The Journal of Cell Biology*. 2002; 157:205-210.

73. Nguyen S, Winnik FM, Buschmann MD. Improved reproducibility in the determination of the molecular weight of chitosan by analytical size exclusion chromatography. *Carbohydrate Polymers*. 2009; 75:528-533.

74. Niesen FH, Vedadi M, Berglund H. The use of differential scanning fluorimetry to detect ligand interactions that promote protein stability. *Nature Protocols*. 2007; 2:2212-2221.

75. Oresnik IJ, Ladner CL, Turner RJ. Identification of a twin-arginine leader-binding protein. *Molecular microbiology*. 2001; 40:323-331.

76. Overduin M, Esmaili M. Native Nanodiscs and the Convergence of Lipidomics, Metabolomics, Interactomics and Proteomics. *Applied Sciences*. 2019; 9:1230.

77. Park S, Liu G, Topping TB, Cover WH, Randall LL. Modulation of Folding Pathways of Exported Proteins by the Leader Sequence. *Science*. 1988; 239:1033-1035.

78. Pierce BG, Hourai Y, Weng Z. Accelerating protein docking in ZDOCK using an advanced 3D convolution library. *PloS one*. 2011; 6:e24657-e24657.

79. Pochapsky TC, Mo H, Al-Mjeni F, Ju T, Pochapsky SS, Maroney MJ. Modeling and experiment yields the structure of acireductone dioxygenase from *Klebsiella pneumoniae*. *Nature Structural Biology*. 2002; 9:966-972.

80. Qiu Y, Zhang R, Binkowski TA, Tereshko V, Joachimiak A, Kossiakoff A. The 1.38 Å crystal structure of DmsD protein from *Salmonella typhimurium*, a proofreading chaperone on the Tat pathway. *Proteins: Structure, Function, and Bioinformatics*. 2008; 71:525-533.

81. Ramasamy SK, Clemons WM. Structure of the twin-arginine signal-binding protein DmsD from *Escherichia coli*. *Acta Crystallographica Section F Structural Biology and Crystallization Communications*. 2009; 65:746-750.

82. Ray N, Oates J, Turner RJ, Robinson C. DmsD is required for the biogenesis of DMSO reductase in *Escherichia coli* but not for the interaction of the DmsA signal peptide with the Tat apparatus. *FEBS Letters*. 2003; 534:156-160.

83. Ray S, Kumar A, Panda D. GTP regulates the interaction between MciZ and FtsZ: a possible role of MciZ in bacterial cell division. *Biochemistry*. 2013; 52:392-401.

84. Rivardo F, Leach TGH, Chan CS, Winstone TML, Ladner CL, Sarfo KJ, Turner RJ. Unique Photobleaching Phenomena of the Twin-Arginine Translocase Respiratory Enzyme Chaperone DmsD. *The open biochemistry journal*. 2014; 8:1-11.

85. Rollauer SE, Tarry MJ, Graham JE, Jääskeläinen M, Jäger F, Johnson S, Krehenbrink M, Liu S, Lukey MJ, Marcoux, J, McDowell MA, Rodriguez F, Roversi P, Stansfeld PJ, Robinson, CV, Sansom MSP, Palmer T, Högbom M, Berks BC, Lea SM. Structure of the TatC core of the twin-arginine protein transport system. *Nature*. 2012; 492:210-214.

86. Rudack T, Xia F, Schlitter J, Kötting C, Gerwert K. The Role of Magnesium for Geometry and Charge in GTP Hydrolysis, Revealed by Quantum Mechanics/Molecular Mechanics Simulations. *Biophysical Journal*. 2012; 103:293-302.

87. Rudack T, Jenrich S, Brucker S, Vetter IR, Gerwert K, Kötting C. Catalysis of GTP hydrolysis by small GTPases at atomic detail by integration of X-ray crystallography, experimental, and theoretical IR spectroscopy. *The Journal of biological chemistry*. 2015; 290:24079-24090.

88. Sarfo K, Turner RJ. Fluorescence spectroscopy study of DmsD. A unique reaction with thiols as a probe for molecular characterization. Poster presented at 47th annual Biophysical Society Meeting; February 14-18, 2004. Baltimore, USA

89. Sarfo KJ, Winstone TL, Papish AL, Howell JM, Kadir H, Vogel HJ, Turner RJ. Folding forms of Escherichia coli DmsD, a twin-arginine leader binding protein. *Biochemical and Biophysical Research Communications*. 2004; 315:397-403.

90. Sargent F. The Model [NiFe]-Hydrogenases of Escherichia coli. *Advances in microbial physiology*. 2016; 68:433-507.

91. Satoh T, Kurihara FN. Purification and properties of dimethylsulfoxide reductase containing a molybdenum cofactor from a photodenitrifier, *Rhodopseudomonas sphaeroides f.s. denitrificans*. *Journal of Biochemistry*. 1987; 102:191-197.

92. Schwemmle M, Staeheli P. The interferon-induced 67-kDa guanylate-binding protein (hGBP1) is a GTPase that converts GTP to GMP. *Journal of Biological Chemistry*. 1994; 269:11299-11305.

93. Shanmugham A, Bakayan A, Völler P, Grosveld J, Lill H, Bollen YJ. The hydrophobic core of twin-arginine signal sequences orchestrates specific binding to Tat-pathway related chaperones. *PLoS One*. 2012; 7:e34159-e34159.

94. Shanmugam SK, Dalbey RE. The Conserved Role of YidC in Membrane Protein Biogenesis. *Microbiology spectrum*. 2019; 7.

95. Shannon RD, Rogers DB, Prewitt CT. Chemistry of noble metal oxides. I. Syntheses and properties of ABO2 delafossite compounds. *Inorganic Chemistry*. 1971; 10:713-718.

96. Shi S, Semple A, Cheung J, Shameem M. DSF Method Optimization and Its Application in Predicting Protein Thermal Aggregation Kinetics. *Journal of Pharmaceutical Sciences*. 2013; 102:2471-2483.

97. Solomon PS, Shaw AL, Lane I, Hanson GR, Palmer T, McEwan AG. Characterization of a molybdenum cofactor biosynthetic gene cluster in *Rhodobacter capsulatus* which is specific for the biogenesis of dimethylsulfoxide reductase. *Microbiology*. 1999; 145:1421-1429.

98. Soufo HJD, Reimold C, Linne U, Knust T, Gescher J, Graumann PL, Losick RM. Bacterial Translation Elongation Factor EF-Tu Interacts and Colocalizes with Actin-like MreB Protein. *Proceedings of the National Academy of Sciences of the United States of America*. 2010; 107:3163-3168.

99. Stephenson K. Sec-dependent protein translocation across biological membranes: evolutionary conservation of an essential protein transport pathway (Review). *Molecular Membrane Biology*. 2005; 22:17-28.

100. Stevens CM, Winstone TML, Turner RJ, Paetzel M. Structural Analysis of a Monomeric Form of the Twin-Arginine Leader Peptide Binding Chaperone *Escherichia coli* DmsD. *Journal of Molecular Biology*. 2009; 389:124-133.

101. Stevens CM, Paetzel M. Crystal structure of Escherichia coli DmsD in space group P212121. PDB: 3U41. 2011; 10.2210/pdb3U41/pdb

102. Styrvold OB, Strøm AR. Dimethylsulphoxide and trimethylamine oxide respiration of Proteus vulgaris. Evidence for a common terminal reductase system. *Archives of microbiology*. 1984; 140:74-78.

103. Tarry MJ, Schäfer E, Chen S, Buchanan G., Greene NP, Lea SM, Palmer T, Saibil HR, Berks BC, Randall LL. Structural Analysis of Substrate Binding by the TatBC Component of the Twin-Arginine Protein Transport System. *Proceedings of the National Academy of Sciences of the United States of America*. 2009; 106:13284-13289.

104. Tran, V. GTP Interactions with the Chaperone, DmsD. MS thesis. 2011. University of Calgary, Canada.

105. Turner RJ, Papish AL, Sargent F. Sequence analysis of bacterial redox enzyme maturation proteins (REMPs). *Canadian Journal of Microbiology*. 2004; 50:225-238.

106. Valent QA, Scotti PA, High S, de Gier JL, von Heijne G, Lentzen G, Wintermeyer W, Oudega B, and Luirink J. The *Escherichia coli* SRP and SecB targeting pathways converge at the translocon. *The EMBO Journal*. 1998; 17:2504-2512.

107. van Amerongen H, van Grondelle R, van der Vliet, P C. Interaction between adenovirus DNA-binding protein and single-stranded polynucleotides studied by circular dichroism and ultraviolet absorption. *Biochemistry*. 1987; 26:4646-4652.

108. van den Berg L, Kiefer D, Serek J, Bauer-Manz G, Struhalla G, Kuhn A, and Dalbey R. *Escherichia coli* YidC is a membrane insertase for Sec-independent proteins. *The EMBO Journal*. 2004; 23:294-301.

109. Wei Y, Thyparambil AA, Latour RA. Protein helical structure determination using CD spectroscopy for solutions with strong background absorbance from 190 to 230nm. *BBA - Proteins and Proteomics*. 2014; 1844:2331-2337.

110. Weiner JH, Rothery RA, Sambasivarao D, Trieber CA. Molecular analysis of dimethylsulfoxide reductase: a complex iron-sulfur molybdoenzyme of *Escherichia coli*. *BBA - Bioenergetics*. 1992; 1102:1-18.

111. Whitaker N, Bageshwar UK, Musser SM. Kinetics of precursor interactions with the bacterial Tat translocase detected by real-time FRET. *The Journal of biological chemistry*. 2012; 287:11252-11260.

112. Williams RJP, Irving H. Order of Stability of Metal Complexes. *Nature*. 1948; 162:746-747.

113. Winstone, TL. Characterization of DmsD - DmsA Twin-Arginine Leader Peptide Binding. PhD thesis. 2013. University of Calgary, Canada.

114. Winstone TL, Workentine ML, Sarfo KJ, Binding AJ, Haslam BD, Turner RJ. Physical nature of signal peptide binding to DmsD. *Archives of Biochemistry and Biophysics*. 2006; 455:89-97.

115. Winstone TML, Tran VA, Turner RJ. The hydrophobic region of the DmsA twin-arginine leader peptide determines specificity with chaperone DmsD. *Biochemistry*. 2013; 52:7532-7541.

116. Winstone TML, Turner RJ. Thermodynamic characterization of the DmsD binding site for the DmsA twin-arginine motif. *Biochemistry*. 2015; 54:2040-2051.

117. Wojnowska M, Gault J, Yong SC, Robinson CV, Berks BC. Precursor-Receptor Interactions in the Twin Arginine Protein Transport Pathway Probed with a New Receptor Complex Preparation. *Biochemistry*. 2018; 57:1663-1671.

118. Yan S, Wu G. Large-scale evolutionary analyses on SecB subunits of bacterial sec system. *PloS one*. 2015; 10:e0120417-e0120417.

119. Yang X, Li H, Lai T, Sun H. UreE-UreG complex facilitates nickel transfer and preactivates GTPase of UreG in *Helicobacter pylori*. *The Journal of biological chemistry*. 2015; 290:12474.

120. Zhang Y, Wang L, Hu Y, Jin C. Solution structure of the TatB component of the twin-arginine translocation system. *BBA - Biomembranes*. 2014; 1838:1881-1888.

Appendix

Permission #1

Title: Identification of Residues in DmsD for Twin-Arginine Leader Peptide Binding, Defined through Random and Bioinformatics-Directed Mutagenesis

Author: Catherine S. Chan, Tara M. L. Winstone, Limei Chang, et al

Publication: Biochemistry

Publisher: American Chemical Society

Date: Mar 1, 2008

PERMISSION/LICENSE IS GRANTED FOR YOUR ORDER AT NO CHARGE

This type of permission/license, instead of the standard Terms & Conditions, is sent to you because no fee is being charged for your order. Please note the following:

- Permission is granted for your request in both print and electronic formats, and translations.
- If figures and/or tables were requested, they may be adapted or used in part.
- Please print this page for your records and send a copy of it to your publisher/graduate school.
- Appropriate credit for the requested material should be given as follows: "Reprinted (adapted) with permission from Chan CS, Winstone TML, Chang L, Stevens CM, Workentine ML, Li H, Wei Y, Ondrechen MJ, Paetzel M, Turner RJ. Identification of residues in DmsD for twin-arginine leader peptide binding, defined through random and bioinformatics-directed mutagenesis. Biochemistry. 2008; 47:2749-2759. Copyright (2008) American Chemical Society."
- One-time permission is granted only for the use specified in your request. No additional uses are granted (such as derivative works or other editions). For any other uses, please submit a new request.

If credit is given to another source for the material you requested, permission must be obtained from that source.

Permission #2

License Number	4641080134994
License date	Aug 02, 2019
Licensed Content Publisher	Elsevier
Licensed Content Publication	Journal of Molecular Biology
Licensed Content Title	Structural Analysis of a Monomeric Form of the Twin-Arginine Leader Peptide Binding Chaperone Escherichia coli DmsD
Licensed Content Author	Charles M. Stevens,Tara M.L. Winstone,Raymond J. Turner,Mark Paetzel
Licensed Content Date	May 29, 2009
Licensed Content Volume	389
Licensed Content Issue	1
Licensed Content Pages	10
Type of Use	reuse in a thesis/dissertation
Portion	figures/tables/illustrations
Number of figures/tables/illustrations	1
Format	both print and electronic
Are you the author of this Elsevier article?	No
Will you be translating?	No
Original figure numbers	Figure 5B
Title of your thesis/dissertation	Characterization of interactions between DmsD, DmsA, and TatB for the docking step for the bacterial twin-arginine translocase".
Expected completion date	Sep 2019
Estimated size (number of pages)	110
Requestor Location	Ms. Elina Levchenko 2440 7th Ave NW Calgary, AB T2N1A2 Canada Attn: Ms. Elina Levchenko
Publisher Tax ID	GB 494 6272 12
Total	0.00 CAD

Permission #3

License Number	4632750731563
License date	Jul 19, 2019
Licensed Content Publisher	John Wiley and Sons
Licensed Content Publication	Proteins: Structure, Function and Bioinformatics
Licensed Content Title	The 1.38 Å crystal structure of DmsD protein from Salmonella typhimurium, a proofreading chaperone on the Tat pathway
Licensed Content Author	Yang Qiu, Rongguang Zhang, T. Andrew Binkowski, et al
Licensed Content Date	Jan 3, 2008
Licensed Content Volume	71
Licensed Content Issue	2
Licensed Content Pages	9
Type of Use	Dissertation/Thesis
Requestor type	University/Academic
Format	Print and electronic
Portion	Figure/table
Number of figures/tables	1
Original Wiley figure/table number(s)	Figure 4 B
Will you be translating?	No
Title of your thesis / dissertation	Characterization of interactions between DmsD, DmsA, and TatB for the docking step for the bacterial twin-arginine translocase".
Expected completion date	Sep 2019
Expected size (number of pages)	110
Requestor Location	Ms. Elina Levchenko 2440 7th Ave NW Calgary, AB T2N1A2 Canada Attn: Ms. Elina Levchenko
Publisher Tax ID	EU826007151
Total	0.00 CAD